SHALLOW-SHELF CARBONATE BUILDUPS IN THE PARADOX BASIN, UTAH— TARGETS FOR INCREASED OIL AND GAS PRODUCTION AND RESERVES USING HORIZONTAL DRILLING TECHNIQUES

Thomas C. Chidsey, Jr., Compiler and Editor

BULLETIN 140
UTAH GEOLOGICAL SURVEY
UTAH DEPARTMENT OF NATURAL RESOURCES
2020

SHALLOW-SHELF CARBONATE BUILDUPS IN THE PARADOX BASIN, UTAH— TARGETS FOR INCREASED OIL AND GAS PRODUCTION AND RESERVES USING HORIZONTAL DRILLING TECHNIQUES

Thomas C. Chidsey, Jr., Compiler and Editor

Cover photos: Reservoir zones in the Pennsylvanian Paradox Formation, Paradox Basin, southeastern Utah.

Top photos—Desert Creek zone, Bug field, San Juan County: (left) slabbed core of a dolomitized phylloid-algal bafflestone with visible porosity, and (right) photomicrograph under plane light of extensive micro-boxwork porosity with some hollow dolomites and pores lined or plugged with bitumen.

Bottom photos—Ismay zone, Cherokee field, San Juan County: (left) photomicrograph under plane light of a peloidal packstone/grainstone dominated by microporosity, and (right) scanning electron microscope photomicrograph showing well-developed dolomite rhombs exhibiting abundant intercrystalline microporosity.

BULLETIN 140
UTAH GEOLOGICAL SURVEY
UTAH DEPARTMENT OF NATURAL RESOURCES
2020

CONTENTS

FIGURES

TABLES

PREFACE

The Pennsylvanian Paradox Formation is the major producer of oil and gas in the Paradox Basin of southeastern Utah and southwestern Colorado. The Paradox was deposited in a warm, shallow-shelf marine environment and contains a wide variety of carbonate lithofacies, which have extensive diagenesis. Traps are stratigraphic formed by carbonate buildups consisting principally of phylloid-algal deposits sealed by organic-rich shale. Complex reservoir heterogeneity has created multiple intervals that represent untested targets for horizontal drilling, which has only been extensively used in the giant Greater Aneth field but not in the more typical small fields of the basin.

This Utah Geological Survey (UGS) Bulletin is based on the final report of a project titled "Heterogeneous Shallow-Shelf Carbonate in the Paradox Basin: Targets for Increased Oil Production and Reserves Using Horizontal Drilling Techniques," which was funded, in part, by the U.S. Department of Energy and conducted by the UGS between 2000 and 2004. The goals of the project were to (1) increase recovery and reserve base by identifying untapped compartments created by reservoir heterogeneity, (2) prevent abandonment of numerous small fields, (3) increase deliverability by horizontal drilling, (4) identify reservoir trends for field extension drilling and stimulating exploration in Paradox Basin fairways, (5) reduce development costs, (6) minimize surface disturbance when drilling, (7) use energy investment dollars more productively, and (8) increase royalty income to the various stakeholders. The project final report was updated, shortened, revised, and peer reviewed to produce this Bulletin.

This Bulletin consists of three components: (1) regional lithofacies evaluation of the Ismay and Desert Creek zones of the Paradox Formation in the Blanding sub-basin (Chapter 2); (2) case studies of Bug and Cherokee fields (general petroleum geology, scanning electron microscopy, epifluorescence and cathodoluminescence petrography, isotope geochemistry, capillary pressure/mercury injection analysis, and well-test and production analysis) (Chapters 3 through 9); and (3) horizontal drilling opportunities (Chapter 10). The research, data, conclusions, and recommendations contained in this Bulletin are anticipated to be a valuable resource for hydrocarbon production and exploration in the Paradox Basin and similar shallow-shelf marine regions worldwide, as well as for students and researchers studying carbonate rocks for years to come.

Thomas C. Chidsey, Jr., Compiler and Editor, Utah Geological Survey

ABSTRACT

The Paradox Basin of Utah, Colorado, Arizona, and New Mexico contains nearly 100 small oil fields producing from carbonate buildups within the Pennsylvanian (Desmoinesian) Paradox Formation. These fields typically have one to 10 wells with primary production ranging from 700,000 to 2,000,000 barrels of oil per field and a 15% to 20% recovery rate of the original oil in place. Millions of barrels of oil as well as billions of cubic feet of gas will not be recovered from these small fields when abandonment leaves undrained heterogeneous reservoirs. With the exception of the giant Greater Aneth field, the value of horizontal drilling has not been demonstrated in the small shallow-shelf carbonate reservoirs in the Paradox Basin. These heterogeneous rocks contain rapid lithofacies changes and extensive diagenesis, resulting in significantly compartmentalized reservoirs that are often untouched by vertical drilling.

Two main producing intervals in the Paradox Formation are referred to as the Desert Creek and Ismay zones. The Desert Creek zone is dominantly dolomite comprising regional, nearshore trends with highly aligned, linear lithofacies tracts. The Desert Creek produces oil and gas in fields in the central Blanding sub-basin. The Ismay zone is dominantly limestone comprising small, equant buildups of phylloid-algal material; locally variable, inner-shelf, skeletal calcarenites; rare, open-marine, bryozoan mounds; and anhydrite caps. The Ismay produces oil and gas from fields in the southern Blanding sub-basin. Both the Desert Creek and Ismay buildups generally trend northwest-southeast.

Two Utah case-study fields were evaluated as candidates for horizontal drilling and enhanced oil recovery based upon geological characterization: Bug field, in the Desert Creek trend; and Cherokee field, in the Ismay trend. Geological characterization on a local scale focused on reservoir heterogeneity, quality, and lateral continuity, as well as possible reservoir compartmentalization to grade the potential in each field, and in other similar fields within the Desert Creek and Ismay trends, for drilling horizontal laterals from existing development wells. From these evaluations, specific untested or under-produced compartments were identified as targets for horizontal drilling.

The primary objective of this report is to enhance petroleum production in the Paradox Basin through an increase in use of horizontal drilling technology. Our research shows that horizontal laterals drilled from existing vertical wells are economically feasible and the wells will likely encounter unproduced oil and gas reserves. This technique could be applied to approximately 100 small fields in the Paradox Basin and could result in the recovery of overlooked millions of barrels of oil and billions of cubic feet of gas. In addition, the results of these studies can be applied to similar fields in the Rocky Mountain region, the Michigan and Illinois Basins, the Midcontinent, and other regions.

The core-derived vertical sequence of lithofacies from the case-study fields was tied to its corresponding log response to identify reservoir and non-reservoir rock and determine potential units suitable for horizontal drilling targets. Reservoir maps show buildup trends, define limits of field potential, and indicate possible horizontal drilling locations. The diagenetic fabrics and porosity types found in the fields are indicators of reservoir flow capacity, storage capacity, and potential for horizontal drilling. The reservoir quality has been affected by multiple generations of dissolution, anhydrite plugging, and various types of cementation, which act as barriers or baffles to fluid flow. The most significant and unique diagenetic characteristics are early-stage micro-boxwork porosity and intense, late-stage microporosity.

Lower Desert Creek cores show open marine, middle shelf, proto-mound, and phylloid-algal mound lithofacies. Cores from the upper Ismay display seven depositional lithofacies: open marine, middle shelf, inner shelf/tidal flat, bryozoan mound, phylloid-algal mound, quartz sand dune, and anhydritic salina. Mapping the Ismay lithofacies delineates very prospective reservoir trends that contain porous, productive buildups around the anhydrite-filled intra-shelf basins. Lithofacies and reservoir controls imposed by the anhydritic intra-shelf basins should be considered when selecting the optimal location and orientation of any horizontal drilling from known phylloid-algal reservoirs to undrained reserves, as well as identifying new exploration trends. Although intra-shelf basins are not present in the lower Desert Creek zone of the Blanding sub-basin, drilling horizontally along linear shoreline trends could also encounter previously undrilled porous intervals and buildups.

Strategies for horizontal drilling developed for case-study and similar fields in the Paradox Basin involve drilling stacked, parallel, horizontal laterals, which could be combined with hydraulic fracturing and water and carbon dioxide flooding. Depositional lithofacies are targeted in both the Desert Creek and Ismay zones where, for example, multiple buildups can be penetrated with two opposed sets of stacked, parallel, horizontal laterals. Similarly, a second strategy involves penetrating multiple zones of diagenetically enhanced reservoir intervals in these mound buildups. Microporosity and micro-boxwork porosity represent important sites for untapped hydrocarbons.

CHAPTER 1:
INTRODUCTION

by

Thomas C. Chidsey, Jr., Utah Geological Survey

CHAPTER 1:
INTRODUCTION

OVERVIEW

Over 550 million barrels of oil (BO) and 1.1 trillion cubic feet of gas (TCFG) have been produced from the shallow-shelf carbonate reservoirs in the Pennsylvanian (Desmoinesian) Paradox Formation in the Paradox Basin, southeastern Utah and southwestern Colorado (figure 1.1) (Colorado Oil and Gas Conservation Commission, 2020; Utah Division of Oil, Gas and Mining, 2020). Two main producing intervals in the Paradox Formation are named the Desert Creek and the Ismay zones (figure 1.2). The Desert Creek zone is dominantly dolomite comprising regional shoreline trends with highly aligned, linear lithofacies tracts. The Desert Creek produces oil and gas in fields in the central Blanding sub-basin (figure 1.3). The Ismay zone is dominantly limestone comprising small, equant buildups of phylloid-algal material; locally variable, inner-shelf, skeletal calcarenites; rare, open-marine, bryozoan mounds; and anhydrite caps. The Ismay produces oil and gas from fields in the southern Blanding sub-basin (figure 1.3). Both the Desert Creek and Ismay buildups generally trend northwest-southeast. Various lithofacies changes and extensive diagenesis have created complex reservoir heterogeneity within these two diverse zones.

We estimate that with the exception of the giant Greater Aneth field (figures 1.1 and 1.3), the other 100-plus oil fields in the basin typically contain 2 to 10 million barrels of original oil in place (OOIP). Most of these fields were characterized by high initial production rates. As a general rule only 15% to 25% of the OOIP is recoverable during primary production from conventional vertical wells.

An extensive and successful horizontal drilling program has been conducted in the giant Greater Aneth field. However, to date, only a few horizontal wells have been drilled in small Desert Creek and Ismay fields. The results from these wells were disappointing due to the poor understanding of the carbonate lithofacies and diagenetic fabrics that create reservoir heterogeneity. Many of these small fields have already been abandoned whereas others are at risk of abandonment. Millions of barrels of oil and billions of cubic feet of gas will be left behind in these small fields because compartments of the heterogeneous reservoirs remain undrained. Through proper geological evaluation of the reservoirs, production may be increased by 20% to 50% through the drilling of low-cost, single, or multilateral horizontal legs from existing vertical development wells (figure 1.4). In addition, horizontal drilling from existing wells minimizes surface disturbance and costs for field development, particularly in the environmentally sensitive areas of southeastern Utah and southwestern Colorado.

The Utah Geological Survey (UGS) selected two diverse, small fields—Bug and Cherokee—for detailed case studies (figure 1.3). These two fields are representative of the two main producing trends in the Paradox Basin of Utah and Colorado—the Desert Creek and Ismay zones of the Paradox Formation. Geological and reservoir characterization of these fields included (1) determination of regional geologic setting; (2) analysis of the reservoir heterogeneity, quality, lateral continuity, and compartmentalization within the fields; (3) construction of lithologic, microfacies, porosity, permeability, and net pay maps of the fields; and (4) integration of geological data to recommend single or multiple horizontal laterals from existing vertical wells. Our research showed that horizontal wells drilled from existing vertical wells in each field would likely economically encounter unproduced oil and gas reserves.

BENEFITS AND POTENTIAL APPLICATION

The overall benefit of this study will hopefully be enhanced petroleum production from small fields in the Paradox Basin. Specifically, the benefits could include (1) increased recovery and reserve base by identification of untapped compartments created by reservoir heterogeneity; (2) prevention of abandonment of numerous small fields; (3) increased deliverability by horizontally drilling along a reservoir's optimal fluid-flow paths; (4) identification of reservoir trends for field extension drilling and stimulating exploration in Paradox Basin fairways; (5) reduced development costs by closely delineating minimum field size and other parameters necessary for horizontal drilling; (6) minimized of surface disturbance by drilling from existing, vertical, field well pads; (7) the ability to use energy investment dollars more productively; and (8) increased in royalty income to the federal, state, tribal, and local governments, and fee owners. These benefits could also apply to other areas, including algal-mound and carbonate buildup reservoirs on the eastern and northwestern shelves of the Permian Basin in Texas, Silurian pinnacle and patch reefs of the Michigan and Illinois Basins, and shoaling carbonate island trends of the Williston Basin.

This Bulletin covers the research and results of the UGS's four-year Paradox Basin study documented in Chidsey (2007). Appendices provide the complete data compilations, maps, core photographs, and thin section descriptions, etc., either collected for or generated by the study. The Bulletin summarizes the research, data, analyses, and results of the study, thus providing the tools for future successful horizontal drilling programs to occur in the small reservoirs found in the Paradox Basin and other shallow-shelf carbonate deposits.
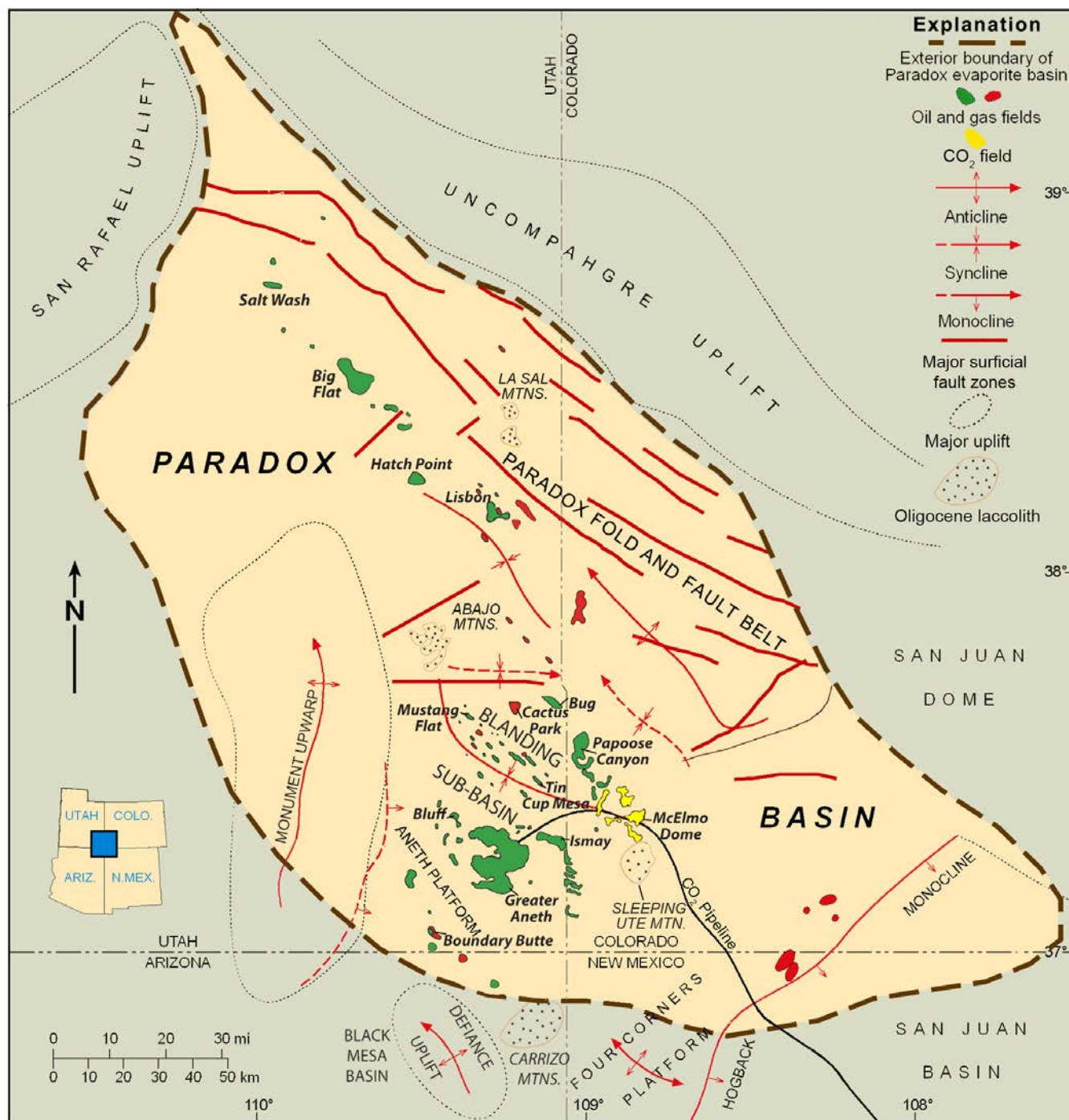
Figure 1.1. *Location map of the Paradox Basin, Utah, Colorado, Arizona, and New Mexico showing producing oil and gas fields, the Paradox fold and fault belt, and Blanding sub-basin as well as surrounding Laramide basins and uplifts. Modified from Kitcho (1981), Harr (1996), and Wood and Chidsey (2015).*

PARADOX BASIN OVERVIEW

Tectonic Setting

The Paradox Basin is located mainly in southeastern Utah and southwestern Colorado with small parts in northeastern Arizona and the northwestern corner of New Mexico (figure 1.1). The Paradox Basin is an elongate, northwest-southeast-trending, evaporitic basin that predominately de-veloped during the Pennsylvanian (Desmoinesian), about 330 to 310 million years ago (Ma). The most obvious struc-tural features in the basin are the spectacular anticlines that extend for miles in the northwesterly trending fold and fault belt. The events that caused these and many other structural features to form began in the Proterozoic, when movement initiated on high-angle basement faults and fractures 1700 to 1600 Ma (Stevenson and Baars, 1986, 1987). During Cambrian through Mississippian time, this region, as well
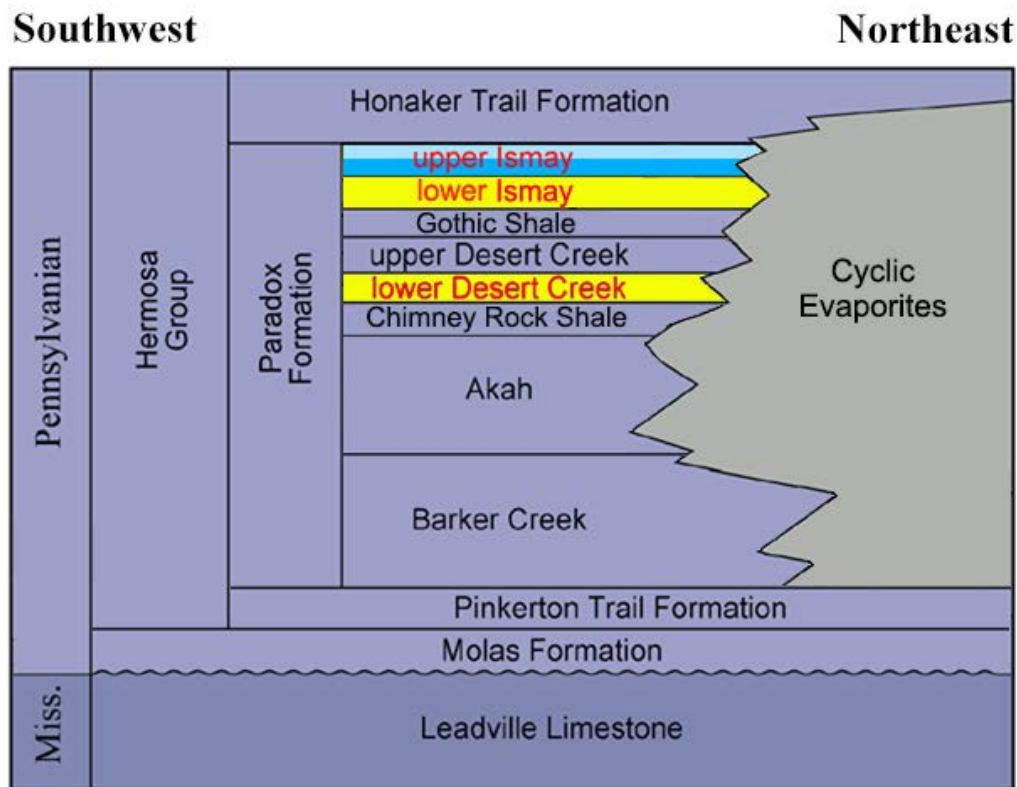
Figure 1.2. *Pennsylvanian stratigraphy of the southern Paradox Basin including informal zones of the Paradox Formation; the Desert Creek and Ismay zones productive in the case-study fields described in this study are highlighted. For the regional lithofacies evaluation the upper Ismay zone has been further divided into two units—the "upper part" and the "lower part."*

as most of eastern Utah, was the site of thin, marine de-position on the craton while thick deposits accumulated in the miogeocline to the west (Hintze and Kowallis, 2009). However, major changes began in the Pennsylvanian when a pattern of basins and fault-bounded uplifts developed from Utah to Oklahoma as a consequence of the collision of South America, Africa, and southeastern North America (Kluth and Coney, 1981; Kluth, 1986), or from a smaller scale collision of a microcontinent with south-central North America (Harry and Mickus, 1998). One result of this tectonic event was the uplift of the Ancestral Rockies in the western United States. The Uncompahgre Highlands (uplift) in eastern Utah and western Colorado initially formed as the westernmost range of the Ancestral Rockies during this ancient mountain-building period.

The Uncompahgre Highlands are bounded along their south-western flank by a large basement-involved, high-angle, re-verse fault identified from seismic surveys and exploration drilling (Frahme and Vaughn, 1983). As the highlands rose, an accompanying depression, or foreland basin, formed to the southwest—the Paradox Basin. The form of the Para-dox Basin was strongly influenced by rejuvenation of pre-existing (Late Precambrian), northwest-trending structures (Baars and Stevenson, 1981). Rapid basin subsidence, par-ticularly during the Pennsylvanian and continuing into the Permian, accommodated large volumes of evaporitic and marine sediments that intertongue with non-marine arkosic

material shed from the highland area to the northeast (figure 1.5) (Hintze and Kowallis, 2009). Deposition in the basin produced a thick cyclical sequence of carbonates, evapo-rites, and organic-rich shale (Peterson and Hite, 1969; Hite and others, 1984). The Paradox Basin is defined for the pur-poses of this study by the maximum extent of anhydrite beds in the Paradox Formation.

The present Paradox Basin includes or is surrounded by other uplifts that formed during the Late Cretaceous-early Tertia-ry Laramide orogeny, such as the Monument upwarp in the west-southwest, and the Uncompahgre uplift, corresponding to earlier Uncompahgre Highlands, forming the northeast boundary (figure 1.1). Oligocene-age laccolithic intrusions form the La Sal and Abajo Mountains in the north and central parts of the basin in Utah whereas the Carrizo Mountains in Arizona, and the Ute, La Plata, and San Miguel Mountains in Colorado were intruded along the southeastern boundary of the basin (figure 1.1).

The Paradox Basin can generally be divided into three areas: the Paradox fold and fault belt in the north, the Paradox fold and fault belt in the south-southwest, and the Aneth platform in the southernmost part in Utah (figure 1.1). The area now occupied by the Paradox fold and fault belt was also the site of greatest Pennsylvanian/Permian subsidence and salt deposi-tion. Folding in the Paradox fold and fault belt began as early as the Late Pennsylvanian as sediments were laid down thinly
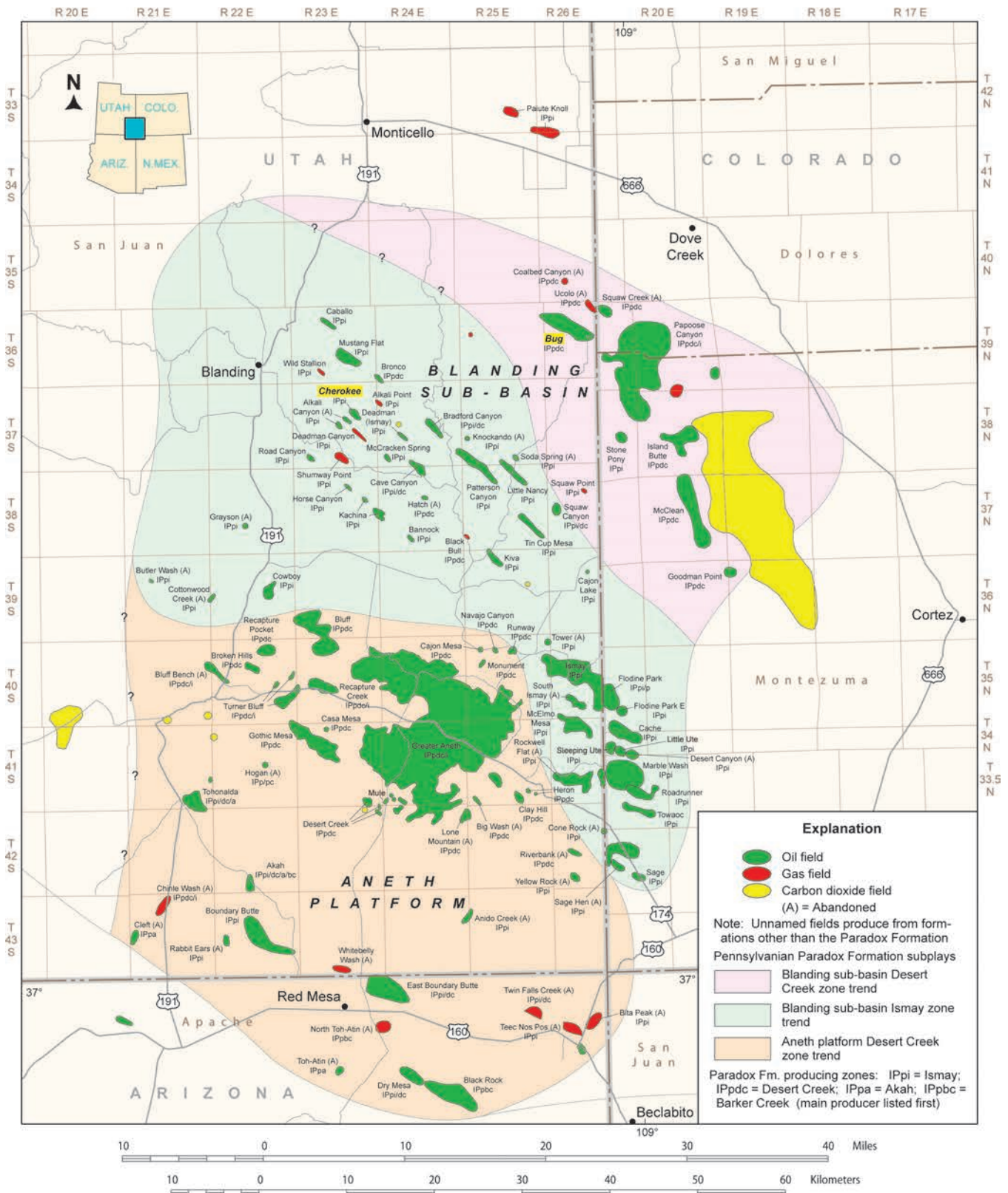
Figure 1.3. *The study area and fields (case-study fields highlighted in yellow) within the Desert Creek and Ismay producing trends in the Blanding sub-basin, Utah and Colorado. Fields shown in the Aneth platform area of the map, including the giant Greater Aneth field, produce primarily from the Desert Creek zone on the shelf margin of the Paradox Basin. Modified from Wray and others (2002) and Wood and Chidsey (2015).*
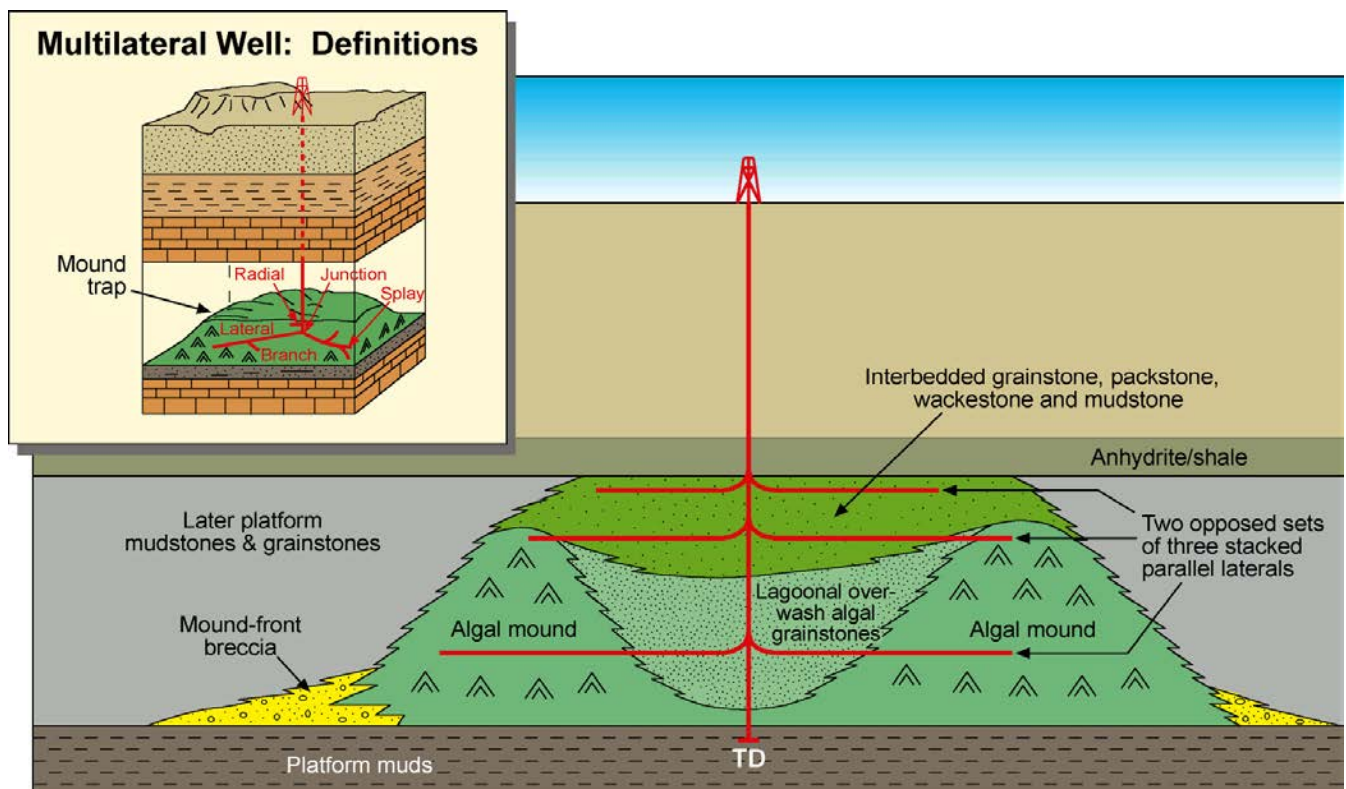
Figure 1.4. *Schematic diagram of Ismay zone drilling targets by multilateral (horizontal) legs from an existing field well. Inset modified from Chambers (1998).*

A.
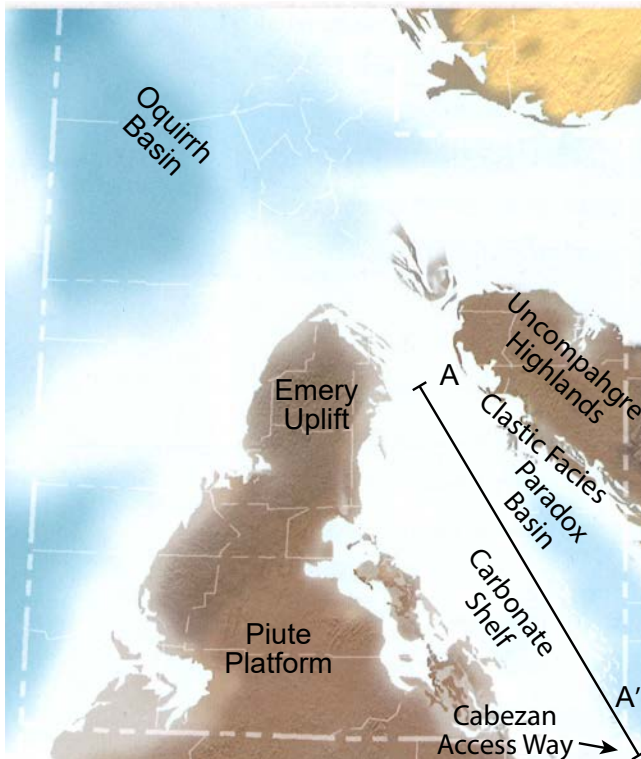
B.
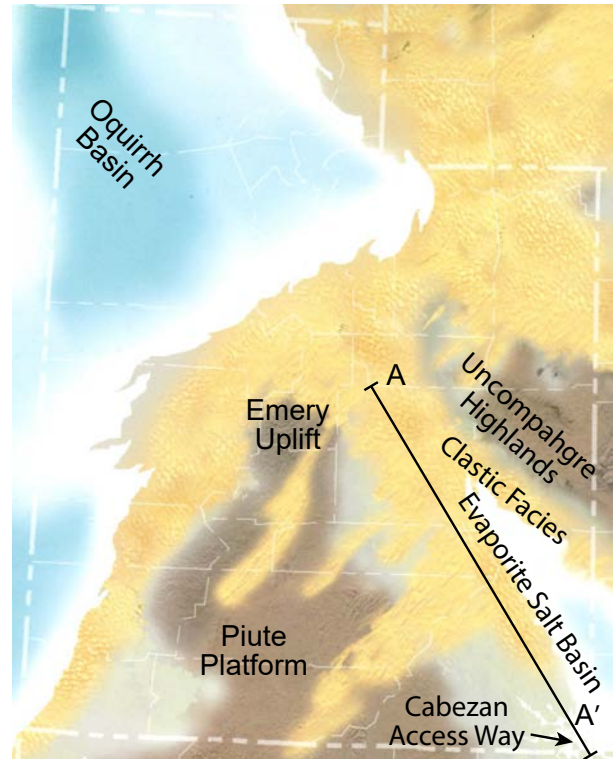
Figure 1.5. *Paleogeography of Utah during Middle (Desmoinesian) Pennsylvanian time. (A) High sea level having normal marine waters and deposition. (B) Low sea level having warm, restricted waters and evaporite deposition. Also indicated is the location of the clastic wedge, evaporite salt basin, and carbonate shelf during deposition of the Paradox Formation. Modified from Blakey and Ranney (2008). Cross section A–A' shown on figure 1.6.*

over areas of rising salt, and thickly in areas in between (Doelling, 2010). The Paradox fold and fault belt was created during the Late Cretaceous through Quaternary by a combination of (1) reactivation of basement normal faults, (2) additional salt flowage followed by dissolution and collapse, and (3) regional uplift (Doelling, 2010). The relatively undeformed Blanding sub-basin and Aneth platform developed on a subsiding shallow-marine shelf.

Paradox Formation

The Paradox Formation was deposited in Pennsylvanian (Desmoinesian) time in the rapidly subsiding northeast margin of the Paradox Basin and on a shallow-marine carbonate shelf on the south and southwest margins of the basin that locally contained algal-mound buildups (figures 1.5 and 1.6). The Paradox Basin during the Pennsylvanian was in subtropical, dry climatic conditions along the trade-wind belt, 10° to 20° north of the paleo-equator. Prevailing winds were from present-day north (Peterson and Hite, 1969; Heckel, 1977; Parrish, 1982). Warm, open-marine waters flowed across the shallow cratonic shelf into the basin during transgressive periods (figure 1.5A). Of the four postulated normal-

marine access ways into the Paradox Basin, the Cabezon access way, located to the southeast, is generally accepted as the most likely conduit for normal marine water to maintain circulation on the shallow shelf (Fetzner, 1960; Ohlen and McIntyre, 1965; Hite, 1970). Periodic decreased circulation in the basin resulted in deposition of thick salts (halite with minor thinner beds of potash and magnesium salts) and anhydrite (figure 1.5B). The deeper interior of the basin to the north and northeast is composed almost entirely of salt deposits and is referred to as the evaporite salt basin (figures 1.5 and 1.6).

Cyclicity in Paradox Formation deposition was primarily controlled by glacio-eustatic fluctuations (Goldhammer and others, 1994). The shape of the sea-level curve reflects rapid marine transgressions (rapid melting of ice caps) and slow, interrupted regression (slow ice cap buildup) (Imbrie and Imbrie, 1980; Denton and Hughes, 1983; Heckel, 1986). Irregular patterns within the transgressive-regressive cycles are thought to be a response to interference of orbital parameters (Imbrie and Imbrie, 1980). These cycles were also influenced by (1) regional tectonic activity and basin subsidence (Baars, 1966; Baars and Stevenson, 1982), (2) proximity to basin margin
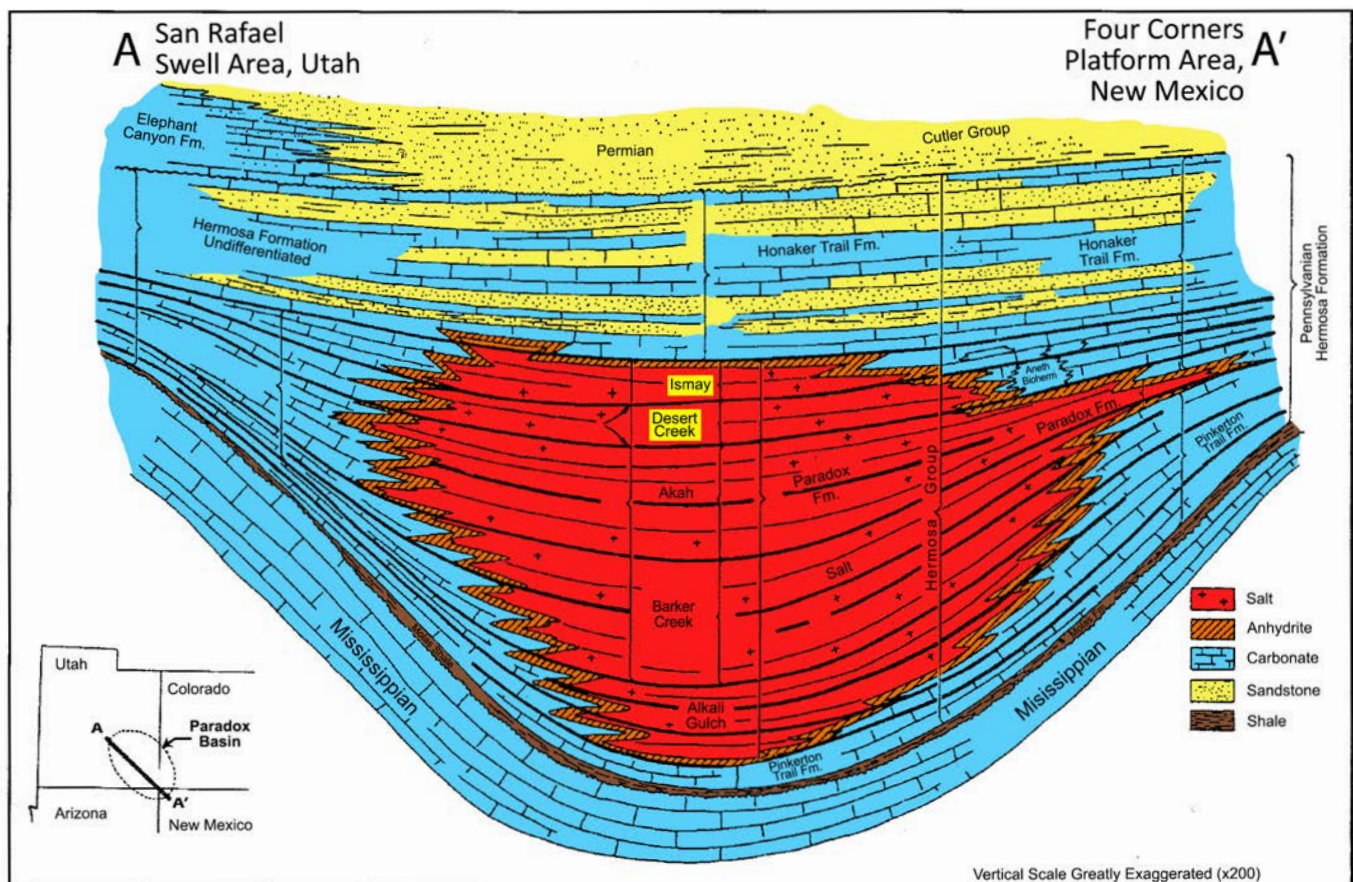
Figure 1.6. *Schematic cross section through the Paradox Basin with gross lithofacies relationships of Middle Pennsylvanian stratigraphy. Maximum extent of anhydrite beds in the Paradox Formation defines the basin. Note that the "salt" actually consists of cycles of interbedded dolomite, dolomitic siltstone, silty limestone, black organic-rich shale, and anhydrite; these cylces are overlain entirely by halite in the interior of the basin. Location of cross section shown on figure 1.5. Modified from Baars (1983) and Hintze and Kowallis (2009).*

and evaporites (Hite, 1960; Hite and Buckner, 1981), (3) climatic variation and episodic blockage of open-marine-water conduits, and (4) fluctuations in water depth and water energy (Peterson and Ohlen, 1963; Peterson, 1966; Hite and Buckner, 1981; Heckel, 1983).

Hydrocarbon Traps

The Paradox fold and fault belt, Blanding sub-basin, and the Aneth platform contain oil and gas fields with structural, stratigraphic, or combination traps formed on discrete, often seismically defined, closures. The sources of the petroleum are several black, organic-rich shales (the Gothic and Chimney Rock, for example, shown on figure 1.2) within the Paradox Formation (Hite and others, 1984; Nuccio and Condon, 1996). Most Paradox Formation hydrocarbon production comes from stratigraphic traps in the Blanding sub-basin and Aneth platform that locally contain algal-mound and other carbonate lithofacies buildups in the Desert Creek and Ismay zones of the Paradox Formation, whereas the fractured Cane Creek shale zone of the Paradox is the primary reservoir in the Paradox fold and fault belt.

The carbonate buildups and the material shed from their flanks in the Desert Creek and Ismay zones formed hydrocarbon traps where reservoir-quality porosity and permeability have developed. Those reservoirs and traps in the Blanding sub-basin are the focus of this study.

CHAPTER 2:
REGIONAL UTAH LITHOFACIES EVALUATION OF THE DESERT CREEK AND ISMAY ZONES, BLANDING SUB-BASIN

by

David E. Eby, Eby Petrography & Consulting, Inc.
and
Thomas C. Chidsey, Jr., and Craig D. Morgan (retired), Utah Geological Survey

CHAPTER 2:
REGIONAL UTAH LITHOFACIES EVALUATION OF THE DESERT CREEK AND ISMAY ZONES, BLANDING SUB-BASIN

INTRODUCTION

An understanding of the basic carbonate lithofacies belts and stratigraphic patterns within the shallow-shelf carbonate Ismay and Desert Creek zones of the Paradox Formation in the Blanding sub-basin is critical to determining the remaining hydrocarbon potential in the region. Geological characterization of lithofacies on a regional scale should focus on reservoir heterogeneity and lateral continuity. Therefore, the objectives of this chapter are to (1) describe lithofacies and depositional environments of the Ismay and Desert Creek zones, (2) map the regional distribution of Ismay and Desert Creek lithofacies, (3) identify reservoir trends for field extension drilling and stimulating exploration in Paradox Basin fairways, and (4) increase understanding of lateral and vertical lithofacies variations on both a regional and reservoir production scale.

We utilized representative cores and geophysical well logs to characterize and initially grade various intervals in the Utah part of the region for horizontal drilling suitability. Detailed examination of cores tied to geophysical well logs showed that the upper Ismay can be divided into two depositional sequences across the study area. We have termed these packages the "upper part" and "lower part" of the upper Ismay (figure 1.2). The top of the lower part is commonly truncated by an erosional or exposure surface.

METHODS AND LOG-BASED CORRELATION SCHEME

The study area covers about 750 square miles (1900 km^2) within the Blanding sub-basin of the Paradox Basin. About 480 wells penetrated the Paradox Formation within the study area. We interpreted all available cores in the area—41 wells in the upper part of the upper Ismay, 40 wells in the lower part of the upper Ismay, and 44 wells in the lower Desert Creek (figure 2.1). Additionally, 82 geophysical well logs were interpreted from the upper Ismay and 38 from the Desert Creek (figure 2.1). We also incorporated the work of Roylance (1984, 1990), Cannizzaro (1985), and Skinner (1996).

A grid of regional geophysical well-log cross sections (figure 2.2; appendix A), thickness relationships of important stratigraphic intervals (figure 1.2), and lithofacies types were combined with examination of cores throughout the Bland-

ing sub-basin to provide a significant database for identifying potential targets for horizontal drilling within the small, heterogeneous, phylloid-algal buildups and associated lithofacies in the upper Ismay and lower Desert Creek zones. The regional cross sections, isochore and structure maps, and regional lithofacies maps (appendices A, B, and C) were constructed using a correlation scheme developed for the study. This correlation scheme tied the typical core-derived, vertical sequence or cycle of depositional lithofacies from the Cherokee and Bug case-study fields (figure 1.3) (described later) to the corresponding gamma-ray and neutron-density curves from geophysical well logs. The correlation scheme identified the major zone contacts, seals or barriers, baffles, producing or potential reservoirs, and depositional lithofacies (figures 2.3 through 2.5, and table 2.1).

Depositionally, rock units are divided into seals or barriers (anhydrites and shales), mound or carbonate buildups (bafflestones, bindstones, grainstones, and packstones), and off-mound lithofacies (mudstones and wackestones). Porosity intervals, and reservoir or potential reservoir layers, are identified within the mound and off-mound intervals. The mound, and some of the off-mound units, are designated as "clean carbonate" lithofacies (see cross sections in appendix A)—intervals containing all of the productive reservoir lithofacies, and where carbonate mudstone and shale are generally absent. The clean carbonate lithofacies abruptly change laterally into thick anhydrite intervals, particularly in the upper Ismay zone where the uppermost is designated as the "upper Ismay anhydrite" and the lower as the "upper Ismay anhydrite 2" (see cross sections in appendix A) (Chidsey and Eby, 2009).

The tops and bases of all these lithofacies (seals, mound, clean carbonate, as well as porosity units) were determined and coded as listed in table 2.1. The unlisted intervening units represent the baffles or non-reservoir rocks, such as non-porous packstone or wackestone (figures 2.3 through 2.5; appendix A). The mound/mound cap intervals usually have porosity greater than 6%, whereas the clean carbonate intervals are defined by lithology only (such as bafflestone or grainstone), although they may contain isolated porosity zones. The top and base of the mound/mound cap intervals are often equivalent to the top and base of the clean carbonate intervals. In addition, the top and base of the mound/mound cap intervals may be equivalent to the top and base of the thinner off-mound clean carbonate intervals (Chidsey and Eby, 2009).
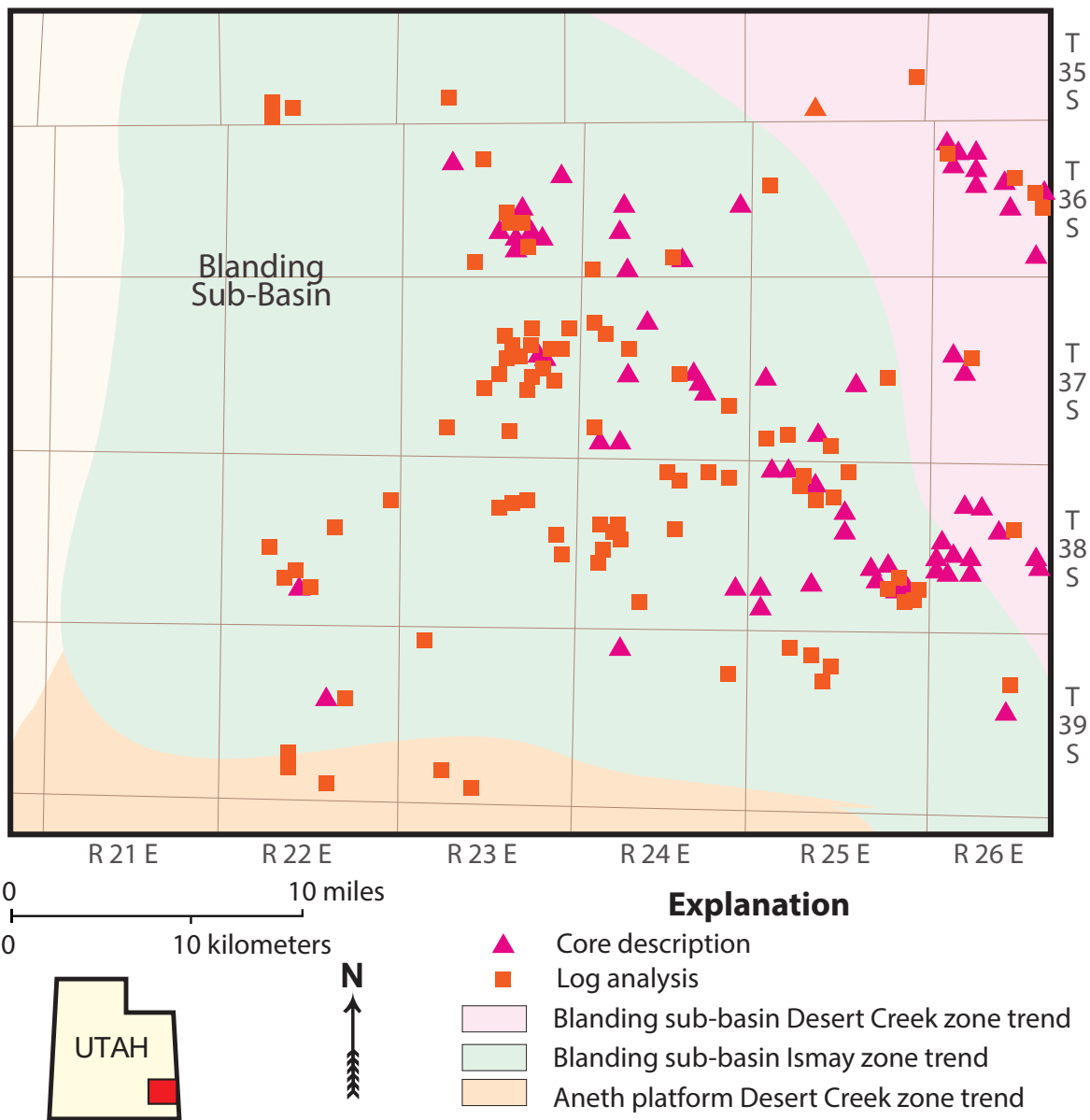
Figure 2.1. *The study area and wells with cores or used for log analysis of the Ismay and Desert Creek producing trends in the Blanding sub-basin, Utah.*

REGIONAL LITHOFACIES TRENDS IN THE UPPER ISMAY AND LOWER DESERT CREEK ZONES OF THE UTAH PART OF THE BLANDING SUB-BASIN

We identified eight major lithofacies based on analysis of cores from the Desert Creek and Ismay zones: lithofacies 1 – open marine, lithofacies 2 – middle shelf, lithofacies 3 – inner shelf/tidal flat, lithofacies 4 – bryozoan mound, lithofacies 5 – proto-mound, lithofacies 6 – phylloid-algal mound, lithofacies 7 – quartz sand dune, and lithofacies 8 – anhydrite salina. Lithofacies 1, 2, and 6 are found in both the Desert Creek and Ismay. Lithofacies 3, 4, 7, and 8 occur only in the Ismay, whereas lithofacies 5 is only in the Desert Creek. The lithofacies or groups of lithofacies in the Desert Creek and Ismay zones represent specific depositional environments, which can be mapped regionally.

Lithology

Lithofacies 1 – Open Marine

Open-marine lithofacies are found in both the Ismay and Desert Creek zones of the Blanding sub-basin (figures 2.6 and 2.7). Rock representing this lithofacies consists of lime mudstone containing well-preserved rugose corals, crinoids, brachiopods, bryozoans, articulated thin-shelled bivalves, and benthic foraminifera indicative of normal-marine salinities and low-energy conditions. Rock units of this lithofacies have very little effective porosity and permeability, and act as barriers and baffles to fluid flow.
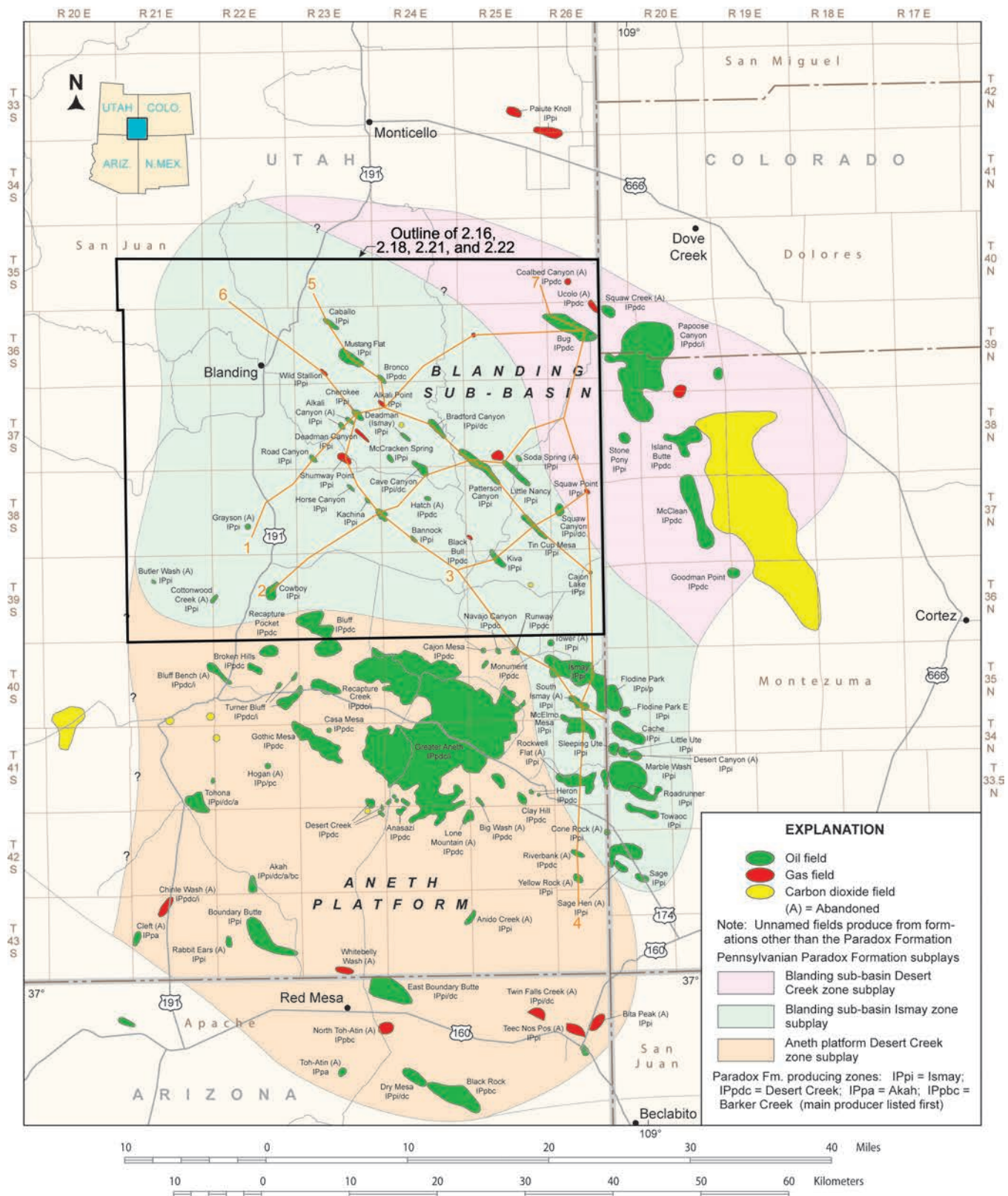
Figure 2.2. *The study area and fields within the Ismay and Desert Creek producing trends in the Blanding sub-basin, Utah and Colorado (numbered lines indicate locations of cross sections generated in this study and included in appendix A). Modified from Wray and others (2002) and Wood and Chidsey (2015).*
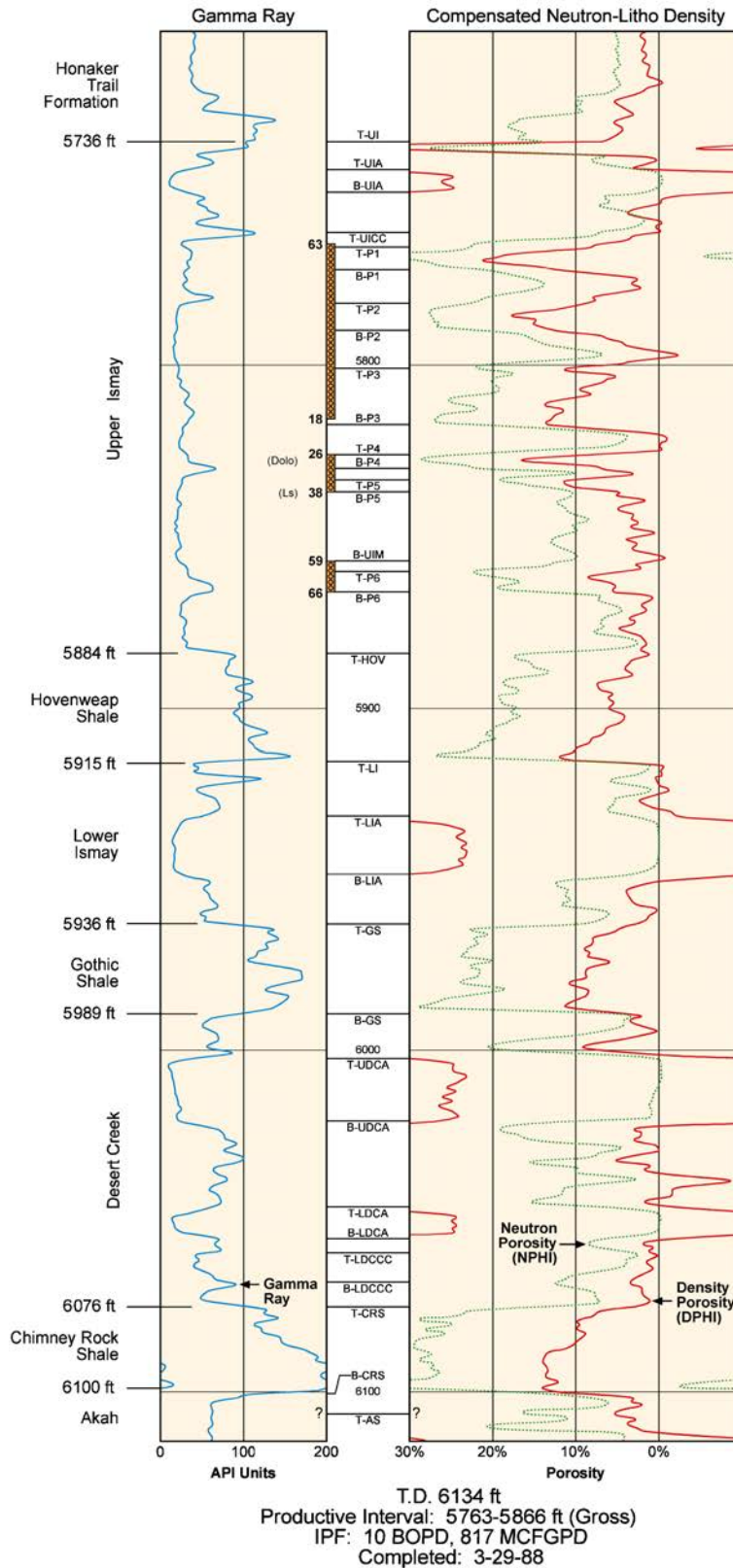
Figure 2.3. *Type log for the Cherokee field (gamma-ray, compensated neutron-litho density) from the Cherokee Federal No. 22-14 well (section 14, T. 37 S., R. 23 E., SLBL&M, San Juan County, Utah), showing the Ismay and Desert Creek correlation scheme, major units, and productive intervals (refer to table 2.1 for explanation of unit abbreviations).*
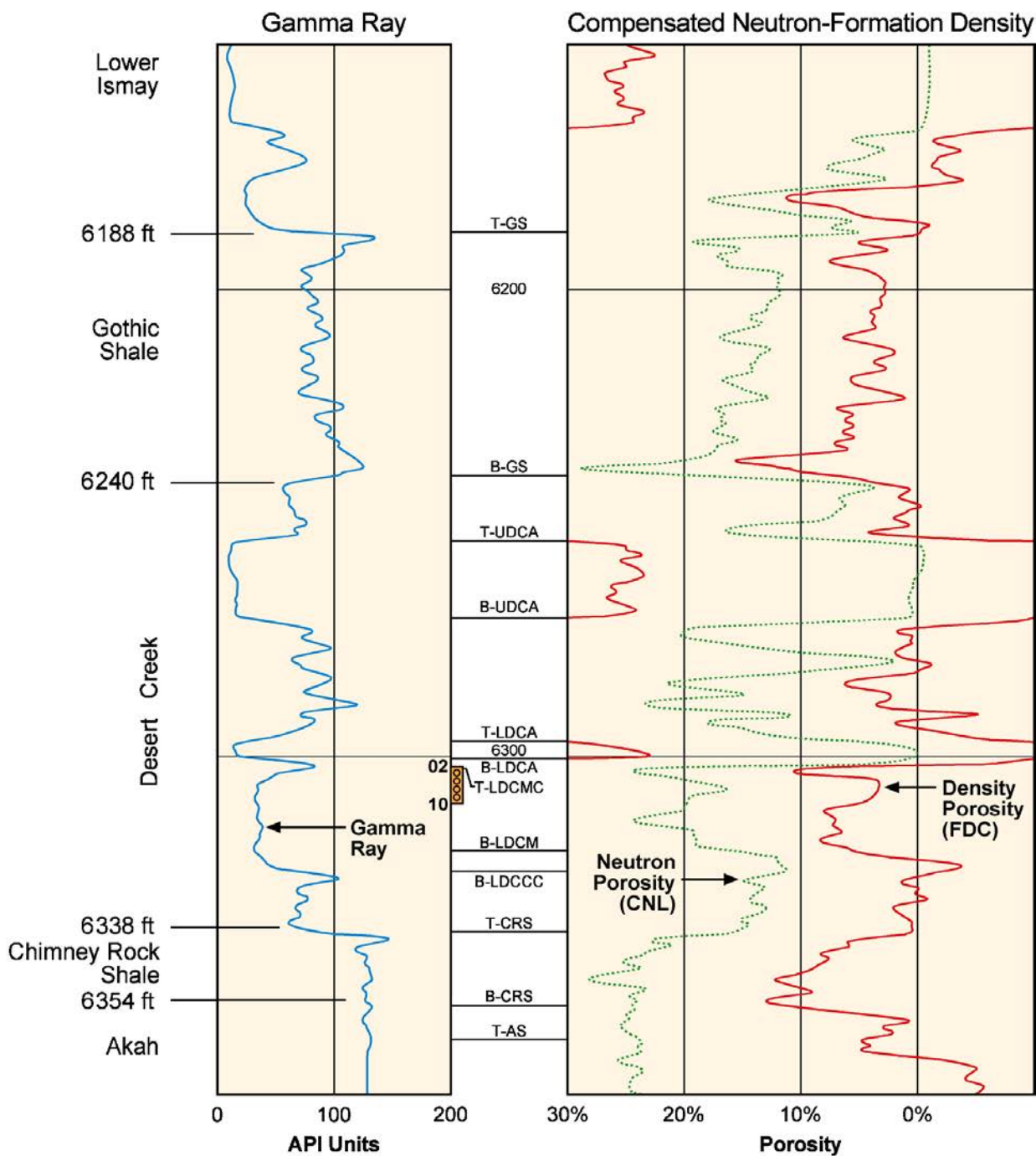
Figure 2.4. *Type log for the Bug field mound (gamma-ray, compensated neutron-formation density) from the Bug No. 16 well (section 17, T. 36 S., R. 26 E., SLBL&M, San Juan County, Utah), showing the Desert Creek correlation scheme, major units, and productive interval (refer to table 2.1 for explanation of unit abbreviations).*
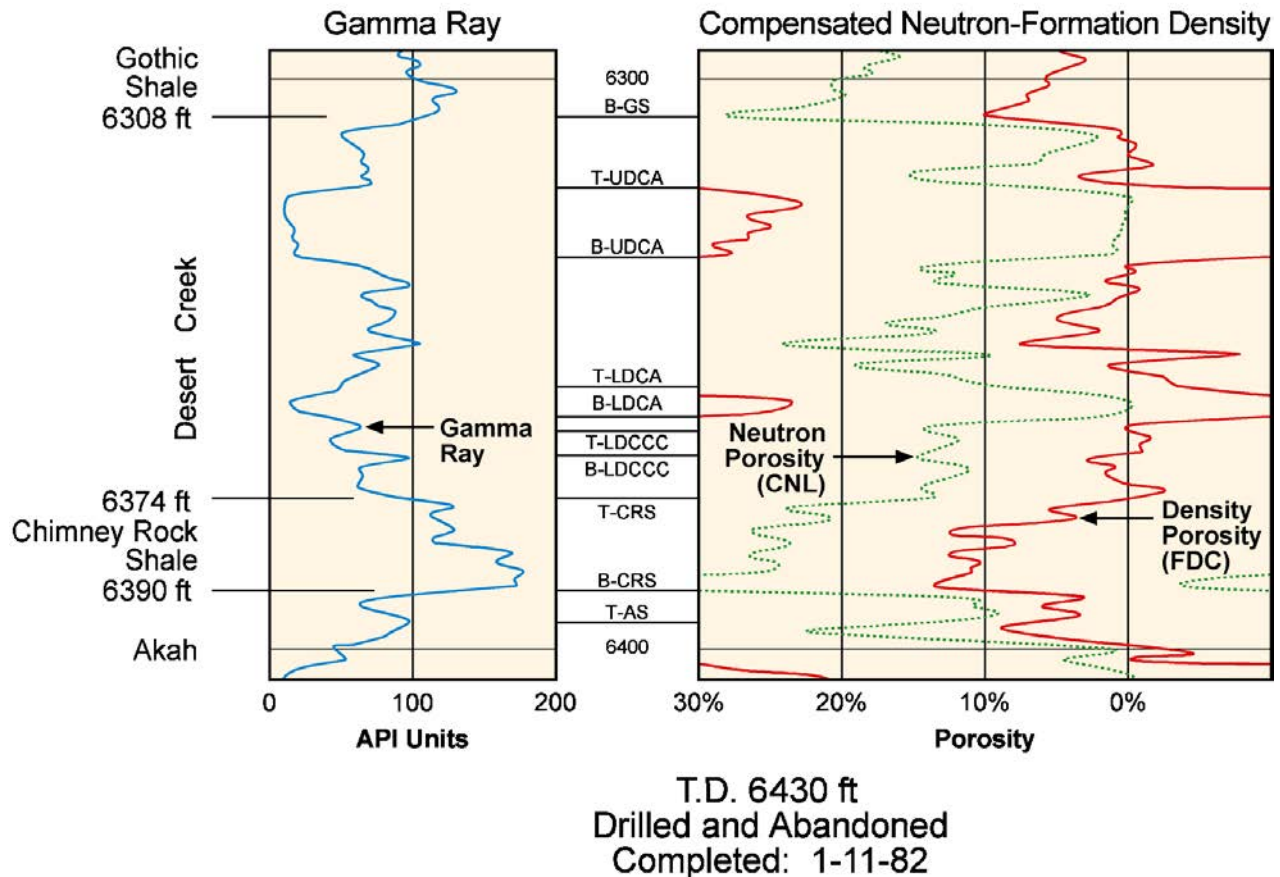
Figure 2.5. Type log for the Bug field off-mound area (gamma-ray, compensated neutron-formation density) from the Bug No. 7-A well (section 7, T. 36 S., R. 26 E., SLBL&M, San Juan County, Utah), showing the Desert Creek correlation scheme and major units (refer to table 2.1 for explanation of unit abbreviations).

Lithofacies 2 – Middle Shelf

Middle-shelf lithofacies are also found in both the Ismay and Desert Creek zones (figure 2.8). The most common depositional fabrics of this lithofacies are bioturbated lime to dolomitic mudstone with ubiquitous sub-horizontal feeding burrows and fossiliferous peloidal wackestone or packstone. There are few megafossils and little visible matrix porosity. However, some fusulinid-rich lime wackestones to packstones are present in very tight, biogenically graded limestone.

Lithofacies 3 – Inner Shelf/Tidal Flat

Inner shelf/tidal flat lithofacies are found in the upper Ismay zone as dolomitized packstone and grainstone (figure 2.9). Clotted, lumpy, and poorly laminated microbial structures resembling small thrombolites and intraclasts are common.

Megafossils and visible porosity are very rare in the inner shelf/tidal flat setting. Non-skeletal grainstone (calcarenite) composed of ooids, coated grains, and "hard peloids" occurs as high-energy deposits in some inner shelf/tidal flat settings. Remnants of interparticle and moldic pores may be present in this lithofacies.

Lithofacies 4 – Bryozoan Mound

Bryozoan mound lithofacies are found in the upper Ismay zone as mesh-like networks of tubular and sheet-type (fenestrate) bryozoans (figure 2.10). These bryozoans provide the binding and baffling agents for lime mud-rich mounds. Crinoids and other open-marine fossils are common. Large, tubular bryozoans and marine cements are also common in areas of high-energy, and possibly shallow water. Porosity is mostly confined to preserved intraparticle spaces.

Table 2.1. *Correlation scheme used for Desert Creek and Ismay zones of the Paradox Formation in Bug and Cherokee fields, Blanding sub-basin, Utah.*

Unit Code	Description
T-UI	Top – Upper Ismay Zone
T-UIA	Top – Upper Ismay Anhydrite
B-UIA	Base – Upper Ismay Anhydrite
T-UIA2	Top – Upper Ismay Anhydrite 2
B-UIA2	Base – Upper Ismay Anhydrite 2
T-UICC	Top – Upper Ismay Clean Carbonate
T-P1	Top – Porosity Unit #1
B-P1	Base – Porosity Unit #1
T-P2	Top – Porosity Unit #2
B-P2	Base – Porosity Unit #2
T-P3	Top – Porosity Unit #3
B-P3	Base – Porosity Unit #3
T-P4	Top – Porosity Unit #4
B-P4	Base – Porosity Unit #4
T-P5	Top – Porosity Unit #5
B-P5	Base – Porosity Unit #5
B-UIM	Base – Upper Ismay Mound
B-UICC	Base – Upper Ismay Clean Carbonate
T-P6	Top – Porosity Unit #6
B-P6	Base – Porosity Unit #6
T-HOV	Top – Hovenweap Shale
T-LI	Top – Lower Ismay Zone
T-LIA	Top – Lower Ismay Anhydrite
B-LIA	Base – Lower Ismay Anhydrite
T-GS	Top – Gothic Shale
B-GS	Base – Gothic Shale
T-UDCA	Top – Upper Desert Creek Anhydrite
B-UDCA	Base – Upper Desert Creek Anhydrite
T-LDCA	Top – Lower Desert Creek Anhydrite
B-LDCA	Base – Lower Desert Creek Anhydrite
T-LDCMC	Top – Lower Desert Creek Mound Cap
B-LDCM	Base – Lower Desert Creek Mound
T-LDCCC	Top – Lower Desert Creek Clean Carbonate
B-LDCCC	Base – Lower Desert Creek Clean Carbonate
T-CRS	Top – Chimney Rock Shale
B-CRS	Base – Chimney Rock Shale
T-AS	Top – Akah Salt

A.
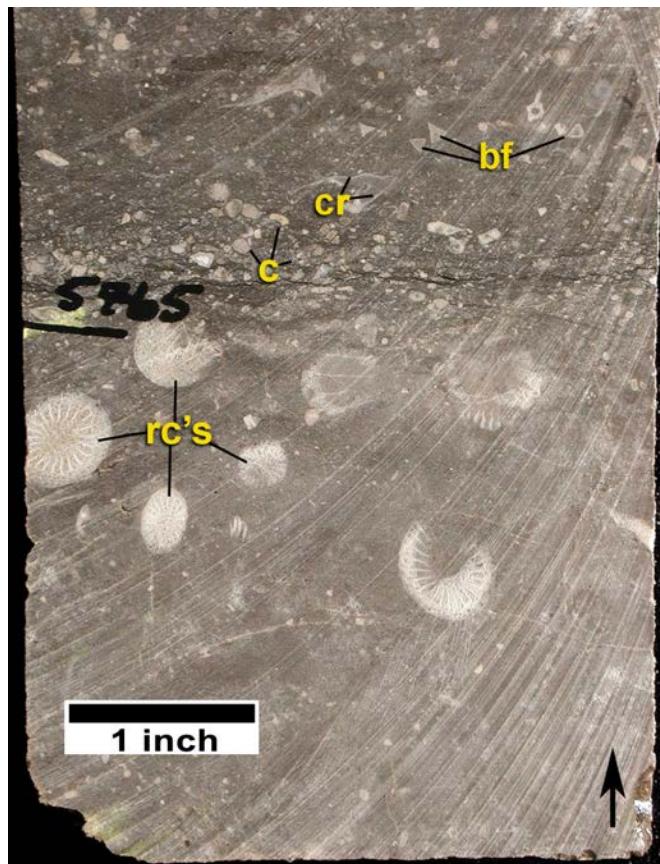
B.
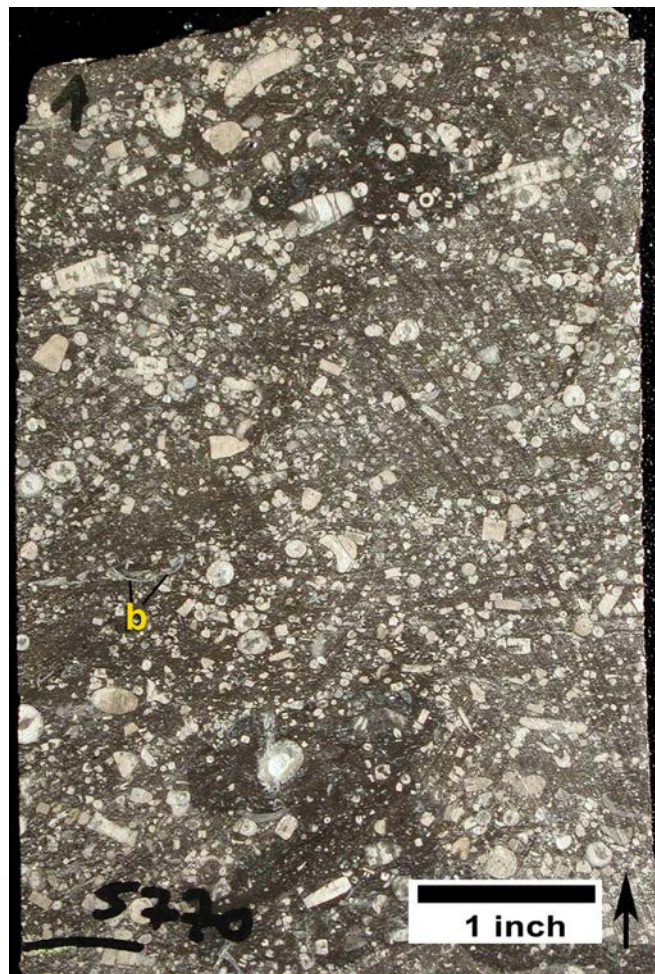
Figure 2.6. *Typical upper Ismay open-marine lithofacies from the Cuthair No. 1-28 well (section 28, T. 38 S., R. 22 E., SLBL&M, San Juan County, Utah). (A) Well-preserved rugose corals (rc), crinoids (c), brachiopods (br), and benthic forams (bf); slabbed core from 5765 feet (1757 m). (B) Well-preserved, partially articulated crinoid stems and parts, as well as articulated thin-shelled bivalves (b); slabbed core from 5770 feet (1759 m).*

Lithofacies 5 – Proto-Mound

Proto-mound lithofacies in the lower Desert Creek zone contain dolomitized and brecciated algal plates, abundant marine cements, and internal sediments suggesting subaerial exposure (figure 2.11). They are usually near or underlie phylloid-algal mound lithofacies, but generally lack any significant porosity.

Lithofacies 6 – Phylloid-Algal Mound

Phylloid-algal mound lithofacies are found in both the Ismay and Desert Creek zones (figures 2.12). This lithofacies contains the dominant petroleum-producing reservoirs in the Paradox Formation. Large phylloid-algal plates of *Ivanovia* (the dominant genus in the upper Ismay zone) and skeletal grains create bafflestone or bindstone fabrics. In mound interiors, algal plates are commonly found in near-growth positions surrounded by lime mud (figure 2.12A). On the high-energy

margins of algal mounds, algal plates and skeletal grains serve as substrates for substantial amounts of botryoids and other early-marine cements, and internal sediments (figure 2.12B). Lower Desert Creek mounds are dolomitized, contain plates of the genus *Kansasphyllum* (figure 2.12C), and show evidence of subaerial exposure (breccia or beach rock). Pore types include primary shelter pores preserved between phylloid-algal plates, secondary moldic pores, and open early fractures.

Lithofacies 7 – Quartz Sand Dune

Quartz sand dune lithofacies are found in the Ismay zone as very fine grained, well-sorted quartzose sandstone that displays moderate- to high-angle cross-bedding (figure 2.13). The well-rounded nature of the individual quartz sand grains (visible in thin sections) is consistent with a possible eolian origin for these nearshore dunes. This lithofacies does not display any preserved porosity due to the very fine grained, well-cemented and compacted nature of the rocks.

Lithofacies 8 – Anhydrite Salina

Anhydrite salina lithofacies are found within locally thick accumulations in upper Ismay (upper and lower parts) intra-shelf basins, described later. Anhydrite growth forms include nodular-mosaic ("chicken-wire"), palmate, and banded anhydrite (figure 2.14). Large palmate crystals probably grew in a gypsum aggregate indicative of subaqueous deposition. Detrital and chemical evaporites (anhydrite) filled in the relief around palmate structures. Thin, banded couplets of pure anhydrite and dolomitic anhydrite are products of very regular chemical changes in the
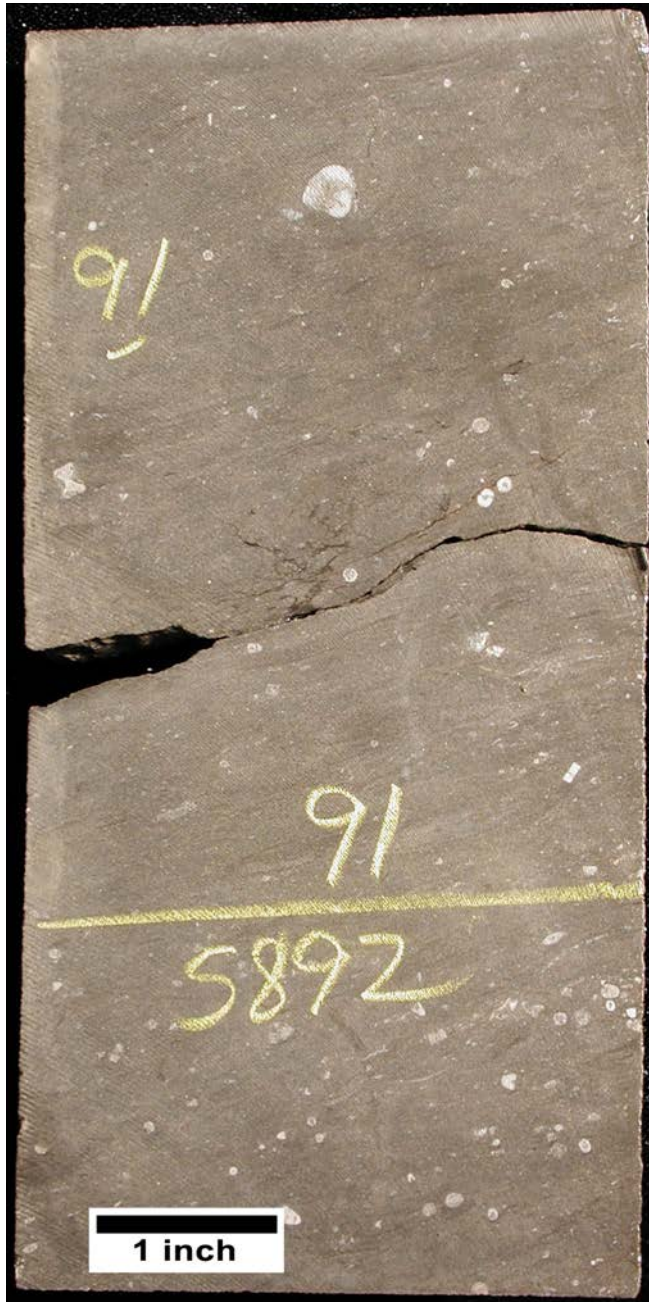
Figure 2.7. *Typical lower Desert Creek open-marine lithofacies from the Scorpion No. 1 well (section 34, T. 36 S., R. 24 E., SLBL&M, San Juan County, Utah) containing dolomitized lime mud, and rugose corals and crinoids; slabbed core from 5892 feet (1796 m).*

evaporite intra-shelf basins. These varve-like couplets are probably indicative of relatively "deep-water" evaporite precipitation. The salinas were probably isolated during relative lowstand sea-level conditions.

Depositional Environments

Depositional environments of the Ismay and Desert Creek zones were determined based on the core descriptions and the lithofacies we identified. These environments are shown schematically on figure 2.15. Reservoirs within the Utah part of the upper Ismay zone of the Paradox Formation are dominantly limestone composed of small, phylloid-algal buildups; locally variable, inner-shelf, skeletal calcarenites; and rarely, open-marine, bryozoan mounds (figure 2.15A). The Desert Creek zone is dominantly dolomite, comprising regional, nearshore, shoreline trends with highly aligned, linear lithofacies tracts (figure 2.15B).

The controls on the development of each depositional environment were water depth, salinity, prevailing wave energy, and paleostructural position. In the upper Ismay zone, the following depositional environments are recognized: open-marine shelf, organic (carbonate) buildups and calcarenites at the edges of small platforms; middle shelf or open platform interior; quartz sand dune; anhydritic salinas; and restricted inner shelf or platform interior. In the lower Desert Creek zone, the following depositional environments are recognized: basinal, open marine calcarenites (carbonate islands); middle shelf or open platform interior; restricted inner shelf or platform interior; platform interior salinas (evaporites); and shoreline to terrestrial (Chidsey and Eby, 2009).

The basinal environment represents sediments deposited in reasonably deep water (we estimate 90 to 120 feet [30–40 m]) and euxinic conditions. Deposition included (1) black to dark gray, non-calcareous, non-fossiliferous mud and silty mud, (2) spiculitic lime mud, (3) pelagic lime mud with microfossils and a few thin-shelled bivalves such as *Halobia*, and (4) deep-water siliciclastic sands.

The open-marine deposition was below wave base under normal-marine salinities, low-energy conditions, and below the photic zone. Deposition consisted of argillaceous and limy mud containing crinoids, brachiopods, and byrozoans.

The middle shelf or open platform interior represents sediments deposited in a well-circulated, low- to moderate-energy, normal salinity, shallow-water (we estimate between 0 and 90 feet [0–30 m]) environment. Lithofacies from this environment form the dominant producing reservoirs in the Ismay and Desert Creek zones across the Blanding sub-basin. Benthic forams, bivalve molluscs, and codiacean green algae (*Ivanovia* and *Kansasphyllum*) are common. Bryozoan mounds developed in the relatively quiet, deeper water of the middle shelf. Echinoderms are rare and open-marine cephalopods are

A.

B.
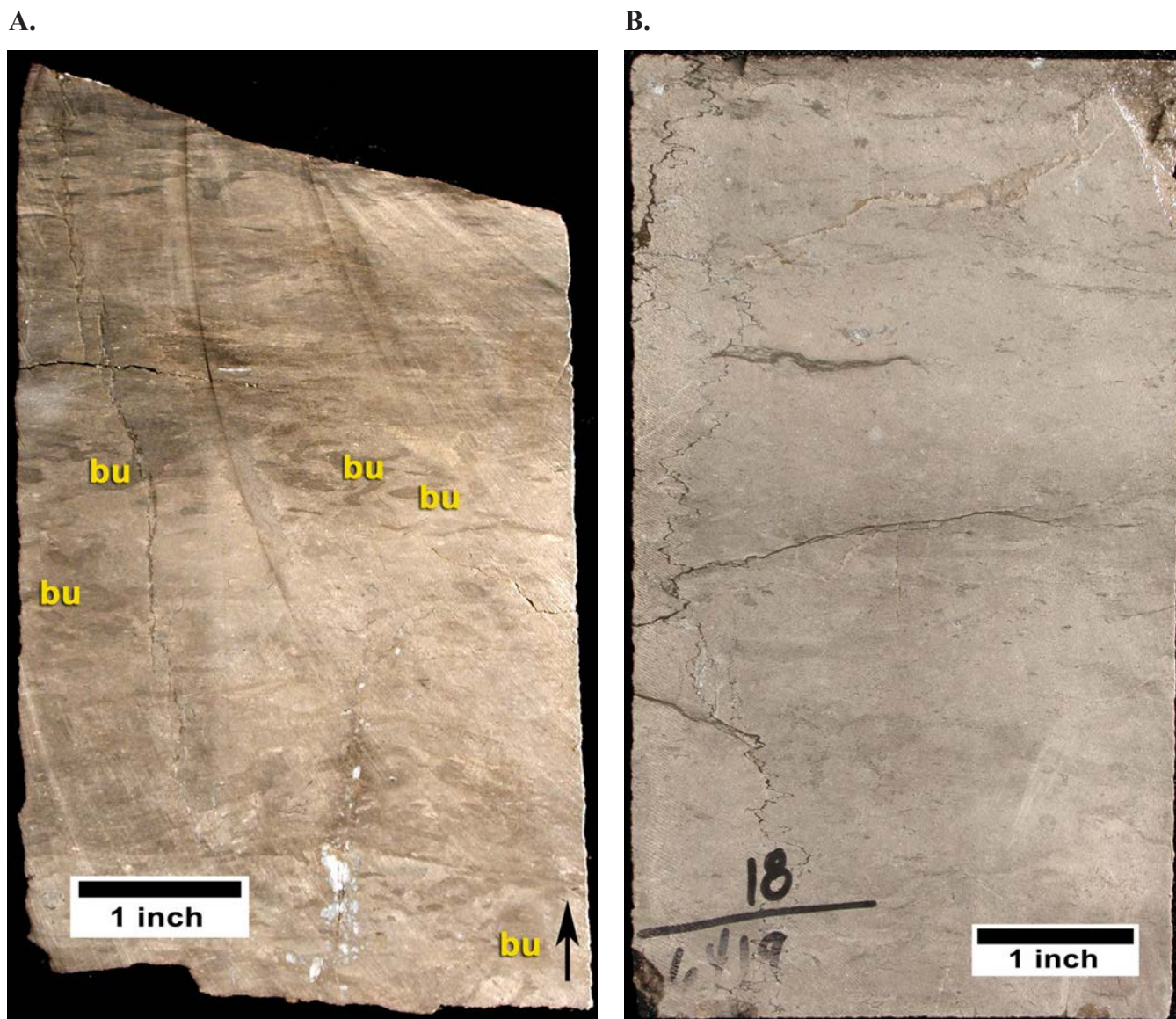
Figure 2.8. *Typical middle-shelf lithofacies. **(A)** Upper Ismay bioturbated lime mudstone containing compacted sub-horizontal feeding burrows (bu); Tank Canyon No. 1-9 well, section 9, T. 37 S., R. 24 E., SLBL&M, San Juan County, Utah, slabbed core from 5412.5 feet (1649.7 m). **(B)** Lower Desert Creek burrowed dolomitic mudstone; Ucolo No. 1-32 well, section 32, T. 35 S., R. 26 E., SLBL&M, San Juan County, Utah, slabbed core from 6418.7 feet (1956.4 m).*

generally absent. The principal buildup process, phylloid-algal growth, occurred during sea-level highstands. Paleotopography from Mississippian-age normal faulting (reactivation of Precambrian faults [Baars, 1966; Baars and Stevenson, 1982]) may have produced the best bathymetric conditions for initial phylloid-algal growth. Isolated dunes, composed of quartz sand, were deposited on the middle shelf of the upper Ismay zone during sea level lowstands with probable subaerial exposure and eolian conditions, although the source of the sand is uncertain.

Calcarenites are recognized in both the upper Ismay and lower Desert Creek zones and represent moderate- to high-energy, regularly agitated, marine environments where shoals and/or islands developed. Sediment deposition and modification probably occurred from 5 feet (1.5 m) above sea level to 50

feet (15 m) below sea level by our estimation. These deposits include (1) oolitic and coated-grain sands, (2) crinoid, foram, algal, and fusilinid sands, (3) small, benthic-foram and hard-peloid sands representing stabilized peloid-grain flats, and (4) shoreline carbonate islands of shell hash.

The restricted inner shelf or platform interior represents sediments deposited in shallow water (we estimate 0 to approximately 45 feet [0–14 m]), and generally in low-energy and poor circulation conditions. Fauna are limited mainly to stromatolitic algae and microbial forms, gastropods, certain benthic forams, and ostracods. Deposits include (1) bioclastic lagoonal to bay lime mud, (2) tidal-flat muds often with early dolomite, and (3) shoreline carbonate islands with birdseye fenestrae, stromatolites, cryptoalgal laminations, and dolomitic crusts. Platform-interior evaporites, now usually anhydrite,

A.   **B.**
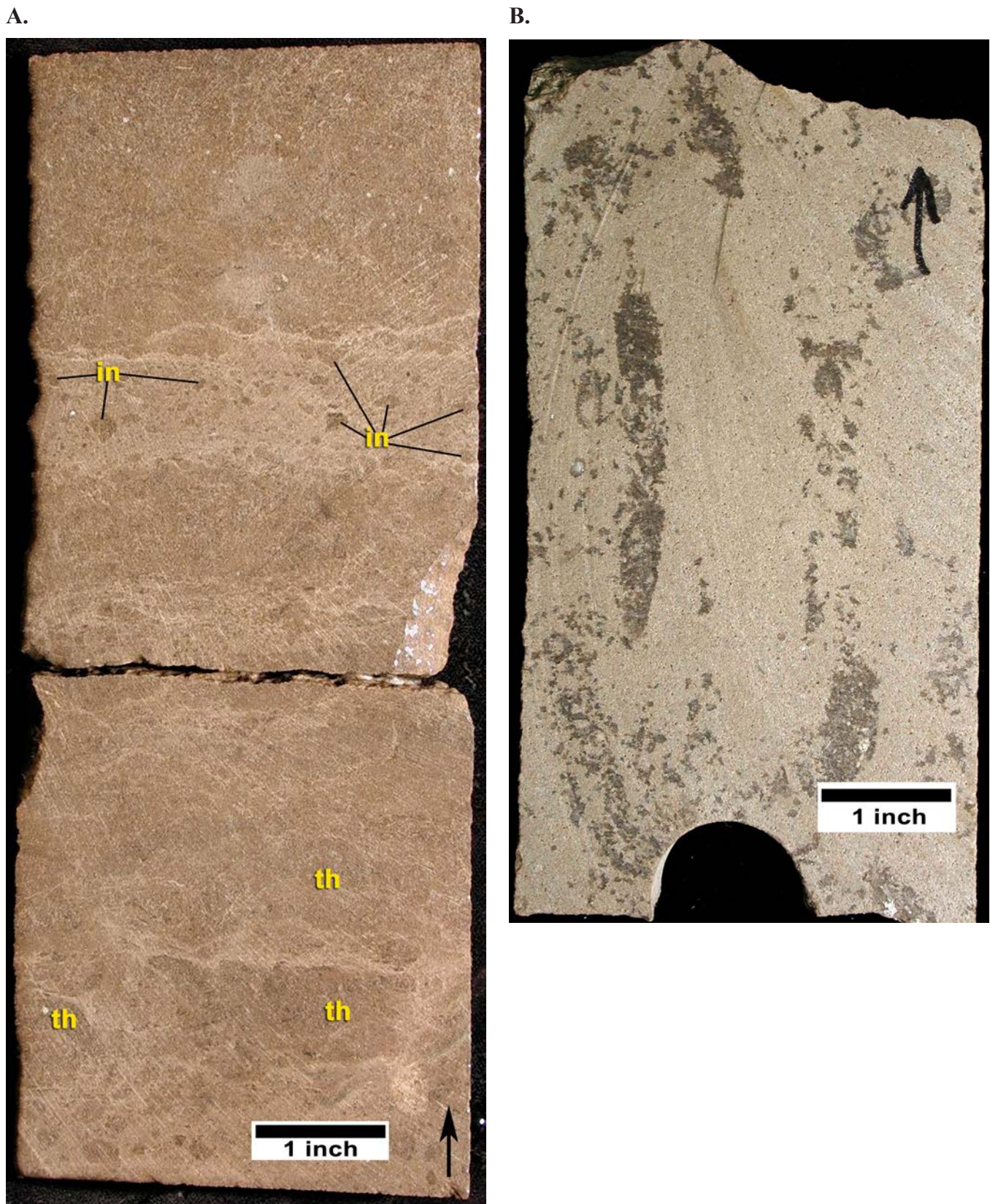
Figure 2.9. *Typical upper Ismay inner shelf/tidal flat lithofacies. (A) Dolomitized lumpy microbial structures resembling small thrombolites (th) and intraclasts (in) composed of desiccated and redeposited thrombolitic fragments; Tin Cup Mesa No. 2-23 well, section 23, T. 38 S., R. 25 E., SLBL&M, San Juan County, Utah, slabbed core from 5460.5 feet (1664.4 m). (B) Non-skeletal grainstone composed of ooids, coated grains, and peloids, with dark gray patches and columns composed of anhydrite-cemented sediments; Patterson No. 5 well, section 4, T. 38 S., R. 25 E., SLBL&M, San Juan County, Utah, slabbed core from 5443.5 feet (1659.2 m).*
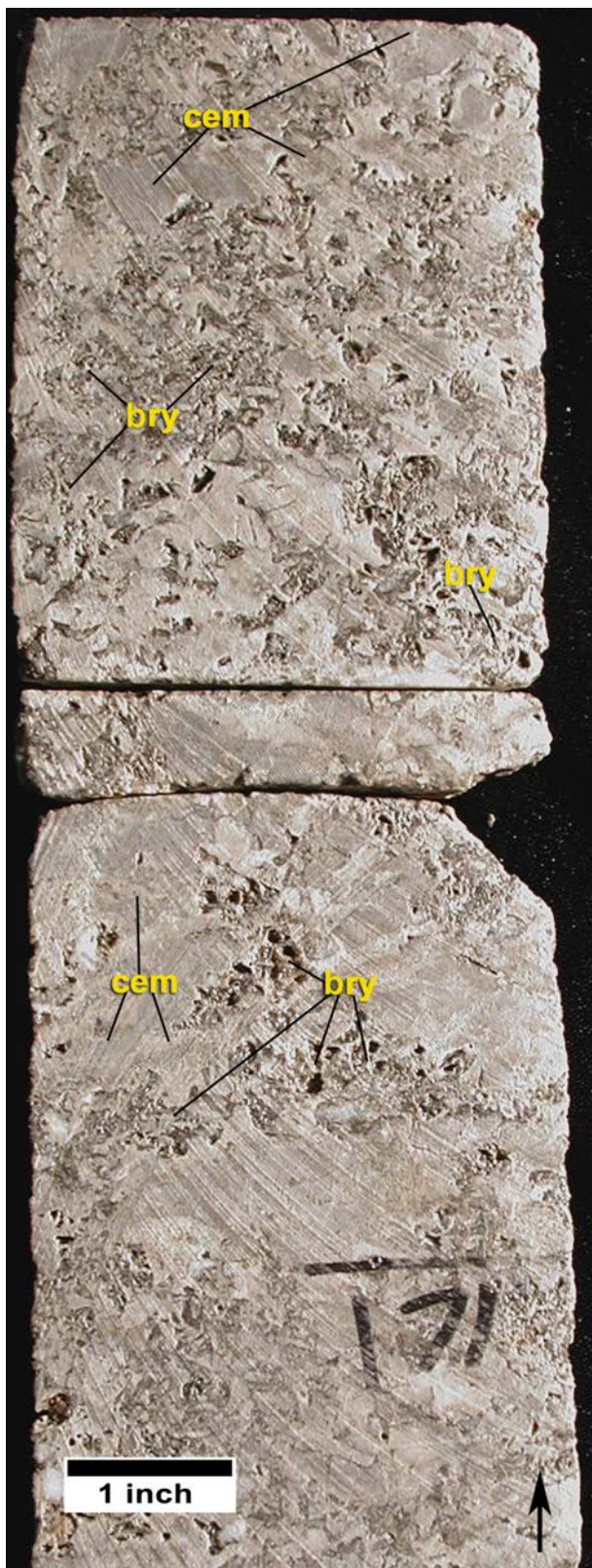
Figure 2.10. *Typical upper Ismay bryozoan-mound lithofacies from the Mustang No. 3 well (section 26, T. 36 S., R. 25 E., SLBL&M, San Juan County, Utah, slabbed core from 6171 feet [1881 m]) containing large tubular bryozoans (bry) and "lumps" of marine cement (cem). Sparse phylloid-algal plates are also present. This mound fabric is typical of higher energy, and possibly shallower water than the mud-dominated fabrics.*

were deposited in restricted areas with high salinity. These areas may have been topographic lows adjacent to phylloid-algal buildups.

Shoreline and terrestrial siliciclastic deposits represent beach, fluvial, and floodplain environments. These siliciclastic deposits include argillaceous to dolomitic silt with rip-up clasts, scour surfaces, or mudcracks.

Many carbonate buildups appear to have developed on subtle anticlinal noses or structural closures. These structures may represent paleobathymetric highs formed by pre-Pennsylvanian reactivation of basement faults, underlying salt structures, or simply longshore current-formed mudbars on the Paradox shallow-marine shelf (Babcock, 1978a, 1978b, 1978c, 1978d). These "highs" provided the substrate for algal growth and mound buildup. An opposite view is presented by Matheny and Longman (1996). They propose that fields such as Bug in Utah and Island Butte in Colorado (figure 1.3) pro-

Figure 2.11. *Typical lower Desert Creek proto-mound from the Ucolo No. 1 well (section 26, T. 38 S., R. 25 E., SLBL&M, San Juan County, Utah, slabbed core from 5506 feet [1678 m]) showing dolomitized, broken algal plates, marine cement, and internal sediment. Note that very little porosity is preserved (white areas are anhydrite).*

A.

B.

C.

Figure 2.12. *Typical Ismay and Desert Creek phylloid-algal mound lithofacies. **(A)** Upper Ismay bafflestone fabric in the Tin Cup Mesa No. 3-26 well (section 26, T. 38 S., R. 25 E., SLBL&M, San Juan County, Utah, slabbed core from 5506 feet [1678 m]) showing large phylloid-algal plates (pa) in near-growth positions surrounded by light gray lime muds. Note the scattered moldic pores (Mo) that appear black here. **(B)** Upper Ismay bindstone (cementstone) from the Bonito No. 41-6-85 well (section 6, T. 38 S., R. 25 E., SLBL&M, San Juan County, Utah, slabbed core from 5590.5 feet [1704.0 m]) showing very large phylloid-algal plates (pa), loose skeletal grains, and black marine botryoids (bc) as well as light brown, banded, internal sediments and marine cements (ws/c). Note the patches of preserved porosity within coarse skeletal sediments between algal plates. **(C)** Lower Desert Creek phylloid-algal mound from the May-Bug No. 2 well (section 7, T. 36 S., R. 26 E., SLBL&M, San Juan County, Utah, slabbed core from 6310 feet [1923 m]) composed of dolomitized algal plates of the genus* Kansasphyllum *(arrows).*

Figure 2.13. Typical upper Ismay (lower part) quartz sand dune lithofacies from the Mustang No. 22-43 well (section 26, T. 36 S., R. 43 E., SLBL&M, San Juan County, Utah, slabbed core from 6219 feet [1896 m]) showing high-angle cross-stratification (see black lines at acute angles) within a 35-foot-thick (11 m) sandstone encountered in wells of Mustang Flat field (figure 1.1).

duce from phylloid-algal buildups deposited in sea-floor lows resulting from dissolution of halite in the underlying Akah zone (figure 1.2). Phylloid-algal lithofacies thickness was dictated by the timing and amount of halite dissolution—the greater the halite dissolution during algal growth, the thicker the potential reservoir (Matheny and Longman, 1996). Our work suggests that both models may be viable explanations for initiating Ismay and Desert Creek carbonate buildups.

Regional Lithofacies Maps

Seven major upper Ismay and four lower Desert Creek lithofacies within these depositional environments are mapped across the Blanding sub-basin study area (figures 2.16 through 2.18; appendix C). Regional subsurface mapping of the lower Desert Creek zone and upper and lower parts of the upper Ismay zone shows considerable lateral heterogeneity of the reservoir and non-reservoir rock types. The lower Desert Creek zone in the Blanding sub-basin contains several of the same lithofacies found in the upper Ismay zone, the most notable exception being the intra-shelf evaporite basins, which are discussed later. Mapping of these lithofacies delineates prospective reservoir trends containing porous and productive buildups. Upper Ismay (both the upper and lower parts) include lithofacies 1 – open marine, 2 – middle shelf, 3 – inner shelf/tidal flat, 4 – bryozoan mound, 6 – phylloid-algal mound, 7 – quartz sand dunes, and 8 – anhydritic salinas. Lower Desert Creek include lithofacies 1 – open marine, 2 – middle shelf, 5 – proto-mound, and 6 – phylloid-algal mound.

Open-marine lithofacies dominate the lower Desert Creek zone in the Blanding sub-basin. Due to the absence of preserved porosity, there is very little hydrocarbon potential (figure 2.18). However, in the upper Ismay, this lithofacies developed in different areas for both the upper part (northeastern and southern regions [figure 2.16]) and lower part (western to north-central regions [figure 2.17]) of the upper Ismay zone.

Middle-shelf lithofacies cover extensive areas of the upper Ismay zone and surround important intra-shelf basins, described later. Bryozoan mounds, proto-mounds and phylloid-algal mounds, quartz sand dunes, and inner shelf/tidal flats developed on the low-energy carbonates of the middle-shelf environment (figures 2.16 through 2.18). Porous lower Desert Creek mound lithofacies, such as the reservoir for Bug field, appear to be linear shorelines (carbonate islands) that developed on the middle shelf (figure 2.18). To date, bryozoan mounds are only recognized in the lower part of the upper Ismay at and near Mustang Flat field (figures 1.3 and 2.17). Quartz sand dune lithofacies probably deposited during low stand sea-level conditions within the upper Ismay zone are also present near Mustang Flat field and a few other isolated locations in the lower part of the upper Ismay zone (figure 2.17). This lithofacies may also be present in the lower Ismay outcrop along the Honaker Trail in the San Juan River canyon near Goosenecks State Park, southern San Juan County, Utah (Pray and Wray, 1963; Ritter and Gianniny, 2012).

A.   **B.**   **C.**
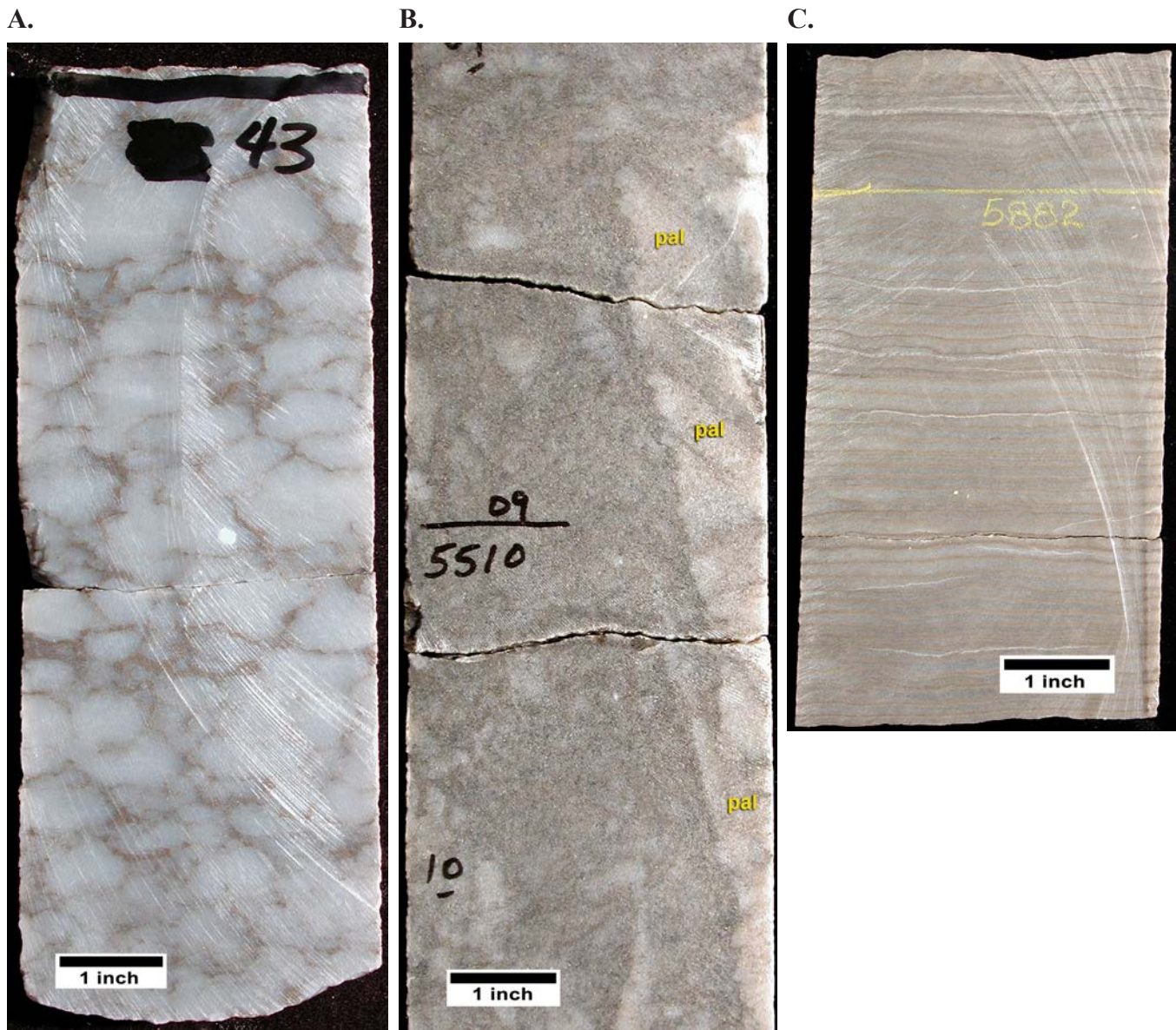
Figure 2.14. *Anhydrite growth forms typically found in anhydrite salina lithofacies of upper Ismay intra-shelf basins. **(A)** Nodular-mosaic ("chicken-wire") anhydrite; Tank Canyon No. 1-9 well, section 9, T. 37 S., R. 24 E., SLBL&M, San Juan County, Utah, slabbed core from 5343 feet (1629 m). **(B)** Large palmate crystals of anhydrite (pal) along the right margin of this core segment probably grew in a gypsum aggregate that resembled an inverted candelabra whereas the remainder of the core segment consists of detrital and chemical anhydrite that filled in the relief around the palmate structure; Sioux Federal No. 30-1 well, section 30, T. 38 S., R. 25 E., SLBL&M, San Juan County, Utah, slabbed core from 5510 feet (1679 m). **(C)** Thin (cm-scale), banded couplets of pure anhydrite (white to light gray) and dolomitic anhydrite (brown); Montezuma No. 41-17-74, section 17, T. 37 S., R. 24 E., SLBL&M, San Juan County, Utah, slabbed core from 5882 feet (1793 m).*

Inner shelf/tidal flat lithofacies represent relatively small areas in geographical extent, especially in the upper part of the upper Ismay zone. However, recognizing this lithofacies is important because inner shelf/tidal flats often form the substrate for subsequent phylloid-algal mound development.

Proto-mound lithofacies are found in the Desert Creek zone and represent the initial stage of a mound buildup or one that never fully developed. They may appear as promising buildups on seismic, but in actuality have poor reservoir quality and little potential other than as guides to nearby fully developed mounds (figure 2.18).

Regional lithofacies mapping clearly defines widespread anhydrite-filled, intra-shelf basins in the upper Ismay zone (figures 2.16 and 2.17). Inner shelf/tidal flat and associated productive, phylloid-algal lithofacies trends of the upper Ismay developed around the anhydritic salinas of intra-shelf basins (figures 2.16, 2.17, 2.19, and 2.20). The topographic relief of these phylloid-algal buildups may have been instrumental in developing the salinity restriction that resulted in anhydrite deposition within adjacent salinas. Although not present in the lower Desert Creek zone in the Blanding sub-basin, the Desert Creek reservoir lithofacies peripheral to Greater Aneth field to the south (figure 1.3) wrap around

A.
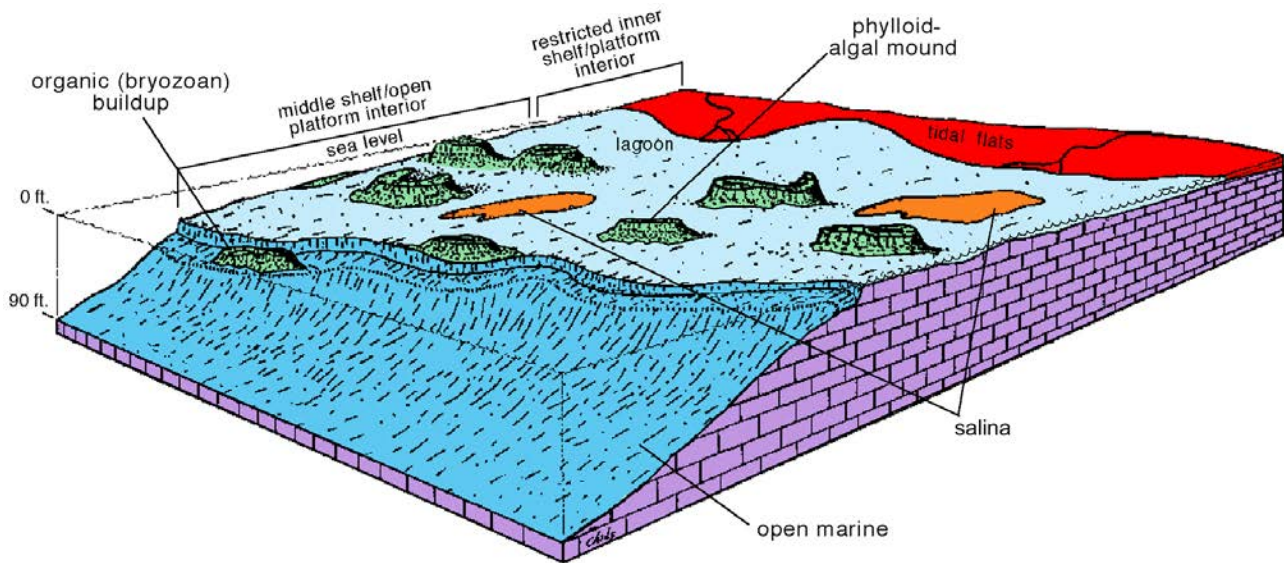
B.
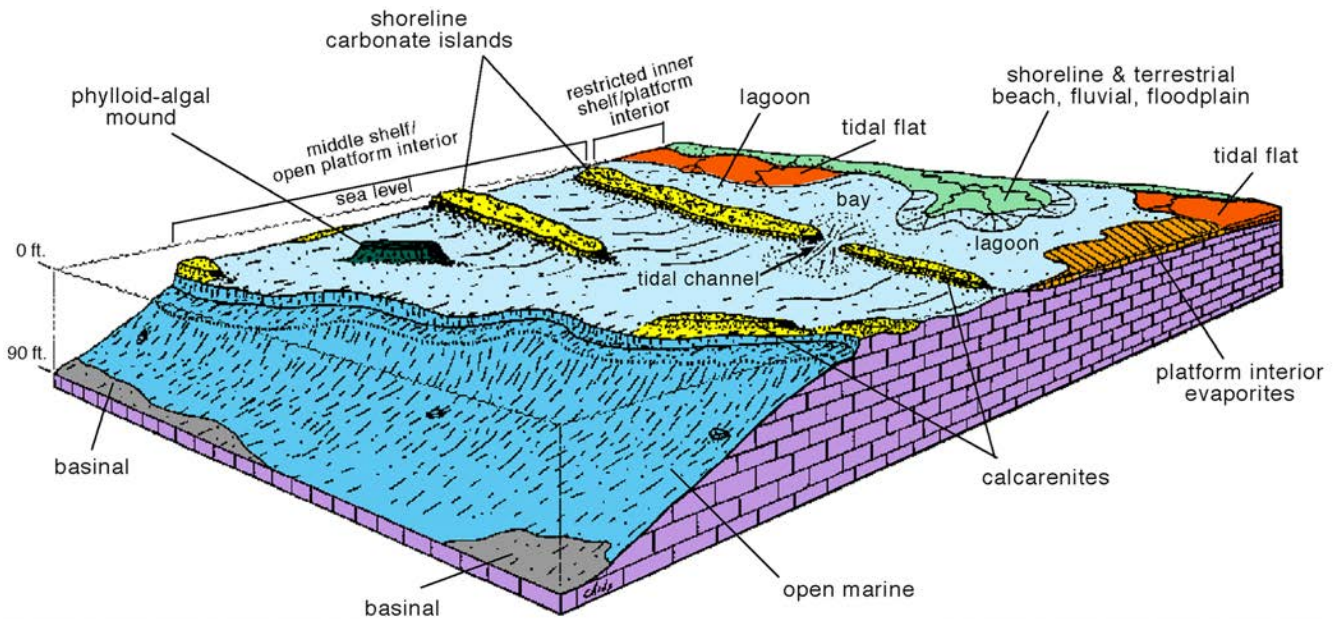
*Figure 2.15. Block diagrams displaying major depositional environments, as determined from core, for the Ismay **(A)** and Desert Creek **(B)** zones, Pennsylvanian Paradox Formation, Utah and Colorado (Blanding sub-basin shown on figure 1.3).*

similar anhydrite-filled, intra-shelf basins (Chidsey and others, 1996b; Chidsey and Eby, 2000).

The location and shape of these anhydrite-rich, intra-shelf basins play major roles in the deposition and orientation of productive phylloid-algal buildups, as well as the shoreline lithofacies that wrap around the basins. Most phylloid-algal buildups and porous inner-shelf lithofacies are very close to the intra-shelf basins, whereas lithofacies distant from the anhydrite-filled basins generally contain less favorable reservoir rocks. The two mapped upper Ismay zone intervals show considerable differences in the distribution of these anhydrite basins and their surrounding lithofacies (compare figure 2.16 with figure 2.17).

Ismay Isochore Relationships

The isochore map of the upper Ismay clean-carbonate interval is shown on figure 2.21. Note that the "thicks" of upper Ismay clean carbonate (the darker green hues on the map) are often connected and nearly surround "thins" (in very pale shades). The thicks are probably the combined effect of upper Ismay platform (middle to inner shelf/tidal flat) deposition and organic (phylloid-algal and bryozoan) buildups. The thins surrounded by thicks are the intra-shelf basins, described above, within the upper Ismay interval. These intra-shelf basins are filled with thick anhydrite deposits (see figure 2.22, upper Ismay anhydrite 2 isochore map). The remaining thins that

are not surrounded by, or near thicks are largely open-marine (deep, outer shelf) deposits. Also see appendices A and B.

The areas of thickest anhydrite on the isochore map of the upper Ismay anhydrite 2 (in darker shades of orange, figure 2.22) roughly correlate with some of the thins on the upper Ismay clean carbonate isochore map (figure 2.21). The anhydrite 2

thicks were deposited within semi-isolated, intra-shelf basins. Also see appendices A and B.

The isochore relationships for the upper Ismay clean-carbonate and upper Ismay anhydrite 2 shown on figures 2.21 and 2.22 are too coarse or complex to accurately define prospective lithofacies tracts and intra-shelf basin boundaries.
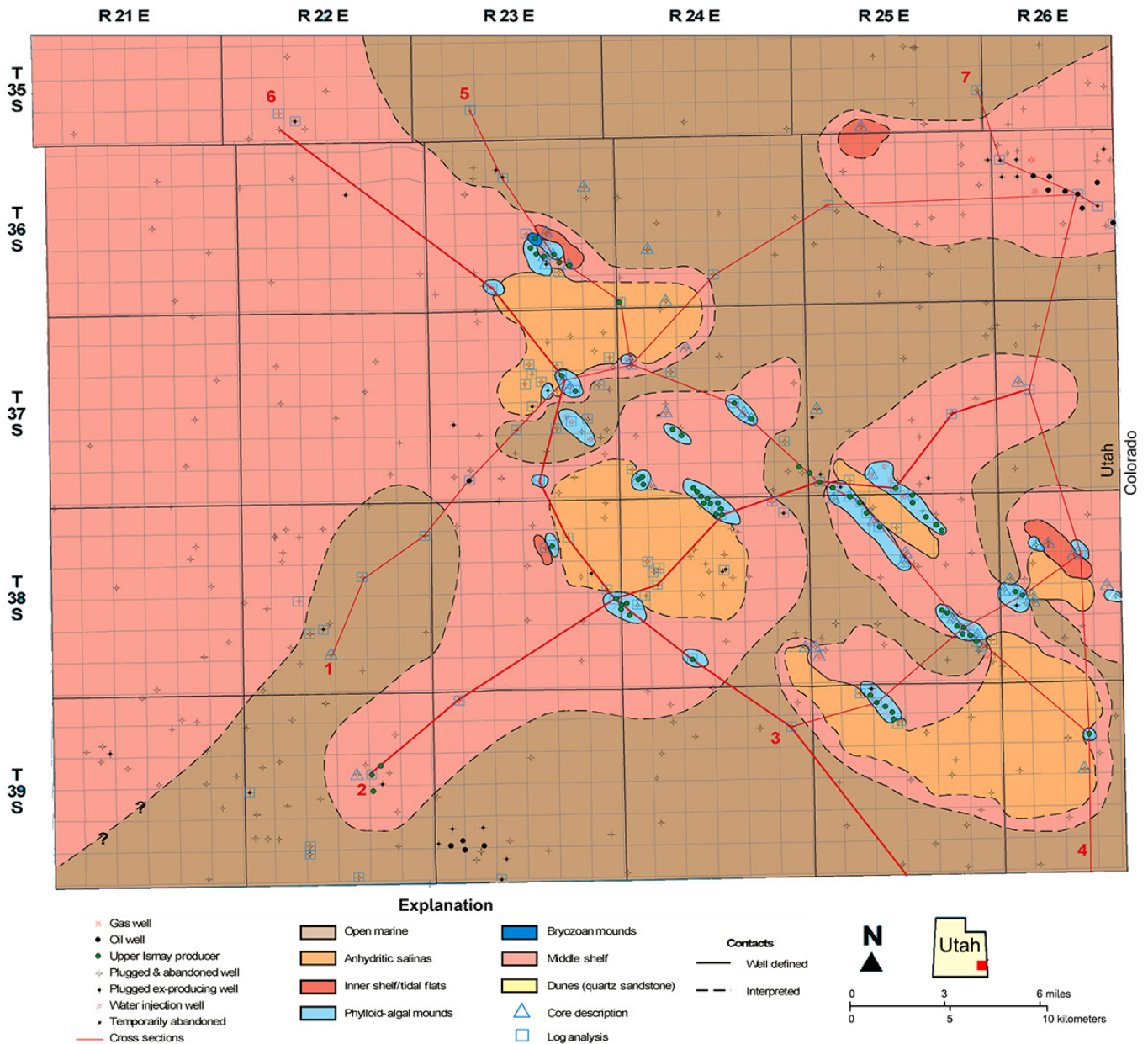
Figure 2.16. *Regional lithofacies (averaged) map of the upper part of the upper Ismay zone, Paradox Formation, in the Blanding sub-basin, Utah. Numbered lines indicate locations of cross sections generated in this study and included in appendix A; also see appendix C, plate C1 for large-scale facies map.*
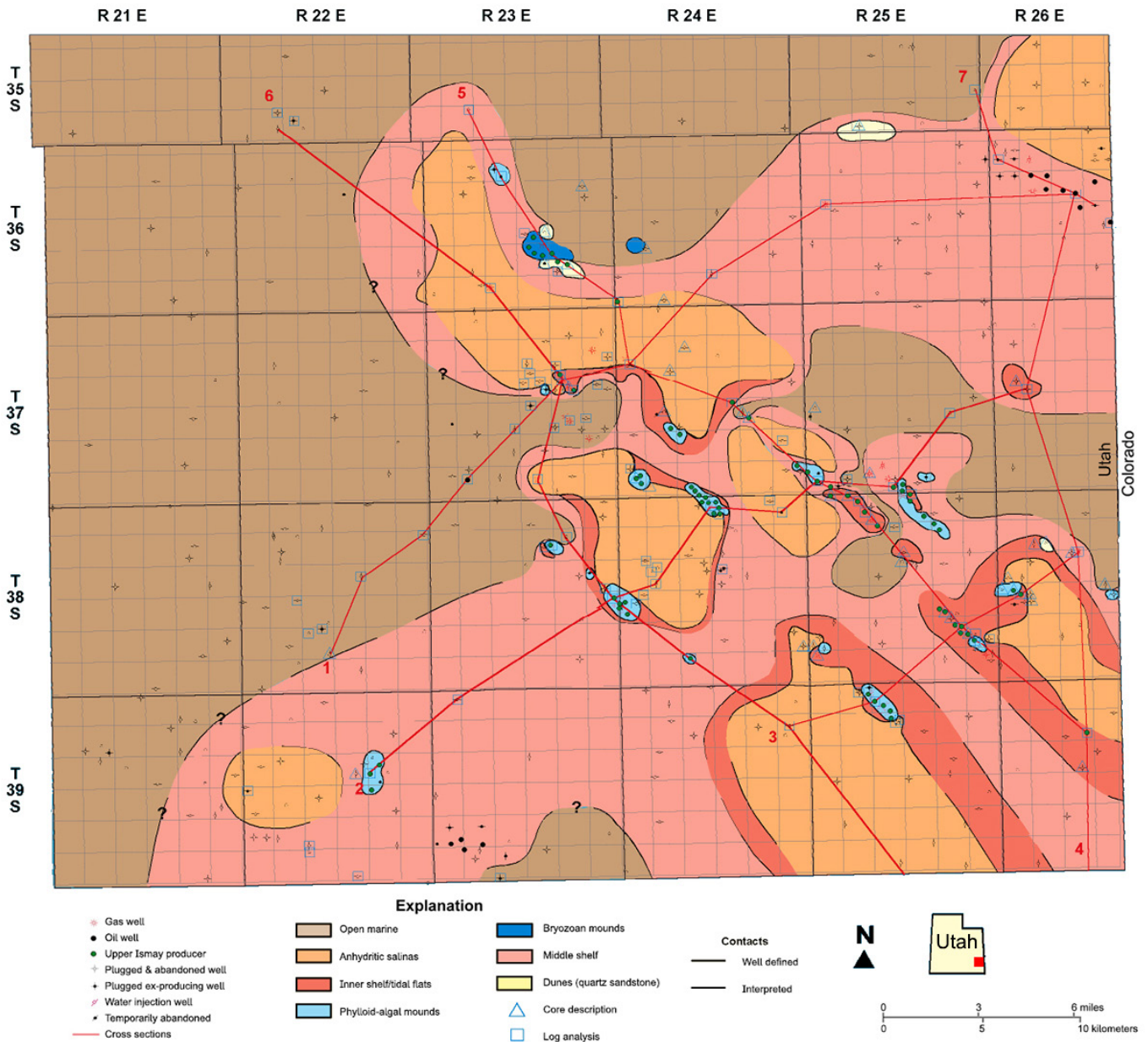
Figure 2.17. *Regional lithofacies (averaged) map of the lower part of the upper Ismay zone, Paradox Formation, in the Blanding sub-basin, Utah. Numbered lines indicate locations of cross sections generated in this study and included in appendix A; also see appendix C, plate C2 for large-scale facies map.*
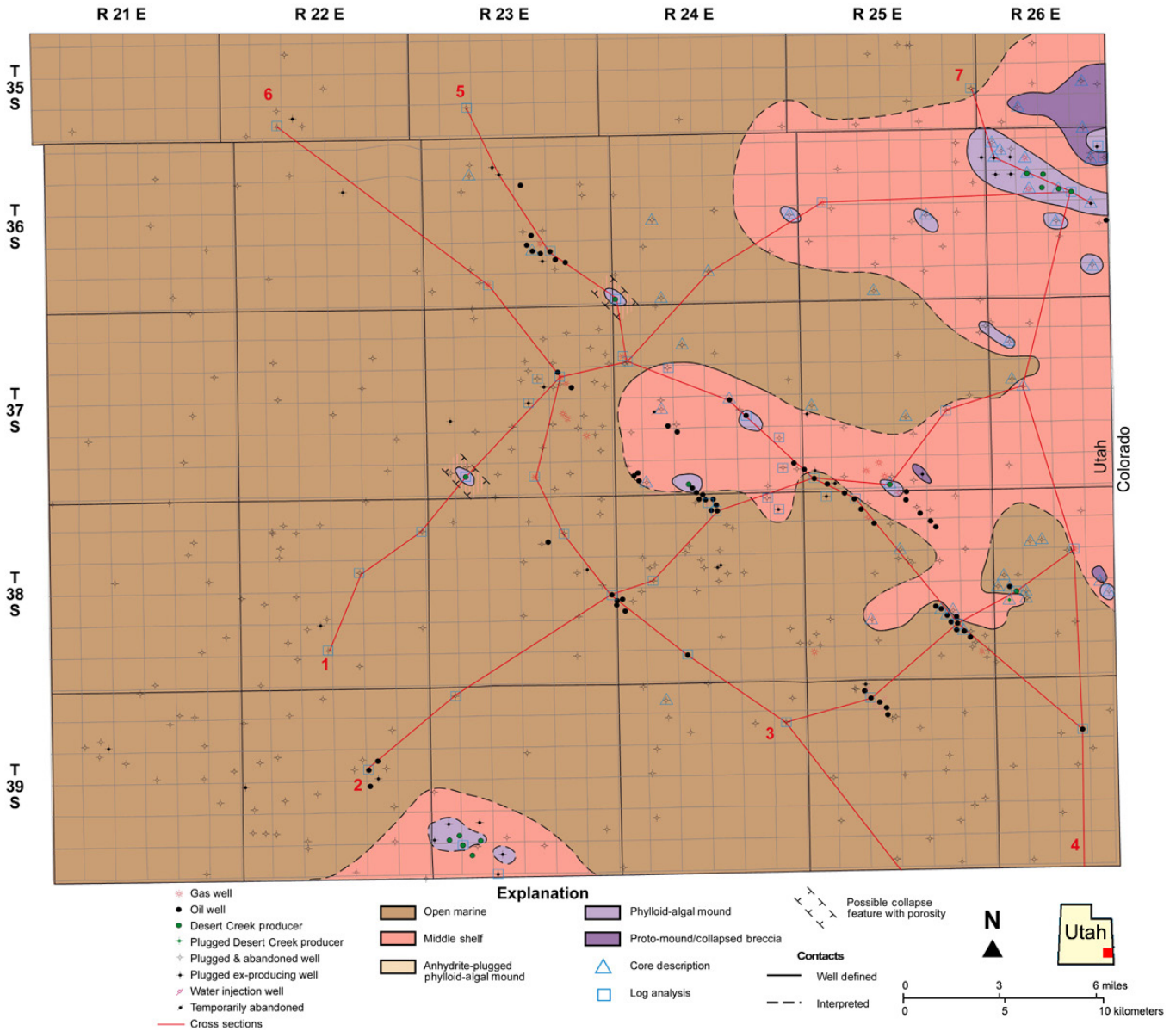
Figure 2.18. *Regional lithofacies map of the lower Desert Creek zone, Paradox Formation, in the Blanding sub-basin, Utah. Numbered lines indicate locations of cross sections generated in this study and included in appendix A; also see appendix C, plate C3 for large-scale facies map.*
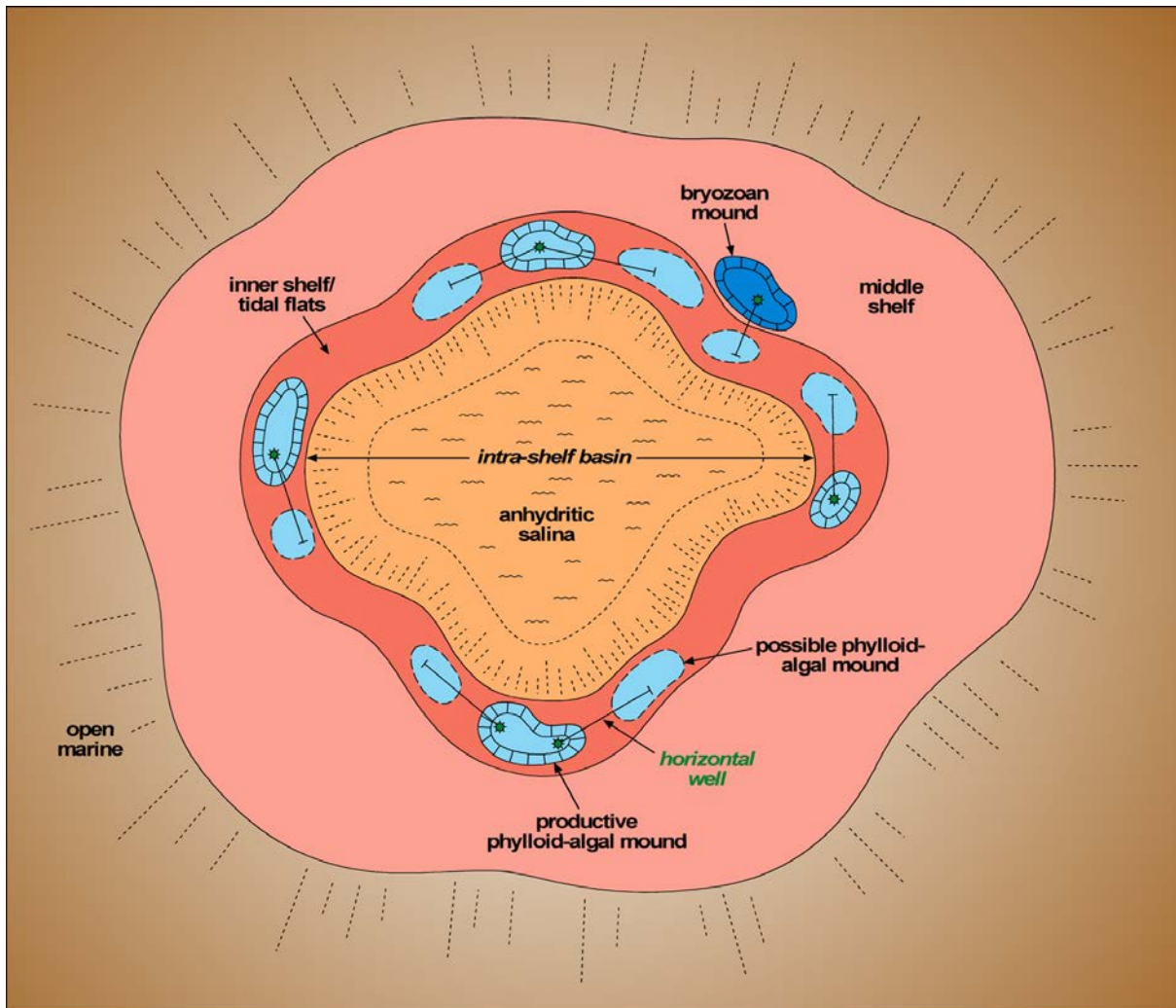
Figure 2.19. *Schematic map view of an ideal upper Ismay intra-shelf basin surrounded by a ring of inner shelf/tidal flat sediments (shown in red), which encase phylloid-algal mound clusters (in light blue). The central part of the intra-shelf basin is the location of thick anhydrite accumulation (in orange). Outboard from the inner shelf/tidal flat and mound fairway are low-energy middle-shelf and open-marine carbonates. No scale intended.*
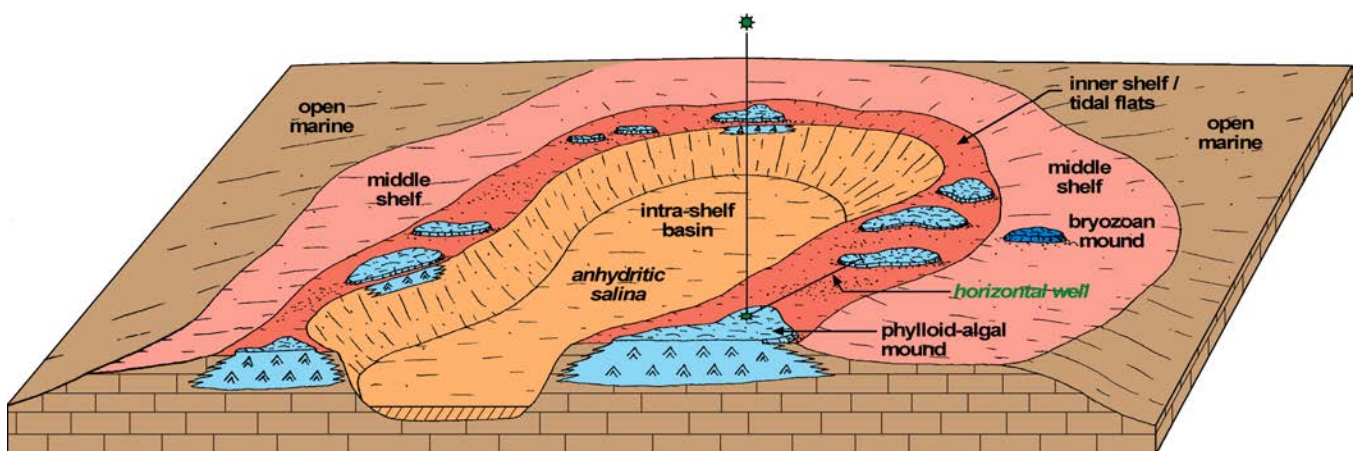
Figure 2.20. *Cut-away block diagram showing the possible spatial relationships of upper Ismay lithofacies types controlled by an intra-shelf basin. Phylloid-algal mounds (in light blue) are the principal reservoir within a curvilinear band that rims the intra-shelf basin. A hypothetical vertical well into a known mound reservoir is used as a kick-off location for horizontal drilling into previously undrained mounds. No scale intended.*
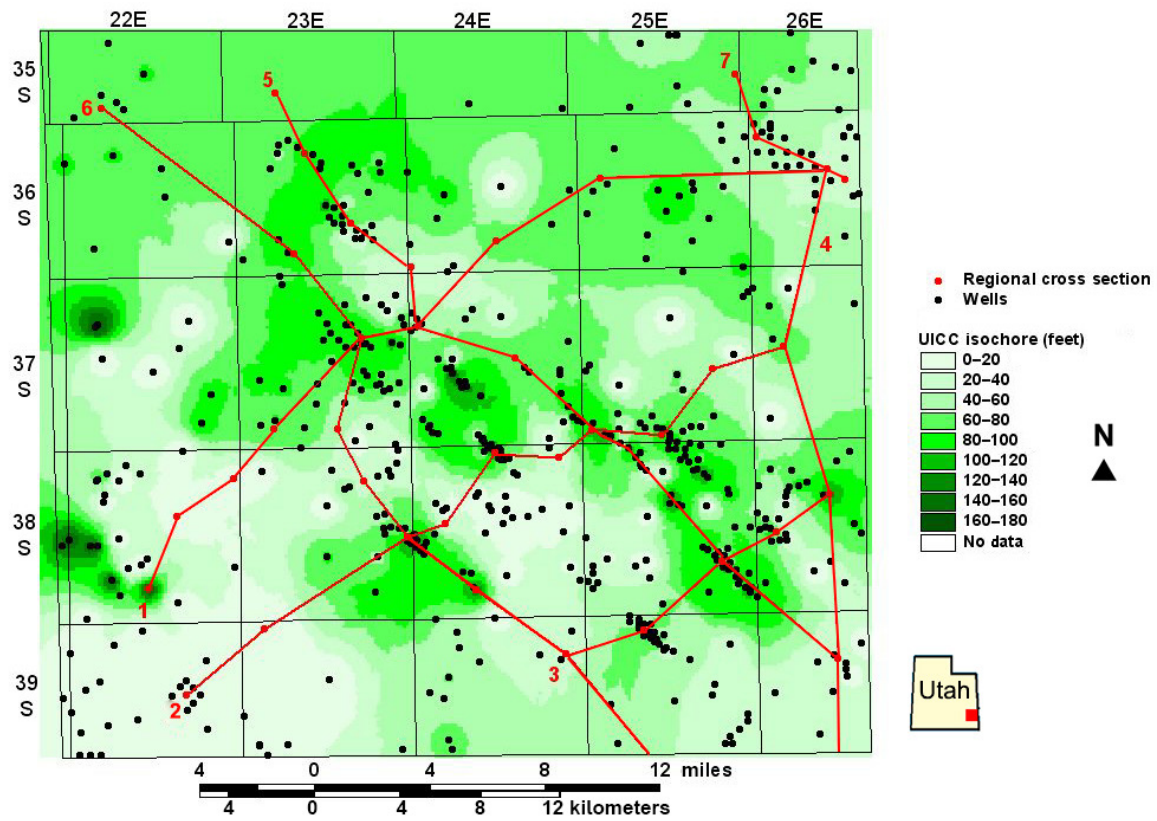
Figure 2.21. *Isochore map of the upper Ismay clean carbonate (UICC) interval. The log picks and correlations of clean carbonate are shown on the regional cross sections represented by the numbered lines included in appendix A.*
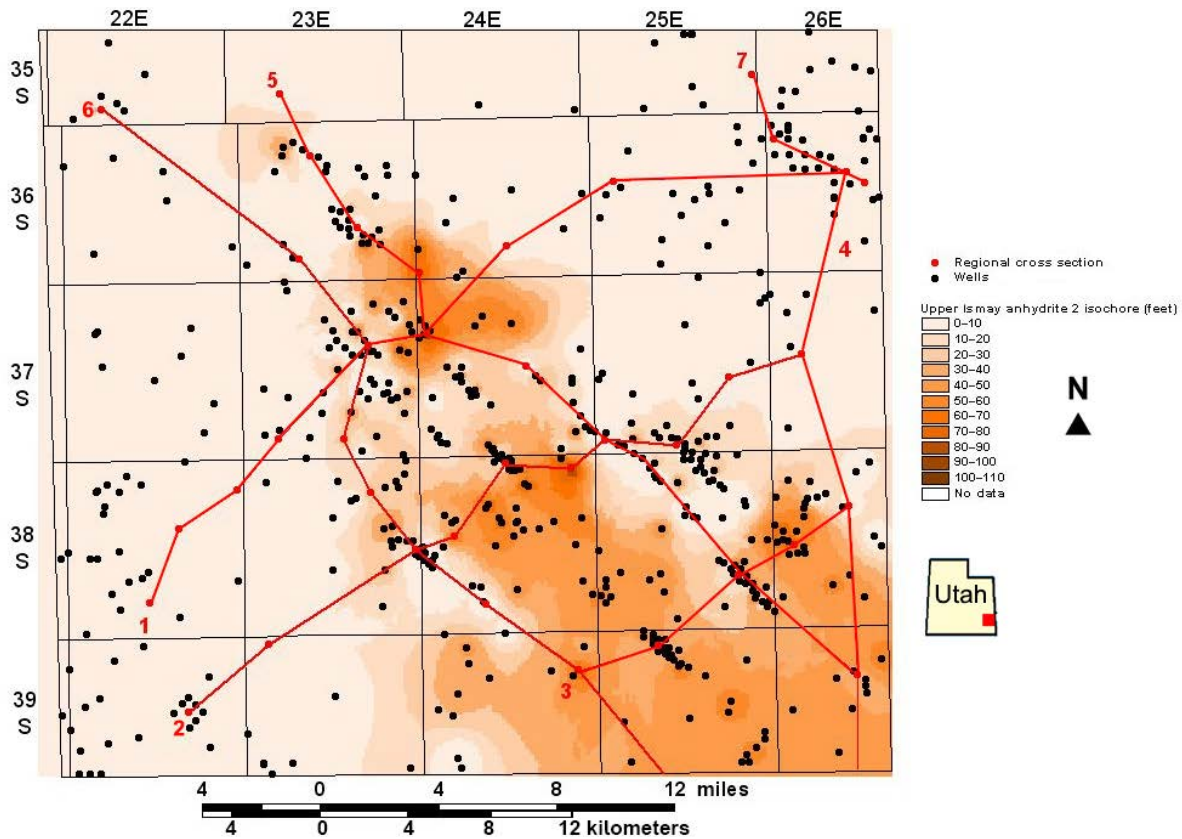
Figure 2.22. *Isochore map of the upper Ismay anhydrite 2. The log picks and correlations of anhydrite 2 are shown on the regional cross sections represented by the numbered lines included in appendix A.*

CHAPTER 3:
GENERAL PETROLEUM GEOLOGY,
BUG AND CHEROKEE CASE-STUDY FIELDS,
SAN JUAN COUNTY, UTAH

by

Thomas C. Chidsey, Jr., and Craig D. Morgan (retired), Utah Geological Survey
and
David E. Eby, Eby Petrography & Consulting, Inc.

CHAPTER 3:
GENERAL PETROLEUM GEOLOGY, BUG AND CHEROKEE CASE-STUDY FIELDS, SAN JUAN COUNTY, UTAH

INTRODUCTION

Two case-study fields were selected for local-scale reservoir characterization and evaluation for this study: Bug field, San Juan County, Utah, in the Desert Creek trend; and Cherokee field, San Juan County, Utah, in the Ismay trend (figure 1.3). These evaluations included data collection, core photography and description, defining a typical vertical sequence from conventional core tied to its corresponding log response, lithofacies identification, reservoir mapping, determination of diagenetic fabrics from thin sections, and comparisons of core plug porosity versus permeability.

The geological characterization of these fields focused on reservoir heterogeneity, quality, and lateral continuity, as well as possible compartmentalization. We used representative core and geophysical well logs to characterize and initially grade various intervals in the fields for horizontal drilling suitability. From these evaluations, untested or under-produced compartments were identified as targets for horizontal drilling. The information generated from the characterization and evaluation of the case-study fields was used for (1) predicting changes in reservoir and non-reservoir rocks across the fields, (2) comparing field to non-field areas, (3) estimating the reservoir properties and identifying lithofacies in wells which were not cored, and (4) determining potential units suitable for horizontal drilling projects. The results from the geological and reservoir characterization of these fields can be applied to similar fields in the basin, or in other carbonate platform plays, where core and other data might be limited.

FIELD DATA COLLECTION, COMPILATION, AND INTERPRETATION

Utah Geological Survey geologists collected reservoir data, cores and cuttings information, geophysical logs, various reservoir maps, and other information from the case-study fields. Well locations, production data, completion tests, basic core analyses, formation tops, and porosity and permeability data were compiled and entered into a database. This database was designed so that geological information, such as lithology, petrophysical analyses, or depositional environment, can be exported to various software programs to produce strip logs, lithofacies maps, various graphs, statistical models, and other types of presentations.

Ten conventional cores from the case-study fields were photographed (examples shown on figures 3.1 and 3.2, and ta-

ble 3.1) and described (appendix D). Special emphasis was placed on identifying each reservoir unit's bounding surfaces and depositional environments. The core descriptions follow the guidelines of Bebout and Loucks (1984) which include (1) basic porosity types, (2) mineral composition (%), (3) nature of contacts, (4) carbonate structures, (5) carbonate textures (%), (6) carbonate fabrics, (7) grain size, (8) fractures, (9) color, (10) fossils, (11) cement, and (12) depositional environment. Carbonate fabrics were determined according to Dunham's (1962) and Embry and Klovan's (1971) classification schemes. Representative samples were selected from the cores for thin section description and geochemical analysis to determine diagenetic history and pore types.

The typical vertical sequence or cycle of lithofacies from the case-study fields, as determined from conventional core, was tied to its corresponding log response from geophysical well logs (examples shown on figures 3.3 and 3.4; appendix D). Gamma-ray and neutron-density curves were analyzed using the log-based correlation scheme described in Chapter 2. These sequences/cycles graphically include (1) carbonate fabric, pore type, physical structure, texture, framework grain, and lithofacies described from core; (2) plotted porosity and permeability analysis from core plugs; and (3) gamma-ray and neutron-density curves from geophysical well logs.

The graphical information was combined with the log-based correlation scheme to identify major Paradox Formation zone contacts, seals or barriers, baffles, and producing or potential reservoirs, and lithofacies. These major zone contacts were used to produce a variety of structure and isochore maps. Seals or barriers include anhydrite layers and thick (black) shales such as the Hovenweep shale, which separates the upper Ismay from the lower Ismay. Baffles are those rock units that restrict fluid flow in some parts of the field but may develop enough porosity and permeability in other parts, through diagenetic processes or lithofacies changes, to provide a conduit for fluid flow or even oil storage. The reservoirs are those units containing 6% or more porosity based on the average of the neutron and density porosity values.

FIELD OVERVIEWS

Bug Field

Bug field (figure 1.3) is an elongate, northwest-trending carbonate buildup in the lower Desert Creek zone. Productive

Figure 3.1. *Representative slabbed core from the lower Desert Creek zone reservoir, Bug No. 13 well, section 17, T. 36 S., R. 26 E., SLBL&M, Bug field, San Juan County, Utah.*

Figure 3.2. *Representative slabbed core from the upper Ismay zone reservoir, Cherokee Federal No. 22-14 well, section 14, T. 37 S., R. 23 E., SLBL&M, Cherokee field, San Juan County, Utah.*

Table 3.1. *List of conventional slabbed cores examined and described from case-study fields in the Paradox Basin of Utah. The repository for the cores is the Utah Core Research Center, Salt Lake City, Utah.*

Well	Location	API No.	Cored Interval (ft)	Field	Stratigraphic Zone
May-Bug 2	7-36S-26E, UT	43-037-30543	6290-6333	Bug	Desert Creek
Bug 3	7-36S-26E, UT	43-037-30544	6316-6358	Bug	Desert Creek
Bug 4	16-36S-26E, UT	43-037-30542	6278-6322	Bug	Desert Creek
Bug 7-A	7-36S-26E, UT	43-037-30730	6345-6400	Bug	Desert Creek
Bug 8	8-36S-26E, UT	43-037-30589	5737-5796.1	Bug	Desert Creek
Bug 10	22-36S-26E, UT	43-037-30591	6300-6346.5	Bug	Desert Creek
Bug 13	17-36S-26E, UT	43-037-30610	5913-5951.3	Bug	Desert Creek
Bug 16	17-36S-26E, UT	43-037-30607	6278-6333	Bug	Desert Creek
Cherokee 22-14	14-37S-23E, UT	43-037-31367	5768-5880	Cherokee	Ismay
Cherokee 33-14	14-37S-23E, UT	43-037-31316	5770-5799	Cherokee	Ismay

lithofacies consist of a phylloid-algal mound capped by shoreline carbonate island deposits (figure 3.5). The buildup is surrounded by non-productive middle shelf fossiliferous/peloidal muds and some platform interior evaporites (figure 3.6) (see Chapter 2 for detailed descriptions of these lithofacies). The producing units vary from porous dolomitized bafflestone (figures 2.26C and 3.5A) to packstone and wackestone (figure 3.5B). The trapping mechanism is an updip porosity pinchout to the northeast (figure 3.7). The net reservoir thickness is 15 feet (4.6 m) over a 2600-acre (1052 ha) area. Porosity averages 11% in moldic, vuggy, and intercrystalline networks. Permeability averages 25 to 30 millidarcies (mD), but ranges from less than 1 to 500 mD. Water saturation is 32% (Martin, 1983; Oline, 1996).

Bug field was discovered in 1980 with the completion of the Wexpro Bug No. 1 well, NE1/SE1/4 section 12, T. 36 S., R. 25 E., Salt Lake Base Line and Meridian (SLBL&M), with an initial flowing potential (IFP) of 608 bbls of oil per day (BOPD), 1128 thousand cubic feet of gas per day (MCFGPD), and 180 barrels of water (BW). There are currently seven producing (or shut-in) wells, six abandoned producers, and two dry holes in the field. The well spacing is 160 acres (65 ha). Cumulative production as of September 1, 2020, was 1,665,520 BO, 5.35 billion cubic feet of gas (BCFG), and 3,315,806 BW (Utah Division of Oil, Gas and Mining, 2020). Estimated primary recovery was 1,600,000 BO and 4 BCFG (Oline, 1996). The fact that both these estimates have been surpassed suggests significant additional reserves remain in Bug and similar mature fields in the lower Desert Creek trend.

Cherokee Field

Cherokee field (figure 1.3) is a phylloid-algal buildup (figure 3.8A) capped by crinoid/fusulinid-bearing sands (figure 3.8B) that produces from porous algal limestone and dolomite in the upper Ismay zone. The buildup is surrounded by productive and non-productive (mound/clean carbonate and off-mound) middle shelf fossiliferous/peloidal muds and anhydrite (figures 3.9 and 3.10) (see Chapter 2 for detailed descriptions of

these lithofacies). The net reservoir thickness is 27 feet (8.2 m), which extends over a 320-acre (130 ha) area. Porosity averages 12% with 8 mD of permeability in vuggy and intercrystalline pore systems. Water saturation is 38.1% (Crawley-Stewart and Riley, 1993).

Cherokee field was discovered in 1987 with the completion of the Meridian Oil Company Cherokee Federal 11-14 well, NE1/4NW1/4 section 14, T. 37 S., R. 23 E., SLBL&M, with an IFP of 53 BOPD, 990 MCFGPD, and 26 BW. There are currently three producing (or shut-in) wells, one abandoned producer, and three dry holes in the field (figure 3.10). The well spacing is 80 acres (32 ha). Cumulative production as of September 1, 2020, was 188,154 BO, 3.8 BCFG, and 5211 BW (Utah Division of Oil, Gas and Mining, 2020). The original estimated primary recovery was 172,000 BO and 3.28 BCFG (Crawley-Stewart and Riley, 1993). Again, since the original reserve estimates have been surpassed and the field is still producing, additional reserves may remain in Cherokee and similar mature fields in the upper Ismay trend.

RESERVOIR MAPPING

Various reservoir maps (top of structure, isochore [anhydrite, shale, porosity, permeability, lithology], lithofacies, etc.) and cross sections were constructed for the case-study fields (appendix E). Examples are shown on figures 3.7 and 3.10 through 3.23. These maps incorporate unit top and thickness picks from all geophysical well logs in the area, which were determined using the log-based correlation scheme (see Chapter 2). The correlation scheme helped identify major Paradox Formation zone contacts, seals or barriers, baffles, producing or potential reservoirs, and depositional lithofacies. Isochore maps of the upper and lower Ismay and lower Desert Creek were generated for reservoir units containing 6% or higher porosity based on the average of the neutron and density porosity values. The maps show well names, Ismay or Desert Creek completions, completion attempts, drill-stem tests, wells with core, and display the subsea
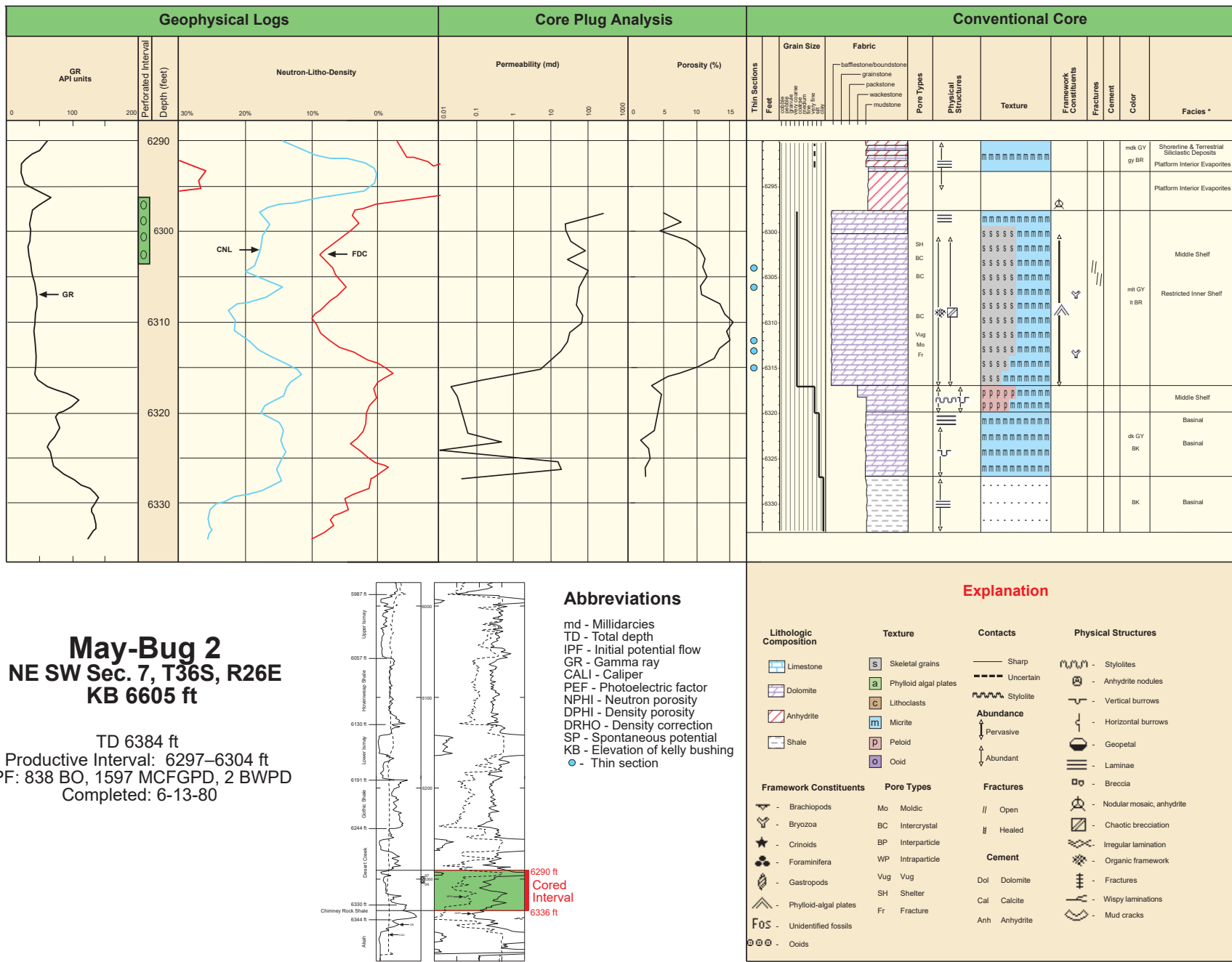
Figure 3.3. *Typical vertical sequence from Bug field, including geophysical well logs, porosity/permeability plots, and core description, of the lower Desert Creek zone, May-Bug No. 2 well.*

Figure 3.4. *Typical vertical sequence from Cherokee field, including geophysical well logs, porosity/permeability plots, and core description, of the upper Ismay zone, Cherokee Federal No. 22-14 well.*

A.

B.

Figure 3.5. *Typical productive lower Desert Creek phylloid-algal mound and shoreline island deposits from Bug field.* ***(A)*** *Dolomitized phylloid-algal bafflestone with botryoidal cements and light-colored internal sediments; Bug No. 16 well, section 17, T. 36 S., R. 26 E., SLBL&M, slabbed core from 6304 feet (1921 m).* ***(B)*** *Dolomitized skeletal calcarenite and peloidal sands and muds (packstone) representing carbonate islands capping the mound; Bug No. 10 well, section 22, T. 36 S., R. 26 E., SLBL&M, slabbed core from 6319.5 to 6320.3 feet (1926.2–1926.4 m).*

A.

B.

Figure 3.6. *Typical non-productive lower Desert Creek middle shelf carbonates and platform interior evaporites from the Bug No. 3 well, section 7, T. 36 S., R. 26 E., SLBL&M, Bug field.* ***(A)*** *Dolomitized, low-energy fossiliferous/peloidal middle shelf wackestone; slabbed core from 6347 feet (1935 m).* ***(B)*** *Finely laminated platform interior anhydrite; slabbed core from 6333 feet (1930 m).*
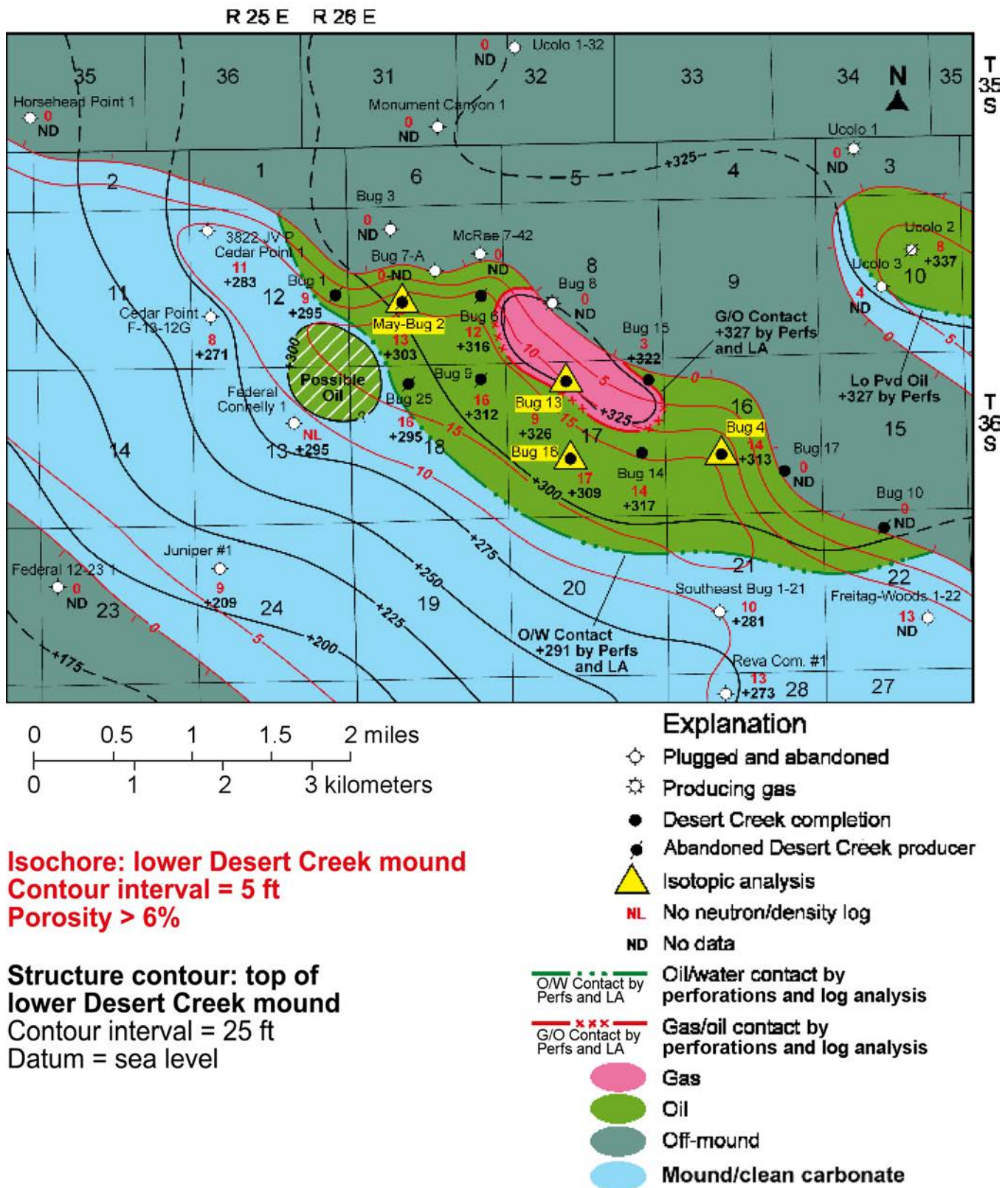
Figure 3.7. *Map of combined top of structure and isochore of lower Desert Creek zone mound, Bug field. Well cores used for isotope sampling for this study are highlighted with a yellow triangle (discussed in Chapter 7).*
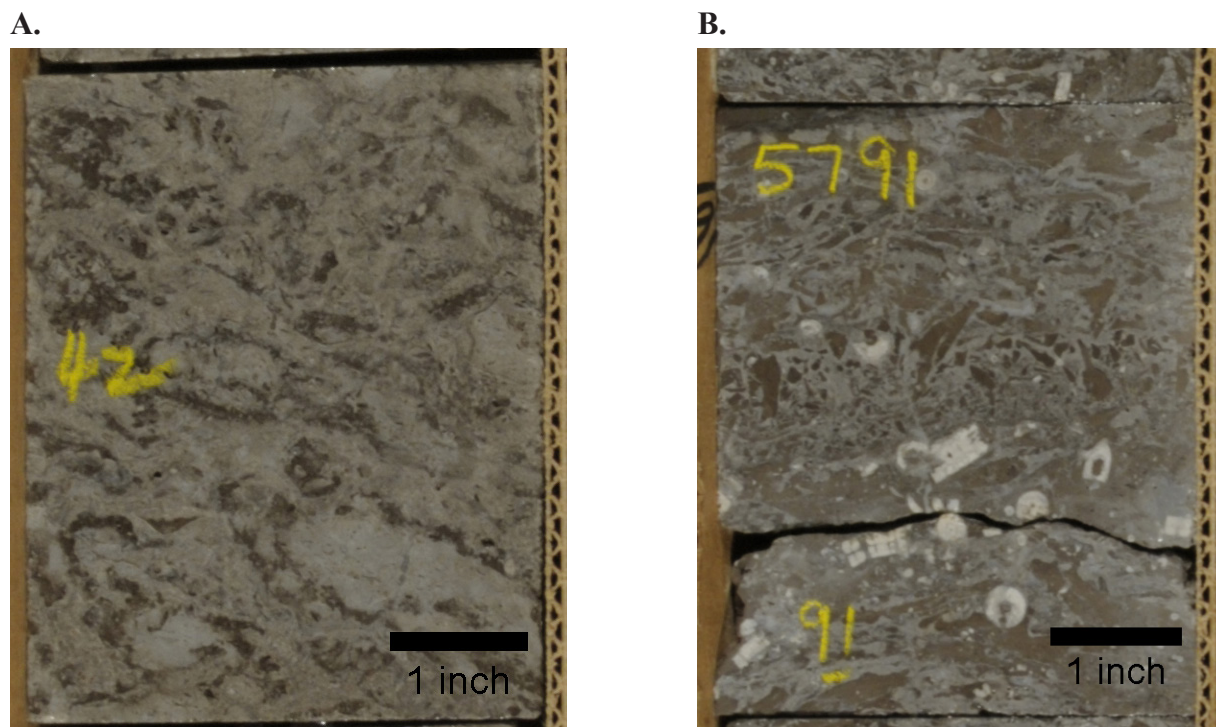
Figure 3.8. *Typical productive upper Ismay limestone represented by phylloid-algal mound and skeletal sands from the Cherokee Federal No. 22-14 well, section 14, T. 37 S., R. 23 E., SLBL&M, Cherokee field. (A) Well-developed phylloid-algal bafflestone with medium-sized phylloid plates and molds of plates plugged with marine cement; slabbed core from 5842 feet (1781 m). (B) Crinoid/fusulinid-bearing packstone that often caps the phylloid-algal mounds; slabbed core from 5791 feet (1765 m).*
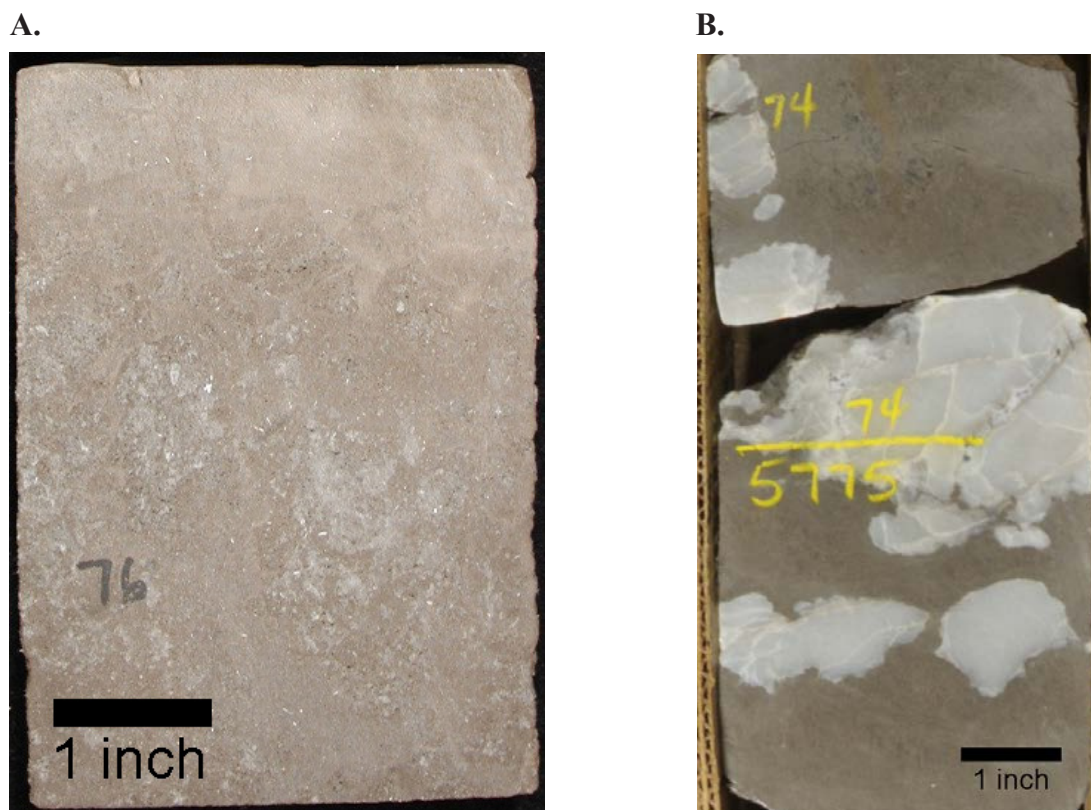
Figure 3.9. *Typical productive and non-productive upper Ismay middle shelf and anhydrite deposits from Cherokee field. (A) Productive, do-lomitized grainstone to packstone contain skeletal debris, ooids, and peloids from the middle shelf; Cherokee Federal No. 33-14 well, section 14, T. 37 S., R. 23 E., SLBL&M, slabbed core from 5776 feet (1761 m). (B) Non-productive, dolomitized mudstone to wackestone composed of soft peloids and anhydrite; Cherokee Federal No. 22-14 well, slabbed core from 5775 feet (1760 m).*
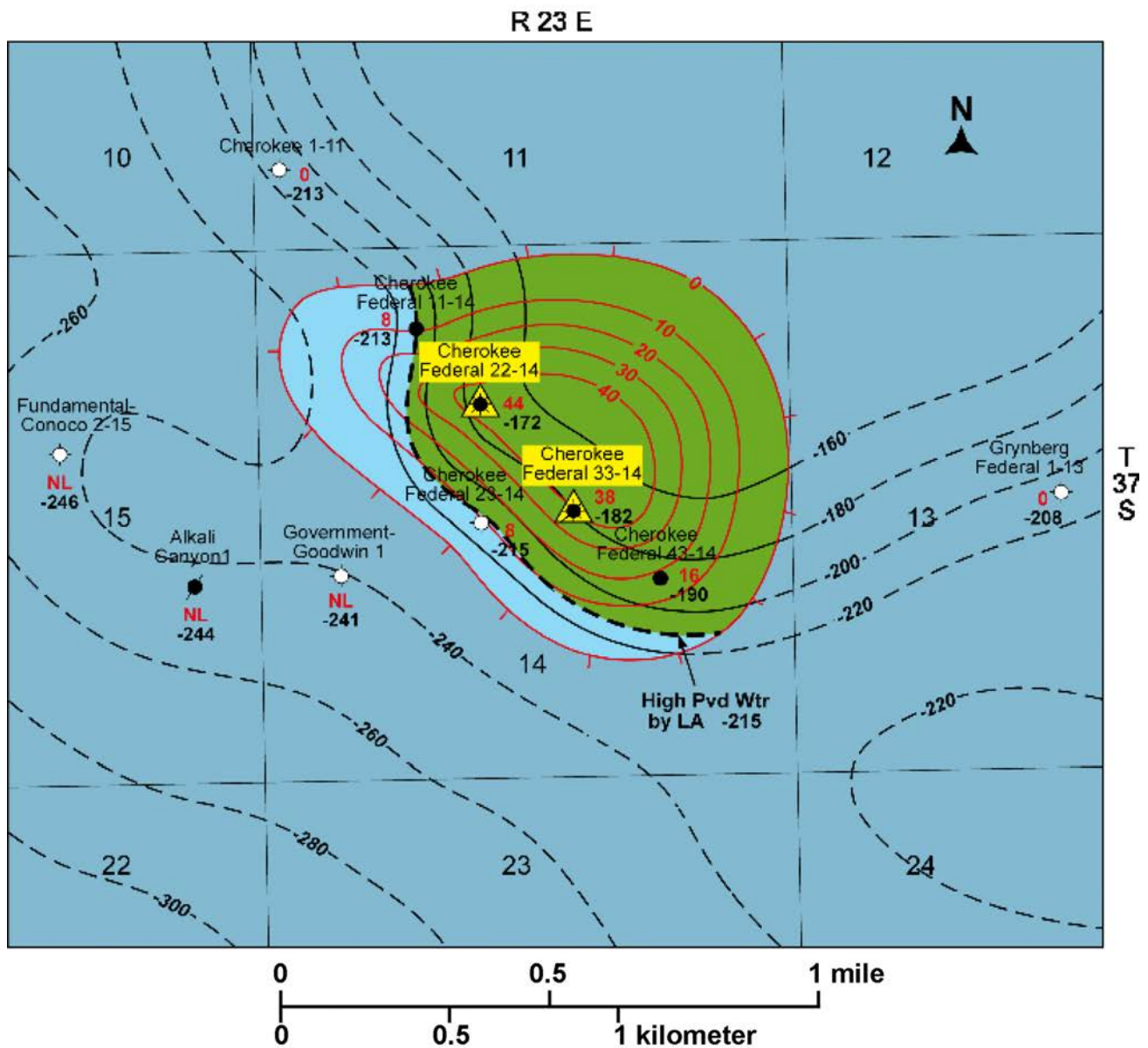
Figure 3.10. *Map of combined top of "clean carbonate" structure and isochore of porosity units 1 through 5, upper Ismay zone, Cherokee field. Well cores used for isotope sampling for this study are highlighted with a yellow triangle (discussed in Chapter 7).*
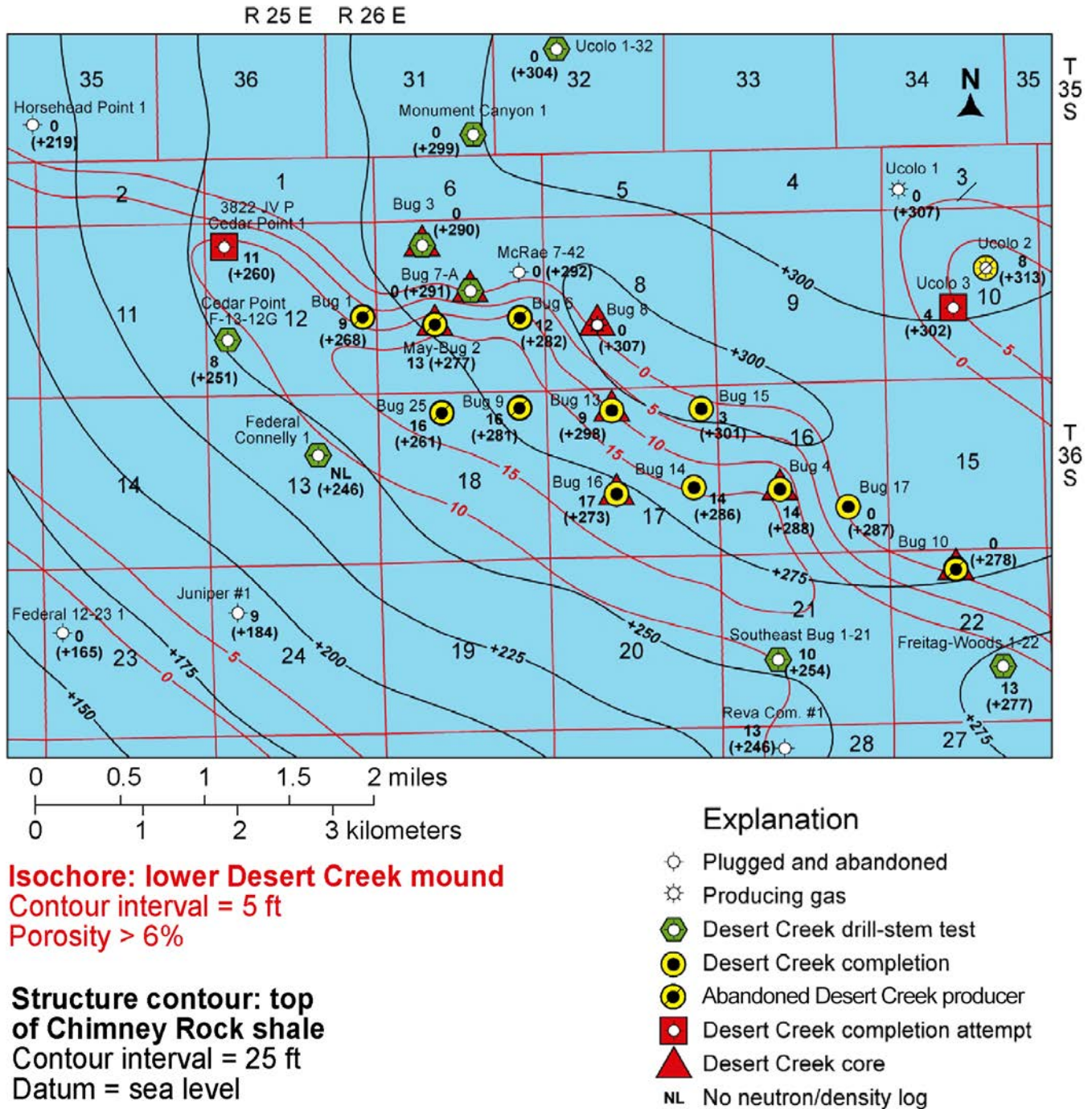
Figure 3.11. *Combined Chimney Rock shale structure contour map and isochore map for the lower Desert Creek mound cap/mound core, Bug field.*
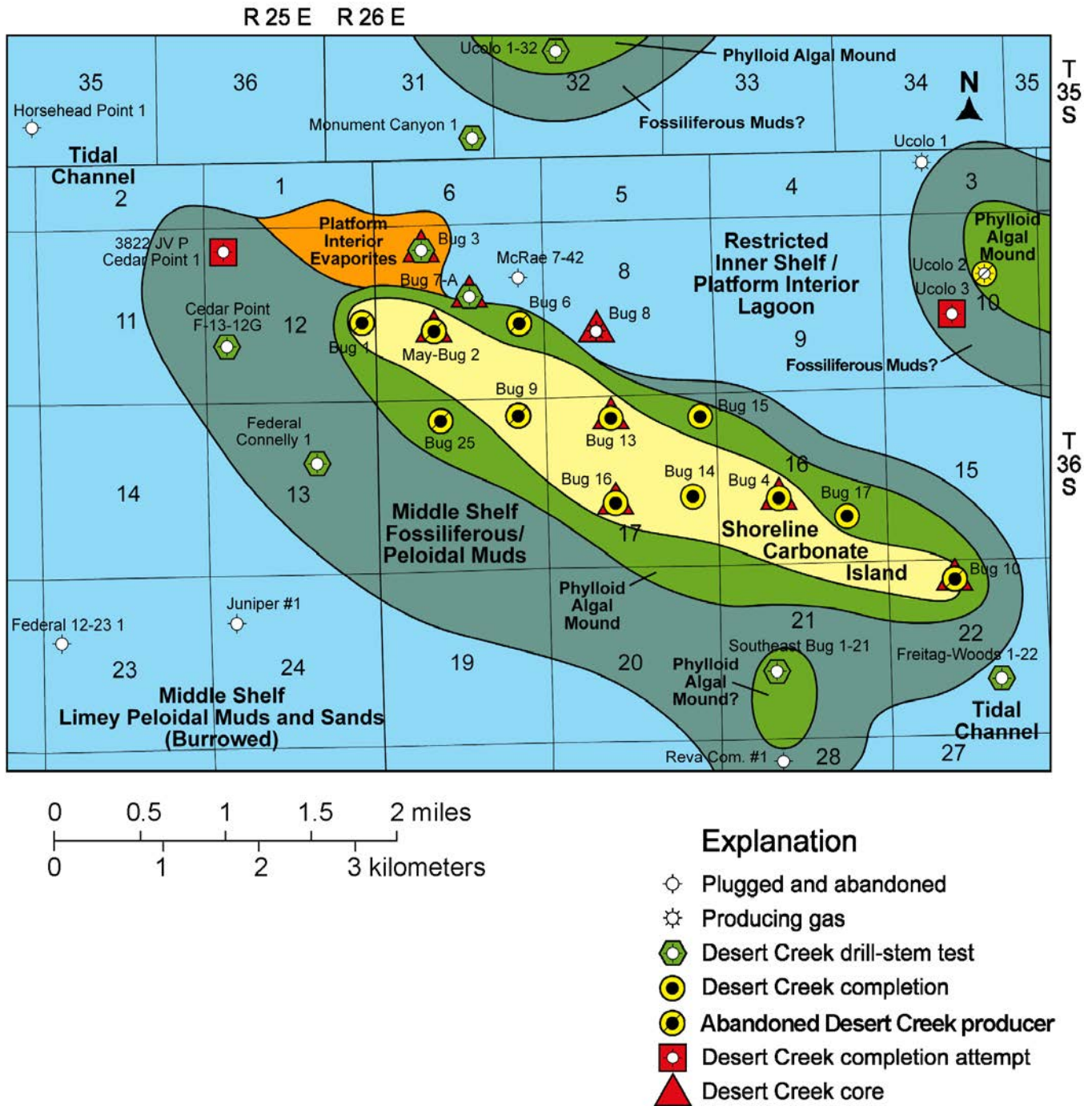
Figure 3.12. *Lower Desert Creek zone lithofacies map, Bug field.*
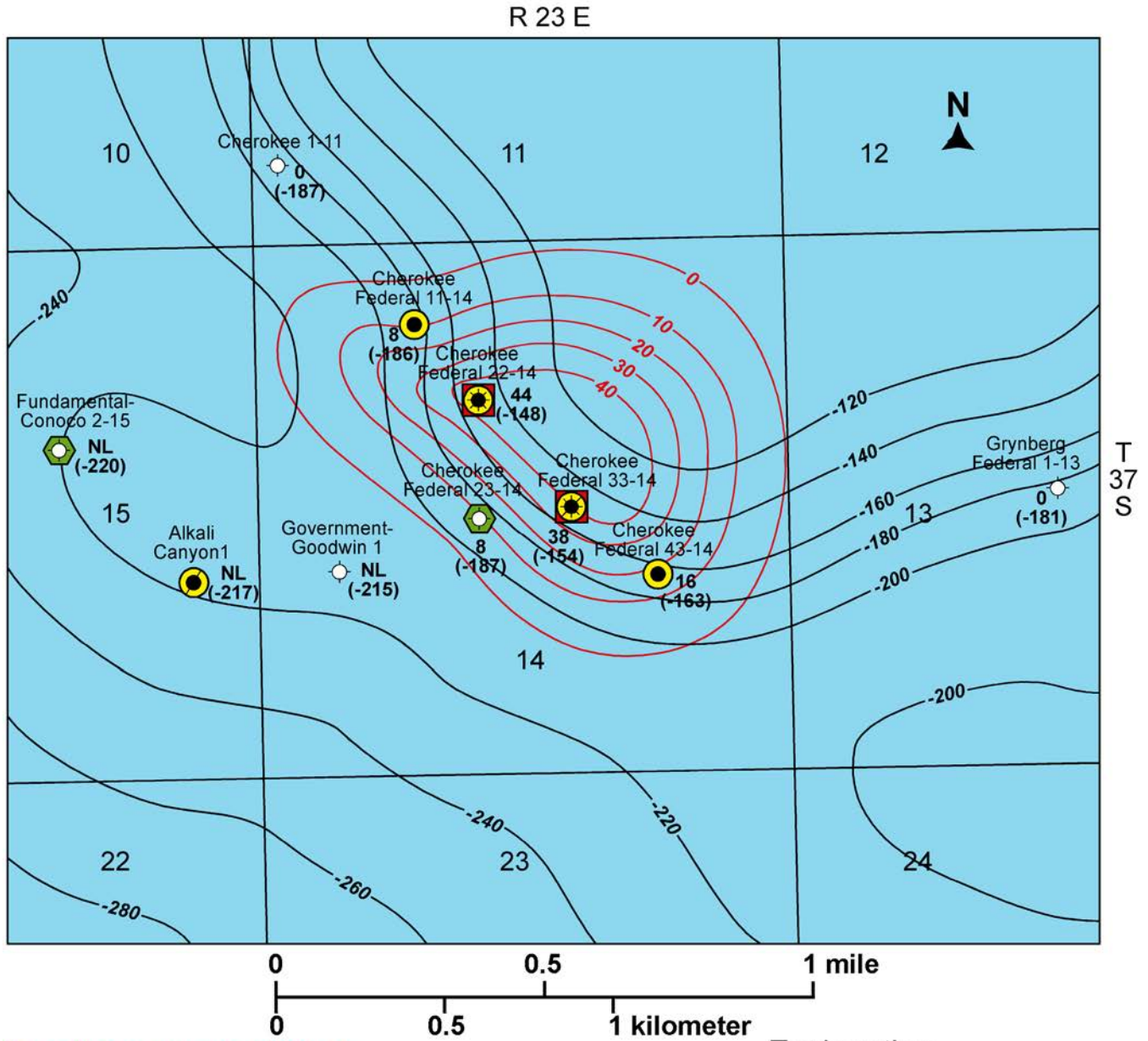
Figure 3.13. *Combined upper Ismay zone structure contour map and isochore map for porosity units 1 through 5, Cherokee field.*
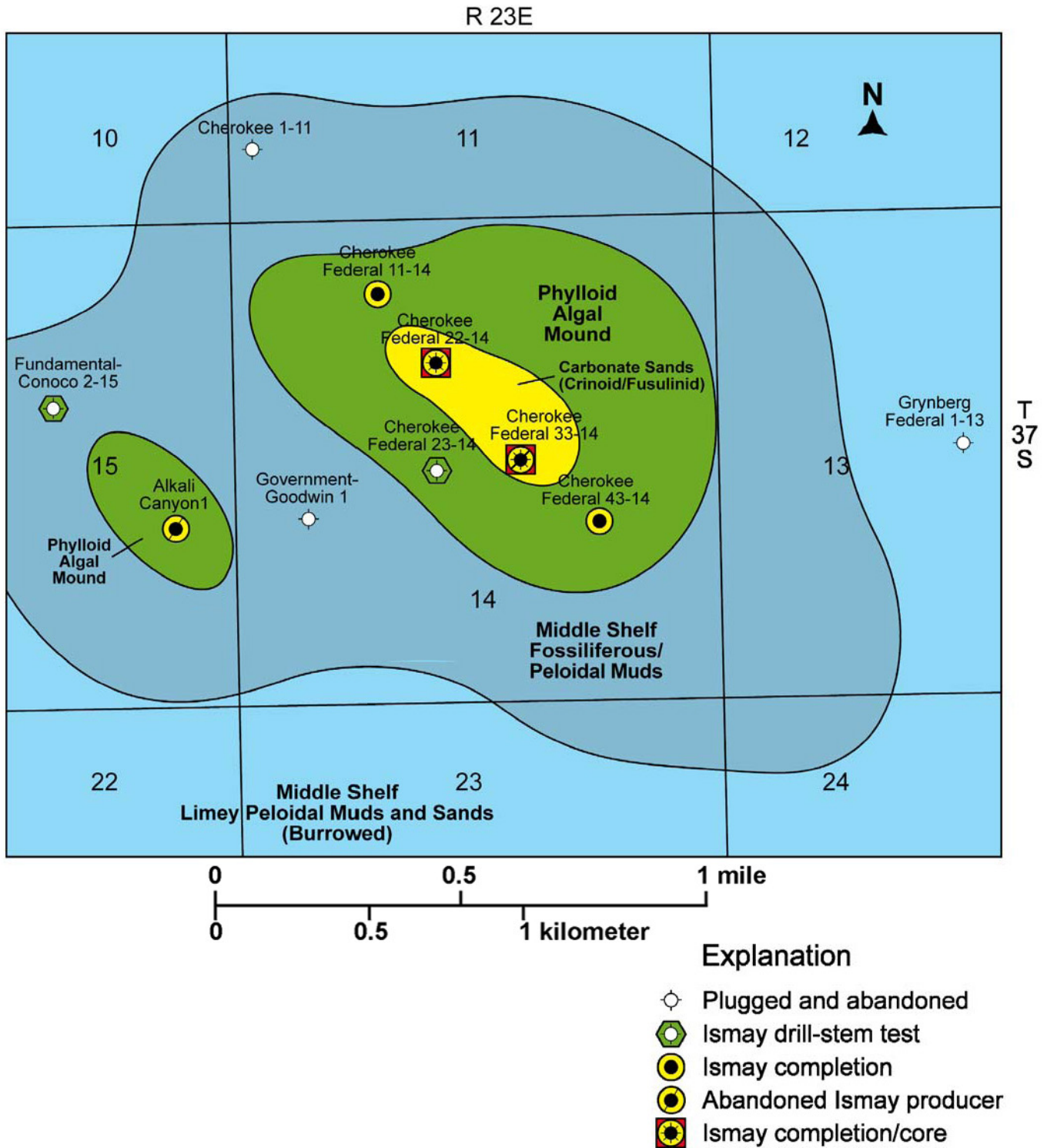
Figure 3.14. *Upper Ismay zone lithofacies map, Cherokee field.*
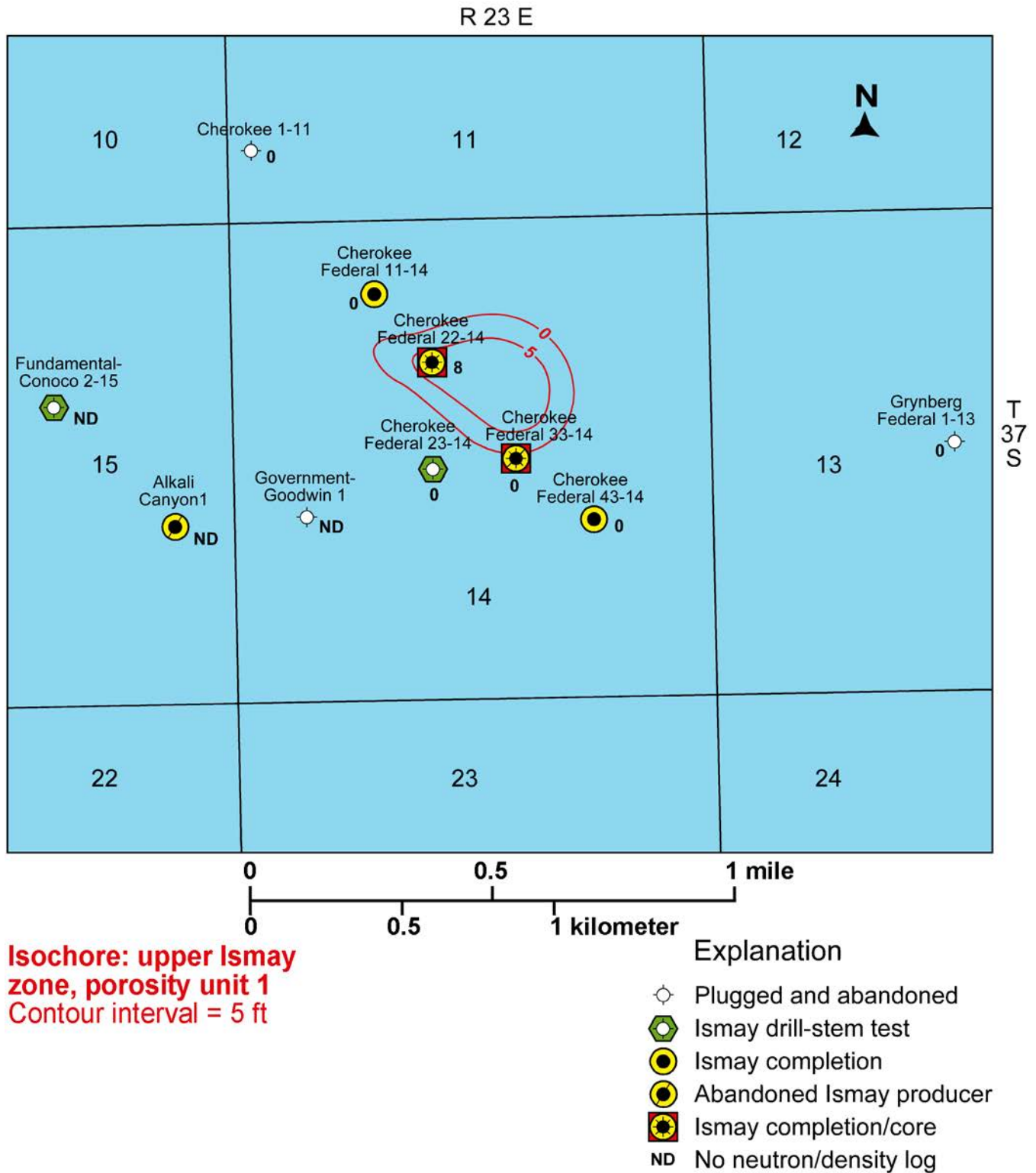
Figure 3.15. *Isochore map for upper Ismay porosity unit 1, Cherokee field.*
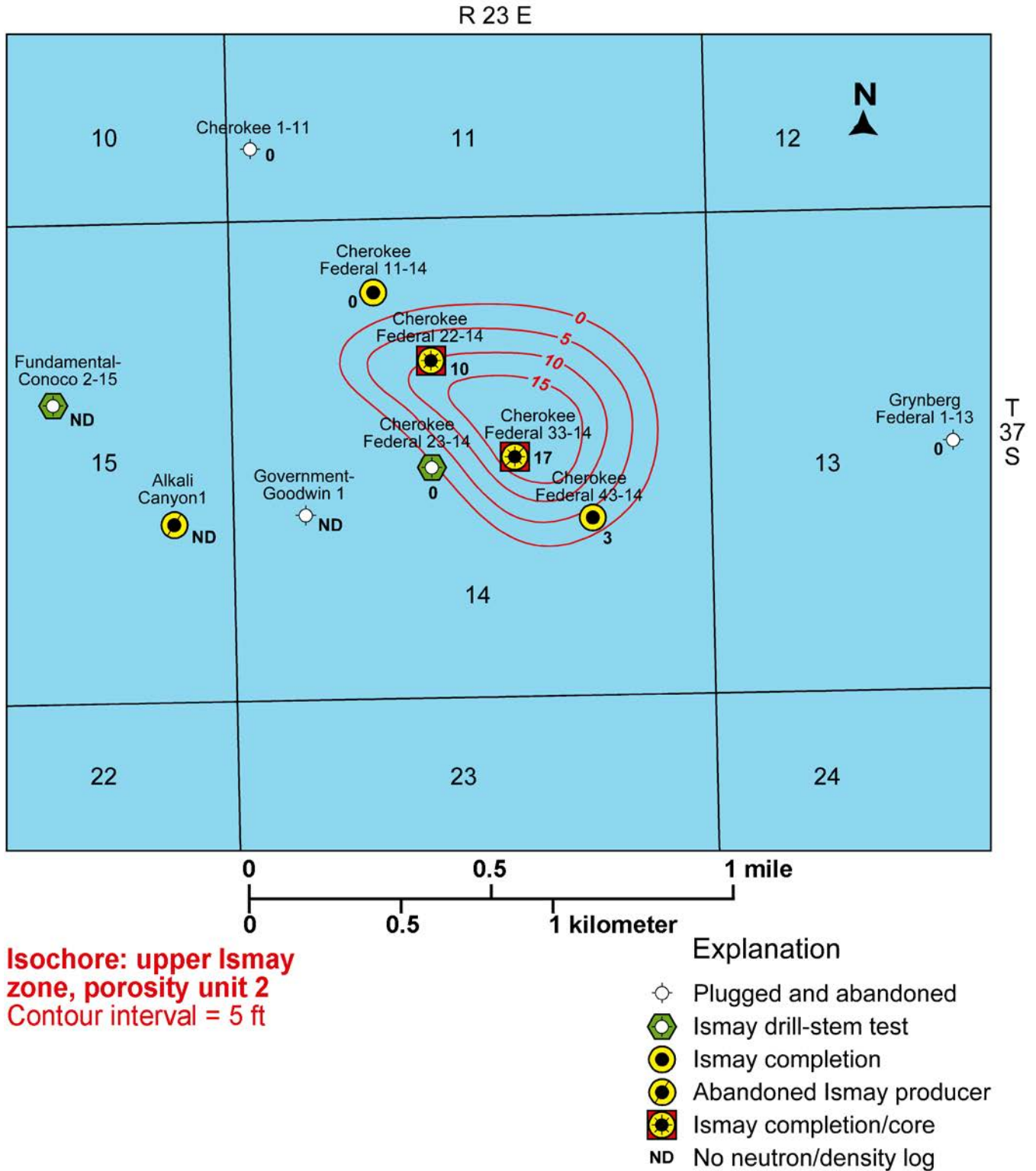
Figure 3.16. *Isochore map for upper Ismay porosity unit 2, Cherokee field.*
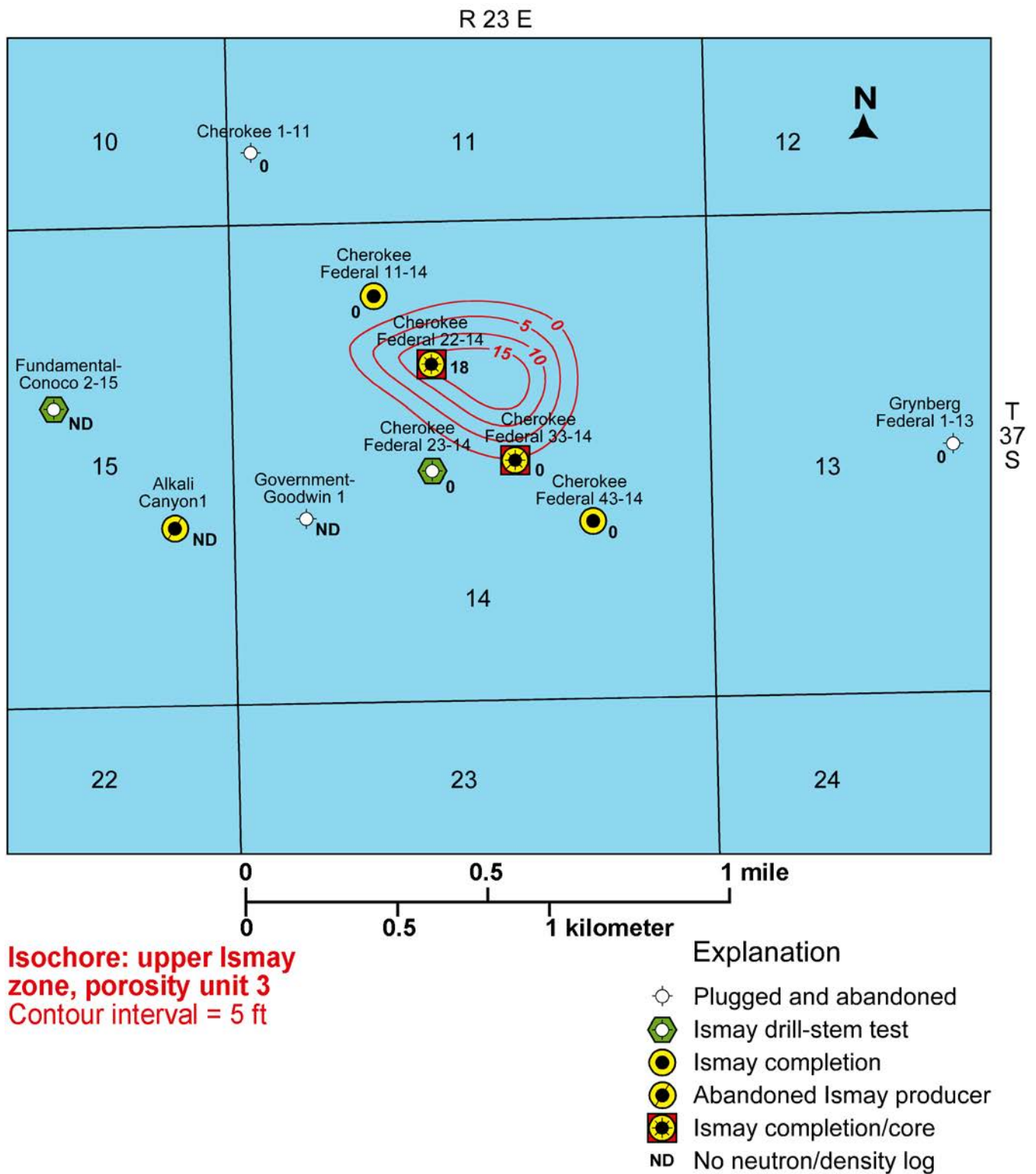
Figure 3.17. *Isochore map for upper Ismay porosity unit 3, Cherokee field.*
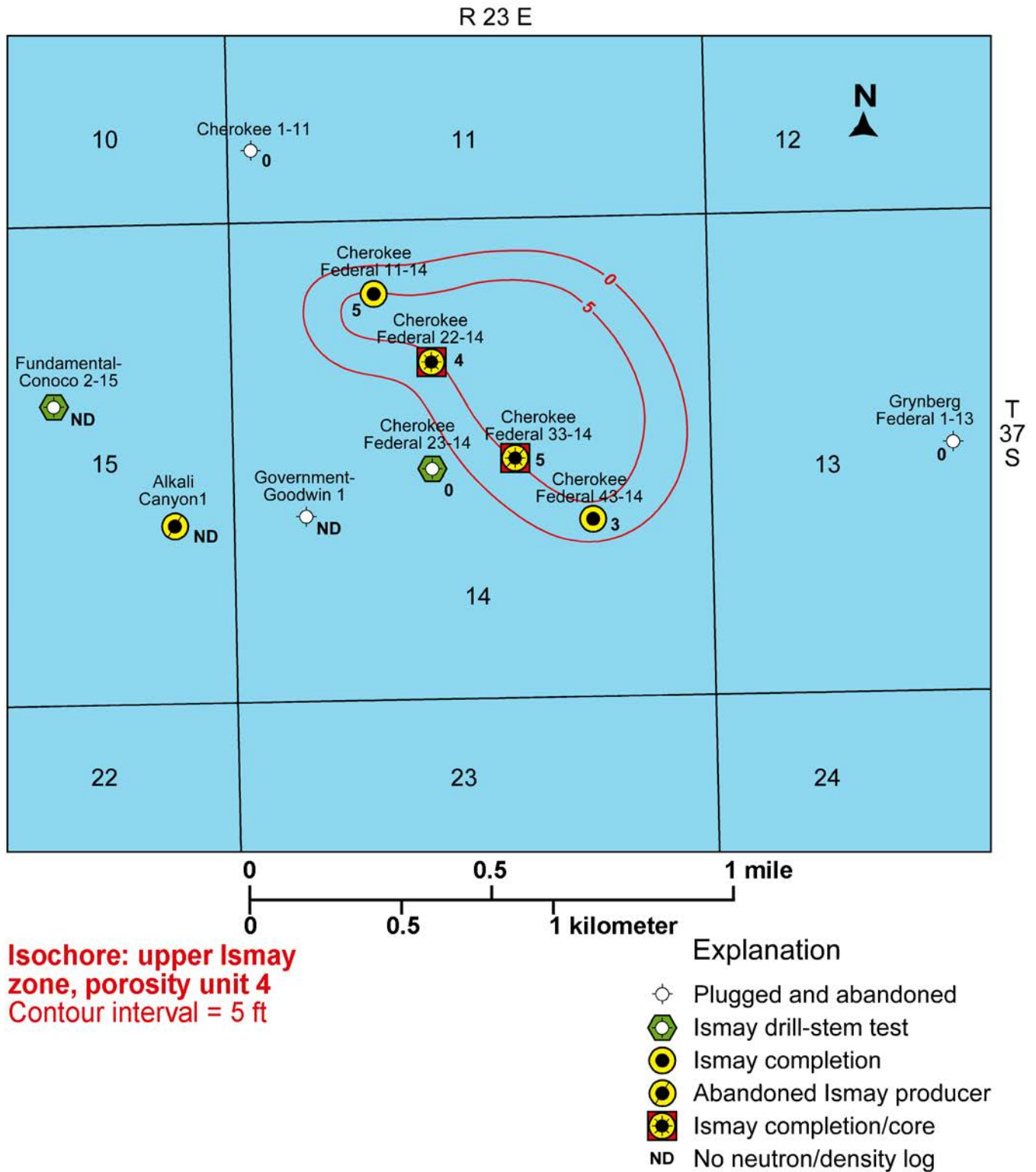
Figure 3.18. *Isochore map for upper Ismay porosity unit 4, Cherokee field.*
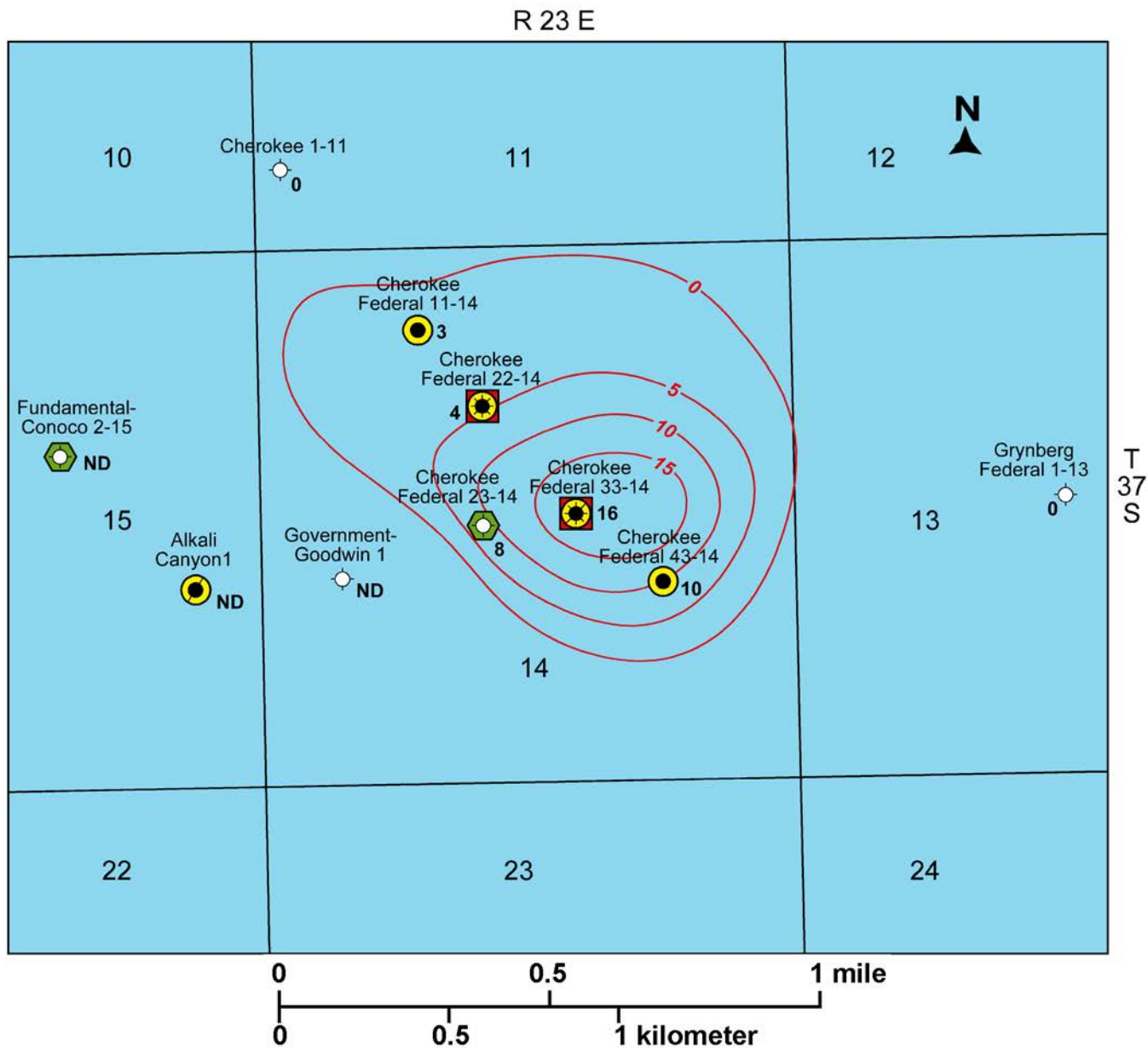
Figure 3.19. *Isochore map for upper Ismay porosity unit 5, Cherokee field.*
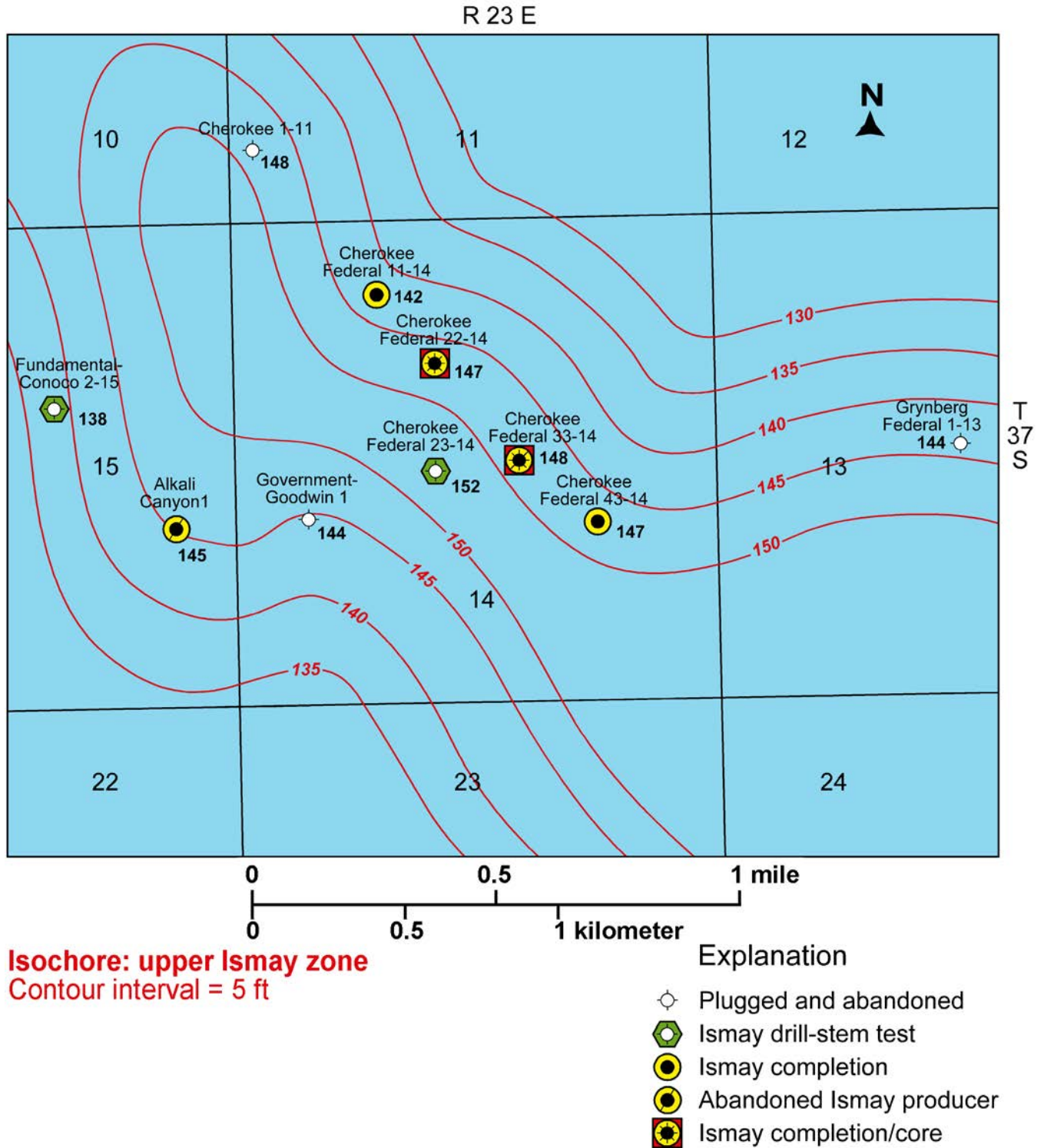
Figure 3.20. Isochore map for upper Ismay zone, Cherokee field.
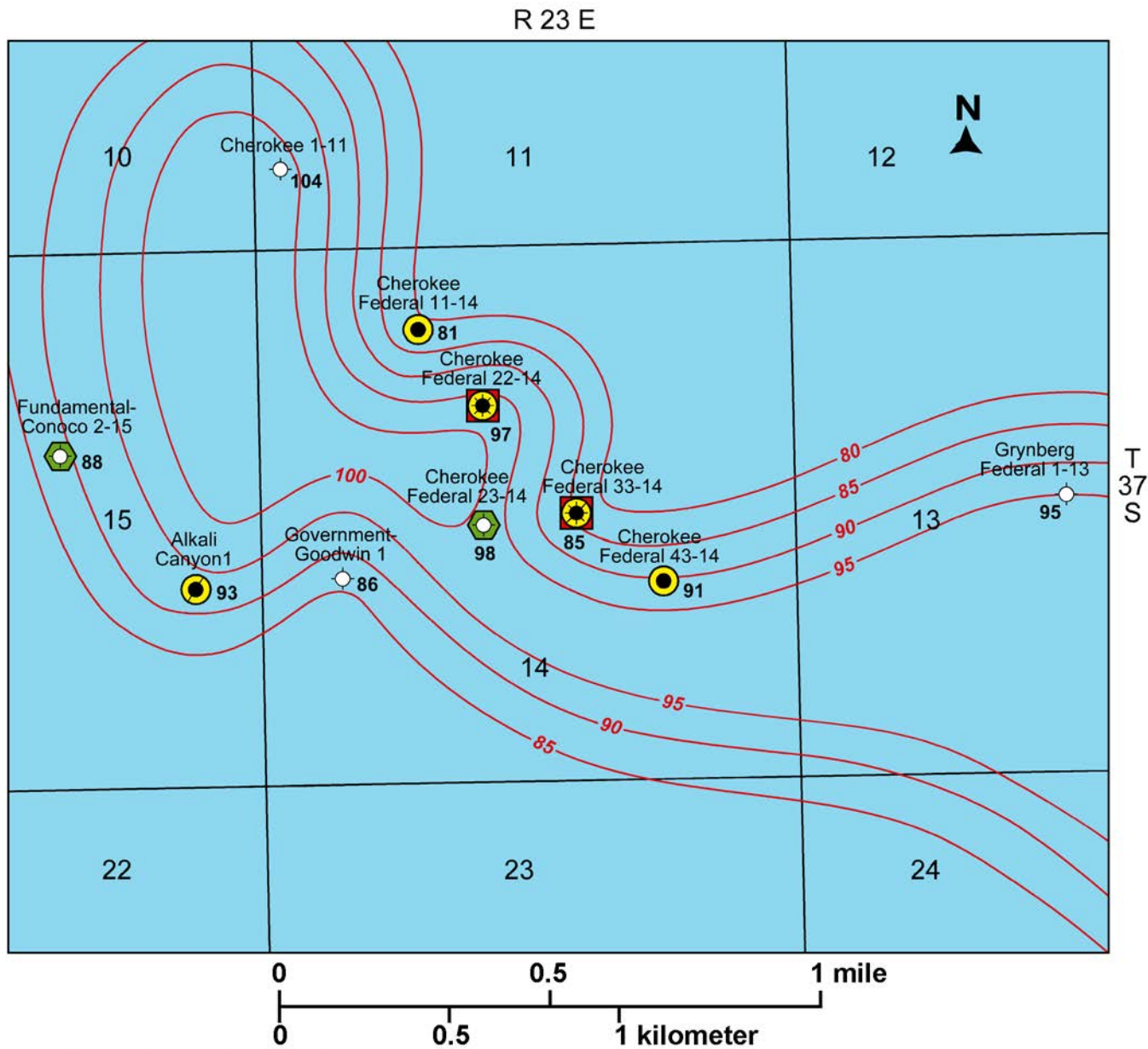
Figure 3.21. Isochore map for upper Ismay clean carbonate, Cherokee field.
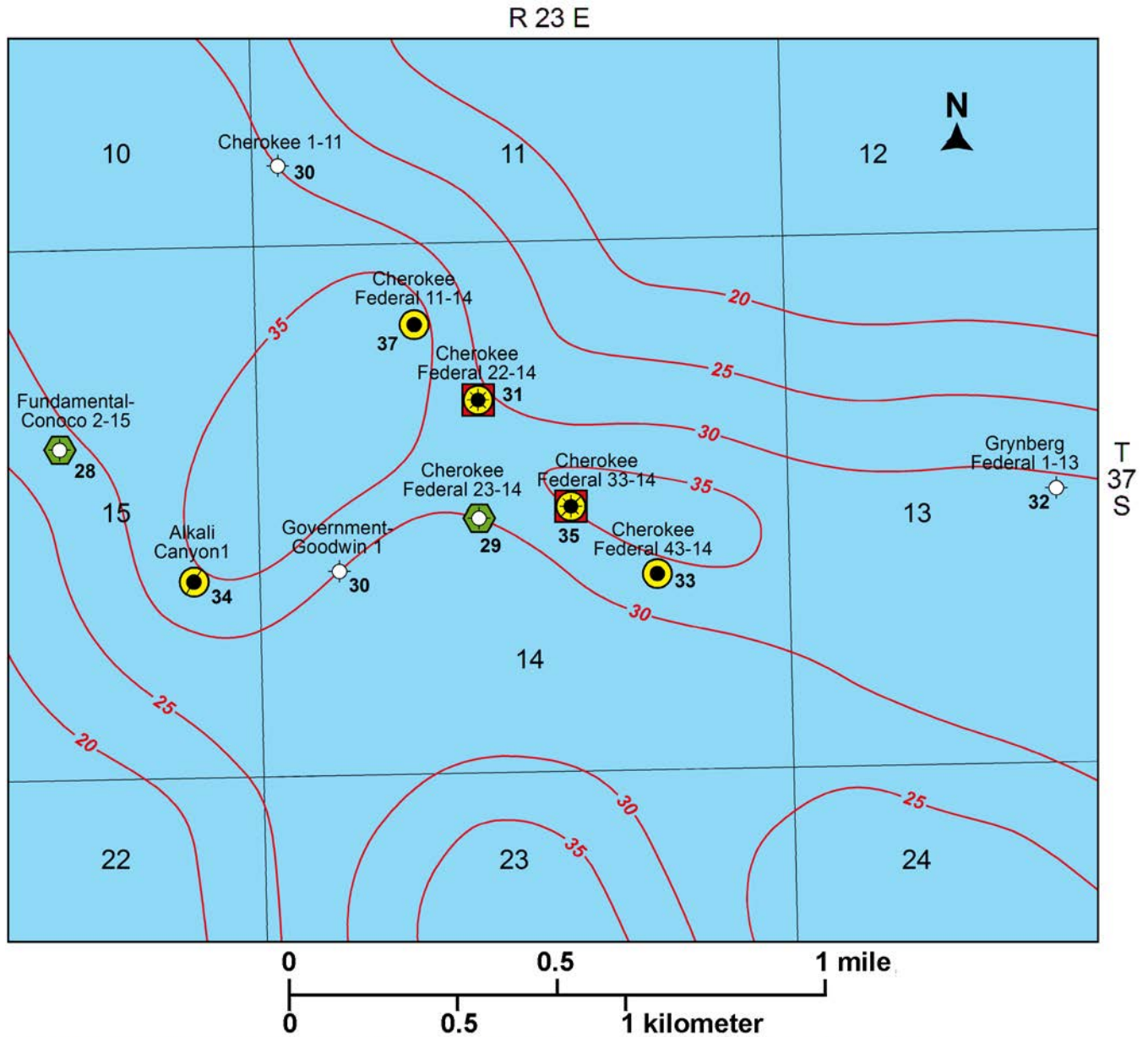
Figure 3.22. *Isochore map for Hovenweep shale of the Ismay zone, Cherokee field.*
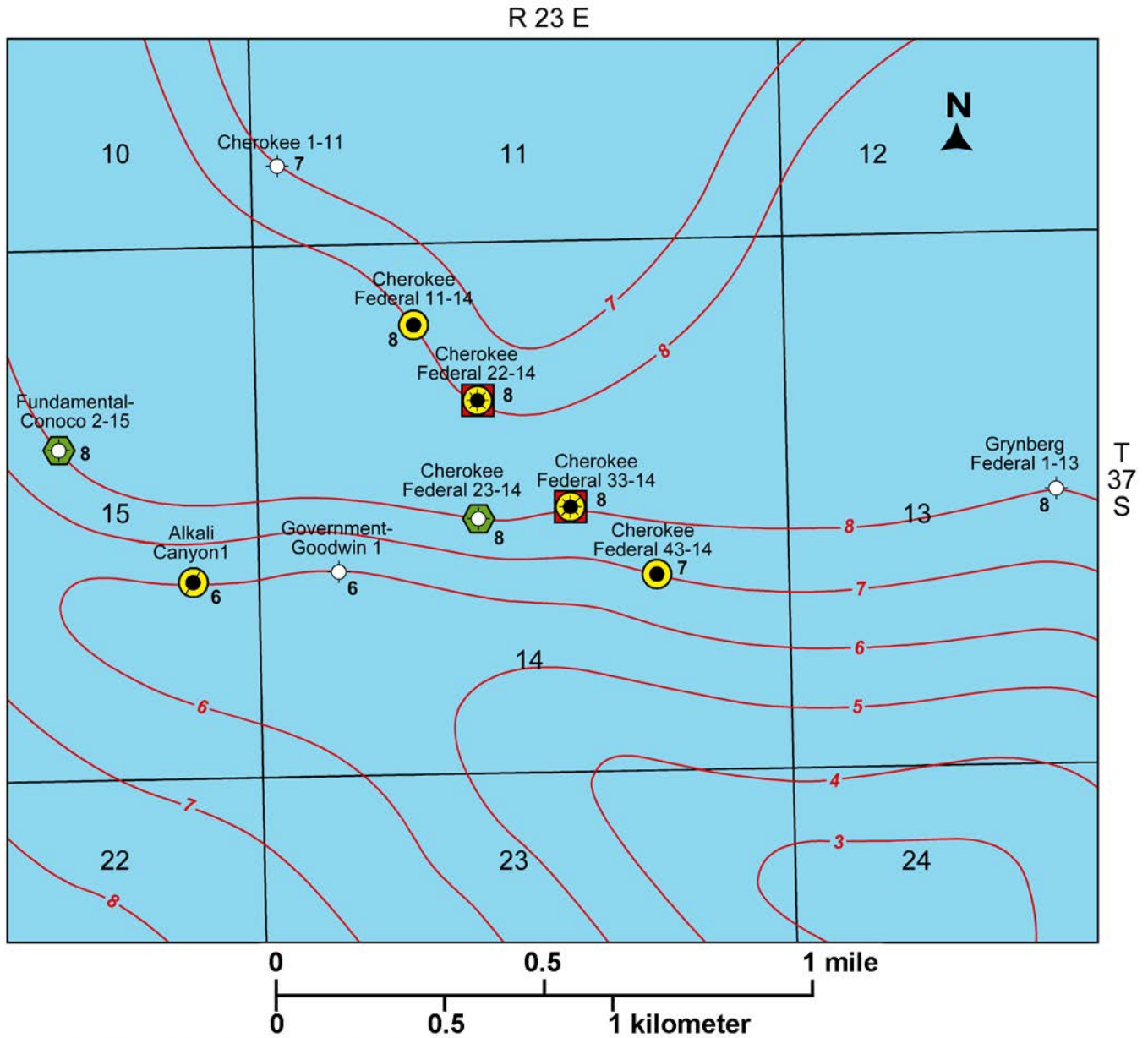
Figure 3.23. *Isochore map for upper Ismay anhydrite, Cherokee field.*

top and interval thickness for each well. These maps were combined to show carbonate buildup trends, define limits of field potential, and indicate possible horizontal drilling targets.

Bug Field

Bug field top of structure and isochore contour maps of the lower Desert Creek zone mound were combined to show the oil/water contact and updip porosity pinchout trap (figure 3.7). A structure contour map on the top of the Chimney Rock shale (the marker bed just below the lower Desert Creek zone) of the Paradox Formation was also constructed for Bug field and combined with the lower Desert Creek zone mound isochore map (figure 3.11). The field limits defined by the isochore maps correspond to the map of porous lithofacies (figure 3.12).

In the lower Desert Creek zone of Bug field, the top of the mound/mound cap interval is equivalent to the top of the clean carbonate interval (figures 2.4 and 2.5; also see appendix A, plates A1-B and A7). In addition, the top mound/mound cap interval is equivalent to the top of the thin off-mound clean carbonate interval. The reservoir porosity unit is the entire mound/mound cap interval.

Cherokee Field

Cherokee field structure contour maps on the top of upper Ismay clean carbonate and the upper Ismay zone were combined with isochore porosity maps of those intervals (figures 3.10 and 3.13). These maps clearly display the equant-shaped carbonate buildup on a gently southwest-plunging structural nose; the trap is especially well defined by the high proved water contact indicated on figure 3.10. These maps also suggest untapped buildup potential to the northeast. The field limits are further defined by the lithofacies map (figure 3.14).

Isochore maps of the upper Ismay zone were generated for five reservoir porosity units containing 6% or higher porosity based on the average of the neutron and density porosity well log values (figures 2.3 and 3.15 through 3.19). Porosity units 1 through 5 are in the upper part of the upper Ismay mound. From geophysical well log analysis, another porosity unit (porosity unit 6 on figure 2.3) is in the lower part of the clean carbonate (i.e., lower part of the upper Ismay). The clean carbonate porosity unit exhibits a "false porosity" on the well logs, which led the operator to perforate the interval and attempt a completion. However, examination of core, thin sections, and porosity and permeability data from core plug analysis shows the unit is incapable of fluid flow due to low permeability. Therefore, porosity units 1 through 5 were mapped together to produce a gross interval isochore (figure 3.13), which represents the actual producing reservoir. Isochore maps were also constructed for the entire upper Ismay zone, upper Ismay clean carbonate, Hovenweep shale, and upper Ismay anhydrite (figures 2.3 and 3.20 through 3.23). The latter two units represent effective seals.

RESERVOIR DIAGENETIC ANALYSIS

The diagenetic fabrics and porosity types found in the various hydrocarbon-bearing rocks of the case-study fields can be indicators of reservoir flow capacity, storage capacity, and potential for horizontal drilling. To determine the diagenetic histories of the various Ismay and Desert Creek reservoirs, thin sections of representative samples were selected from the conventional cores of each field for petrographic description and possible geochemical analysis (appendix F). Carbonate fabrics were again determined according to Dunham's (1962) and Embry and Klovan's (1971) classification schemes. Each thin section was photographed with additional close-up photos of (1) typical preserved primary and secondary pore types, (2) cements, (3) sedimentary structures, (4) fractures, and (5) pore plugging anhydrite and halite. Porosity types and associated abbreviations used in this chapter are from Choquette and Pray (1970) (figure 3.24).

Reservoir diagenetic fabrics and porosity types of these carbonate buildups were analyzed to determine the sequence of diagenetic events and predict lithofacies patterns. Diagenetic characterization focused on reservoir heterogeneity, quality, and compartmentalization within the case-study fields. All depositional, diagenetic, and porosity information can be combined with each field's production history to analyze the potential for success of each horizontal drilling candidate. Of special interest is the determination of the most effective pore systems for oil drainage versus storage.

Bug and Cherokee fields were also selected for additional petrographic, geochemical, and petrophysical techniques (described in later chapters). These techniques included (1) scanning electron microscope analysis of various dolomites to determine reservoir quality of the dolomites as a function of diagenetic history, (2) epifluorescence and cathodoluminescence petrography for the sequence of diagenesis, (3) stable carbon and oxygen isotope analysis of diagenetic components such as cementing minerals and different generations of dolomites, and (4) capillary pressure/mercury injection analysis.

Bug Field

The lower Desert Creek zone in Bug field consists entirely of dolomite. In thin section, the phylloid-algal mound is represented by bafflestone consisting of in-place algal plates grading into early-marine micrite or botryoidal (aragonite) cements; primary shelter pores can be preserved and micrite rims mark the outlines of former phylloid plates (figure 3.25). The pore system observed in thin section also shows a reservoir that has been predominantly affected by subaerial exposure. Solution-enlarged grain molds and vugs (sometimes originally phylloid-algal plates) and fractures are common; these and other types of pores are often lined with dogtooth spar (figure 3.25A). The remaining matrix typically consists of low-permeability dolomite. Remnants of primary, interpar-

BASIC POROSITY TYPES

FABRIC SELECTIVE

	INTERPARTICLE	BP
	INTRAPARTICLE	WP
	INTERCRYSTAL	BC
	MOLDIC	MO
	FENESTRAL	FE
	SHELTER	SH
	GROWTH-FRAMEWORK	GF

NOT FABRIC SELECTIVE

	FRACTURE	FR
	CHANNEL*	CH
	VUG*	VUG
	CAVERN*	CV

*Cavern applies to human-sized or larger pores of channel or vug shapes.

FABRIC SELECTIVE OR NOT

BRECCIA BR	BORING BO	BURROW BU	SHRINKAGE SK

MODIFYING TERMS

GENETIC MODIFIERS

PROCESS

SOLUTION	s
CEMENTATION	c
INTERNAL SEDIMENT	i

DIRECTION OR STAGE

ENLARGED	x
REDUCED	r
FILLED	f

TIME OF FORMATION

PRIMARY	P
pre-depositional	Pp
depositional	Pd
SECONDARY	S
eogenetic	Se
mesogenetic	Sm
telogenetic	St

Genetic modifiers are combined as follows:

[PROCESS] + [DIRECTION] + [TIME]

EXAMPLES:
solution-enlarged	sx
cement-reduced primary	crP
sediment-filled eogenetic	ifSe

SIZE* MODIFIERS

CLASSES				mm†
				256
MEGAPORE	mg	large	lmg	
		small	smg	32
				4
MESOPORE	ms	large	lms	
		small	sms	1/2
				1/16
MICROPORE	mc			

Use size prefixes with basic porosity types:
mesovug	msVUG
small mesomold	smsMO
microinterparticle	mcBP

*For regular-shaped pores smaller than cavern size.

†Measures refer to average pore diameter of a single pore or the range in size of a pore assemblage. For tubular pores use average cross-section. For platy pores use width and note shape.

ABUNDANCE MODIFIERS

percent porosity	(15%)
or	
ratio of porosity types	(1:2)
or	
ratio and percent	(1:2) (15%)

Figure 3.24. *Classification of pores and pore systems in carbonate rocks (after Choquette and Pray, 1970).*

A.
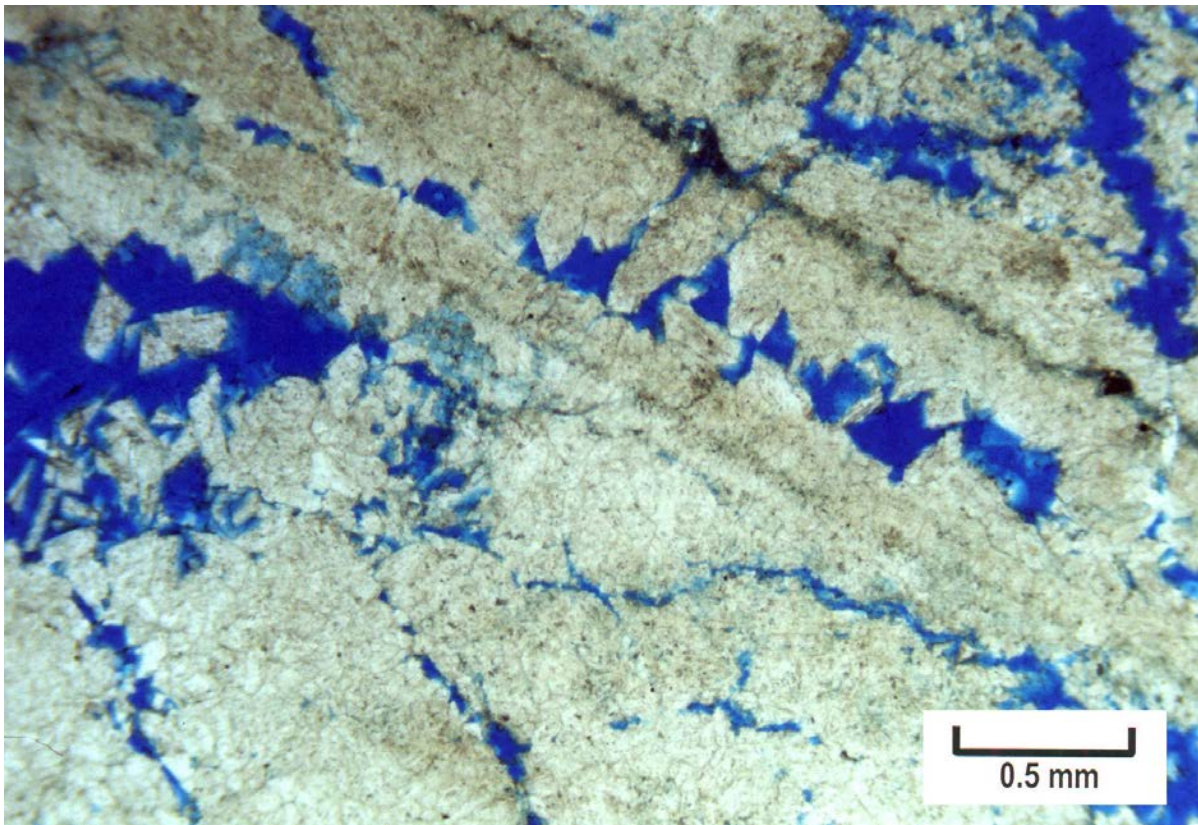
B.
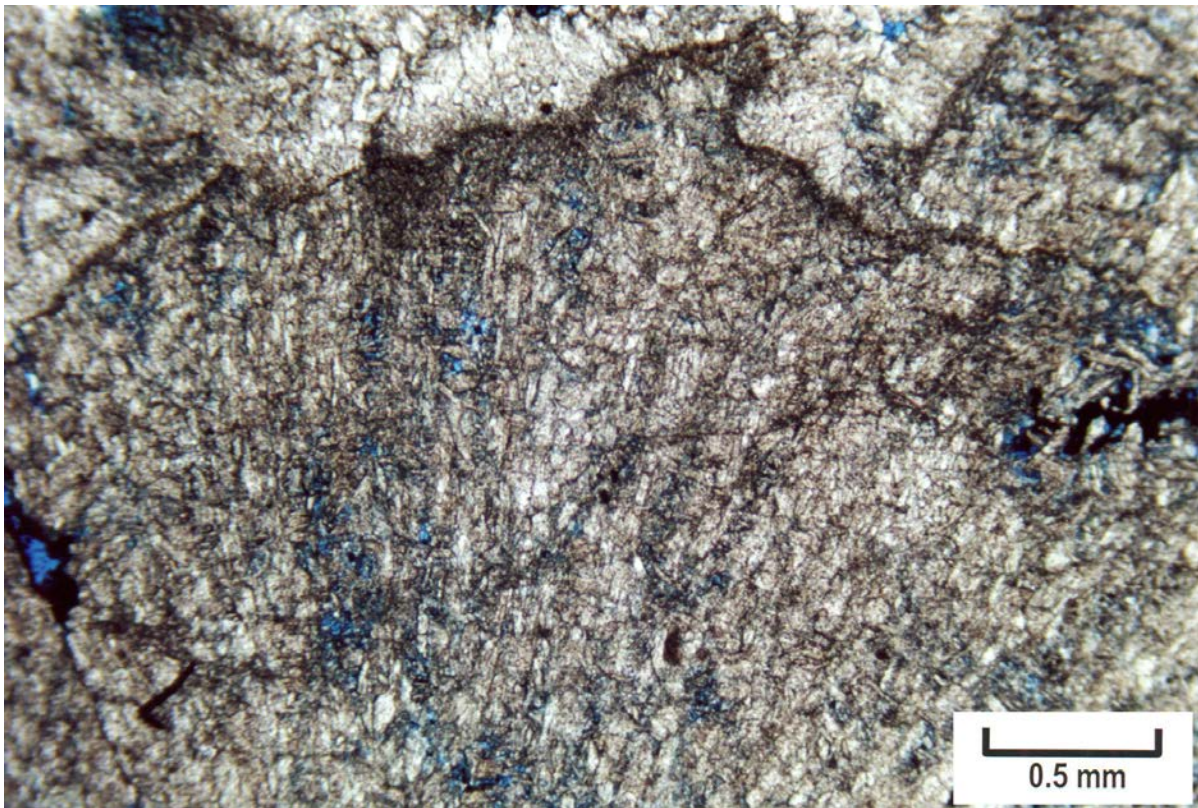
Figure 3.25. Photomicrographs (plane light) of diagenetic characteristics of phylloid-algal bafflestone, Desert Creek zone, Bug field. (A) Dolomitized phylloid-algal plates, grading into early-marine cement (micrite rims that mark the outlines of a former phylloid plates), and remnant primary shelter pores lined with freshwater dogtooth spar; May-Bug No. 2 well, 6304 feet (1921 m), porosity = 10.9%, permeability = 99 mD. (B) Phylloid-algal plates with bladed botryoidal early marine cement and later dissolution; Bug No. 4 well, section 16, T. 36 S., R. 26 E., SLBL&M, 6289.7 feet (1917.1 m), porosity = 14.5%, permeability = 92 mD.

ticle pores are also observed between small pisolites/peloids and grain aggregates; the remaining matrix typically consists of low-permeability dolomite (figure 3.26). Soil pisolites indicate subaerial exposure of the mound cap. Pores are often lined or plugged with anhydrite cements or late black bitumen (figure 3.26). The result is that both effective and ineffective pores are present. The extensive dolomitization has also created some intercrystalline and micro-intercrystalline porosity.

The most significant and unique diagenetic characteristic observed in the Bug field thin sections was extensive "micro-boxwork" porosity. Figure 3.27 shows the pattern of patchy dolomite dissolution which includes a micro-boxwork pattern of pores. These pores occur between elongate, rectilinear networks of dolomite "lathes." Some late anhydrite and bitumen plugging may be present in some intervals (figure 3.27). Our interpretation is that the intense micro-boxwork porosity developed early from subaerial exposure of the phylloid-algal buildup. The micro-boxwork porosity represents an important site for untapped hydrocarbons.

Cherokee Field

The upper Ismay zone in Cherokee field consists of both limestone and dolomite, although there appears to be more dolomite in core than observed in thin section. Petrographic analysis shows the typical mound-lithofacies limestone consists of skeletal phylloid-algal bafflestone with fibrous fans of early-marine magnesium calcite cement with anhydrite plugging pore space (figure 3.28A). The calcarenite lithofacies consists of skeletal grainstone limestone, with primary interparticle and intraparticle porosity, and early moldic porosity (figure 3.28B). Some early mixing-zone dolomitization (often micritic, figure 3.29A) and dogtooth spar (meteoric cement) are present (figure 3.29B). The low-energy, middle-shelf lithofacies typically consists of dolomite, packstone/wackestone, with peloids, crinoids, and bryozoans. Late solution-enlarged molds or channels, and anhydrite and bitumen plugging are common.

The most significant and unique diagenetic characteristic observed in the Cherokee field thin sections is extensive microporosity (figure 3.30A). In fact, much of the "dolomite" observed on the slabbed surface of the core is the result of alteration that features microporosity. The sequence of diagenetic events consisted of (1) early dolomitization by hypersaline or mixing zone brines, (2) stylolitization, (3) late dissolution/micropores, (4) anhydrite replacement, and (5) bitumen plugging. There were two generations of oil migration—the first was thermally altered ("cooked" out) leaving pyrobitumen (solid) bridging micro-intercrystalline porosity, then the second generation of oil migrated into the smaller pore throats. Some fracturing is also present.

We believe the intense microporosity developed late, along solution fronts by the action of aggressive hydrothermal solutions from depth, carbon dioxide escaping from the Mississip-

pian Leadville Limestone, or deep decarboxylation of organic matter (figure 3.30B). At any rate, like the microporosity in Bug field, this microporosity represents an important site for untapped hydrocarbons.

POROSITY AND PERMEABILITY CROSSPLOTS

Porosity and permeability data from core plugs were available from five of the eight Bug wells that were cored and the two cored Cherokee wells (table 3.1). Crossplots of these data are used to (1) determine the most effective pore systems for oil storage versus drainage, (2) identify reservoir heterogeneity, (3) predict potential untested compartments, (4) infer porosity and permeability trends where core-plug data are not available, and (5) match diagenetic processes, pore types, mineralogy, and other attributes to porosity and permeability distribution. Approximately 50 porosity and permeability crossplots were constructed using the available data (appendix G). Data classes within the plots included perforated limestone intervals, perforated dolomite intervals, total perforated intervals, reservoir lithofacies, carbonate fabric, pore type, and core with a 6% porosity cutoff.

Bug Field

The graph for the May-Bug No. 2 well from Bug field indicates that those samples representing intercrystalline porosity with micro-boxwork dolomite have the best reservoir potential (figure 3.31). The dominant lithofacies types (mound/breccia, calcarenites, and open marine and middle/inner shelf) were also assigned to each porosity/permeability data point (figure 3.32); however, no specific trend between lithofacies type and porosity/permeability was identified. In general, the better reservoir qualities are found in mound/breccia lithofacies. Thus, our initial conclusion is that the reservoir quality of the rocks in Bug field is most dependent on pore types and diagenesis.

Cherokee Field

In general, analysis of these plots for Cherokee field shows that those zones that have been dolomitized have better reservoir potential than those that remain limestone (figure 3.33). The dominant pore type (microporosity/channel, moldic, intercrystalline, interparticle, and shelter/vuggy) was assigned to each porosity/permeability data point and the data were crossplotted (figure 3.34). The graph for the Cherokee Federal No. 22-14 well from Cherokee field indicates that those samples representing microporosity have the best reservoir potential, whereas those representing intercrystalline porosity have the poorest reservoir potential. Finally, in Cherokee field better reservoir qualities are generally found in calcarenite lithofacies. As with Bug field, our conclusion is that the reservoir quality of the rocks in Cherokee field is most dependent on pore types and diagenesis.

A.

B.
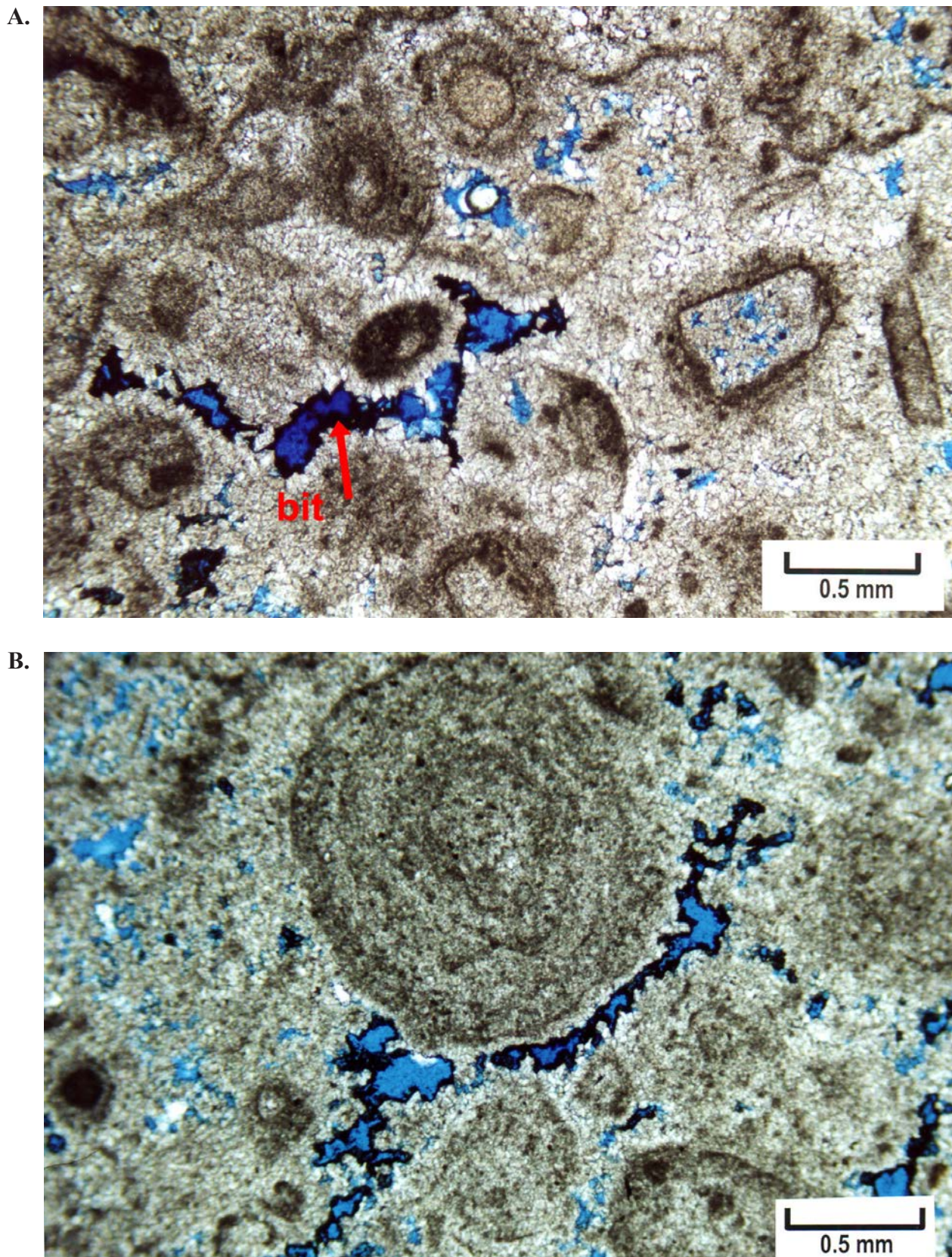
Figure 3.26. *Photomicrographs (plane light) of diagenetic characteristics of pisolitc/peloidal grainstone/packstone of the mound cap, Desert Creek zone, Bug field.* ***(A)*** *Skeletal peloidal grainstone/packstone in a dolomite matrix showing a few remnant interparticle pores (blue) lined with black bitumen (bit); Bug No. 4 well, 6284.2 feet (1915.4 m), porosity = 6.9%, permeability = 2.5 mD.* ***(B)*** *Pisolitic/peloidal grainstone in a dolomite matrix with micro-intercrystalline porosity and solution-enlarged channels and remnant interparticle pores lined with black bitumen; Bug No.13 well, 5930.6 feet (1807.6 m), porosity = 9.3%, permeability = 15 mD.*

A.
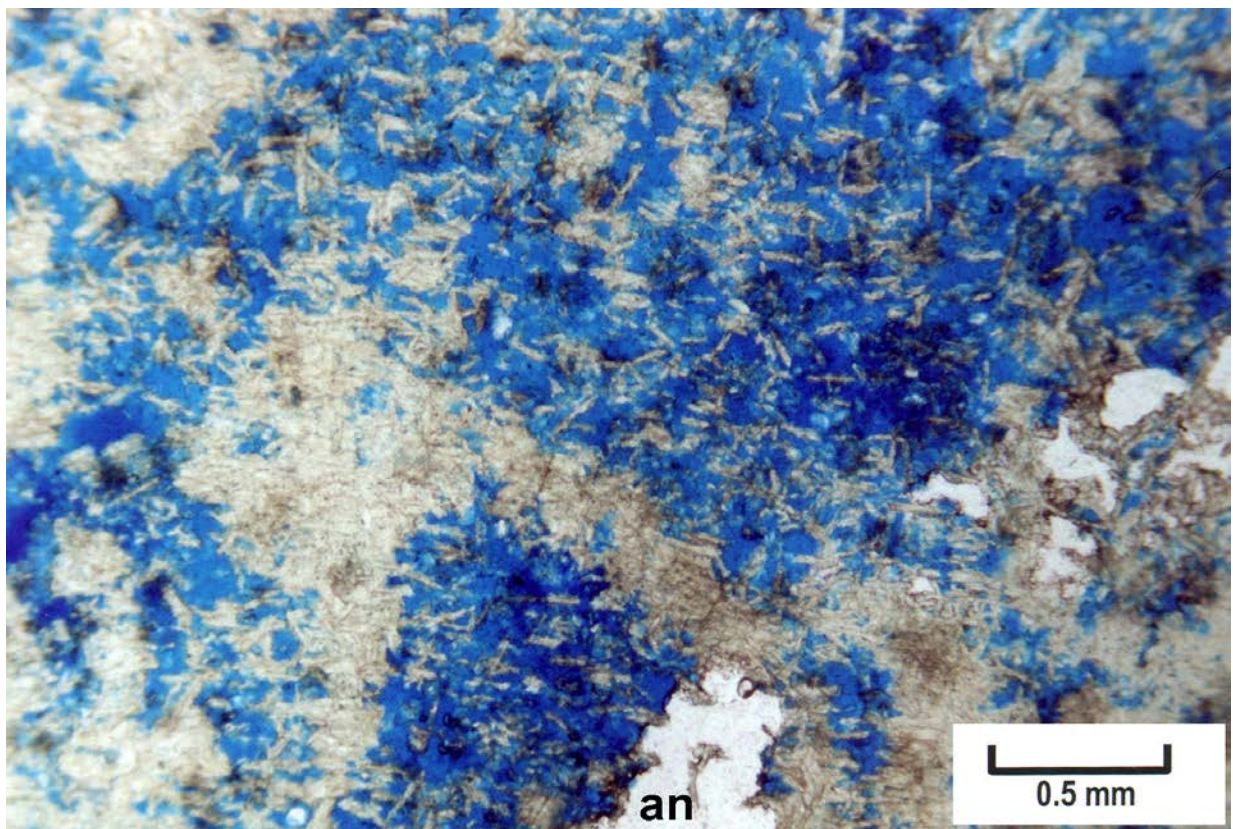
B.
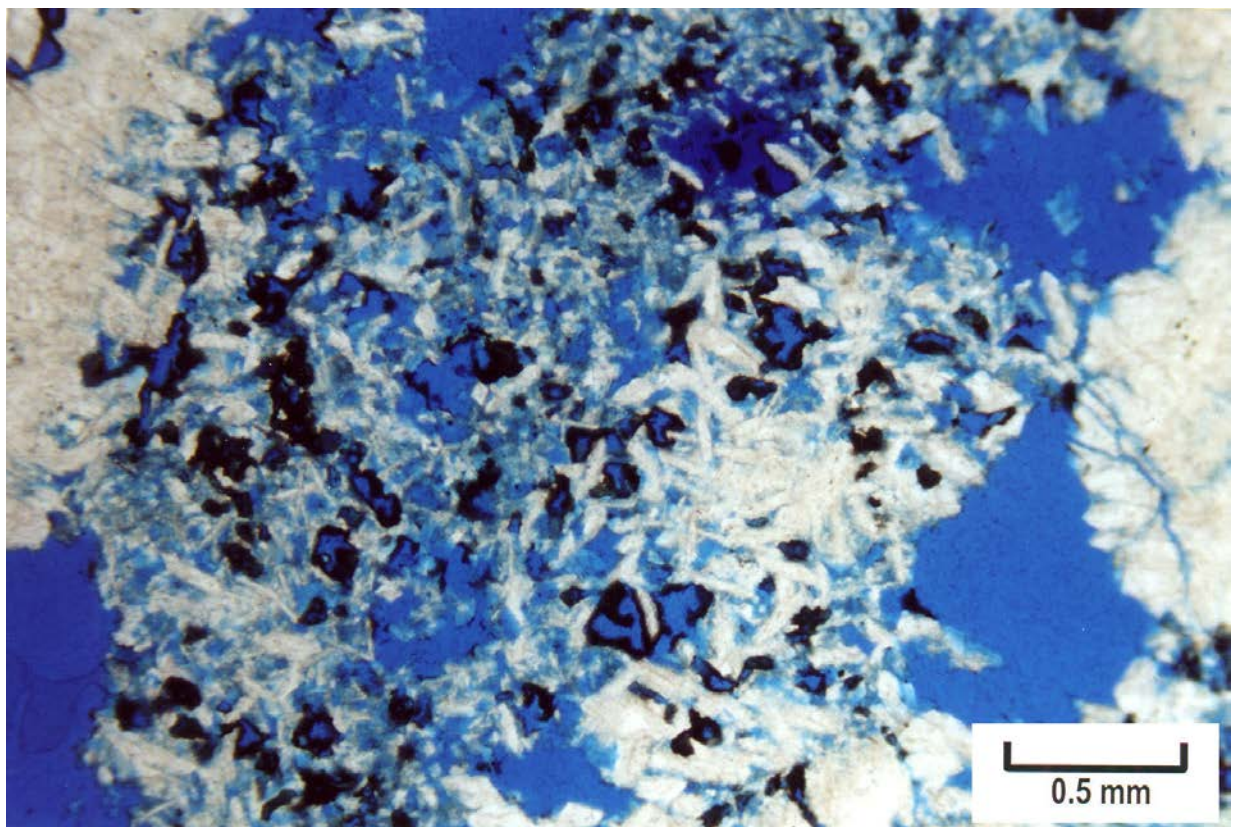
Figure 3.27. *Photomicrographs (plane light) of "micro-boxwork" porosity, Desert Creek zone, Bug field. **(A)** Patchy dolomite dissolution which produces a micro-boxwork pattern of pores (in blue) and dolomite lathes with some late anhydrite replacement (an); Bug No. 10 well, 6327.5 feet (1928.6 m), porosity = 10.5%, permeability = 7.5 mD. **(B)** Extensive micro-boxwork porosity with some hollow dolomites and pores lined or plugged with bitumen; Bug No. 4 well, 6289.7 feet (1917.1 m), porosity = 14.5%, permeability = 92 mD.*

A.

B.
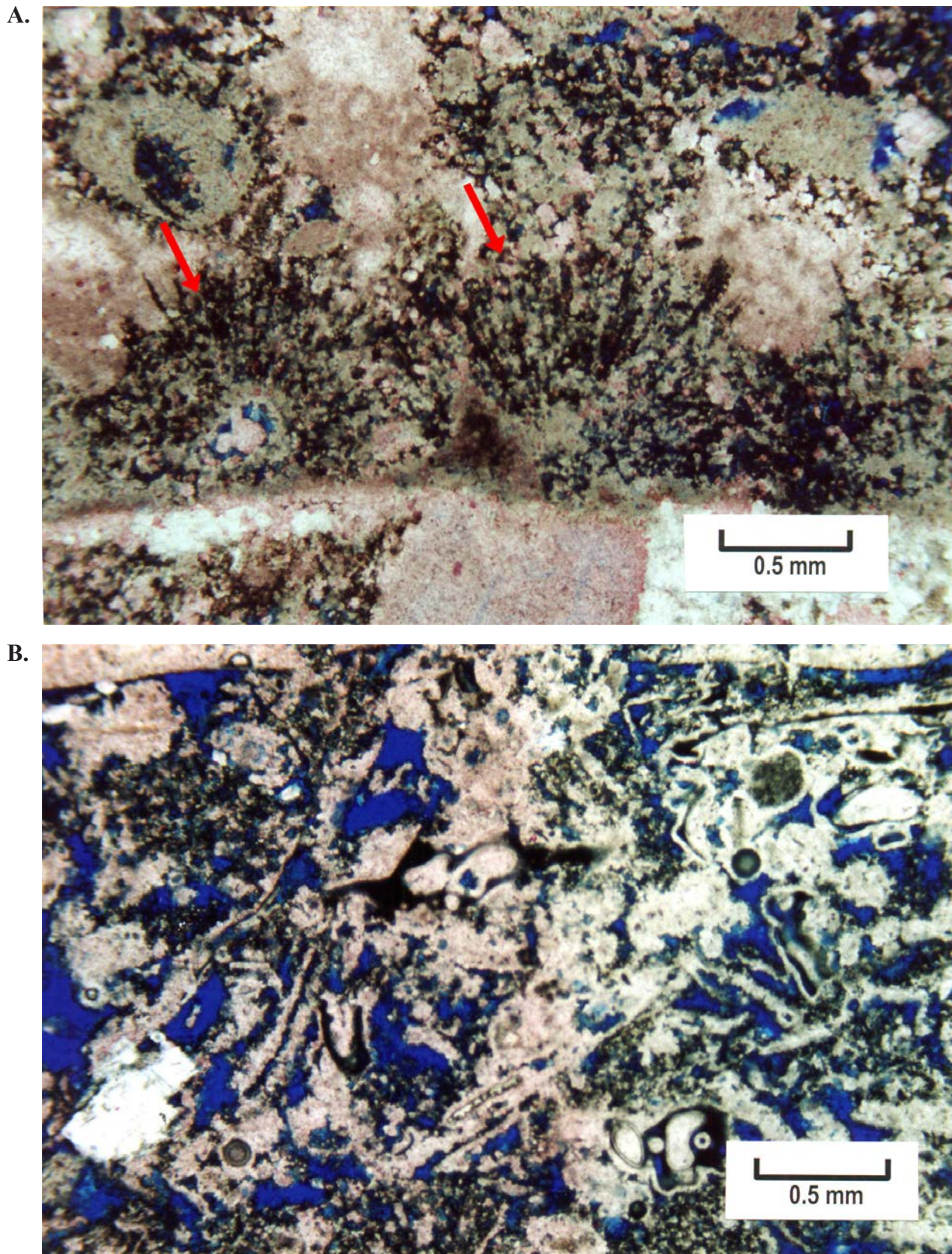
Figure 3.28. Photomicrographs (plane light) of early-marine cementation and moldic porosity, Ismay zone, Cherokee Federal No. 22-14 well, Cherokee field. (A) Dolomitic limestone, phylloid-algal bafflestone with encrusting forams and fibrous fans of early-marine calcite cement along phylloid plates (red arrows) that show corroded dissolution porosity and late anhydrite and bitumen plugging; 5821.2 feet (1774.3 m), porosity = 8.5%, permeability = 0.8 mD. (B) Skeletal limestone, grainstone having primary interparticle and intraparticle porosity as well as early dissolution molds; 5833.4 feet (1778.0 m), porosity = 14.7%, permeability = 4.7 mD.

A.
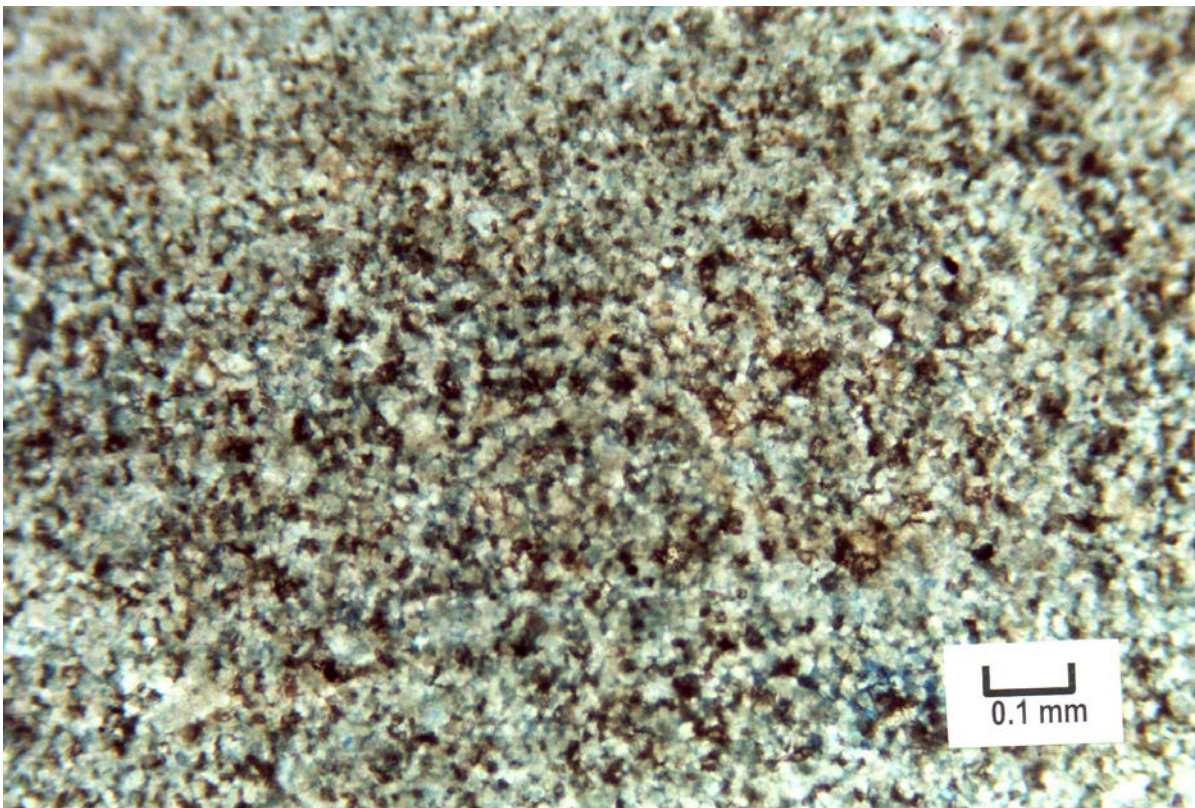
B.
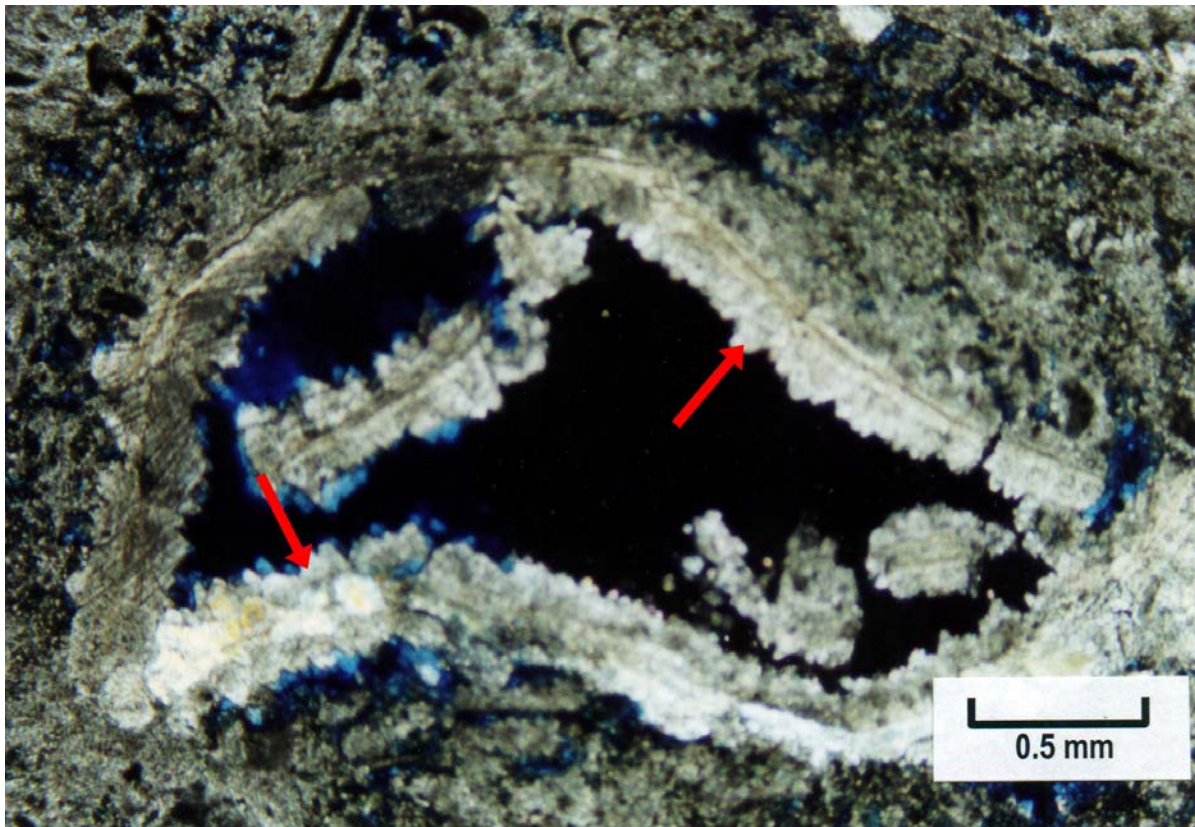
Figure 3.29. *Photomicrographs (plane light) of early dolomitization and meteoric cement, Ismay zone, Cherokee field. **(A)** Early micritic dolomite, mudstone to wackestone, completely altered by late-stage dissolution with some late anhydrite replacement and a great amount of bitumen; Cherokee Federal No. 33-14 well, 5781.2 feet (1762.1 m), porosity = 23.5%, permeability = 103 mD. **(B)** Large moldic pore from the same skeletal grainstone shown on figure 3.28B, lined with meteoric dogtooth sparry calcite cement (red arrows).*
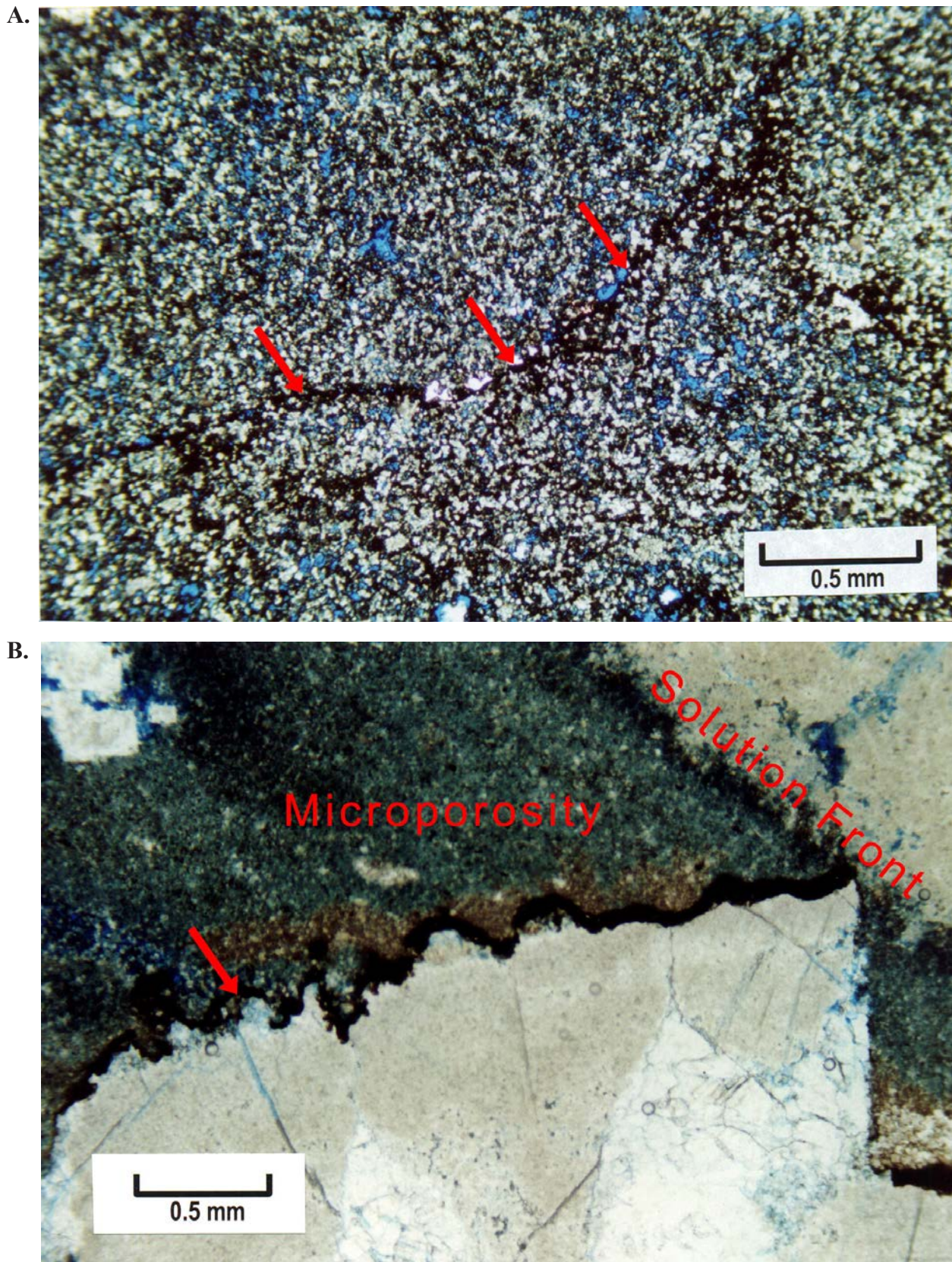
Figure 3.30. *Photomicrograph (plane light) of microporosity, Ismay zone, Cherokee Federal No. 22-14 well, Cherokee field.* **(A)** *Dolomitic peloidal packstone/grainstone dominated by late dissolution and microporosity with extensive bitumen plugging (red arrows indicate possible remnant dissolution front); 5768.7 feet (1758.3 m), porosity = 22.9%, permeability = 215 mD.* **(B)** *Dolomitic wackestone with bitumen-lined stylolite (red arrow), solution front, patchy microporosity with intense bitumen plugging (dark clay-looking material), and pseudo brecciation; 5801.3 feet (1768.2 m), porosity = 18.4%, permeability = 8.3 mD.*
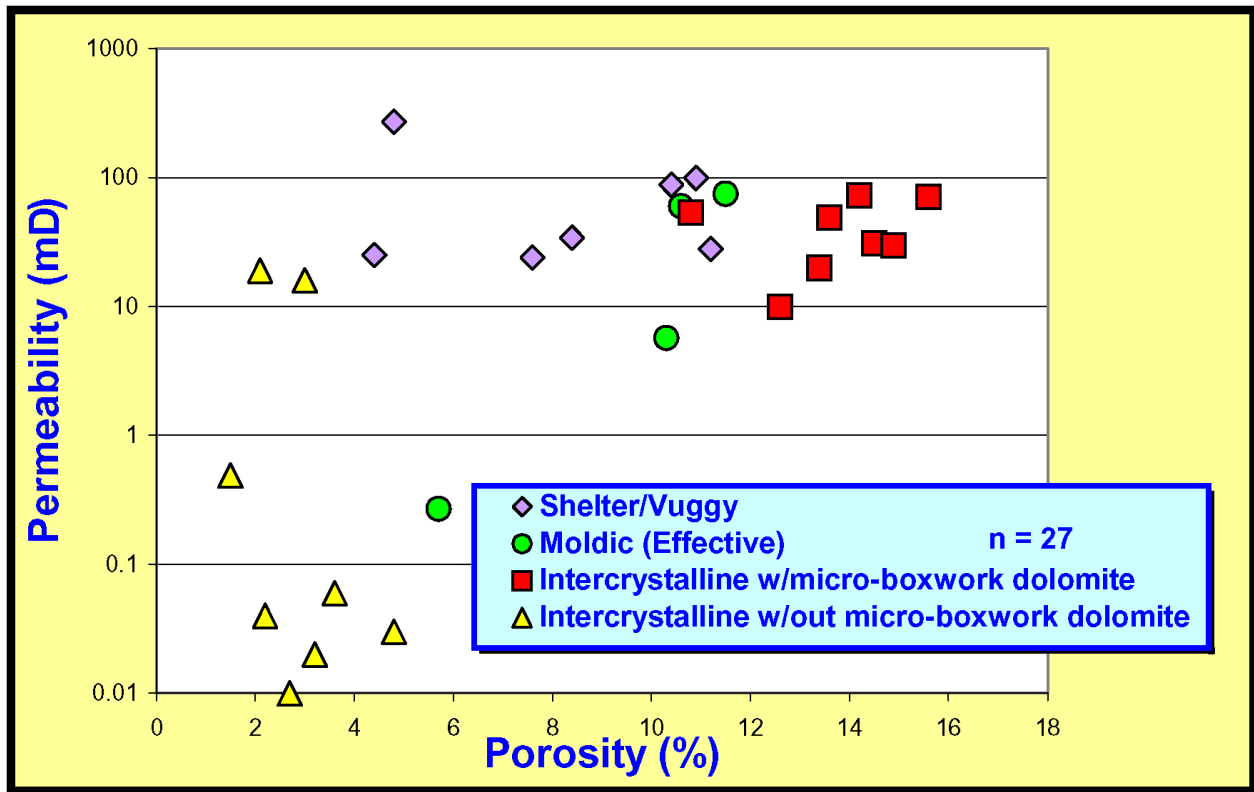
Figure 3.31. *May-Bug No. 2 well permeability versus porosity crossplot by pore types and diagenesis.*
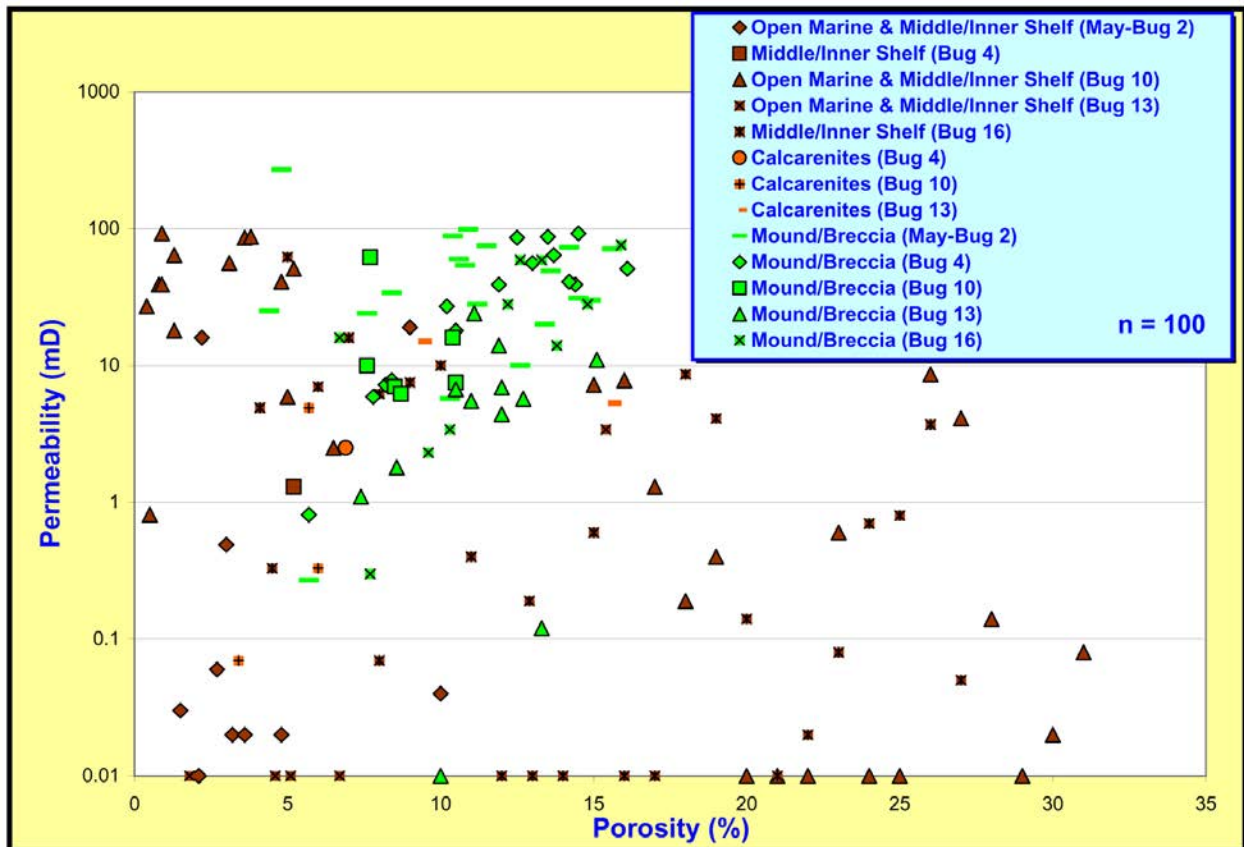
Figure 3.32. *Bug field permeability versus porosity crossplot by lithofacies.*
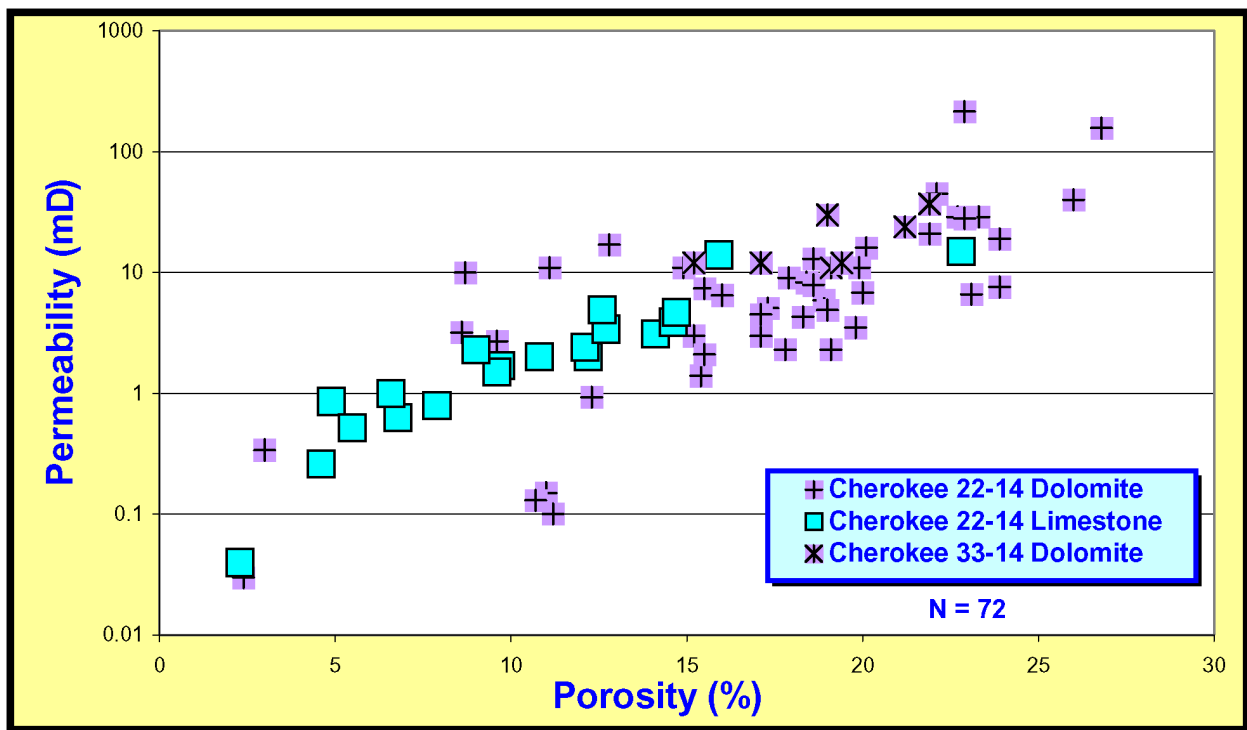
Figure 3.33. *Cherokee field permeability versus porosity crossplot of perforated limestone and dolomite intervals.*
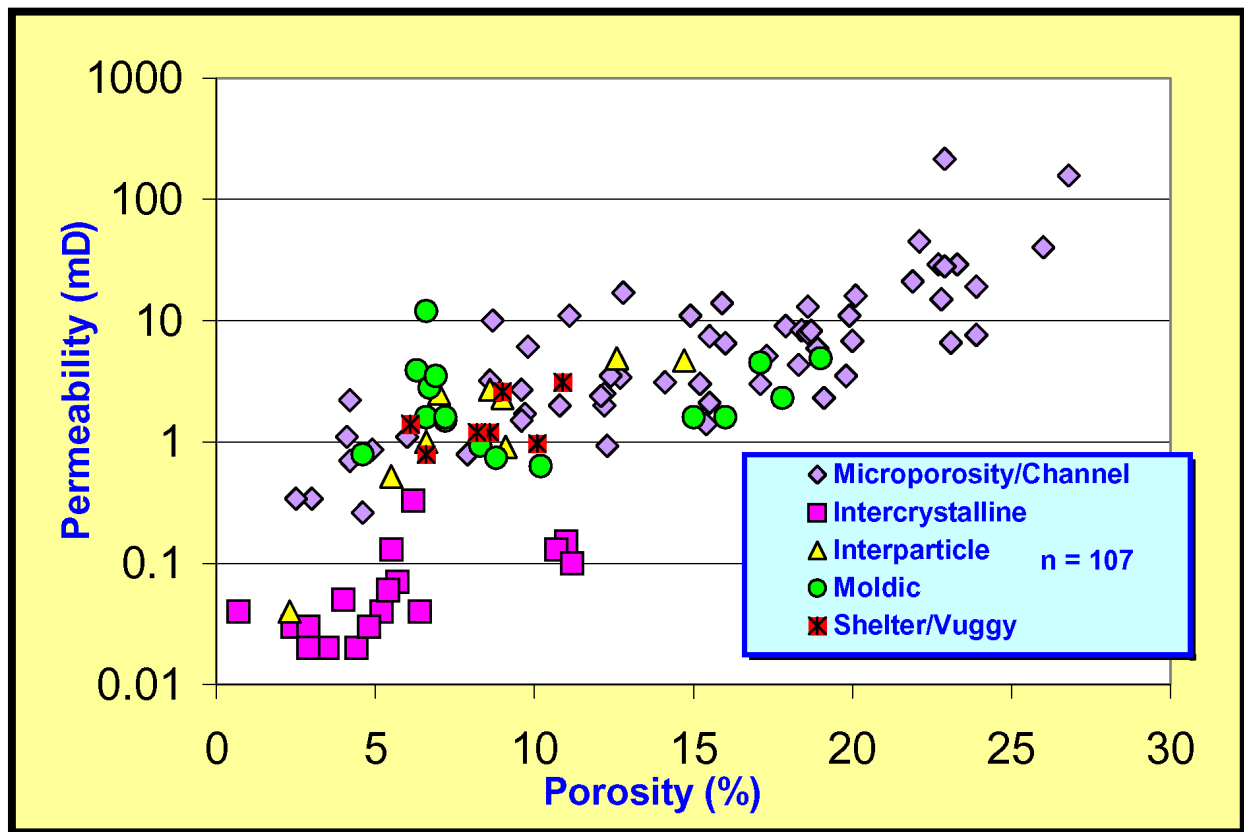
Figure 3.34. *Cherokee Federal No. 22-14 well permeability versus porosity crossplot by pore types and diagenesis.*

CHAPTER 4:

SCANNING ELECTRON MICROSCOPY AND PORE CASTING, BUG AND CHEROKEE CASE-STUDY FIELDS, SAN JUAN COUNTY, UTAH

---

by

Thomas C. Chidsey, Jr., Utah Geological Survey

Louis H. Taylor, Standard Geologic Services, Inc.
(now at the Denver Museum of Nature & Science)

and

David E. Eby, Eby Petrography & Consulting, Inc.

CHAPTER 4:
SCANNING ELECTRON MICROSCOPY AND PORE CASTING, BUG AND CHEROKEE CASE-STUDY FIELDS, SAN JUAN COUNTY, UTAH

INTRODUCTION

Bug and Cherokee fields (figure 1.3) were selected for scanning electron microscope (SEM) and/or pore casting analyses because they had high-quality core material available and exhibit a variety of diagenetic fabrics and porosity types as observed in thin sections. These characteristics, when found in various hydrocarbon-bearing rocks, can be indicators of reservoir flow capacity, storage capacity, and horizontal drilling potential. Scanning electron microscope and pore casting analyses were conducted on eight thin section blanks from core samples that displayed particular characteristics of interest (table 4.1; appendix H). The objectives of these analyses were to (1) characterize the cements, (2) identify the types of porosity, and (3) determine diagenetic events.

METHODOLOGY

To determine the diagenetic histories of the various Desert Creek and Ismay reservoirs, representative examples of key lithofacies were selected from the suite of 44 samples used for thin sections, which had been taken from conventional cores of each field (table 3.1). As with the core descriptions and diagenetic analysis of thin sections, carbonate fabrics were determined according to Dunham's (1962) and Embry and Klovan's (1971) classification schemes. Porosity types and associated abbreviations used in this chapter are also from Choquette and Pray (1970) (figure 3.26). A scanning electron microscope was used to photograph (1) typical preserved primary and secondary pore types and pore throats, (2) cements, (3) sedimentary structures, (4) fractures, and (5) pore-plugging anhydrite, halite, and bitumen.

Pore casting is a special technique where the carbonate matrix of an epoxy-impregnated thin section blank is dissolved by hydrochloric acid. What remains is only the epoxy that represents the entire pore system of the sample (pores and pore throats). The pore cast is then coated with gold and studied and photographed with the SEM (the same method used on the actual thin section blank).

RESULTS AND INTERPRETATION

The results of this SEM work are summarized in table 4.2. Some porosity descriptions provided here vary from those determined by the thin section analysis (see Chapter 3 and appendix F). The descriptions presented in this chapter are from SEM examination and measurement only.

Porosity Types

All samples exhibit microporosity in the form of intercrystalline microporosity (figure 4.1) and micro-boxwork porosity (figure 4.2). Microporosity represents an important site for untapped hydrocarbons and possible targets for horizontal drilling. Dissolution has contributed to porosity in most samples (figure 4.2) and has created moldic, vuggy, and channel porosity. Dissolution pores are most often in the mesopore size range (see figure 3.26 for definition of pore-size classes).

Table 4.1. List of samples examined in this study and the characteristics of interest.

Well	Depth (ft)	SEM	Pore Casting	Characteristics of Interest
May-Bug 2	6304	X	X	Micro-boxwork dolomite/hollow dolomite fabric
May-Bug 2	6312B	X		B – (second sample) botryoidal cement/dolomite
May-Bug 2	6315A	X	X	A – yellow internal sediment/dolomite
Bug 4	6289.7	X	X	Microporosity/with bitumen and micro-boxwork dolomite
Cherokee Fed. 22-14	5768.7	X	X	Microporosity dolomite with bitumen
Cherokee Fed. 22-14	5827.7	X		Moldic porosity and micro-crystalline dolomite
Cherokee Fed. 33-14	5773.9	X		Dolomite, microporosity and moldic porosity, relatively low porosity and permeability
Cherokee Fed. 33-14	5781.2	X	X	Microporosity only dolomite, high porosity and permeability
TOTAL	-	8	5	

Table 4.2. *Summary of porosity, cement, and diagenetic characters of samples examined.*

WELL	Cherokee Fed. 22-14		Cherokee Fed. 33-14		May-Bug 2*			Bug 4
DEPTH (ft)	5768.7'	5826.7'	5773.9'	5781.2'	6304.0'	6312.0' B	6315.0' A	6289.7'
POROSITY								
Intergranular/Microcrystalline	X	X	X	X	X	X	X	X
Dissolution (moldic)	X	X	X			X		
Dissolution (vug)	X				X	X		X
Dissolution (channel)	X	X	X					X
Fractures	X				X			X
CEMENTS								
Anhydrite	X	X	X			X		X
Calcite		X	X			X		
Quartz		X	X	X		X		
Dolomite					X			
Smectite	X	X	X					
Pyrobitumen	X	X	X	X				
DIAGENESIS								
Botryoidal Calcite Deposition					X	X	X	X
Dolomitization	X	X	X	X	X	X	X	X
Dissolution	X	X	X	X	X	X		X
Calcite Cementation		X	X					
Quartz Cementation		X	X	X		X		
Smectite Deposition	X	X	X	X				
Anhydrite Cementation	X	X	X			X		X
Pyrobitumen Emplacement	X	X	X	X				
Fracturing					X			

* Limited observation of the 6312-foot B specimen.

Permeability is related to the size and number of pore throats, and, particularly, to the connectivity of pore throats (figures 4.3 and 4.4). In general, permeability is limited in these samples by the presence of "dead end" pore throats, as well as the presence of pore-throat-blocking cements, pyrobitumen, and tight dissolution remnants.

Fractures enhance the permeability in three samples (table 4.2): the sample from the depth of 5768.7 feet (1758.2 m) from the Cherokee Federal No. 22-14 well, the sample from the depth of 6304.0 feet (1921.5 m) from the May-Bug No. 2 well (figure 4.5), and the sample from the depth of 6289.7 feet (1917.0 m) from the Bug No. 4 well (figure 4.6). The permeability of these three samples is among the highest of those examined.

Lithology, Cements, and Diagenesis

All samples examined contain dolomite (figures 4.1, 4.2, 4.5, 4.7, and 4.8). Anhydrite, calcite, smectite clays, and pyrobitumen are present in some samples. The dominant cement occluding porosity and permeability in the Cherokee wells is anhydrite (figure 4.8). Although we did not observe anhydrite in the sample from the depth of 5781.2 feet (1762.0 m) from the Cherokee Federal No. 33-14 well during SEM analysis, thin section analyses suggest that it is present.

Porosity reduction in the Bug wells is the result of dolomitization of former calcite cements. Later anhydrite cementation also contributes to porosity and permeability reduction in these wells; anhydrite was found at the following sample depths: 6312.0 feet (1923.9 m) from the May-Bug No. 2 well and 6289.7 feet (1917.0 m) from the Bug No. 4 well. Pyrobitumen commonly lines pores and plugs pore throats in many samples (figure 4.9).

Calcite (figure 4.10) and quartz (figure 4.11) cementation are very rare but are present in the Cherokee wells and in one sample (6312.0 feet [1923.9 m]) of the May-Bug No. 2 well. Smectite clay deposition (figure 4.10) is also extremely rare, and is only visible in the Cherokee wells. The minor cement constituents of calcite, quartz, and smectite contribute little to the overall lithology and are relatively insignificant to reservoir quality.
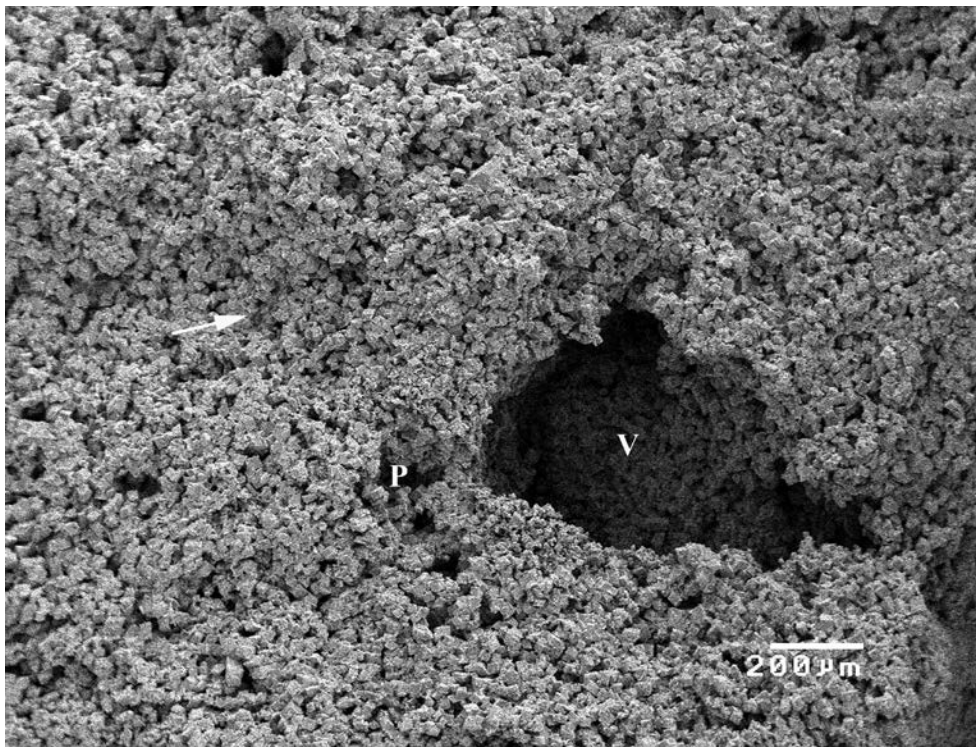
Figure 4.1. *Scanning electron microscope photomicrograph of a core plug from 5768.7 feet (1758.3 m), Cherokee Federal No. 22-14 well. Dolomite exhibits three porosity types: intercrystalline microporosity (arrow), moldic microporosity (P), and a large mesovug (V). Oil drainage is mainly from macro- and mesopores, but not from micropores. Scale represents 200 microns (0.2 mm). Porosity = 22.9%, permeability = 215 mD, based on core-plug analysis.*
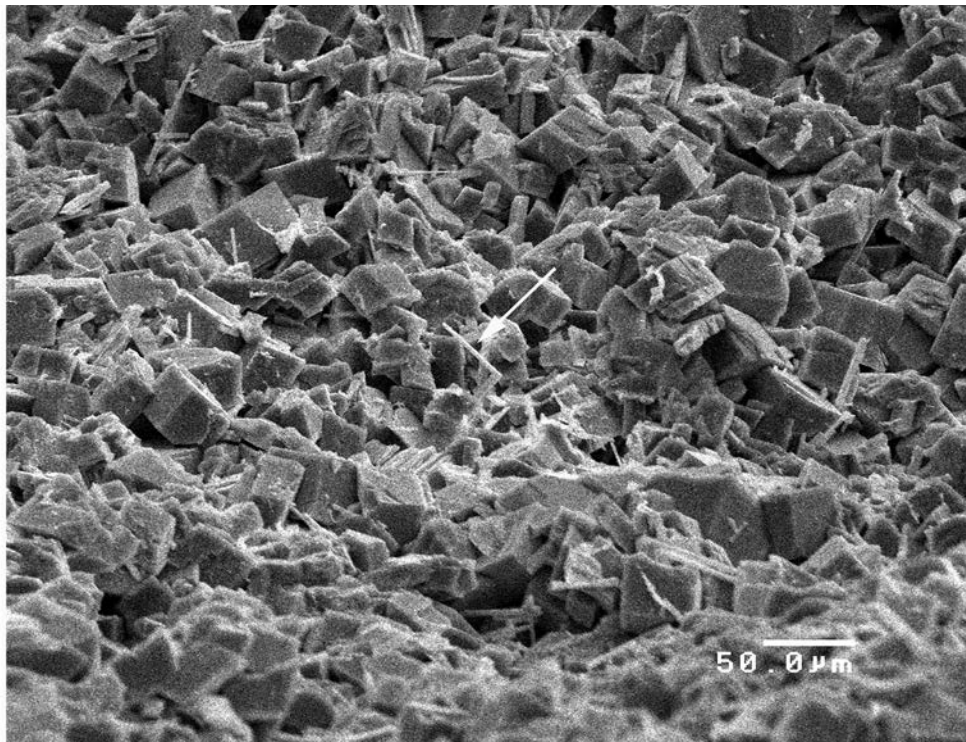
Figure 4.2. *Scanning electron microscope photomicrograph of a core plug from 6315 feet (1925 m), May-Bug No. 2 well, showing dolomite with intercrystalline microporosity (black). Fragments (lathes) (arrow) of dolomite represent partially dissolved dolomite rhombs present within a part of the sample. The collapse and/or crushing of dolomite rhombs within the internal hollow dolomite sediment indicate early dolomitization and early meteoric dissolution resulting in micro-boxwork porosity. Scale represents 50 microns (0.05 mm). Porosity = 10.3%, permeability = 5.7 mD, based on core-plug analysis.*

A.

B.
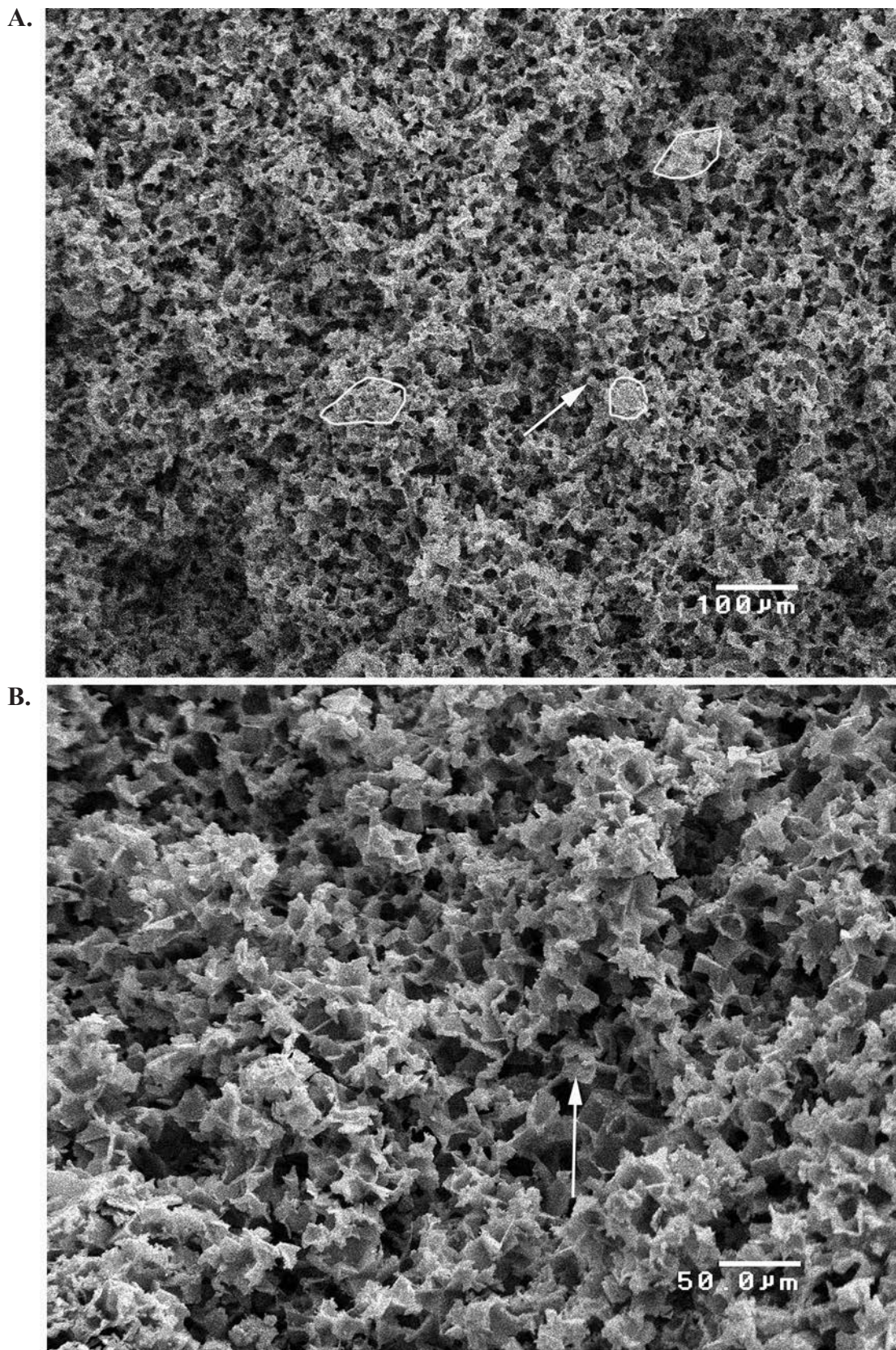
Figure 4.3. *Scanning electron microscope photomicrograph of a pore cast from 5768.7 feet (1758.3 m), Cherokee Federal No. 22-14 well.* ***(A)*** *The overall intercrystalline microporosity (arrow) is relatively uniform. A few larger micropores are visible (outlined). Note that the solid areas (light gray) represent porosity and the open areas (dark gray to black) represent matrix. Scale represents 100 microns (0.1 mm).* ***(B)*** *Enlargement of (A) showing microporosity. Impressions of dolomite rhombs are visible (arrow). Scale represents 50 microns (0.05 mm). Porosity = 22.9%, permeability = 215 mD, based on core-plug analysis.*
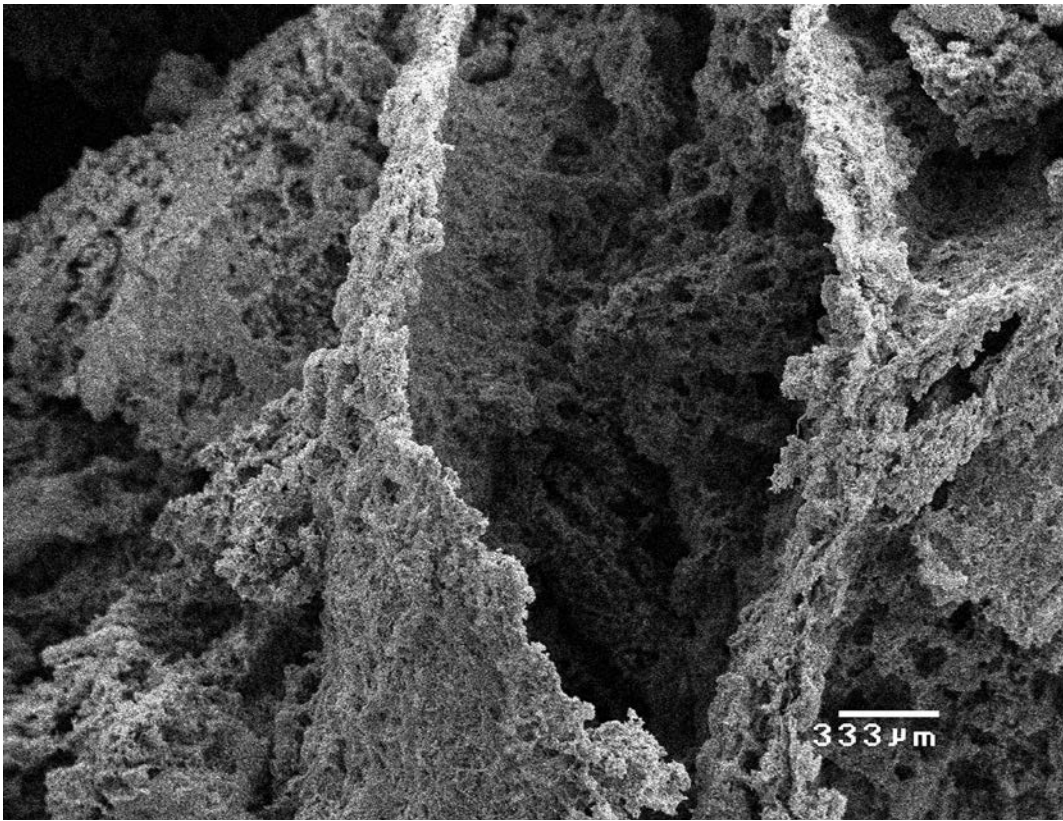
Figure 4.4. *Scanning electron microscope photomicrograph of a pore cast from 6304 feet (1921 m), May-Bug No. 2 well. Sheet-like linear pores are associated with phylloid-algal fronds. Note that the solid areas represent porosity. Scale represents 333 microns (0.333 mm). Porosity = 10.9%, permeability = 99 mD, based on core-plug analysis.*
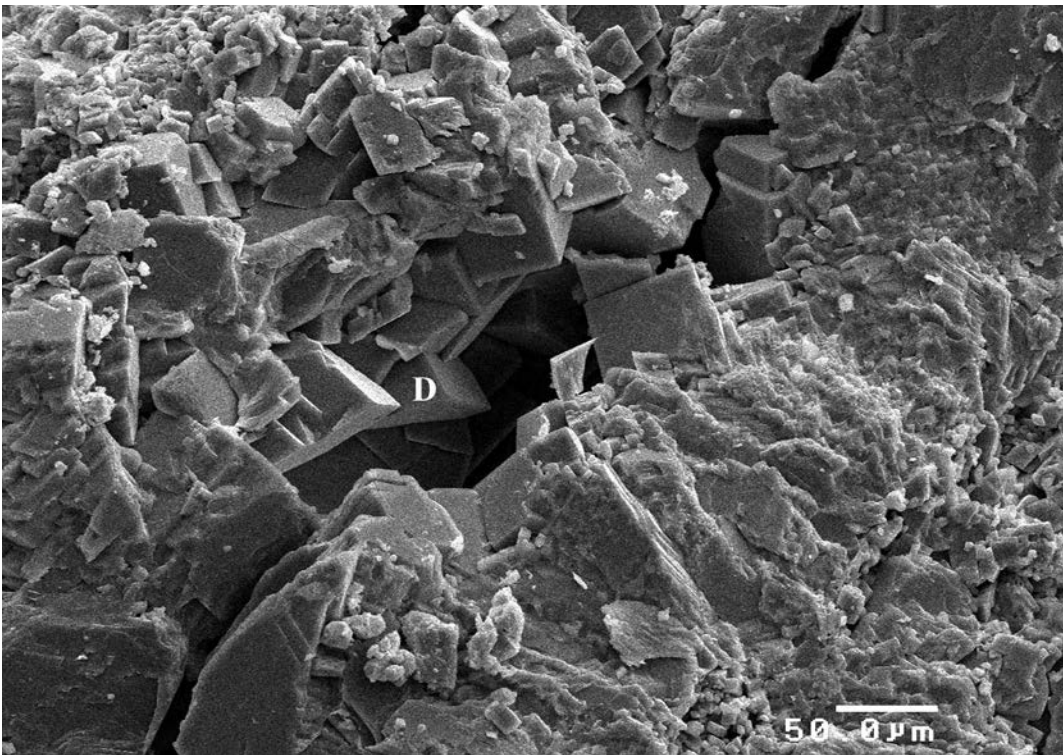
Figure 4.5. *Scanning electron microscope photomicrograph of a core plug from 6304 feet (1921 m), May-Bug No. 2 well, showing a fracture pore and dolomite (D) within it. This demonstrates that the fracture was open during dolomite deposition. Scale represents 50 microns (0.5 mm). Porosity = 10.9%, permeability = 99 mD, based on core-plug analysis.*
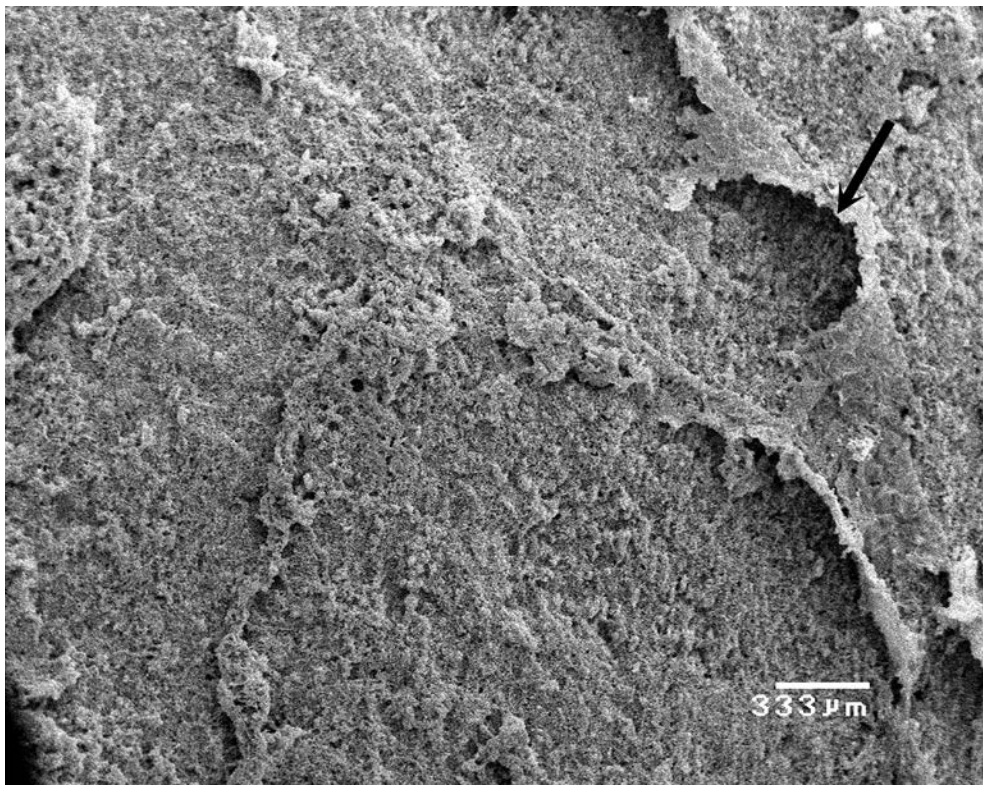
Figure 4.6. *Scanning electron microscope photomicrograph of a pore cast from 6289.7 feet (1917.1 m), Bug No. 4 well, showing pattern of intersecting fractures in a low permeable part of the sample. The curvilinear feature in the upper right (black arrow) may represent artificially bent fracture-filling epoxy. The circular feature is a grain. Note that the solid areas represent porosity. Scale represents 333 microns (0.333 mm). Porosity = 14.5%, permeability = 92 mD, based on core-plug analysis.*
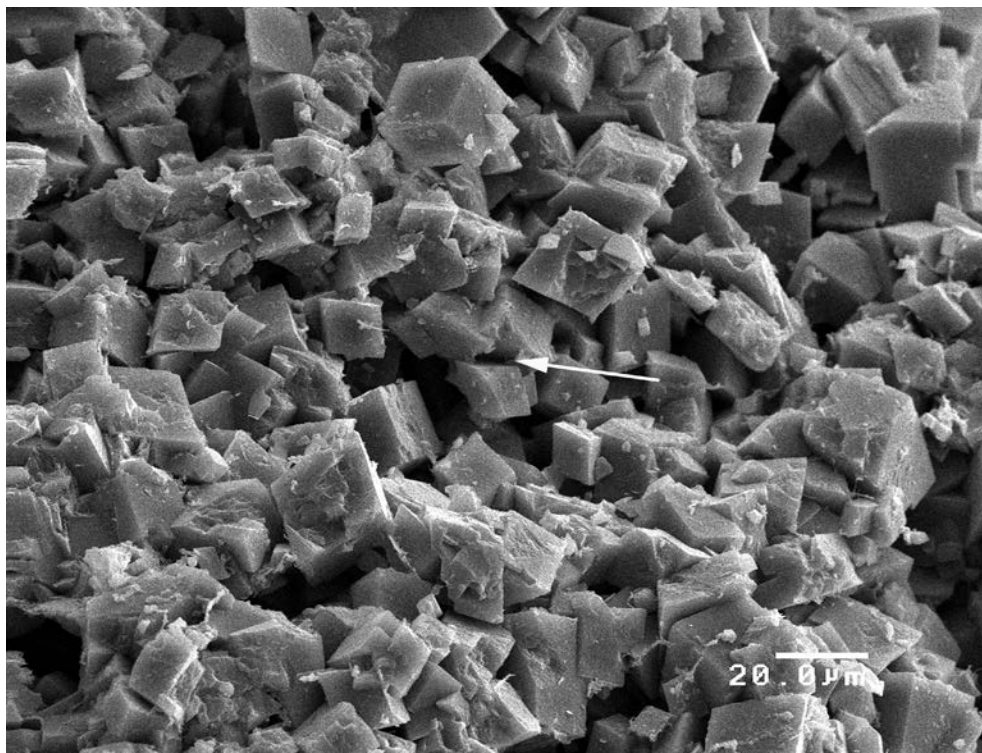
Figure 4.7. *Scanning electron microscope photomicrograph of a core plug from 5781.2 feet (1762.1 m), Cherokee Federal No. 33-14 well, showing well-developed dolomite rhombs exhibiting abundant intercrystalline microporosity (arrow). Scale represents 20 microns (0.02 mm). Porosity = 23.6%, permeability = 103 mD, based on core-plug analysis.*
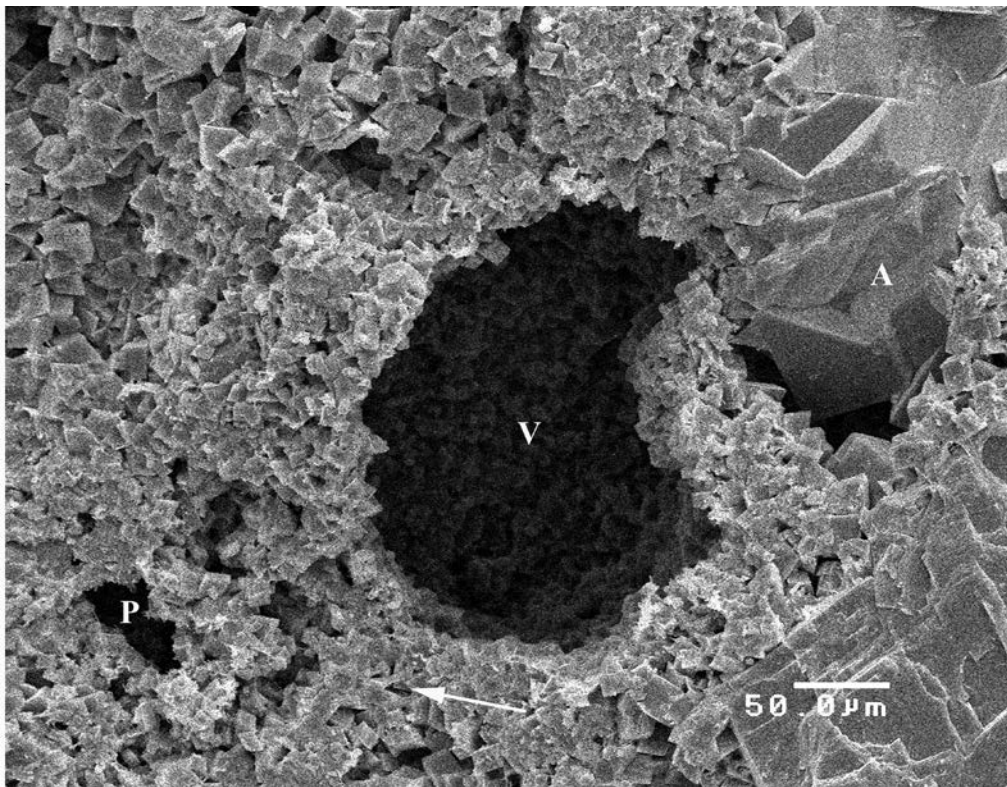
Figure 4.8. *Scanning electron microscope photomicrograph of a core plug from 5827.7 feet (1776.2 m), Cherokee Federal No. 22-14 well, showing dolomite with a mesovug (V) and visible anhydrite (A) cement, smaller mesopores (P), and intercrystalline micropores (arrow). Scale represents 50 microns (0.05 mm). Porosity = 17.1%, permeability = 4.5 mD, based on core-plug analysis.*
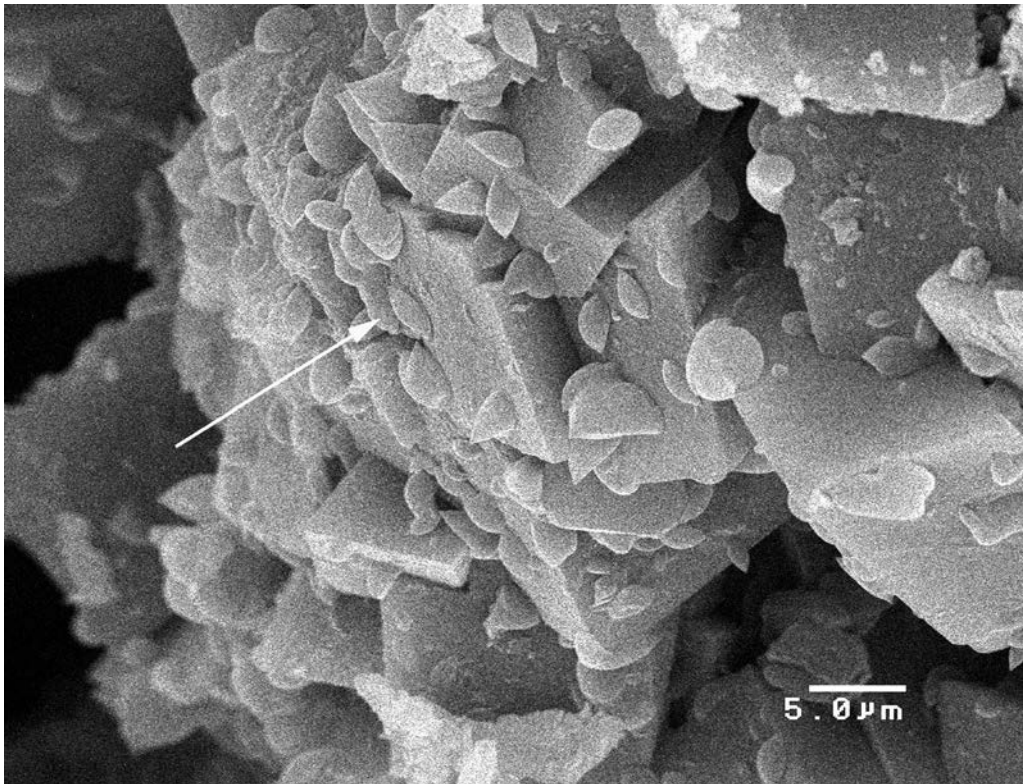
Figure 4.9. *Scanning electron microscope photomicrograph of a core plug from 5768.7 feet (1758.3 m), Cherokee Federal No. 22-14 well, showing pyrobitumen (arrow) on dolomite within a microfracture. Micropores are black areas. Scale represents 5 microns (0.005 mm). Porosity = 22.9%, permeability = 215 mD, based on core-plug analysis.*
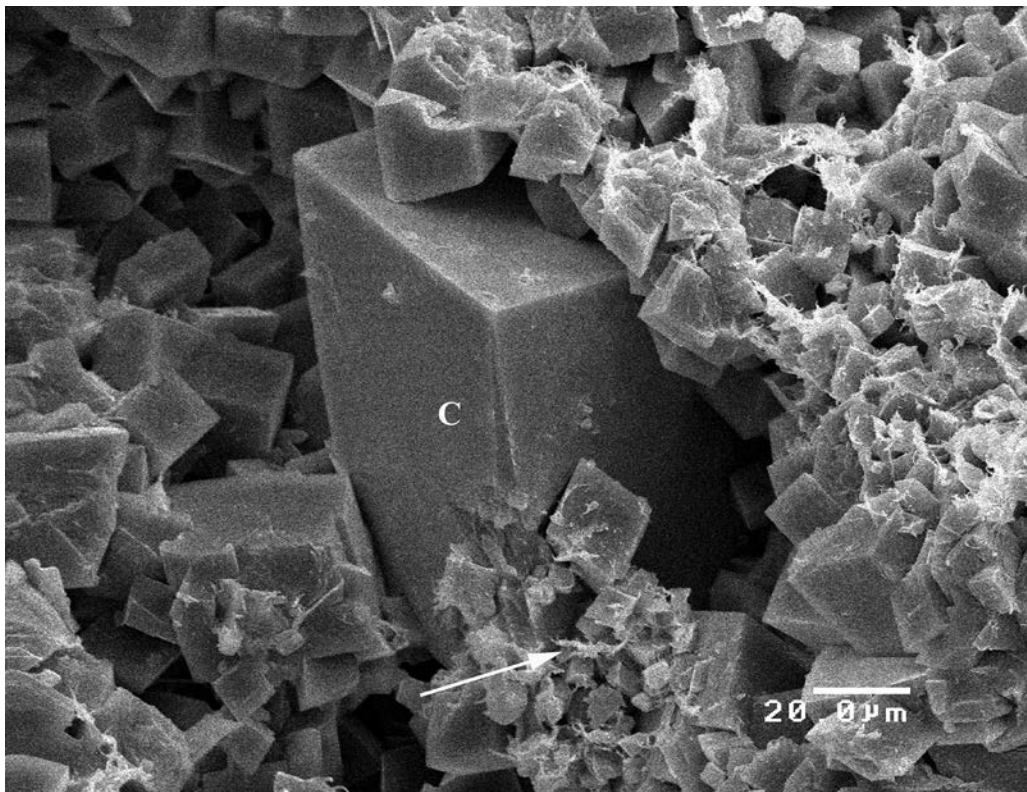
Figure 4.10. *Scanning electron microscope photomicrograph of a core plug from 5827.7 feet (1776.3 m), Cherokee Federal No. 22-14 well, showing equant spar calcite (C), a burial cement, as well as minor smectite clay (arrow) present in a large moldic pore on the dolomite. Scale represents 20 microns (0.02 mm). Porosity = 17.1%, permeability = 4.5 mD, based on core-plug analysis.*
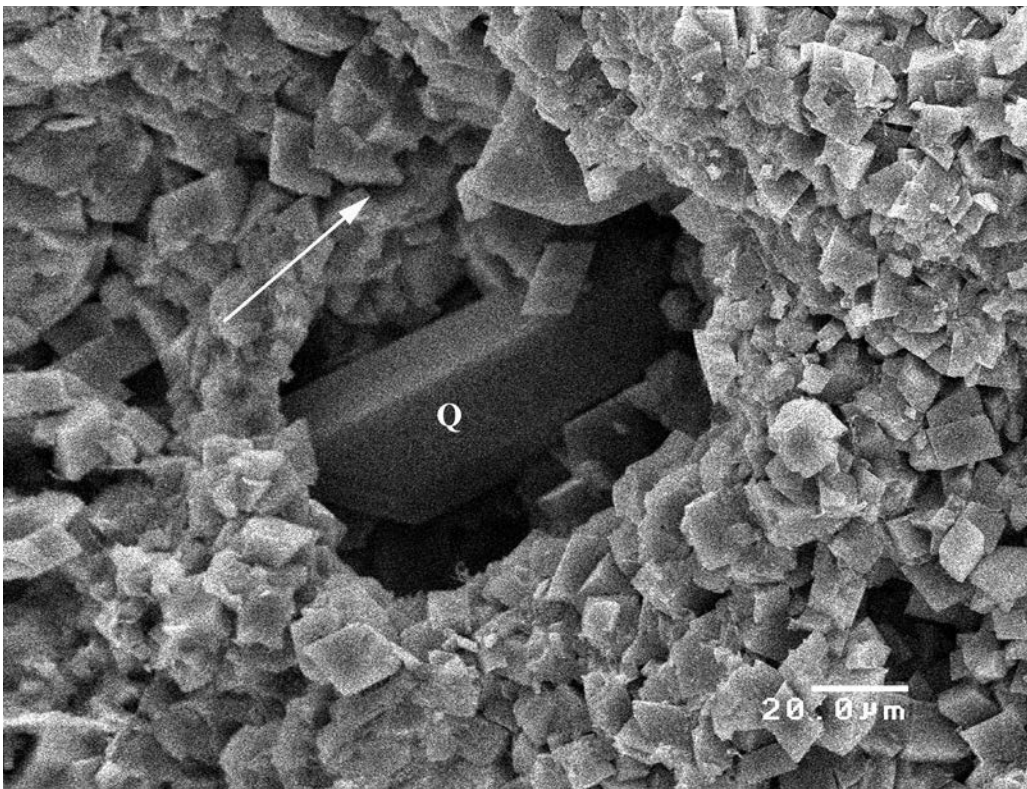
Figure 4.11. *Scanning electron microscope photomicrograph of a core plug from 5773.9 feet (1759.9 m), Cherokee Federal No. 33-14 well, showing authigenic quartz crystal (Q) within a mesovug. Note the presence of intercrystalline microporosity (arrow). Scale represents 20 microns (0.02 mm). Porosity = 19.1%, permeability = 11 mD, based on core-plug analysis.*

Sequence of Diagenetic Events

The general diagenetic sequence for the Paradox Formation samples, based on SEM and pore casting analyses, is listed below (not all diagenetic events were identified in every sample). The various diagenetic events are included in table 4.2.

1. Calcite cementation
2. Dissolution
3. Dolomitization
4. Dissolution
5. Fracturing
6. Calcite cementation
7. Quartz cementation
8. Clay deposition
9. Anyhydite cementation
10. Pyrobitumen emplacement

Diagenesis played a major role in the development of reservoir heterogeneity in Bug and Cherokee fields as well as throughout all of the Paradox Formation fields. Based on the combined examination of samples in thin sections, core, and SEM of thin section blanks and pore casts, the diagenetic processes started during Paradox Formation deposition and continued throughout its burial history. A complete listing of diagenetic events through time and their individual significance is shown on figure 4.12. Major early (eogenetic) events were dominated by marine cementation, seepage reflux/hypersaline and mixing zone dolomitization, and micro-boxwork dissolution. Late (mesogenetic) events were dominated by micro-porosity dissolution and fracturing.
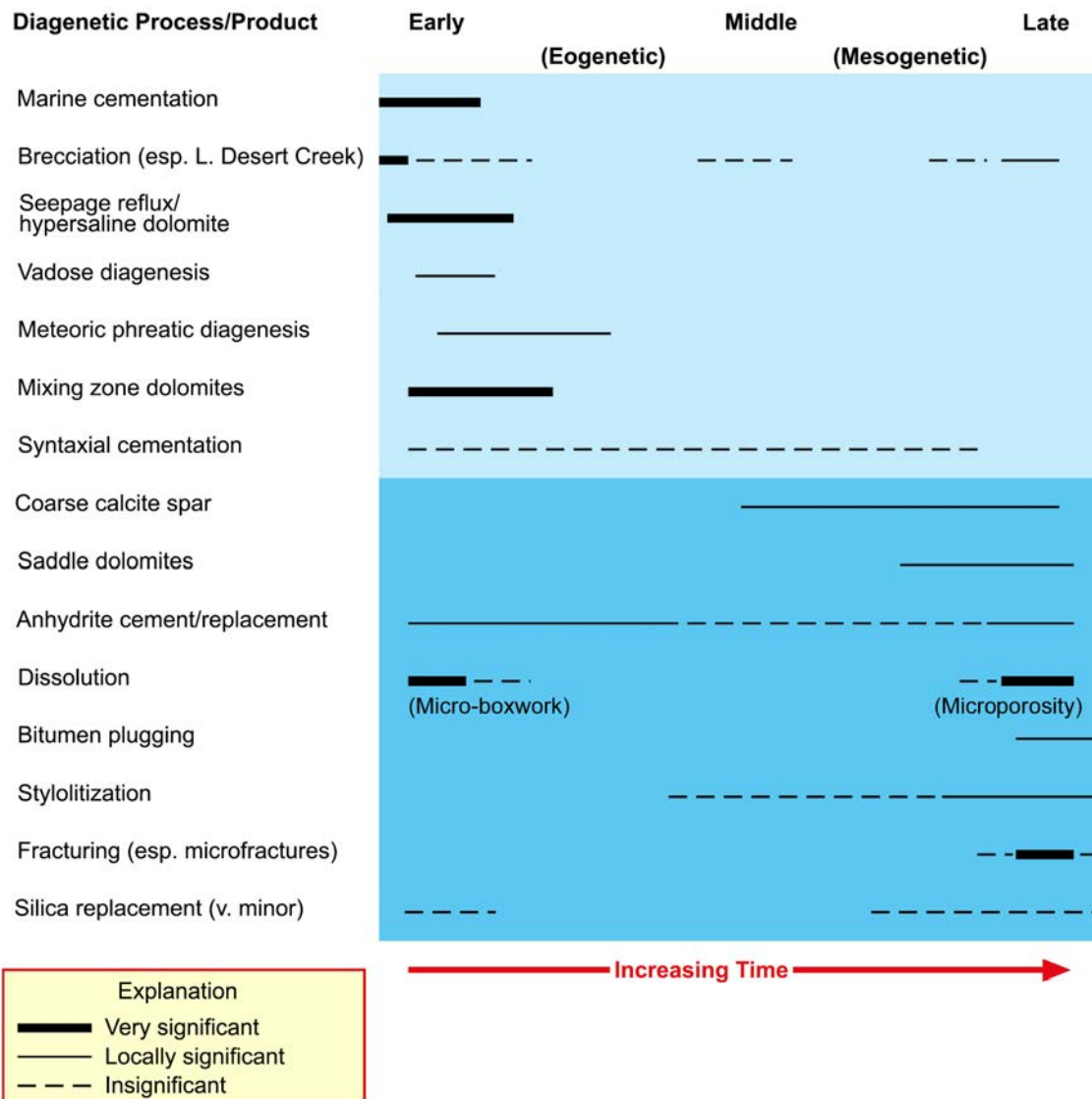
Figure 4.12. *Ideal diagenetic sequence through time based on thin sections, core, and scanning electron microscopy of core plugs and pore casts from the Desert Creek and Ismay zones, Bug and Cherokee fields.*

CHAPTER 5:
EPIFLUORESCENCE ANALYSIS,
BUG AND CHEROKEE CASE-STUDY FIELDS,
SAN JUAN COUNTY, UTAH

by

David E. Eby, Eby Petrography & Consulting, Inc.
and
Thomas C. Chidsey, Jr., Utah Geological Survey

CHAPTER 5:
EPIFLUORESCENCE ANALYSIS, BUG AND CHEROKEE CASE-STUDY FIELDS, SAN JUAN COUNTY, UTAH

INTRODUCTION

Diagenesis of the carbonate rocks in the Paradox Formation may have created significant untested reservoir compartments that could be targets for horizontal drilling. To better understand the role that diagenesis has played in potential reservoir development in the Desert Creek and Ismay zones, we conducted epifluorescence (EF) (described in this chapter), cathodoluminescence (Chapter 6), isotopic geochemistry (Chapter 7), and capillary pressure/mercury injection (Chapter 8) analyses.

Bug and Cherokee case-study fields (figure 1.3) were chosen for blue-light EF photomicroscopy examination, description, and interpretation of selected thin sections of samples taken from wells in the fields (appendix I). Epifluorescence microscopy is a technique that has been used successfully to provide additional information on diagenesis, pores, and organic matter (including "live" hydrocarbons) within sedimentary rocks (see Eby and others, 2008; Chidsey and Eby, 2017). The procedure uses a petrographic (polarizing) microscope equipped with reflected-light capabilities, a mercury-vapor lamp, and appropriate filtering. The basic principles and equipment for EF were largely developed in the 1960s and 1970s for applications in coal petrology and palynology (van Gijzel, 1967; Teichmuller and Wolf, 1977). All applications depend upon the emission of light (by a material capable of producing fluorescence) that continues only during absorption of the excitation-generating light beam (Rost, 1992; Scholle and Ulmer-Scholle, 2003).

Epifluorescence techniques have been used within industry and research for three objectives. Firstly, EF microscopy has been used extensively for enhancing petrographic observations, including the recognition of depositional and diagenetic fabrics within recrystallized limestone and massive dolomite (Dravis and Yurewicz, 1985; Cercone and Pedone, 1987; Dravis, 1991; LaFlamme, 1992). Secondly, the study of pore structures, microfractures, and microporosity within both carbonates and sandstones has been greatly facilitated by impregnating these voids with epoxy spiked with fluorescing dyes (Yanguas and Dravis, 1985; Gies, 1987; Cather and others, 1989a, 1989b; Soeder, 1990; Dravis, 1991). Thirdly, the evaluation of "oil shows" (Eby and Hager, 1986; Kirby and Tinker, 1992; Chidsey and Eby, 2017) and determination of the gravity or type cements and minerals has been facilitated by EF microscopy (Burruss, 1981, 1991; Burruss and others, 1986; Guihaumou and others, 1990; Lavoie and others, 2001). Only the first two objectives were pursued in this study. Also, fluid inclusions were not evaluated.

Previous Work

We know of no published use of EF microscopy on the lower Desert Creek and upper Ismay subsurface rocks of the Blanding sub-basin. However, applications to carbonate reservoirs include Eby and Hager (1986) who studied a Permian Basin carbonate field in West Texas; case studies documented by Dravis (1988) on limestones in the Upper Jurassic Haynesville Shale of East Texas and dolomites in the Upper Devonian Elk Point Group of Western Canada by Dravis (1992); and regional "oil show" analyses within the Devonian Keg River/Winnipegosis petroleum system in Alberta by Kirby and Tinker (1992), and more recently the Cane Creek shale of the Paradox Formation in the Paradox Basin by Chidsey and Eby (2017). These studies provided justification to apply EF petrography to Desert Creek and Ismay reservoir rocks within the Bug and Cherokee case-study fields, respectively.

Methodology

Epifluorescence petrography for this study used incident (reflected) blue light fluorescence microscopy employing the general procedures outlined by Dravis and Yurewicz (1985). Ultraviolet (UV) fluorescence did not effectively add any textural or pore structure information that could not otherwise be seen under blue-light excitation, even though some researchers use UV fluorescence for evaluating fluid inclusions and compositional zoning within dolomite crystals (Scholle and Ulmer-Scholle, 2003). Fluorescence data and observations collected for this study used a Jena (now part of Carl Zeiss) research-grade combination polarizing-reflected light microscope equipped with a high-pressure mercury vapor lamp for EF excitation, and a Zeiss IIIRS EF nosepiece. Magnification ranges for examination and photo-documentation were between about 130X and 320X. The EF optical configuration used is similar to that shown on figure 5.1.

The light pathways and mechanics of the EF used in this study have been generally described by Soeder (1990). As described by Burruss (1991):

> "These excitation wavelengths are reflected to the microscope objective and sample by a dichroic beamsplitter which has a dielectric coating that reflects a specific short wavelength range. Fluorescence emission and reflected short wavelength excitation light is collected by the objective. The dichroic beamsplitter transmits the long wavelength fluorescence emission, but reflects the short

wavelengths back toward the light source. The fluorescence emission passes through a barrier filter which removes any remaining short wavelength excitation light."

Blue light (about 420 to 490 nanometer [nm] exciter filter/520 nm barrier filter) was used to excite the samples on the thin sections. Broad-band, blue-light EF was found to be the most helpful in observational work on dolomite, although some workers report applications using UV light (330 to 380 nm exciter filter/420 nm barrier filter) or narrow-band, blue-violet light (400 to 440 nm exciter filter/480 nm barrier filter). Finally, the greater depth of investigation into a sample by the reflected fluorescence technique than by transmitted polarized light or other forms of reflected light makes it possible to resolve grain boundary and compositional features that are normally not appreciated by thin-section petrography only.

Sample preparation is inexpensive and rapid, involving standard thin section preparation techniques. Thin sections were prepared from representative upper Ismay fabrics. These thin sections were vacuum- and pressure-impregnated with blue-dyed epoxy (Gardner, 1980) that was spiked with a fluorescing compound. Microscopy used only uncovered polished

Figure 5.1. Generalized microscope optical configuration for observing fluorescence under incident light. Modified from Soeder (1990).

surfaces. Examination for each thin section area of interest included image-photography and petrographic descriptions (compositional, textural, and pore structure attributes) under EF and plane-polarized light at the same magnification (see appendix I). Since the image brightness is directly proportional to magnification, we obtained the best images at relatively high magnifications (such as greater than 100X). Low-power fluorescence is often too dim to effectively record. These techniques are applicable to thin sections from both core and cuttings samples.

EPIFLUORESCENCE PETROGRAPHY OF LOWER DESERT CREEK THIN SECTIONS, BUG FIELD

Blue-light EF microscopy was completed on four samples for a variety of rock textures and diagenetic phases in core samples from oil-productive, lower Desert Creek zone dolomites within Bug field. These samples were selected to be representative of the compositional, diagenetic, pore, and fracture types encountered within the three cored wells (Bug Nos. 7, 10, and 16 [two samples]) from Bug field. A detailed description and interpretation of the fluorescence petrography of each sample follows below along with photomicrographs (figures 5.2 through 5.5) to show representative views under both blue-light EF and plane-polarized light.

Bug No. 7-A Well

Blue-light EF microscopy of the sample from 6359.3 feet (1938.3 m) shows very tight dolomites having fairly uniform oil saturation throughout (figure 5.2). Much of the dolomite fluoresces a dull to bright yellow, due in part to the presence of "live oil" films around many of the tight intercrystalline spaces. Non-fluorescent areas (which appear red to black in the photomicrographs) indicate extremely low-permeability areas where oil could not penetrate. In places, fluorescence petrography makes it possible to see outlines of carbonate grains as well as sparse larger dolomite rhombs. Perhaps the best application of EF in this sample is to determine open, oil-bearing fractures and "stylo-fractures" from healed fractures and tight microstylolites.

Bug No. 10 Well

Epifluorescence examination of the sample from 6327.9 feet (1928.7 m) aids in two very important aspects of the Bug dolomite oil reservoir. First, the definition of open, crystal-lined microfractures within dense portions of this dolomite is aided considerably with EF. Second, this sample displays well-developed micro-boxworks of dolomite crystal aggregates that serve to isolate a number of the open pores within some of the most porous parts of this sample (figure 5.3). Whereas some pore throats are wide and open, other megascopic pores are
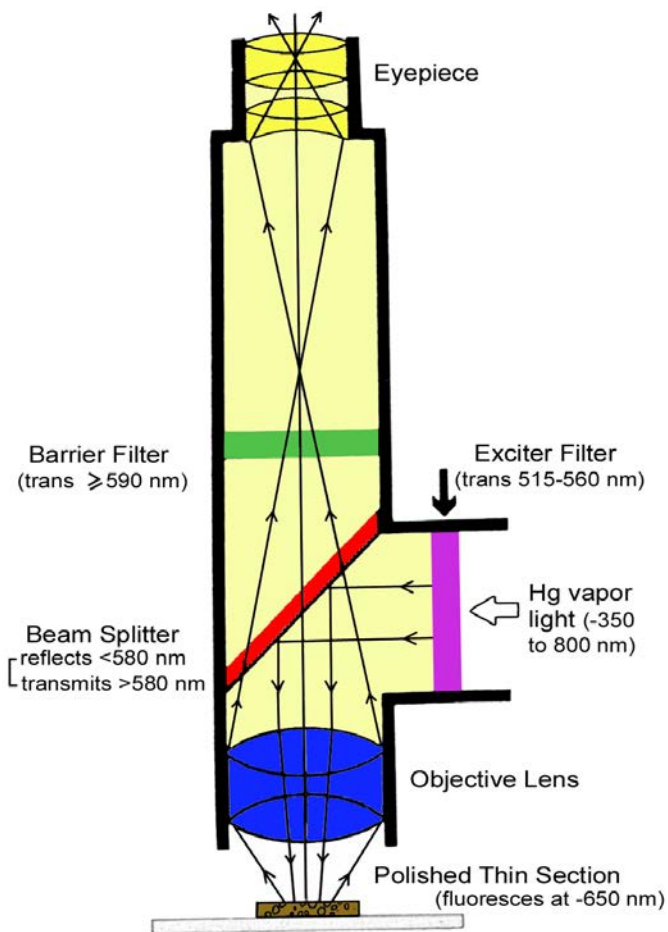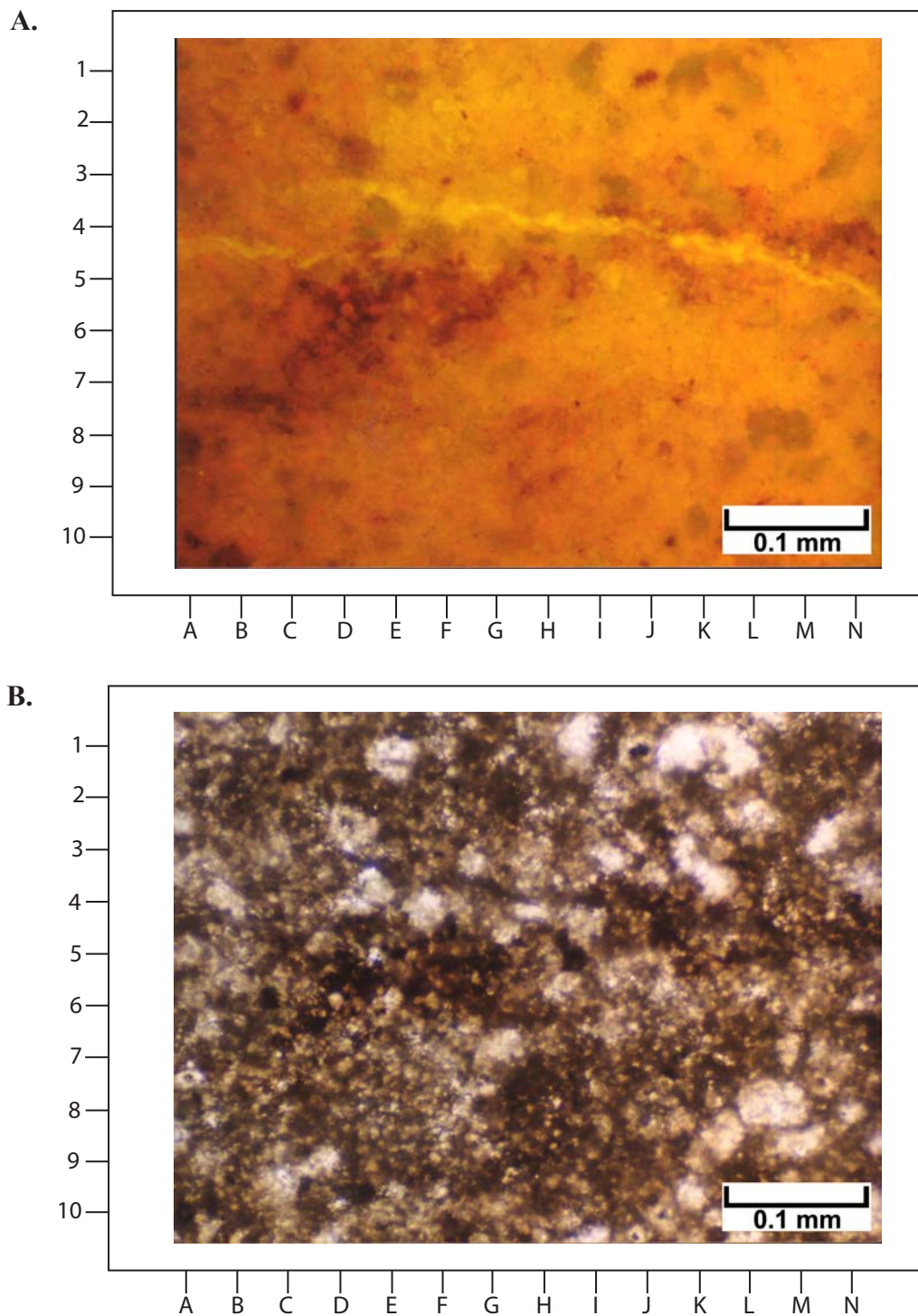
Figure 5.2. *Photomicrographs from Bug No. 7-A well at 6359.3 feet (1938.3 m).* ***(A)*** *Representative EF view of a very low-permeability microcrystalline dolomite shows the absence of any significant megascopic matrix porosity. However, the matrix displays a yellowish-orange color, indicating probable "live oil" saturation of this low-permeability dolomite. Notably, there is an open microfracture, with an offset in the upper left center part of the photomicrograph. It appears bright yellow here due to the fluorescence of "live" hydrocarbons. This microfracture crosses and postdates a microstylolite marked by the black, jagged pattern across this view from lower left to right center. Most of the rest of the massive (mud-rich) matrix displays a mottled yellow and orange color due to oil saturation in this dolomite. Although there are no readily visible grains in the field of view, there are a few discrete dolomite crystals that appear as the dark green areas.* ***(B)*** *The same field of view as above is shown under plane light at the same magnification. Some of the medium to dark-brown color of this dolomite may be the result of oil staining as indicated by the yellowish-orange color in the EF view above. Note the poorly preserved peloids and possible fossils in this aphanitic to anhedral dolomite. Some of the larger non-planar dolomite crystals appear white in this view. The open, en echelon (offset) fractures and the wispy microstylolites seen in the top image are very indistinct across the length of this photomicrograph.*

A.

B.
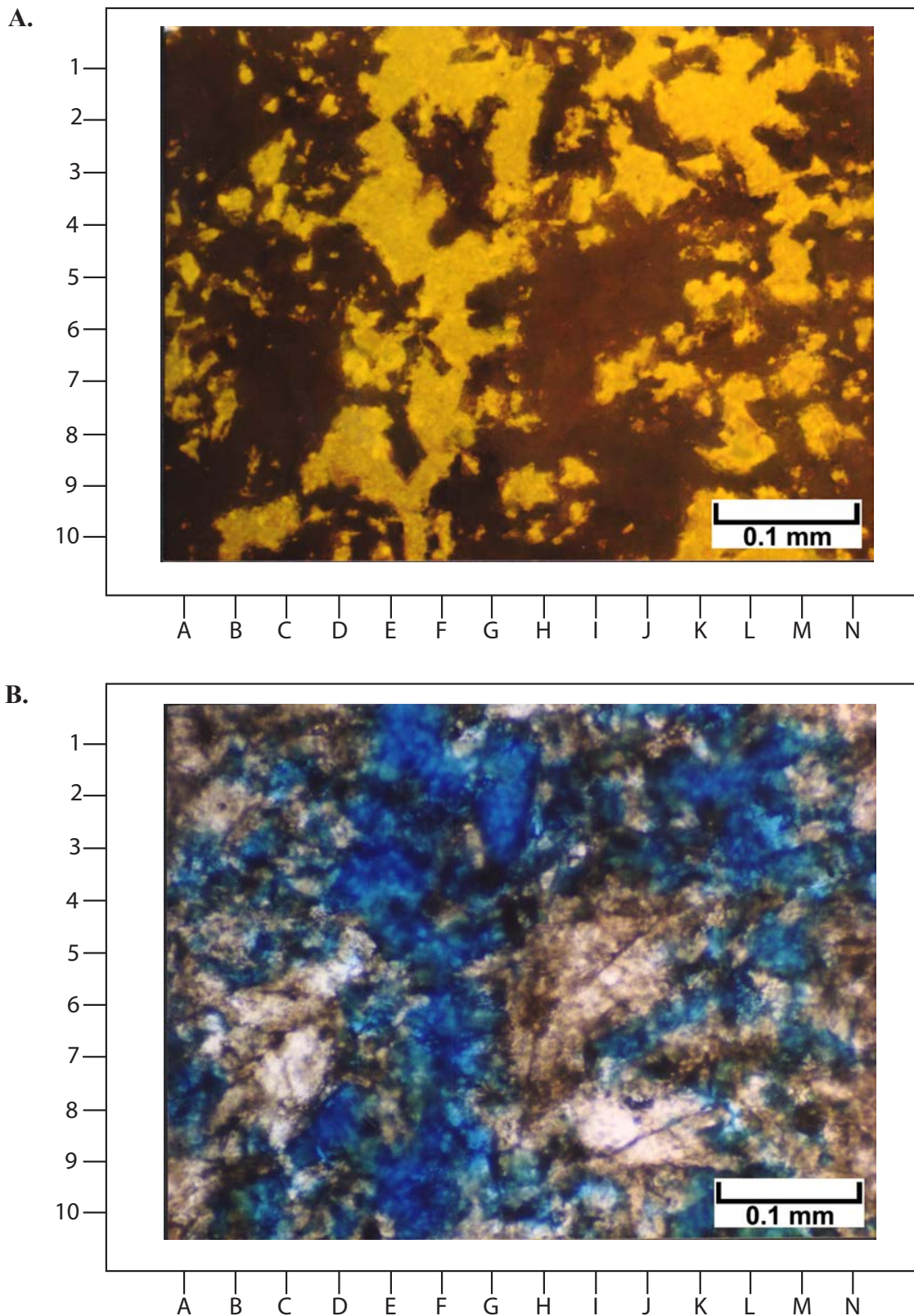
Figure 5.3. Photomicrographs from Bug No. 10 well at 6327.9 feet (1928.7 m). (A) Heterogeneous micro-boxwork of dolomite is displayed here, where the dolomite crystal aggregates appear dark gray and the open pores between the dolomite are bright yellow (due to spiked epoxy and "live oil" lining pores). Some of the pores appear to be well connected whereas others are isolated by interlocking dolomite crystals. Hence, some of these large pores may be "blind" or lack interconnections. Note that there is very little evidence of intercrystalline porosity within the dense dolomite areas. (B) The same field of view as above under plane light at the same magnification shows fuzzy relationships between the cross section of pores (impregnated with blue epoxy) and the poorly sorted dolomite crystal matrix. No grains or structures are visible within the dolomites in this image.

A.

B.
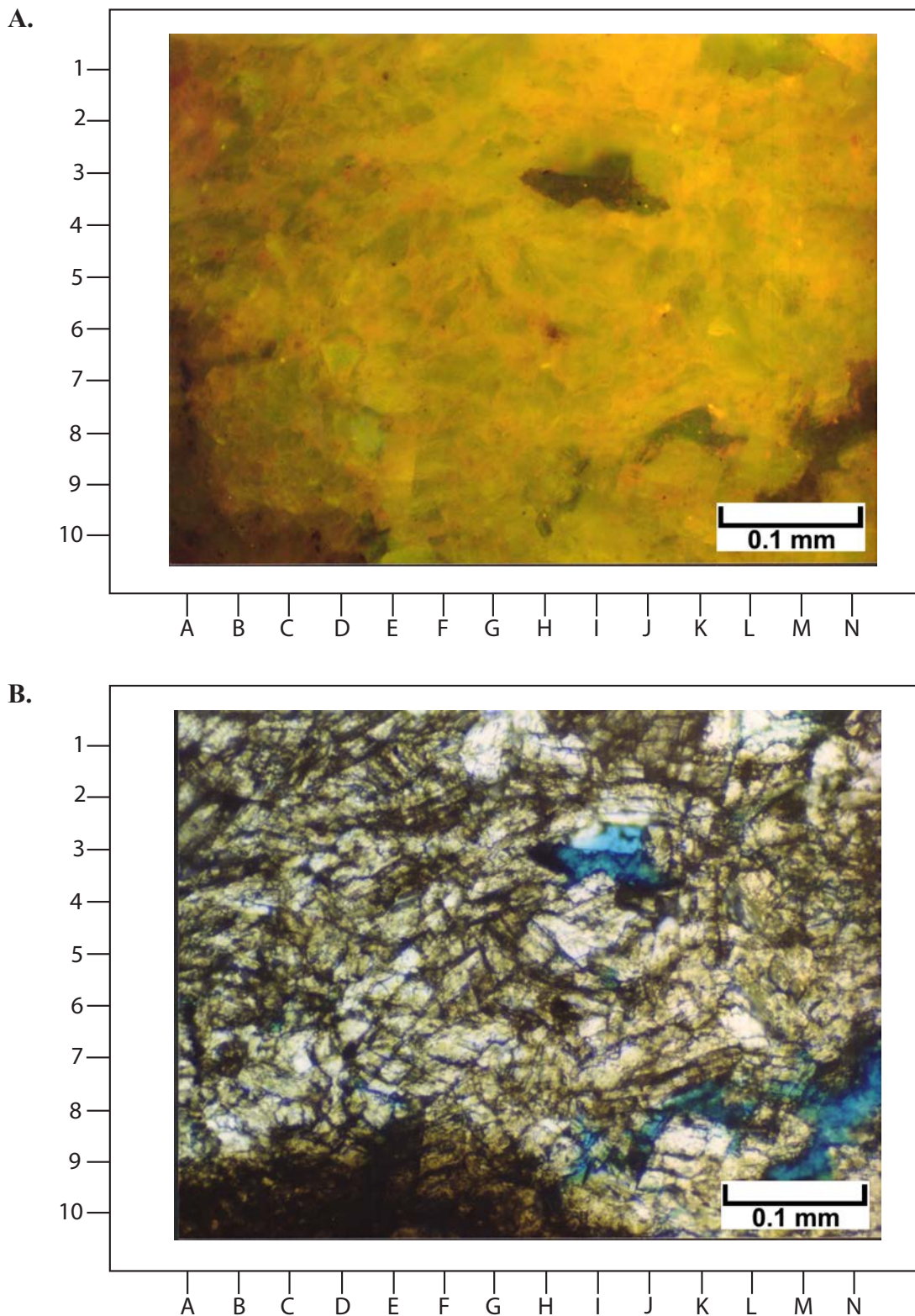
Figure 5.4. Photomicrographs from Bug No. 16 well at 6299.3 feet (1920.0 m). (A) This part of the sample displays very low-permeability, moderately coarse, interlocking dolomite crystals having low visible porosity. Note the intense yellow to orangish-yellow fluorescence that appears to surround the dolomite subcrystals and microfractures. This yellow fluorescence is probably due to the presence of "live" and/or relict hydrocarbons within the low-permeability intercrystalline spaces. Some of the black and reddish colors in this view may be the result of bitumen lining some of the few isolated open pores. (B) The same field of view as above is shown under plane light at the same magnification. The dark gray areas within the interlocking dolomite crystals are probably due to organic matter or oil staining. This staining makes it possible to see the subcrystal boundaries and probable microfractures within them. The small amount of open pore space in this view is shown in blue, with black bitumen linings.
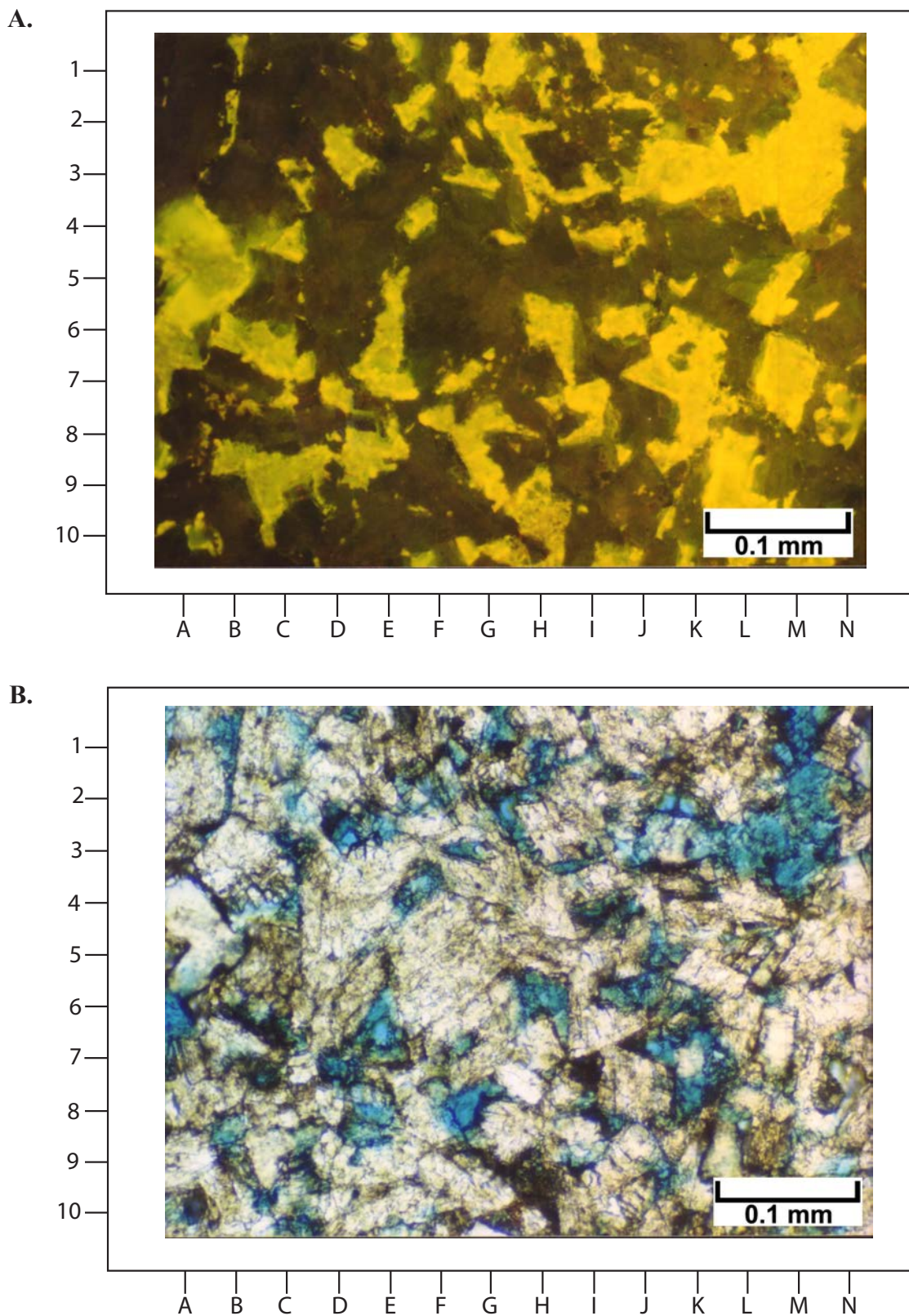
Figure 5.5. *Photomicrographs from Bug No. 16 well at 6300.5 feet (1920.4 m). (A) This EF view nicely displays rhombic and highly angular pores that fluoresce bright yellow. The rhombic dolomite crystals and crystal aggregates are dull gray and gray-green in color. Note the sharp contacts between the dolomite crystals and the intercrystalline pores. This image is probably representative of a cross-sectional view of a typical sucrosic dolomite from the lower Desert Creek interval at Bug field. (B) The same field of view as above is shown under plane light at the same magnification. Although this view shows the sucrosic dolomite crystals well (in the white to light-brown areas), the definition of pore/dolomite contacts is indistinct, in part because of bitumen linings. Pore outlines are enhanced in the EF image.*

"blind" and dead end into dolomite partitions. Only EF petrography techniques allow visual definition of this type of reservoir heterogeneity, as standard plane-light petrography does not image the micro-boxwork patterns very well.

Bug No. 16 Well

Blue-light EF microscopy of the sample from 6299.3 feet (1920.0 m) shows fine- to medium-sized, interlocking crystals in a sucrosic dolomite that displays some intercrystalline porosity (figure 5.4). Epifluorescence examination nicely shows that many of these types of rhombic, sucrosic, dolomite crystals display internal zonation with some ghosts of the original replaced carbonate grains. As in other Bug field samples, the definition of pore to matrix boundaries, especially where there are bitumen linings, can be seen much more clearly under EF.

Blue-light EF microscopy of the sample from 6300.5 feet (1920.4 m) shows excellent examples of rhombic dolomite crystals and crystal aggregates. Fluorescence photomicrographs show sharp contacts between the dolomite crystals and the intercrystalline pores (figure 5.5). This thin section is representative of a cross-sectional view of a typical sucrosic dolomite from the lower Desert Creek interval at Bug field. In addition, this sample contains complex networks of micro-boxwork structure. Many of the pores within this network appear to be isolated or "blind." Therefore, drainage of oil from this type of pore system may be inefficient. Under high magnification, EF imaging makes it easy to see highly corroded or scalloped margins of many dolomite crystals in this sample. The corroded dolomite rhomb contacts indicate that there has been some partial dissolution of dolomite rhombs.

EPIFLUORESCENCE PETROGRAPHY OF UPPER ISMAY THIN SECTIONS, CHEROKEE FIELD

Blue-light EF microscopy was completed on thin sections from six core samples for a variety of rock textures and diagenetic phases from upper Ismay zone limestone and dolomite within Cherokee field. These samples were selected to be representative of compositional, diagenetic, and pore types encountered within the two cored wells (Cherokee Federal Nos. 22-14 and 33-14). A detailed description and interpretation of the fluorescence petrography of each sample follows below along with photomicrographs (figures 5.6 through 5.11) to show representative views under both blue-light EF and plane-polarized light.

Cherokee Federal No. 22-14 Well

Blue-light EF microscopy of the sample from 5768.7 feet (1758.3 m) nicely shows pore spaces and structures that are not readily seen under transmitted, plane-polarized lighting

(figure 5.6). Black bitumen linings and interlocking, dolomite crystalline aggregates mask clear definition of the blue-dyed epoxy that has been impregnated into the open pore spaces. However, the reddish fluorescence of the epoxy makes it possible to image pores in cross section. Despite the significant amount of open porosity visible under EF, many of these voids appear to be completely surrounded by a micro-boxwork of dolomite crystals. Much of the dolomite has a dull-to bright-yellow fluorescence, due in part to the presence of live-oil films around many of the tight intercrystalline spaces. There are no identifiable remnants of the original depositional fabric of this carbonate rock, although the appearance of probable micro-moldic and slightly larger dissolution pores (figure 5.6) suggests that there were original detrital carbonate grains present.

Blue-light EF microscopy assists with the identification of fossil fragments and peloids that populate this massive, partially dolomitized limestone. Under plane polarized lighting, the sample from 5778.1 feet (1761.1 m) appears dense and muddy; however, the fluorescence petrography reveals depositional textures that range from a fine grainstone to packstone (figure 5.7). In addition, the distribution and types of pores are difficult to identify without examination under fluorescence. Abundant open micropores (reddish areas on figure 5.7) with some bitumen linings are enhanced under EF microscopy than by trying to resolve the blue-dyed epoxy that has been impregnated into the sample.

Blue-light EF microscopy of the sample from 5783.5 feet (1762.7 m) displays considerable heterogeneity of porosity and its effect on permeability (figure 5.8). The EF petrography shows the location and distribution of pores in cross sections (black and dark-red areas) and provides good visual discrimination boundaries. Areas of low porosity and permeability show up particularly well because fluorescent "live oil" is trapped in the low-permeability (tighter) parts of this sample. In addition, this sample displays some relatively large dolomite crystals (>100 μm across) that have replaced the finer carbonate matrix. Without EF, the size variation of dolomite crystals and some of the related intercrystalline pore space would be nearly impossible to resolve. Finally, an amoeboid-shaped nodule of anhydrite surrounded by finely crystalline dolomite is well displayed in the center of figure 5.8.

Blue-light EF microscopy of the sample from 5801.3 feet (1768.2 m) also displays significant heterogeneity in porosity distribution. Blue-light EF made it possible to image the quantity and quality of microporosity throughout the sample (figure 5.9). "Micro-sucrosic" dolomite appears to dominate this sample with an excellent micro-intercrystalline pore structure that could not be resolved without EF microscopy.

Blue-light EF microscopy of the sample from 5864.1 feet (1787.3 m) shows a very dense limestone and reveals some very interesting textural and porosity information (figure 5.10). Under plane transmitted light, this sample appears to

A.

B.
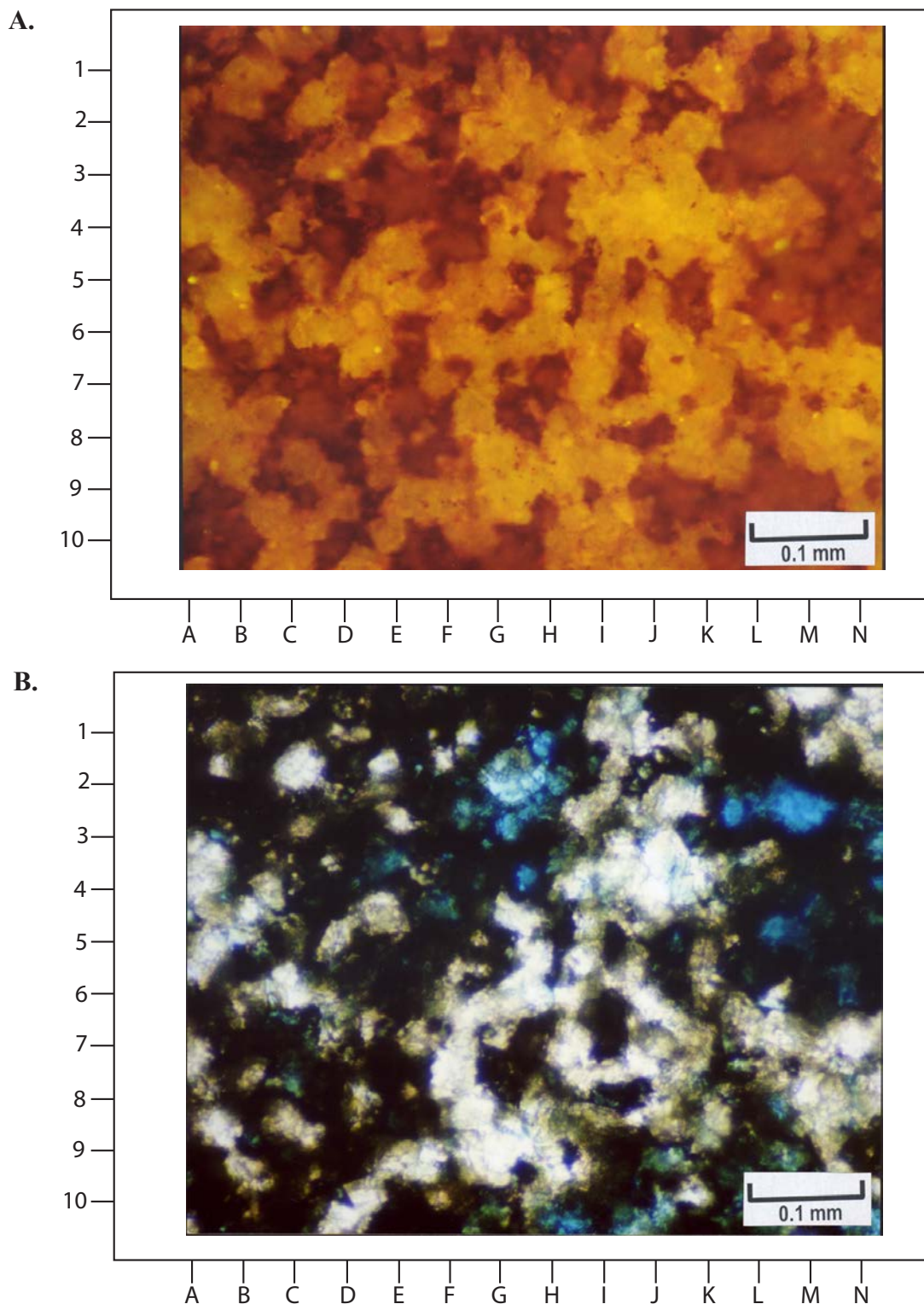
Figure 5.6. Photomicrographs from Cherokee Federal No. 22-14 well at 5768.7 feet (1758.3 m). (A) Epifluorescence under moderate magnification of a representative area of microporosity shows outlines of small dolomite crystals (fluorescing yellow here due to oil staining). The reddish areas are pores with abundant bitumen linings and plugging (see figure 5.6B). Fluorescence petrography makes it possible to clearly see the dolomite crystals versus the pore space. In places, very small rhombic outlines of dolomite crystals can be resolved (see, for instance, E-9, G-4, and N-1). Most of the pores appear in cross section to be poorly size-sorted and of dissolution origin. Many of these pores are completely surrounded by an interlocking network of dolomite crystals (see, for instance, H-3, H-6.5, and J-4). (B) The same field of view as above is shown under plane light at the same magnification. Note that the black (and opaque) areas composed of bitumen mask the crystal boundaries of the dolomite as well as individual pore outlines. The white and gray areas are remnants of the dolomite matrix that are not masked by the bitumen. Only a small amount of pore space (blue-dyed areas) can be seen in this view compared to the fluorescence photomicrograph above.
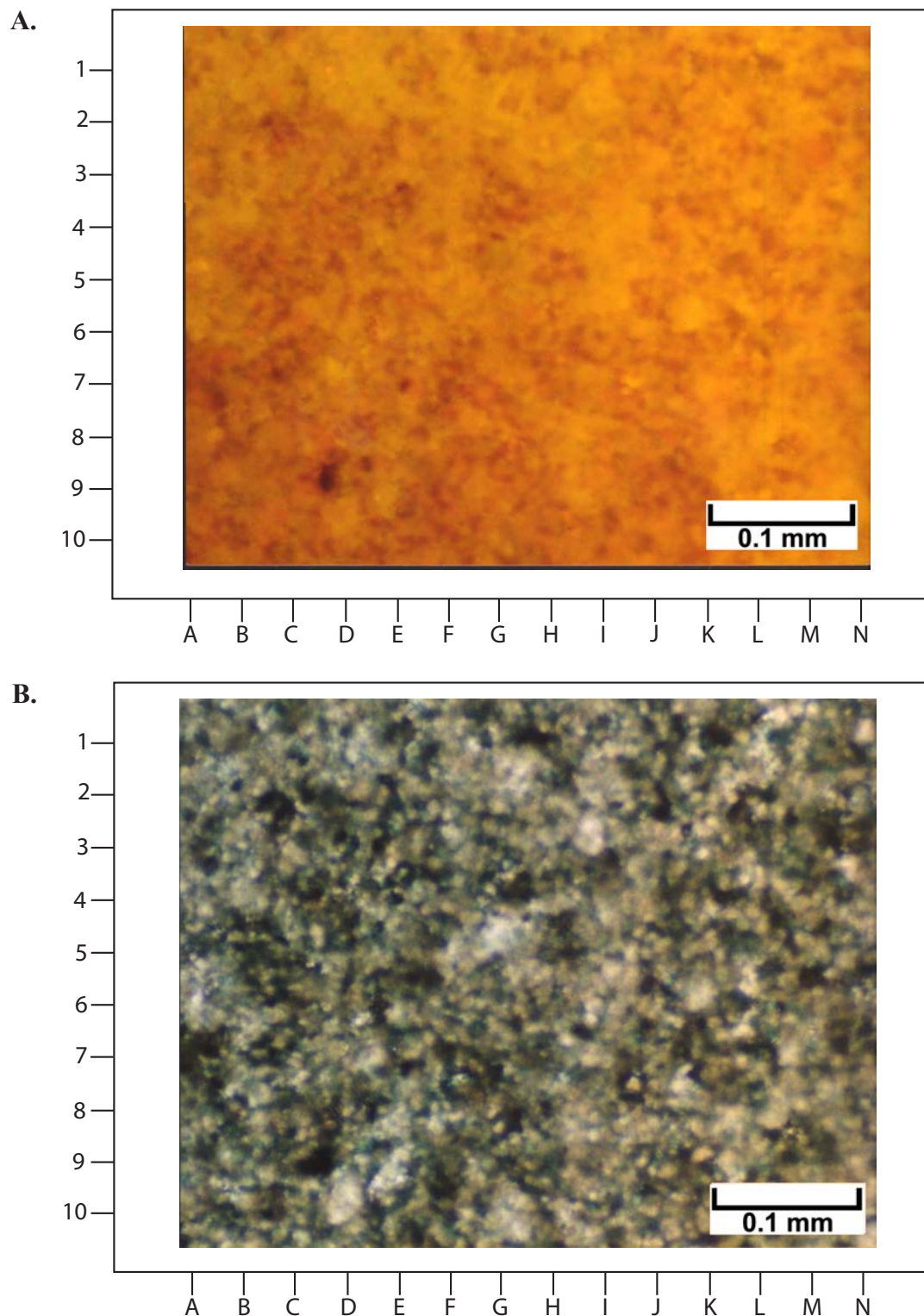
Figure 5.7. *Photomicrographs from Cherokee Federal No. 22-14 well at 5778.1 feet (1761.2 m). (A) Representative EF photomicrograph of a dense dolomitic limestone under moderate magnification distinguishes porosity from oil-stained matrix. The reddish areas represent the epoxy-impregnated pores within this sample. The yellow areas are the oil-stained, carbonate, mineral matrix. Note that the fluorescence image helps to identify occult carbonate grains such as probable fossils (e.g., G-2, H-2, and J-9) and small peloids (e.g., C-1, I-5, K-8, etc.) that are not visible in the plane-light image. This dense limestone was deposited as a bioclastic-peloidal grainstone to packstone. (B) The same field of view as above is shown under plane light at the same magnification. This part of the sample has been artificially stained with Alizarin Red-S solution. The pink areas are calcite whereas the white and gray areas are mostly dolomite. The indistinct black patches are indicative of some bitumen plugging within microporous spaces. The bluish areas within this view are due to the impregnation of blue-dyed epoxy into the micropores. However, it is impossible to see any of the carbonate components, the depositional texture, or the open pores without use of EF lighting as shown above.*

A.

B.
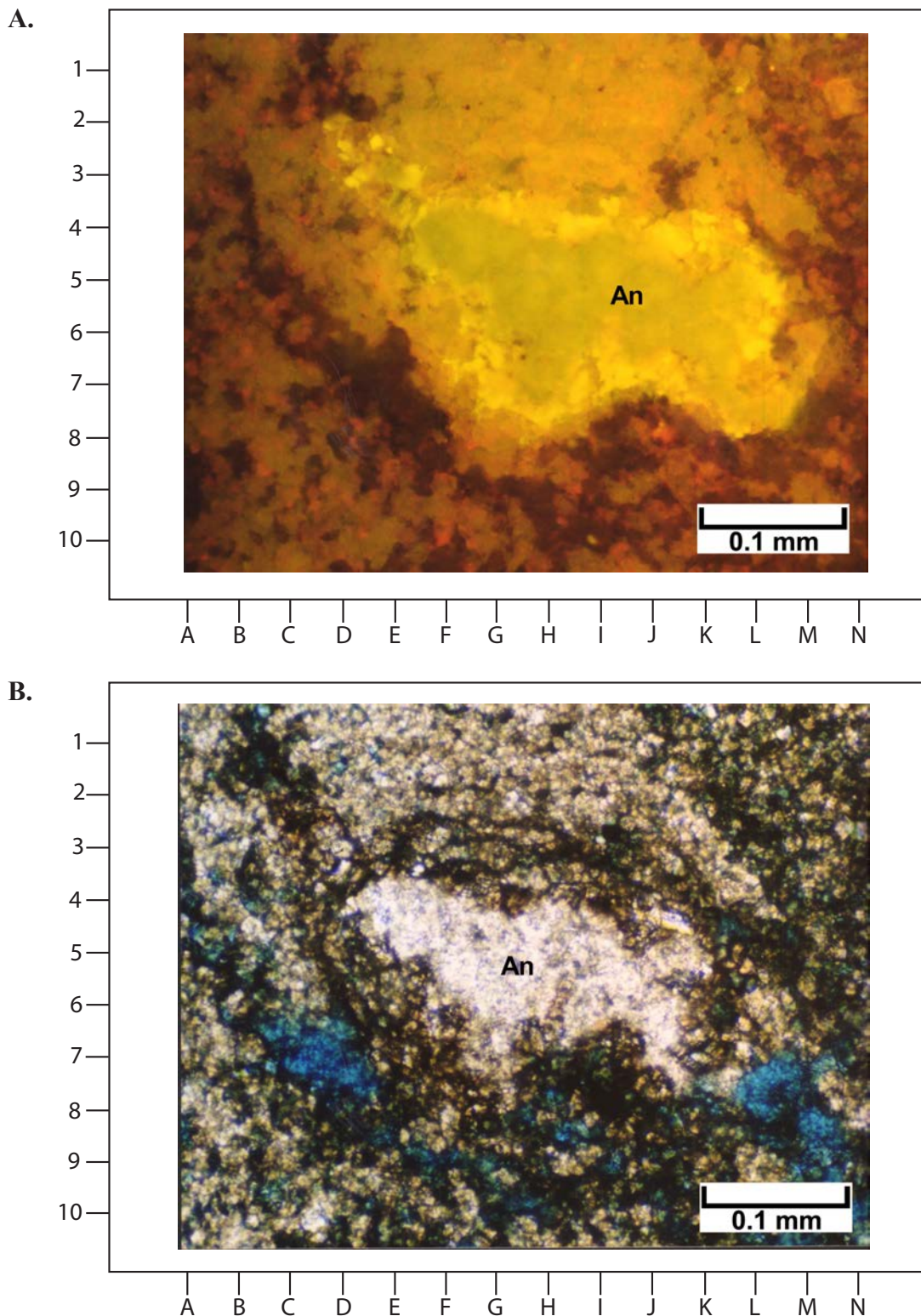
Figure 5.8. *Photomicrographs from Cherokee Federal No. 22-14 well at 5783.5 feet (1762.8 m). **(A)** A wide range of information can be seen in this EF image. The amoeboid, greenish-yellow feature in the center (from F-4 to M-7) is a small nodule of anhydrite (An) surrounded by finely crystalline dolomite. The bright-yellow rim around the anhydrite is due to "live oil" bleeding out of the dolomite and trapped against the impervious nodule. The dull-yellow areas throughout the remainder of this image consist of dolomite containing small amounts of fluorescing oils. The solid patch of dull fluorescence across the top of this photomicrograph (from E-2 to K-2) is a low-permeability area with interlocking dolomite crystals. The black and dark-red areas show where the open pore spaces occur, including pores with some bitumen coatings. Finally, the orangish areas are mostly likely weakly fluorescing bitumen. **(B)** The same field of view as above is shown under plane light at the same magnification. Even though it is possible to identify the white nodule of anhydrite (An) in the center of this field of view, the details of pore distribution, as well as the fluorescence of live oils and bitumen distribution, are not easy to see in this transmitted-light image.*

A.

B.
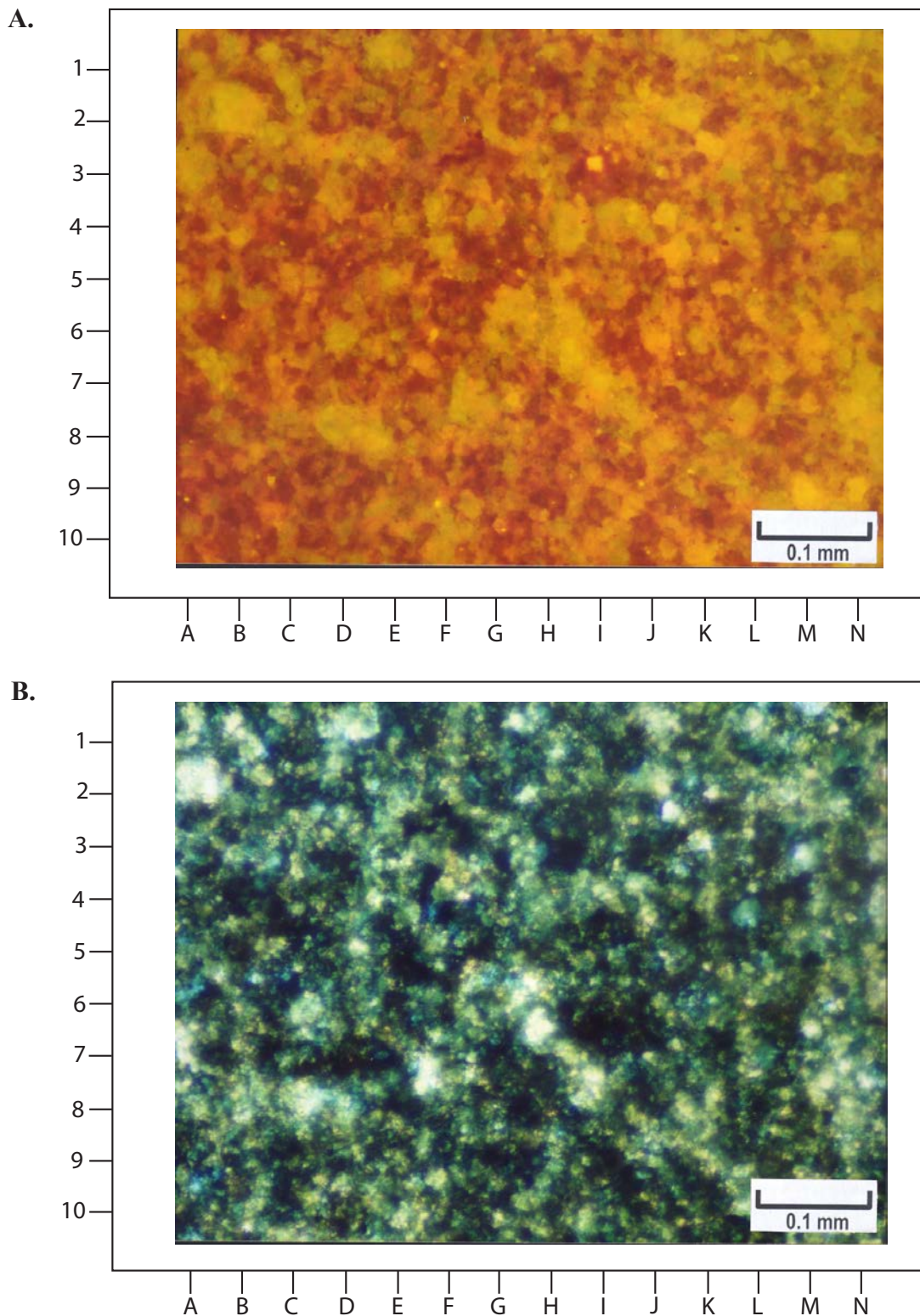
Figure 5.9. *Photomicrographs from Cherokee Federal No. 22-14 well at 5801.3 feet (1768.2 m). **(A)** Abundant pore space can be seen in this fluorescence image, where the epoxy-impregnated pores appear red. Despite the heterogeneity of the distribution of pores, most of this microporosity seems to be moderately well connected. The greenish-yellow and yellow colors in this image are from matrix areas composed of dolomite and limestone. The brightest yellow areas reflect staining of the matrix by "live oil." Note the hints of earlier sand-sized carbonate grains (e.g., F-1.5, H-2, and L-5) and sparse, isolated, larger dolomite rhombs (e.g., B-1.5, G-7, and K-2). **(B)** The same field of view as above is shown under plane light at the same magnification. Note that the details of the pore sizes and shapes cannot be seen in this plane transmitted light photo. Abundant black bitumen throughout this microporous network makes it nearly impossible to see the amount of visible porosity. At best, the microporosity in this image shows up as an indistinct "blue haze." In addition, it is not possible to see any hints of original grains or the sizes of dolomite crystals.*
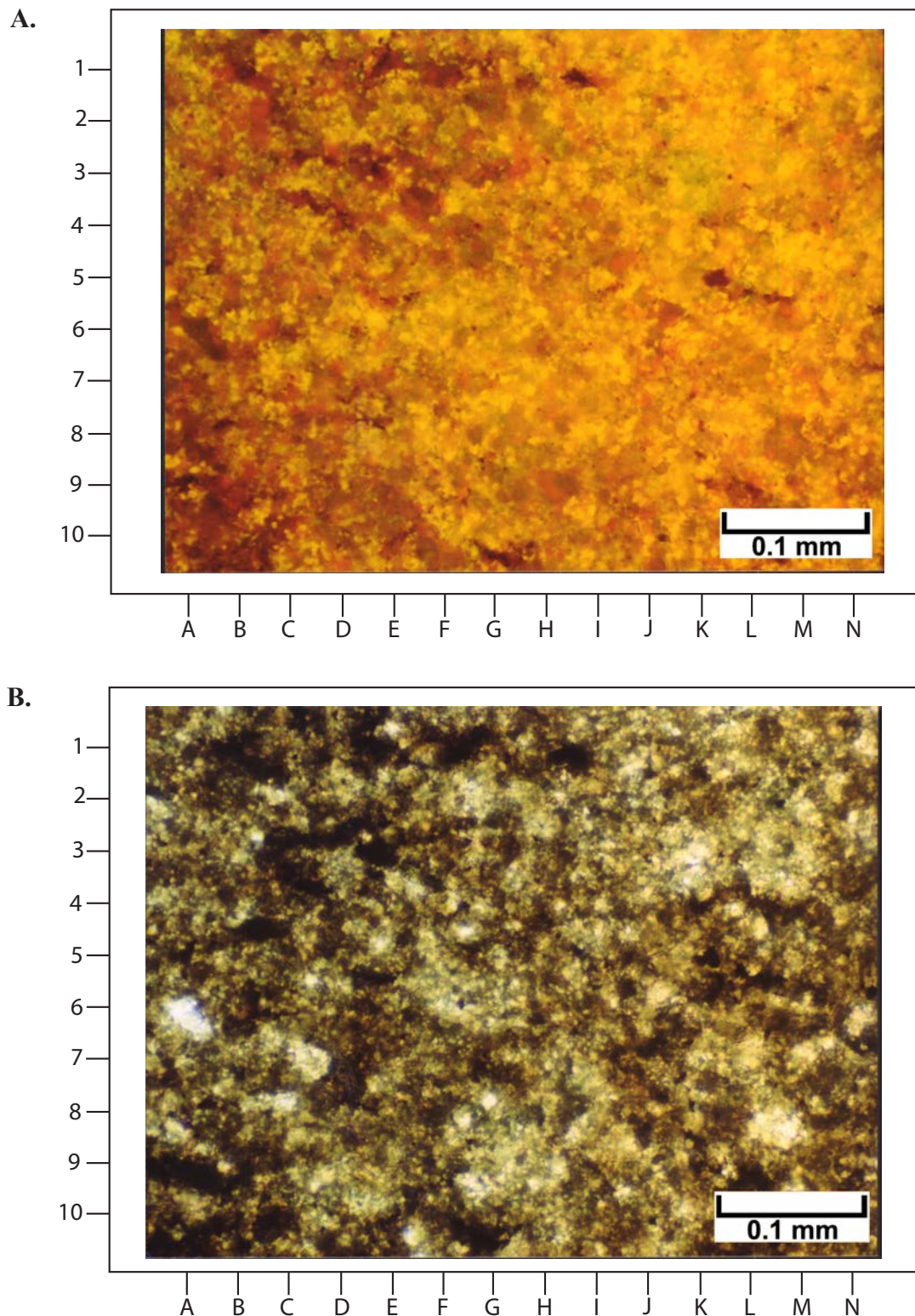
Figure 5.10. *Photomicrographs from Cherokee Federal No. 22-14 well at 5864.1 feet (1787.4 m). (A) This sample comes from a rather low-permeability limestone than has no visible matrix porosity under transmitted lighting (see photomicrograph below). However, under EF microscopy, there is some red fluorescence from spike epoxy that has been impregnated into matrix pore spaces. Therefore, the scattered red spots in this image show the presence of some porosity. The abundant bright-yellow specks across the image are probably the result of "live-oil" staining throughout this relatively low-porosity sample. Note the dull-green areas that show some relict preservation of the peloids (e.g., E-3, F-4, and L-8) that were the principal constituent of this carbonate rock. (B) The same field of view as above is shown under plane light at the same magnification. There is no visible matrix porosity in this image (i.e., no blue colors) despite the appearance in some areas of fluorescing epoxy-filled pores in the image above. In addition, the peloids that can be seen in the fluorescence view are very difficult to make out in this transmitted-light view.*

A.

B.
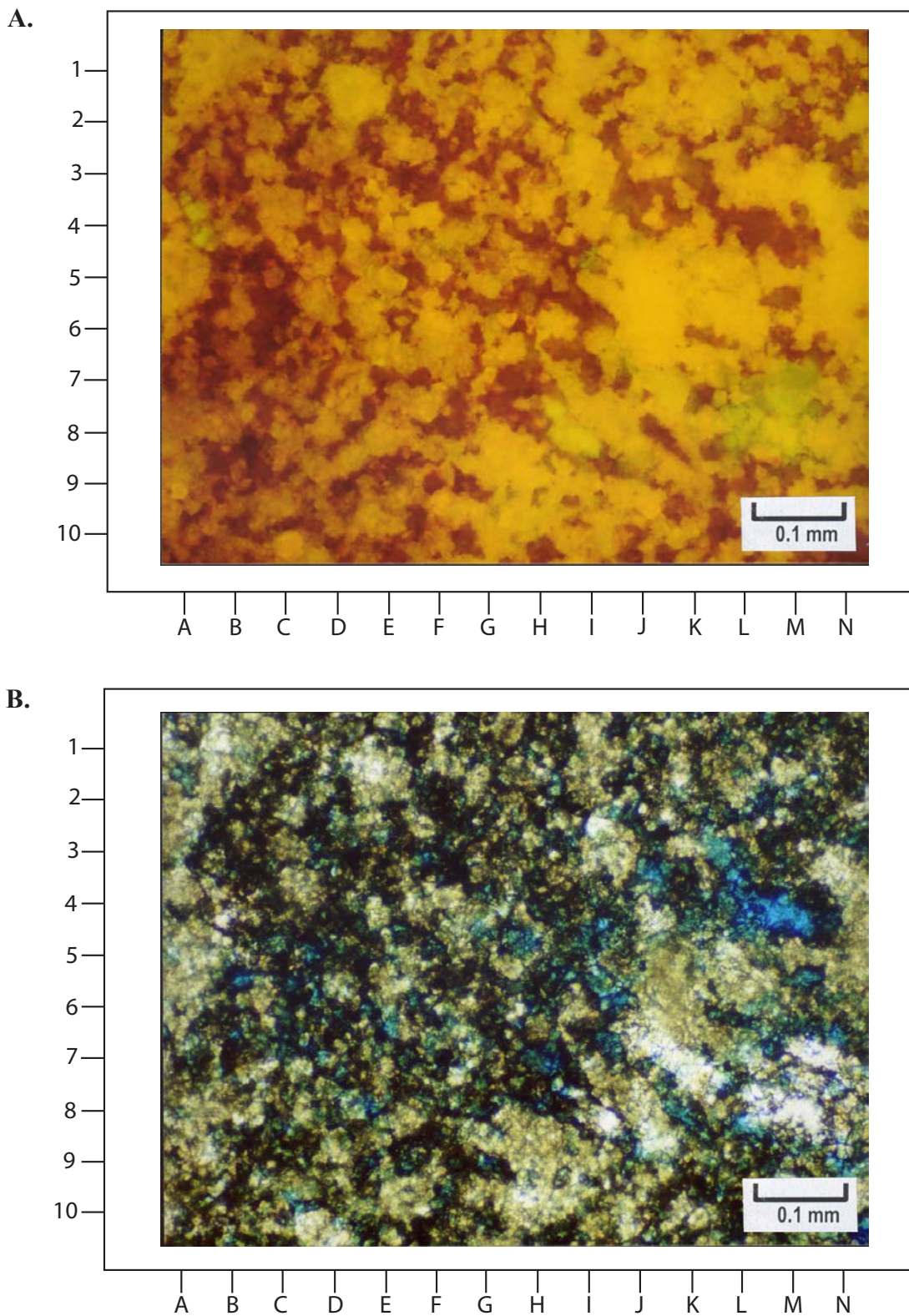
Figure 5.11. *Photomicrographs from Cherokee Federal No. 33-14 well at 5773.9 feet (1759.9 m).* **(A)** *Representative EF photomicrograph nicely shows the distribution and shapes of open pores that appear here in shades of red. Many of these pores are somewhat elongate and are moldic in origin. Most result from the dissolution of small, phylloid-algal plates and possibly other fossil skeletons. Many of these dissolution pores appear to be well connected. The yellow areas are oil-stained carbonates, which are mostly composed of limestone here. The light green areas (e.g., B-3.5 and M-7) are patches of anhydrite cementation.* **(B)** *The same field of view as above is shown under plane light at the same magnification. Note that the areas of blue-dye colored epoxy are not abundant or as distinct as the areas in red within the fluorescence photomicrograph above. Without the aid of the fluorescence view, the amount of visible open pore space would be underestimated in the plane-light image.*

be a dense lime mudstone, whereas fluorescence examination shows grain-supported peloids (dull-green areas). More importantly, EF reveals small compartments of good porosity separated from areas of much lower porosity rocks. Hence, epifluorescence suggests that the origin of the porosity may be related to dissolution of the peloidal limestone matrix.

Cherokee Federal No. 33-14 Well

Blue-light EF microscopy of the sample from 5773.9 feet (1759.9 m) shows slightly dolomitic limestone with high amounts of microporosity and solution-enlarged pores that are difficult to image under plane-polarized lighting. Blue-light EF images nicely show the open pores and their shapes despite the presence of variable amounts of black bitumen lining pore walls and some anhydrite replacement (figure 5.11). In addition, EF nicely shows remnants of fossils and non-skeletal grains (peloids and possibly ooids), as well as excellent examples of zoned, replacement, dolomite crystals. Where anhydrite has secondarily plugged earlier intercrystalline pores (figure 5.11), the differences in fluorescence between oil-impregated dolomite and very massive anhydrite cement are easy to see.

CHAPTER 6:
CATHODOLUMINESCENCE ANALYSIS, BUG AND CHEROKEE CASE-STUDY FIELDS, SAN JUAN COUNTY, UTAH

by

David E. Eby, Eby Petrography & Consulting, Inc.
and
Thomas C. Chidsey, Jr., Utah Geological Survey

CHAPTER 6:
CATHODOLUMINESCENCE ANALYSIS, BUG AND CHEROKEE CASE-STUDY FIELDS, SAN JUAN COUNTY, UTAH

INTRODUCTION

Bug and Cherokee case-study fields (figure 1.3) were selected for cathodoluminescence (CL) photomicroscopy, examination, description, and interpretation of selected thin sections of samples taken from wells in the fields (appendix J). Cathodoluminescence is the emission of light resulting from the bombardment of materials using a cathode ray (Allan and Wiggins, 1993). This technique, which can be an invaluable tool in petrographic studies of carbonate rocks, provides important information about the complex modification of rock fabrics and porosity within the lower Desert Creek and upper Ismay zones of the Blanding sub-basin (see figure 4.12 for sequence of diagenetic events). A complete discussion of the diagenetic history based upon visual core examination, thin section petrography, SEM, and pore casting is documented in appendices F and H, and discussed previously in Chapters 3 and 4.

Cathodoluminescence is used to provide insights into the chemical differences between preserved remnants of depositional components resulting from various diagenetic events in carbonate rocks as recognized from core examination and thin section petrography. In particular, CL provides visual information on the spatial distribution of certain trace elements, especially manganese (Mn^{2+}) and iron (Fe^{2+}) in calcite and dolomite (Machel and Burton, 1991; Scholle and Ulmer-Scholle, 2003). The visible CL responses are red to orange in color, and their intensity is usually described as non-luminescent, dully luminescent, and brightly luminescent. As a general rule, incorporation of Mn^{2+} into the calcite lattice stimulates luminescence and the incorporation of Fe^{2+} quenches or reduces luminescence (Fairchild, 1983; Allan and Wiggins, 1993; Scholle and Ulmer-Scholle, 2003).

Qualitative interpretation of CL usually assigns nonluminescent responses to oxidizing settings in which the reduced forms of both Mn and Fe are unavailable for incorporation into the lattices of carbonate mineral precipitates. Oxidized forms of Mn and Fe are not incorporated into calcite or dolomite crystals. Therefore, nothing in these crystals will excite luminescence. Bright luminescence is related to carbonate precipitates having high Mn/Fe trace element ratios, typically as a result of reducing environments during early (near-surface) to intermediate stages of burial diagenesis. Dull luminescence seems to happen where the Mn/Fe trace element ratios are present but not high in carbonate precipitates. Thus, dull luminescence is usually thought to be the result of intermediate to late stages of burial diagenesis. Apparently, elements other than Mn and Fe do not have any appreciable effect in enhancing or reducing luminescence (Budd and others, 2000).

References that discuss the use and limitations of CL interpretations in carbonate studies include Sipple and Glover (1965), Frank and others (1982, 1996), Marshall (1988), Hemming and others (1989), Barker and Kopp (1991), Gregg and Karakus (1991), Machel (2000), Lavoie and others (2001), Coniglio and others (2003), and Lavoie and Morin (2004).

Previous Work

Research of the application of CL petrography to Pennsylvanian rocks from the Blanding sub-basin has not been published. Unpublished thesis research includes observations of carbonate cements and dolomite in thin sections from Ismay-zone outcrop samples along the San Juan River and from five Ismay-zone cores in Ismay field by Brinton (1986).

Methodology

The CL analysis performed in this study was completed using uncovered, polished thin sections, although rock chips and unpolished thin sections could be used. The equipment needed for CL can be installed on almost any polarizing microscope (Marshall, 1988; Miller, 1988). A Nulcide Corporation luminocope model (figure 6.1) belonging to the Colorado School of Mines Department of Geological Engineering was used for this analysis. Operating conditions were generally at 10 to 12 kilovolts (kV) accelerating potential, 0.5 to 0.7 milliamps (mA) of beam current and a beam focused at about 2 centimeters. Observations were mostly visual, with some photographic documentation. No attempt was made to measure intensities or spectral information on the CL responses (e.g., Marshall, 1991; Filippelli and Delaney, 1992). Image analysis and regional mapping of cement zones (i.e., "cement stratigraphy") have been done by some workers on carbonate cements (e.g., Meyers, 1974, 1978; Dorobek and others, 1987; Cander and others, 1988; Dansereau and Bourque, 2001), but these applications are beyond the scope of diagenesis documentation attempted in this study.

CATHODOLUMINESCENCE PETROGRAPHY OF LOWER DESERT CREEK AND UPPER ISMAY DOLOMITE AND LIMESTONE THIN SECTIONS

Cathodoluminescence examination was completed on five thin section samples of lower Desert Creek zone dolomite from Bug field and five thin section samples from upper Is-
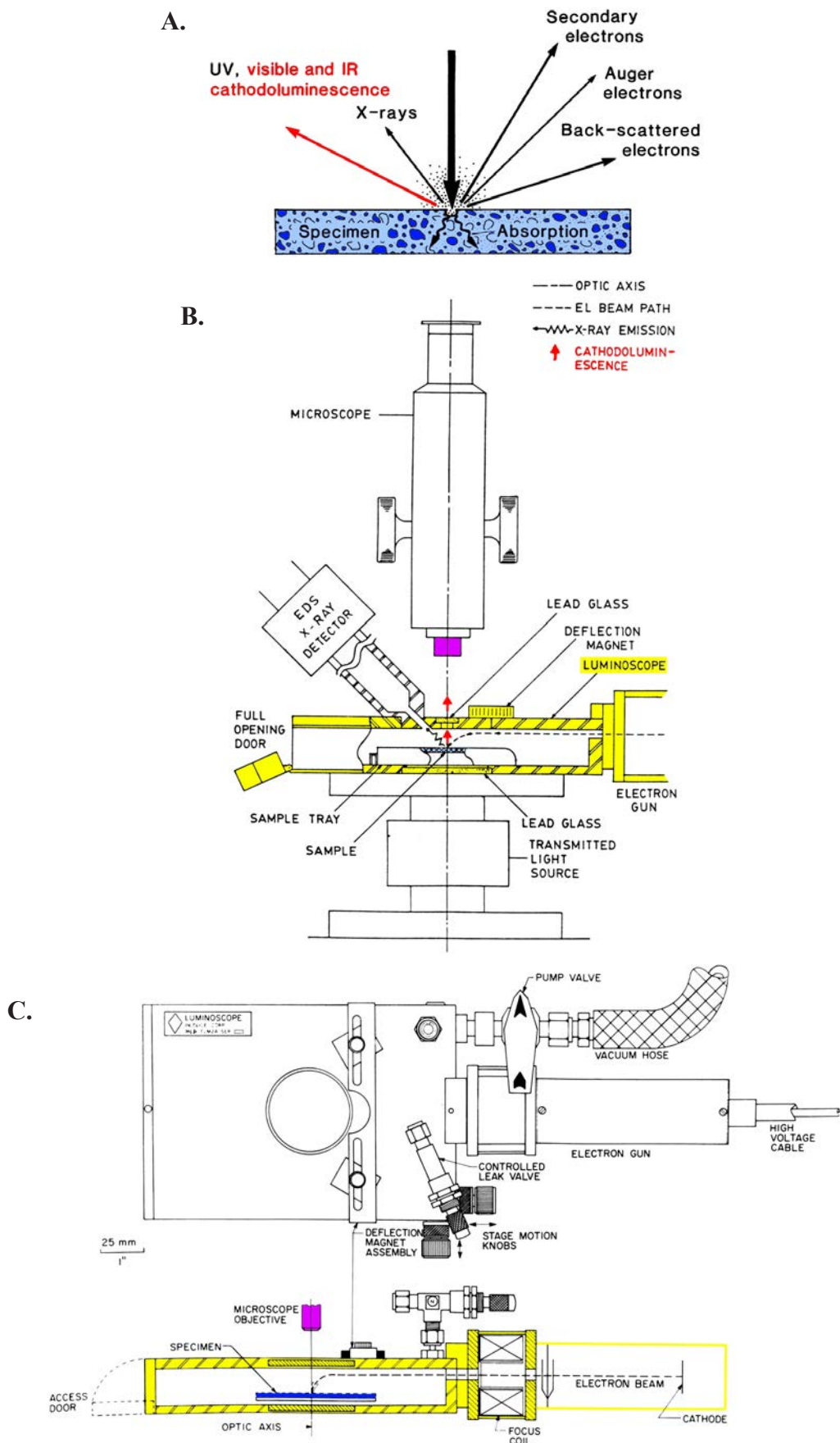
Figure 6.1. Generalized microscope optical configuration for observing cathodoluminescence (A – modified from Walker and Burley, 1991; B – modified from Marshall, 1991; and C – modified from Marshall, 1988).

may zone limestones and dolomites within Cherokee field (table 6.1). These thin section samples were selected to be representative of mineralogical (e.g., calcite, dolomite, anhydrite, and quartz), compositional, diagenetic, and pore types encountered within four cores from the lower Desert Creek dolomites of Bug field and one core from the upper Ismay limestones of Cherokee field.

Appendix J has 34 paired CL and transmitted plane light photomicrographs, as well as figures 6.2 through 6.10, from the lower Desert Creek of Bug field and upper Ismay Cherokee Federal No. 22-14 well samples.

Cathodoluminescence Petrography of Lower Desert Creek Thin Sections from Bug Field

Cathodoluminescence microscopy was completed on core-sample thin sections exhibiting a variety of rock textures and diagenetic phases from the lower Desert Creek zone reservoir dolomites within the May-Bug No. 2, Bug No. 10, Bug No. 13, and Bug No. 16 wells (table 6.1). Cathodoluminescence imaging was used to examine the details of early, fibrous marine cements that occur as distinct botryoidal fans within the sample from the May-Bug No. 2 well core at 6306 feet (1922 m) (figure 6.2). Most of these fibrous cements exhibit fairly uniform orange and red luminescence. Hints or ghosts of the radiating cement fibers are visible. The blunt to square ends of several radiating bundles of fibrous cements can be seen. These blunt ends have been used by some carbonate research-

ers (Frank and others, 1982; Goldstein, 1988, 1991) to suggest original aragonite mineralogy of these cements, since modern aragonite botryoidal cements exhibit similar morphologies. In addition, small, internal dissolution pores crossing these early marine cements are also more readily visible using CL.

Cathodoluminescence imaging enhances the contacts between dolomite matrix and pores. The dolomites replacing brecciated phylloid-algal mound fabrics are distinctly zoned when viewed under CL (figure 6.3) in the sample from the May-Bug No. 2 well core at 6312 feet (1924 m). Replacement dolomite crystals and crystal aggregates that average 100 to 200 μm display dull to non-luminescent cores and bright red luminescent rims. In one of the photomicrographs from this sample, up to four growth zones can be seen within individual dolomite rhombs. The resulting dolomitization and crystal size growth creates small sucrosic crystals that form an effective intercrystalline pore system. These intercrystalline pores augment the vuggy and shelter pores created by the brecciated phylloid-algal mound fabric.

Cathodoluminescence imaging of the sample from the Bug No. 10 well core at 6327.5 feet (1928.5 m) was particularly useful in identifying the shape and distribution of phylloid-algal plates, even though most of the plates have been partially dissolved, lined with early cements, and dolomitized (figure 6.4). Micro-boxwork arrays of bladed dolomite crystals are also very distinctive. In addition, CL provides a very vivid image of the distribution of both megapores and micropores within this dolomite. In particular, CL provides sharp definition of the

Table 6.1. *Lower Desert Creek (Bug field) and upper Ismay (Cherokee field) samples used for cathodoluminescence microscopy.*

Well	Depth (ft)	Comments
May-Bug 2	6306	Dolomitized micro-fibrous botryoidal cements. One pair of photomicrographs included in this study.
May-Bug 2	6312	Zone mega- and micro-dolomite crystals within brecciated fabric. One pair of photomicrographs included in this study.
Bug 10	6327.5	Alternating tight and streaks within dolomites. One pair of photomicrographs included in this study.
Bug 13	5930.6	"Soil" pisolites and coated grain aggregates (grapestone?). One pair of photomicrographs included in this study.
Bug 16	6300.5	Micro-boxwork dolomite. One pair of photomicrographs included in this study.
Cherokee Fed. 22-14	5773.9	Tight dolomite with no visible fabrics or differences under CL. No photomicrograph examples in this study.
Cherokee Fed. 22-14	5778.1	Micro-porous dolomite; only dim to no visible CL differences. No photomicrograph examples in this study.
Cherokee Fed. 22-14	5821.2	Radiating cement crystals and microporosity. No photomicrograph examples in this study.
Cherokee Fed. 22-14	5836.8	Micro-zoned dolomite cements and bladed to equant calcite cements. Two pairs of photomicrographs included in this study.
Cherokee Fed. 22-14	5870.3	Saddle dolomite replacement of limestone matrix and saddle dolomite cements. Two pairs of photomicrographs included in this study.
TOTAL	10 thin sections	18 CL-PL pairs of photomicrographs included in this study.
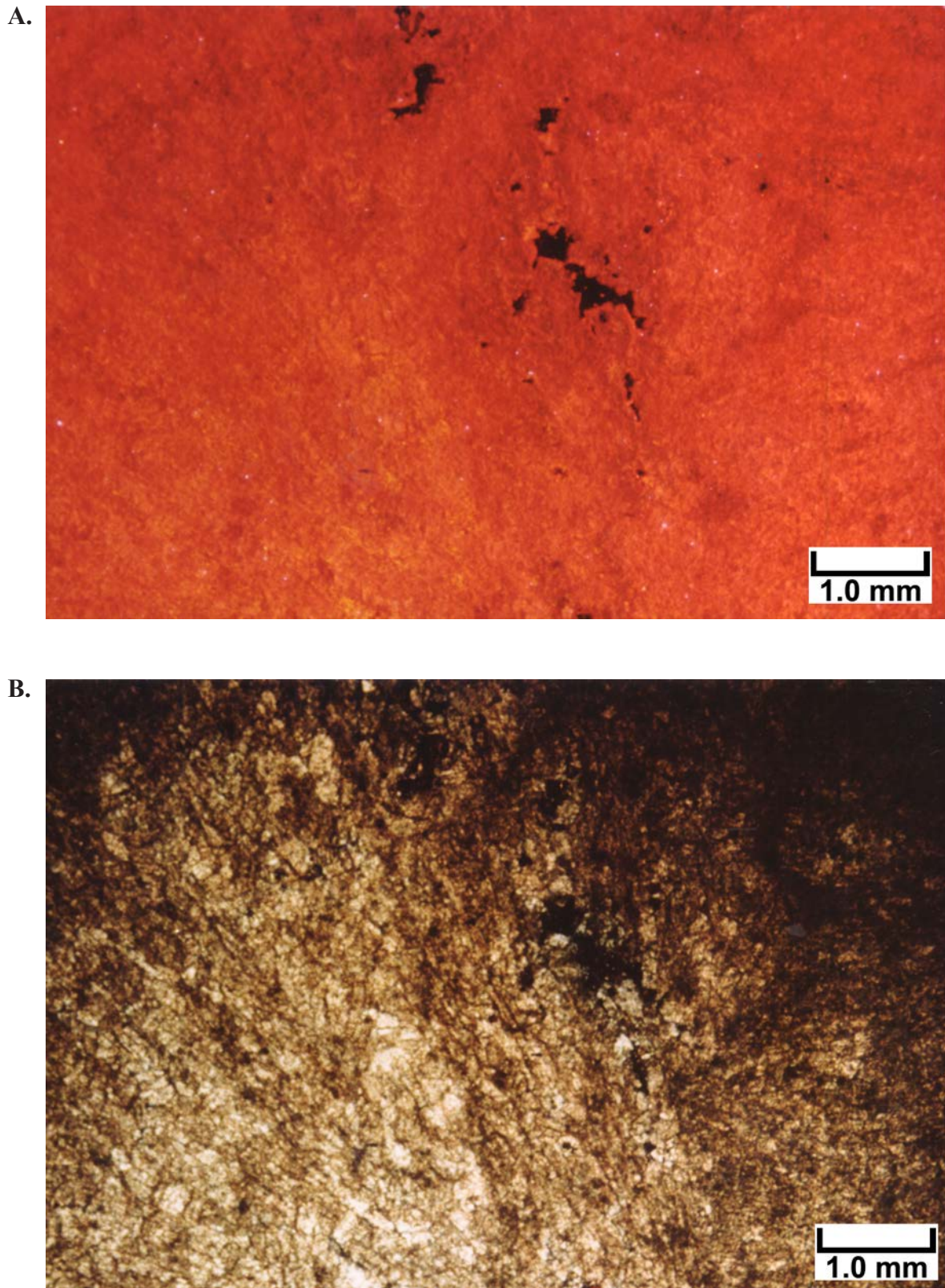
Figure 6.2. *Photomicrographs from May-Bug No. 2 well at 6306 feet (1922 m).* ***(A)*** *Cathodoluminescence imaging of a large botryoidal fan of dolomitized cements (originally aragonite) shows reasonably uniform orange and red luminescence. Note the blunt-shaped or square-ended crystal bundles evident in the area just to the right of center. Hints of radiating fibrous cements can be seen from the bottom of the photograph to the top in this view. The black (non-luminescent) patches represent secondary pores within these early marine botryoidal cements.* ***(B)*** *The same field of view is shown here under plane light at the same magnification. This photomicrograph shows ghosts of the radiating fibrous crystal habit of these completely dolomitized, early marine botryoidal cements. Without the CL view (see A above), it would be difficult to see either the blunt crystal fan terminations or the dissolution pores.*
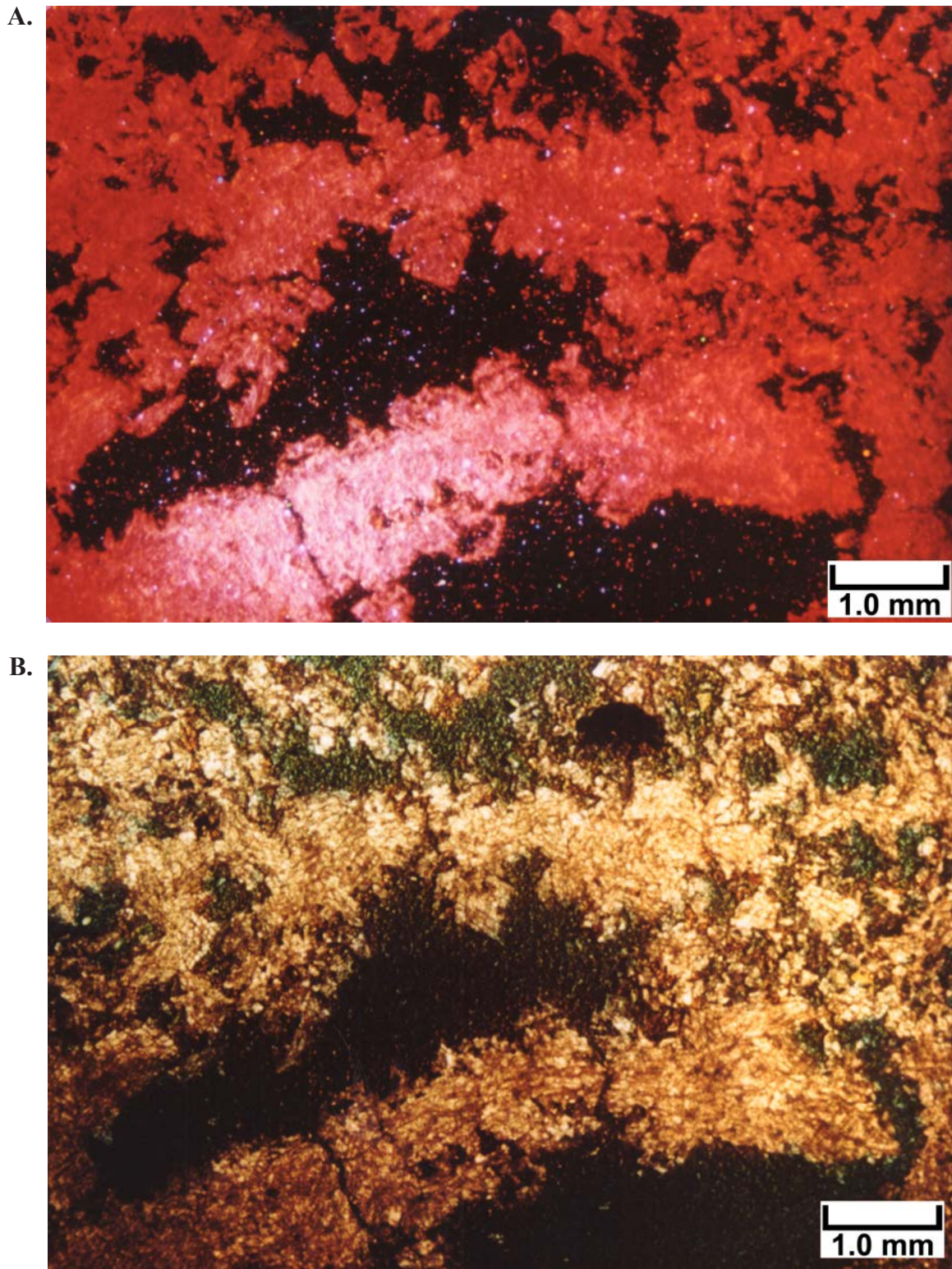
Figure 6.3. *Photomicrographs from May-Bug No. 2 well at 6312 feet (1924 m). (A) This CL view nicely shows micro-rhombic dolomites that have completely replaced a brecciated phylloid-algal mound fabric. Despite the dull red luminescence of these dolomites, growth zones and different crystal sizes can readily be seen within the replacement fabric. For instance, note the dolomite crystals (in the upper center part of this photomicrograph) with dead (black) cores and bright luminescent (red) rims. This zonation is probably related to two distinct growth stages of this replacement dolomite. The resulting dolomitization of this mound fabric creates small sucrosic or rhombic crystals that produce an effective intercrystalline pore system. The large black patches in the lower half of this photomicrograph consist of open pores within this brecciated phylloid-algal mound fabric. (B) The same field of view is shown here under plane light at the same magnification. Note that there is very little detail within this replacement dolomite that is visible under plane-transmitted light. For instance, it is impossible to see any of the zoned dolomite rhombs or the precursor fabrics before dolomite replacement without the use of CL.*
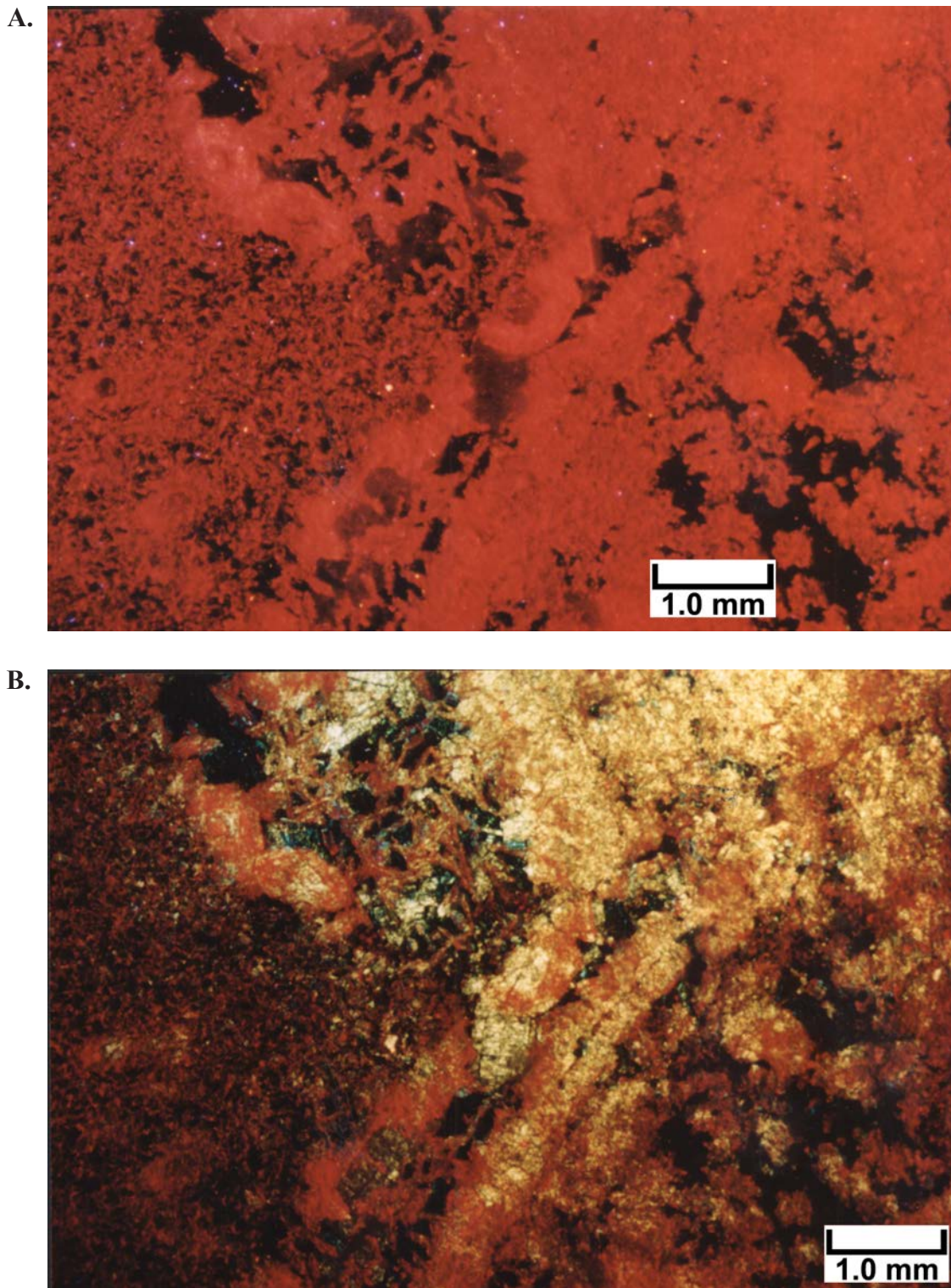
Figure 6.4. *Photomicrographs from Bug No. 10 well at 6327.5 feet (1928.6 m). **(A)** Cathodoluminescence imaging clearly shows some of the distinctive fabric elements within a completely dolomitized, phylloid-algal/skeletal, grain-rich rock. Note the elongate blades of poorly preserved phylloid-algal plates from bottom center to upper right in this photomicrograph. Within these blades are preserved remnants of skeletal materials in bright red, and cements in dull reddish-gray. For the most part, dolomitized skeletal grains, or their remnants, appear as bright red luminescent areas with clear skeletal shapes. Some of the grains easily visible in this field of view are rounded crinoids with their distinctive circular cores and single crystal, red luminescent rims. Early cements (prior to dolomitization) are very dull red. Porous microdolomites dominate the left quarter of this photomicrograph. Note also the remnants of dolomitized bladed cements and micro-boxwork dolomite fabrics visible in the upper left center of this view. The black areas throughout this field of view are open pores. **(B)** The same field of view is shown here under combined plane light and CL (i.e., a double exposed image) at the same magnification. In this view, remnants of bright red luminescence show through the coarse and fine dolomite crystal patterns. The blue and black areas of this slide consist of open pores.*

A.

B.
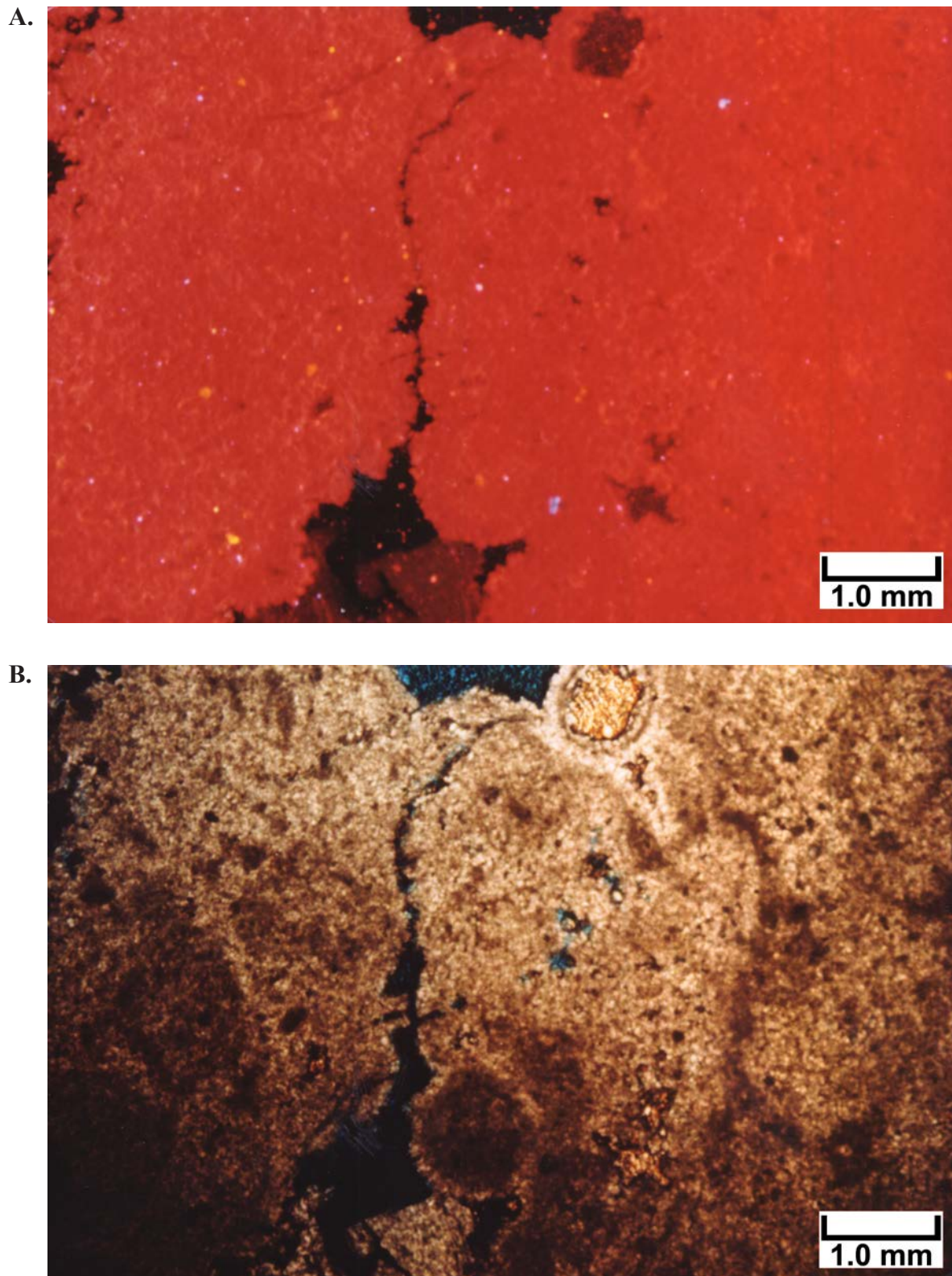
Figure 6.5. *Photomicrographs from Bug No. 13 well at 5930.6 feet (1807.6 m). **(A)** This CL view is from a sample of pisolites and coated-grain aggregates. Note that it is possible to see the carbonate-grain outlines (in uniformly dull red) versus early carbonate cements (in orangish-red). Late-stage, dolomitized, spar crystals can be seen in the dull-gray patches in the lowermost and uppermost center of this view. The black (non-luminescent) areas clearly image the open pores and microfractures. **(B)** The same field of view is shown here under plane light at the same magnification. In this view, it is possible to see the large coated grain aggregates (pisolites and possible grapestones). However, plane light viewing does not show the individual carbonate grains that compose the larger grain aggregates as well as the CL imaging.*
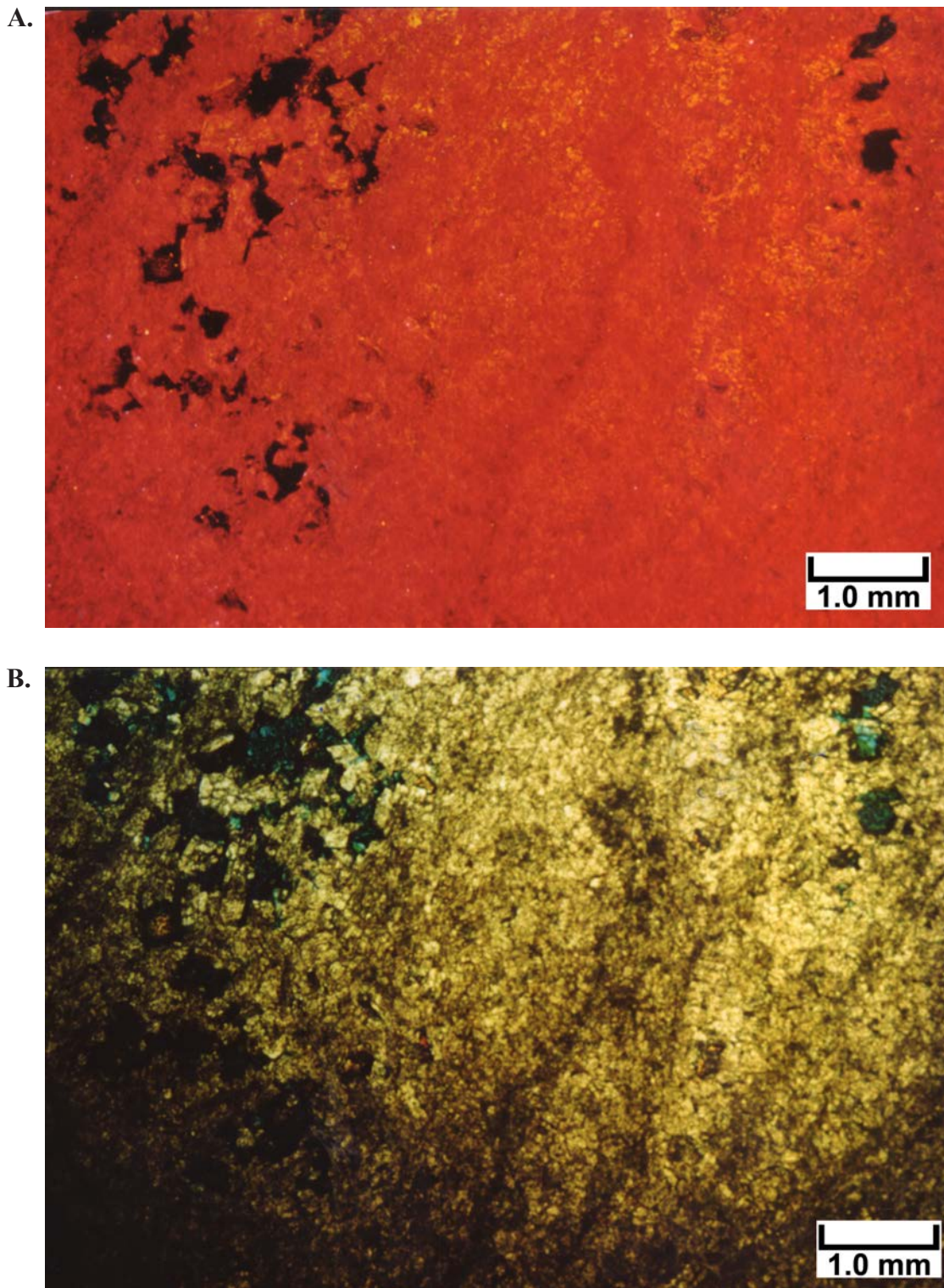
Figure 6.6. *Photomicrographs from Bug No. 16 well at 6300.5 feet (1920.4 m).* ***(A)*** *Cathodoluminescence of an area displaying micro-boxwork dolomite and early fibrous marine cements is imaged here. Note the patterns of dull red, bright red, and orangish-red throughout this dense, tight dolomite. Most of the original carbonate fabric associated with carbonate sediment and early marine cements can be seen in the dull and bright red patterns. The orangish-red areas represent later dolomite cement growth bands. In some areas of this view (especially in the left third of the image), dolomite crystals have developed a clear rhombic shape. The black areas clearly define open pores associated with dissolution as well as the development of intercrystalline porosity.* ***(B)*** *The same field of view is shown here under plane light at the same magnification. Only the outlines of larger dolomite crystals are visible. Cathodoluminescence imaging, as shown above, brings out the internal original fabric versus later dolomite growth zones much more clearly. The blue patches are open pores lined with black bitumen. The presence of bitumen makes it difficult to clearly discern the outlines of dolomite matrix versus open pores under plane light. Cathodoluminescence (above) images the pore/rock boundaries very well.*
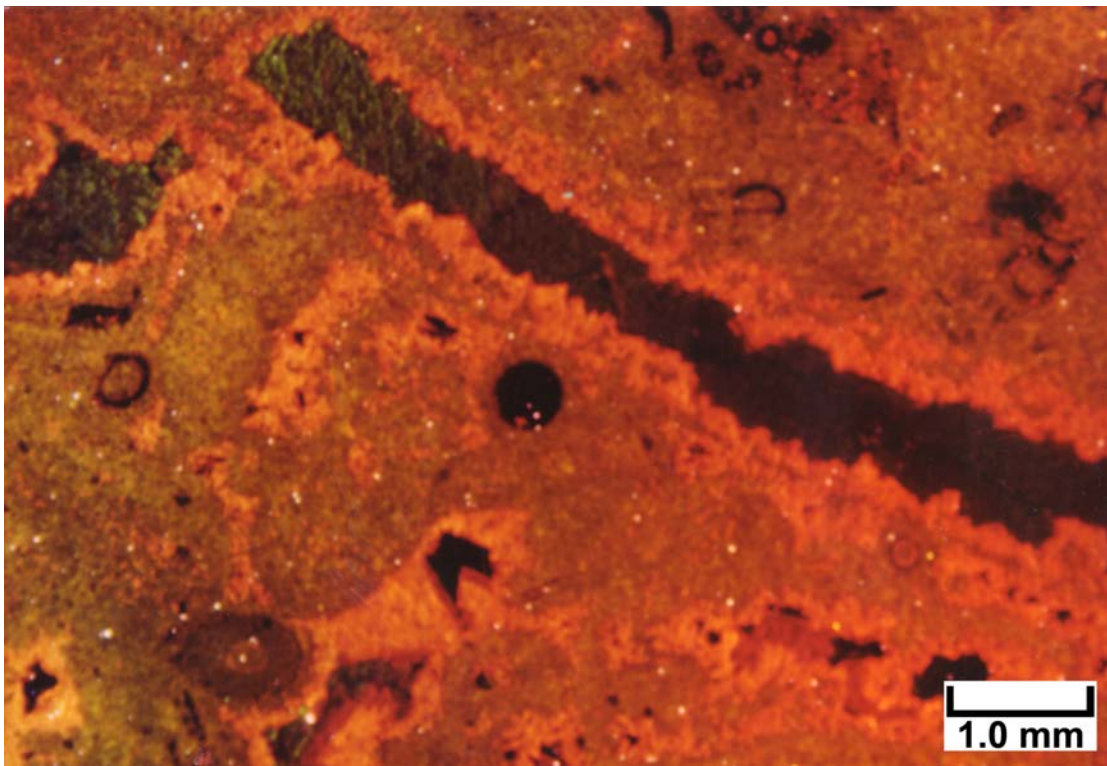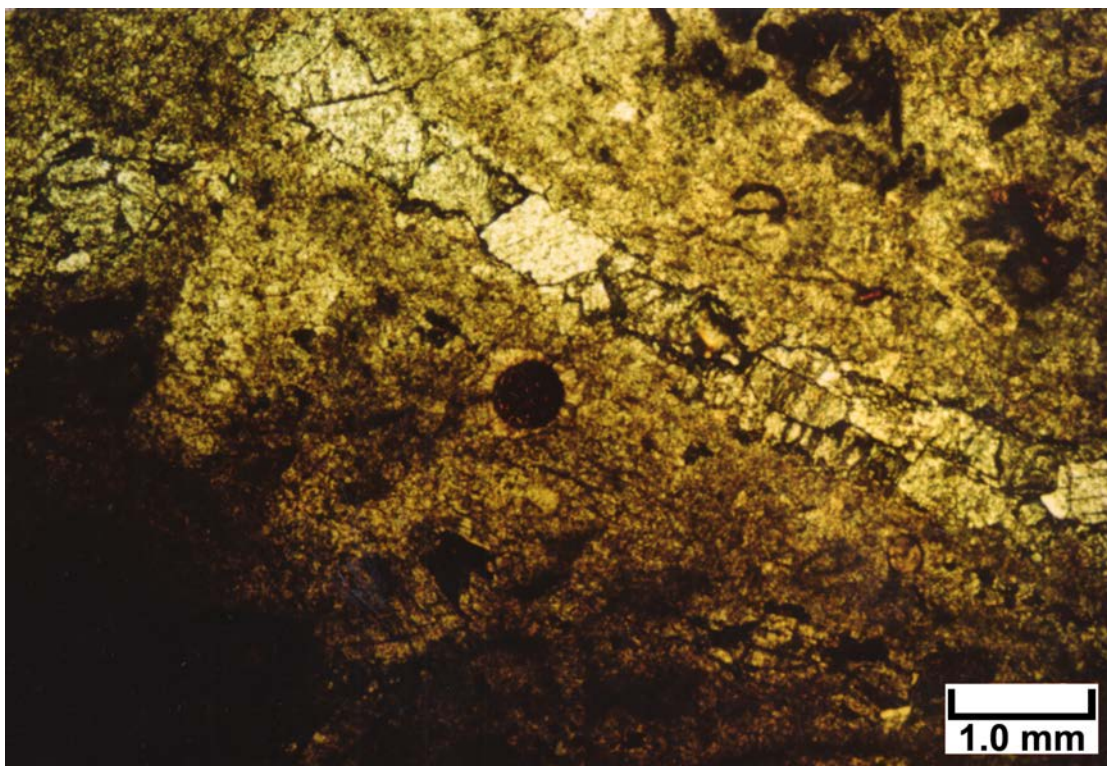
Figure 6.7. *Photomicrographs from Cherokee Federal No. 22-14 well at 5836.8 feet (1779.1 m). **(A)** Cathodoluminescence overview of a representative skeletal/peloidal grainstone shows the details of grain preservation as well as different generations of calcite cement. Note the elongate non-luminescent area (from the upper left to right-central sections of this photomicrograph) which represents a dissolved phylloid-algal plate which is now a moldic pore. Other non-luminescent (black) parts of this view are also open pores or are filled with the same generation of calcite cement. A series of banded bright and dull cement generations represent an earlier generation of pore-filling cements. **(B)** The same field of view is shown here under plane light at the same magnification. Note that the preservation of original grains, leached skeletal grains such as the dissolved phylloid-algal plate, and the multiple generations of cement are not visible under plane light. Without CL, many of these features would be difficult to identify.*

A.

B.
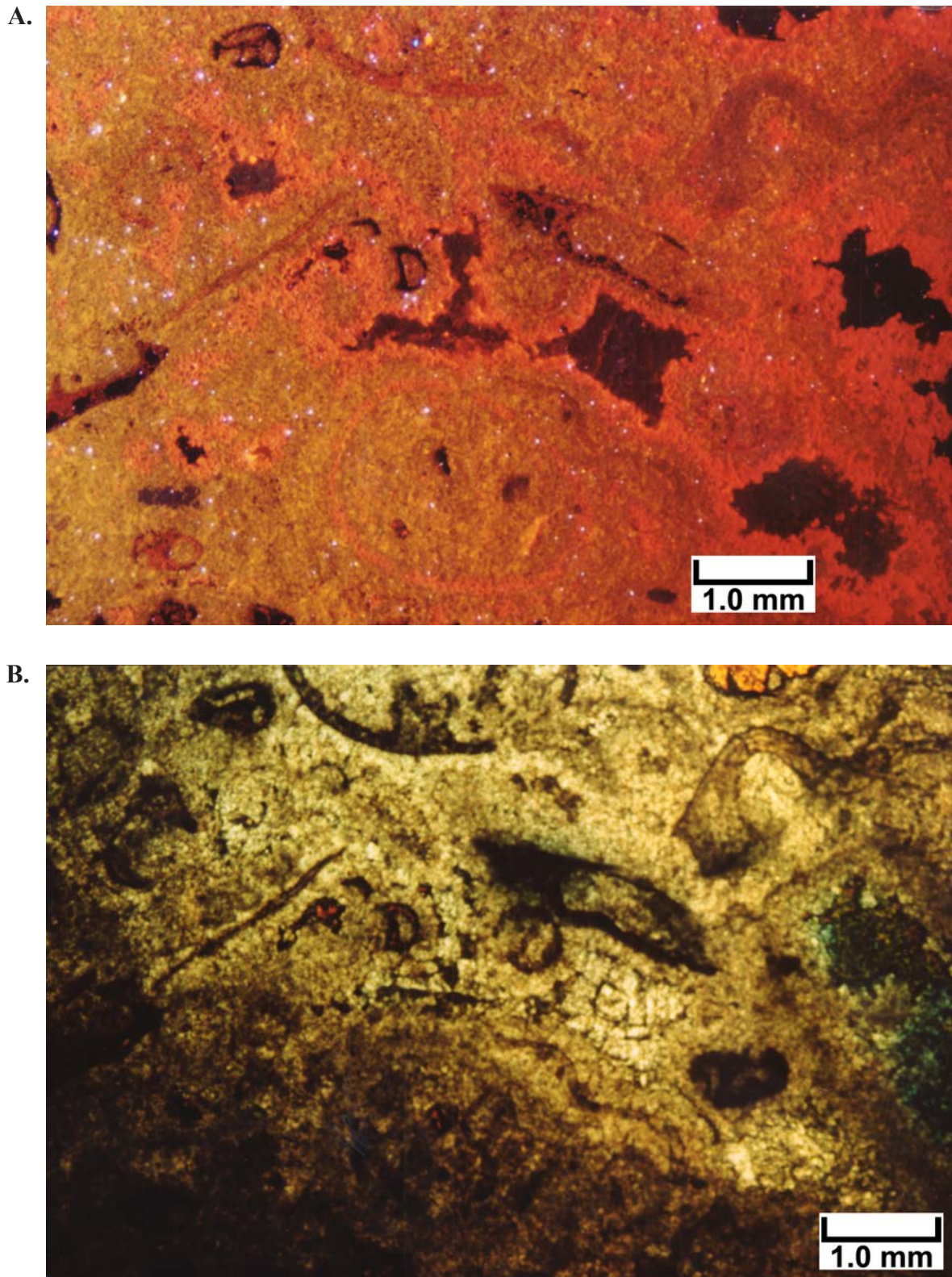
Figure 6.8. *Photomicrographs from Cherokee Federal No. 22-14 well at 5836.8 feet (1779.1 m). **(A)** This CL view shows various skeletal grains in the dull red shapes and colors surrounded by banded generations of early pore-filling cements. Note the non-luminescent (black) patches that represent largely secondary pores that have either been filled with equant calcite spar cement, or are isolated, open moldic pores. The numerous light blue specs across this photomicrograph are mostly detrital quartz silt grains within this carbonate sediment. **(B)** The same field of view is shown here under plane light at the same magnification. Vague outlines of skeletal grains, including broken phylloid-algal plates, brachiopod shells, and bryozoan fragments, are seen in the dark grains. This view does not provide much detail to differentiate various generations of calcite cement seen in the CL view above.*
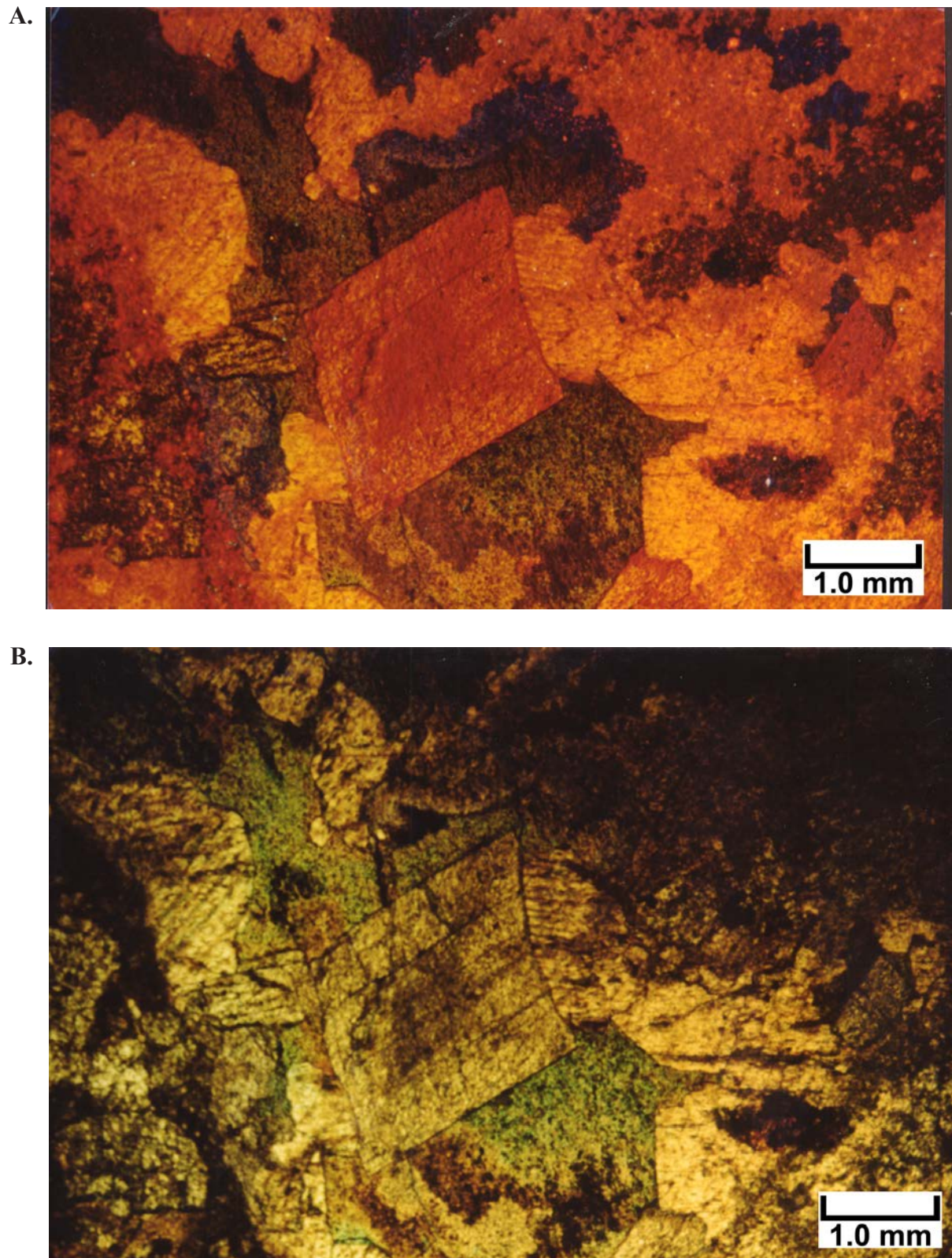
Figure 6.9. *Photomicrographs from Cherokee Federal No. 22-14 well at 5870.3 feet (1789.3 m).* **(A)** *Most of the large crystals in this CL view consist of dolomite. Note, in particular, that the large crystal in the center displays strongly curved crystal faces. This "saddle dolomite" (Radke and Mathis, 1980) as well as the other coarse dolomite crystals with reddish luminescence are probably late, burial or hydrothermal dolomites that precipitated under elevated temperatures.* **(B)** *The same field of view is shown here under cross-polarized light at the same magnification. Note the sweeping extinction within the large crystal in the center, indicative of a strained crystal lattice. The bluish areas surrounding these replacement dolomites are remnants of intercrystalline pores.*
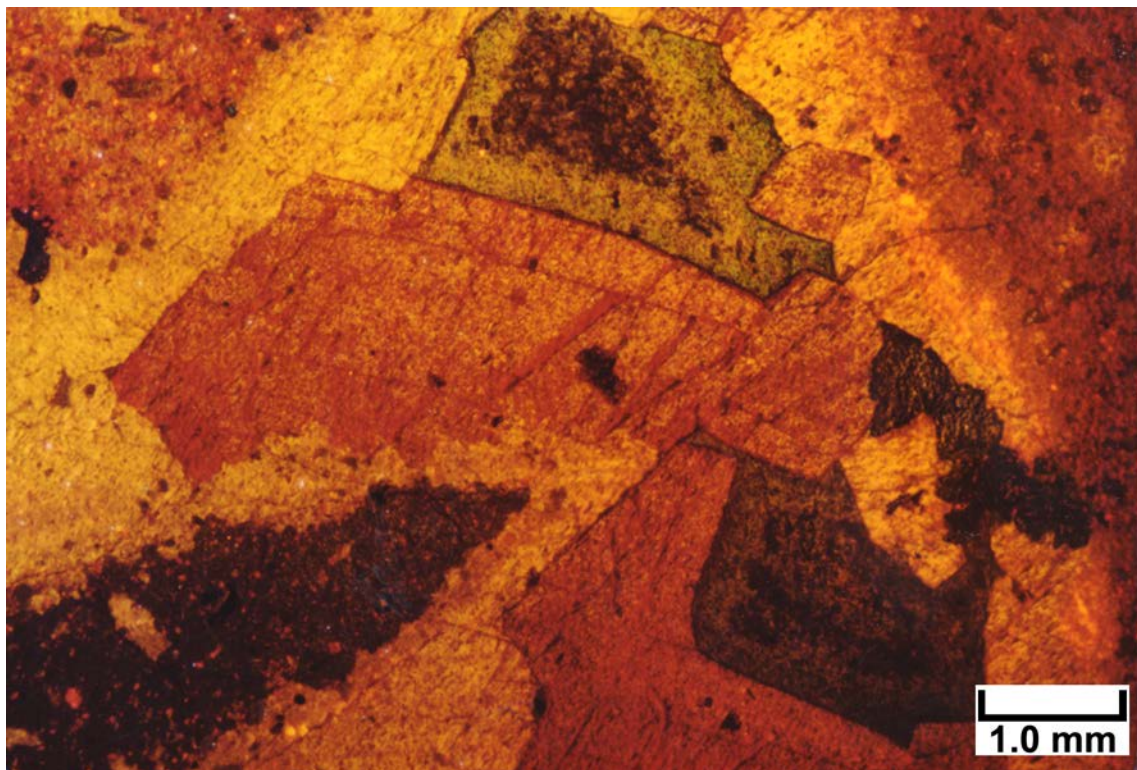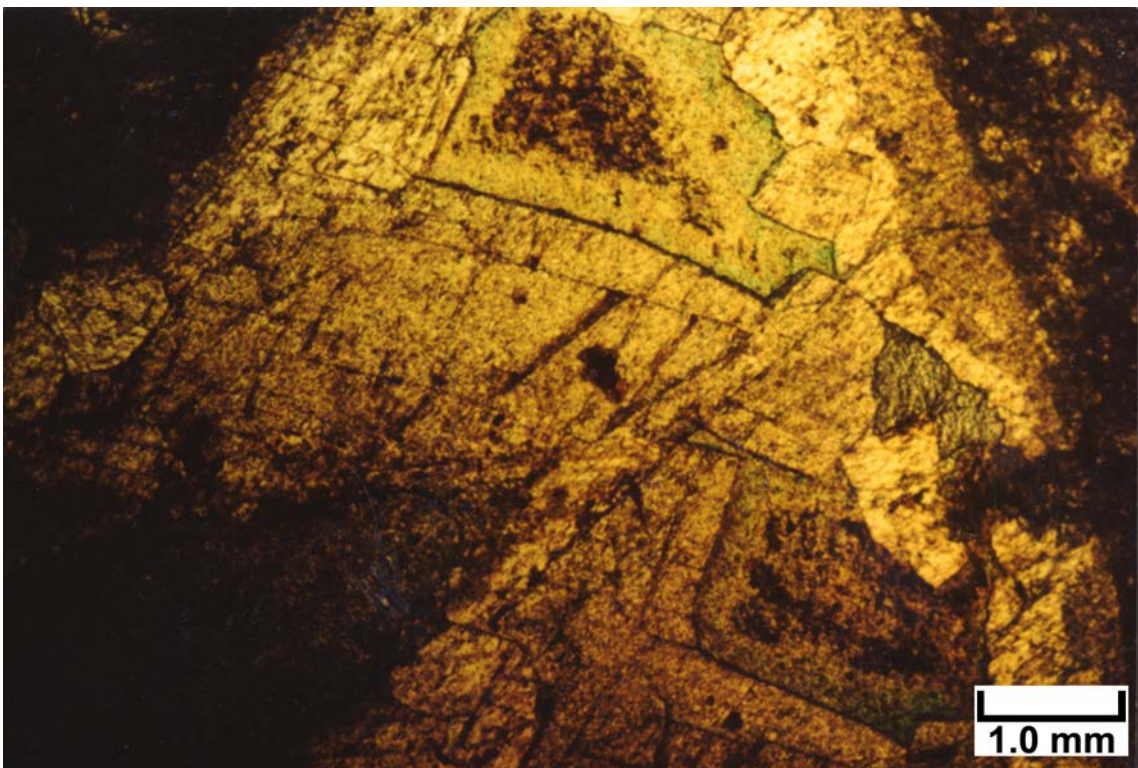
Figure 6.10. *Photomicrographs from Cherokee Federal No. 22-14 well at 5870.3 feet (1789.3 m).* **(A)** *This CL view shows remnants of a muddy limestone matrix (wackestone) in the lower left and upper right corners that has been partially replaced by coarse dolomite crystals displaying curved faces. These "saddle dolomites" have a distinctive dull red and orange luminescence in which hints of the dolomite growth bands can be seen. Small inclusions of dark-colored, lime, wackestone matrix can be seen scattered throughout the coarse dolomite saddles, indicating that these saddle dolomites replaced previous carbonates rather than being entirely cements.* **(B)** *The same field of view is shown here under cross-polarized light at the same magnification. Note the intercrystalline pores (blue areas) between some of the saddle dolomites. This view shows where dolomite has replaced lime wackestone matrix (in the medium and dark-brown areas) and where dolomite is a cement growing into open pores (the clear areas).*

pore boundaries with the dolomite matrix and crystal boundaries. Evidence of a brecciated fabric, as well as dissolution and corrosion of early sediments and cement, are enhanced in this sample under CL than under plane polarized light.

A sample from the Bug No. 13 well at 5930.6 feet (1807.6 m) consists of dolomitized pisolites and coated grain aggregates (similar to "grapestone"). Cathodoluminescence imaging aids in distinguishing the smaller grains incorporated into the grapestone, or aggregate grains, versus the early marine cements (figure 6.5). Parts of this sample consist of internal sediment composed of carbonate mud and silt-sized, detrital quartz. The pelleted nature of the muddy part of this sample is very evident under CL, despite the complete dolomitization of this interval. Interestingly, detrital quartz silt grains of probable eolian origin are easily visible within the internal sediments of this sample. In addition, CL imaging enhances open (versus cemented) pores and microfractures within this sample.

Cathodoluminescence imaging of the sample from the Bug No. 16 well core at 6300.5 feet (1920.3 m) was particularly useful in identifying dense, dolomitized, micro-boxwork arrays as well as bundles of fibrous marine cements (figure 6.6). Original grains and cement fabrics can be seen in the brighter red parts of the luminescing dolomites. Somewhat later cements and zonation within coarser dolomites can be seen in the orangish-red areas. Cathodoluminescence imaging also provides sharp definition of rhombic dolomite crystal terminations as well as intercrystalline pores.

Carbonate grains such as peloids and fragmented skeletal debris can be distinguished from carbonate cements in completely dolomitized intervals (see examples in appendix J). The dolomitized grains exhibit deep red colors under CL whereas the carbonate cements are bright reddish-orange. Cathodoluminescence also brings out significant detail in areas of anhydrite replacement of the dolomitized sediment (see examples in appendix J). Islands of red luminescing dolomite can be easily seen within the plethora of bladed-anhydrite crystal aggregates. Finally, CL does an excellent job in imaging microfractures and microfracture swarms cutting through the lower Desert Creek dolomites (see examples in appendix J). Most microfractures can be seen as dark-gray to black (non-luminescent) curvilinear lines. Some of these open microfractures possibly may have originated from dissolution along microstylolites.

Cathodoluminescence Petrography of Upper Ismay Thin Sections from Cherokee Field

Cathodoluminescence microscopy was completed on core-sample thin sections having a variety of rock textures and diagenetic phases from the upper Ismay zone limestones within the Cherokee Federal No. 22-14 well (table 6.1). However, only two of the five samples showed any significant visible response to CL.

Cathodoluminescence imaging provides good to excellent resolution of grains (both skeletal and non-skeletal) as well as different generations of calcite cements within the limestone in the thin section from 5836.8 feet (1778.9 m) in the Cherokee Federal No. 22-14 well (figures 6.7 and 6.8). Fine details of the microstructures within skeletal fragments, such as brachiopods, bryozoans, and phylloid-algal plates, are more readily visible under CL than with transmitted plane light. In addition, calcite cements that rim leached skeletal grains, as well as early generations of isopachous cements, can be easily seen. Some of the cements display a series of concentric bright and dull luminescent bands that represent multiple generations of cementation under varying water chemistry. Such concentrically banded cements are similar to those cements used in calcite cement stratigraphy within Carboniferous carbonate systems in North America by Meyers (1974, 1978, 1991) and Goldstein (1988, 1991). Finally, CL enhances the pore outlines and boundaries better than under plane light viewing. Thus, it becomes possible to qualitatively interpret how interconnected the remaining pore systems are within this sample.

Cathodoluminescence imaging was very useful in identifying the presence of saddle dolomites (Radke and Mathis, 1980) within microporous dolomites in the sample from the Cherokee Federal No. 22-14 well core at 5870.3 feet (1789.2 m). Large dolomite crystals (1.0 to 2.0 mm in diameter) with distinctly curved crystal faces occur as both replacements of finer, earlier dolomites and as pore-filling cements (figures 6.9 and 6.10). These saddle dolomites display dull, red luminescence in their core areas and slightly bright, orange-red luminescence toward their rim areas. In addition, CL makes it possible to see the growth bands in these coarse dolomite crystals due to slight luminescent differences between each growth zone.

In general, the presence of saddle dolomites within a carbonate sample is indicative of the growth of strained, slightly iron-rich, dolomite replacements and cements under elevated temperatures during burial conditions (Radke and Mathis, 1980). Additional published descriptive work on saddle dolomites using CL can be found in Lavoie and Morin (2004).

CHAPTER 7:
ISOTOPE GEOCHEMISTRY, BUG, CHEROKEE, TIN CUP MESA, AND PATTERSON CANYON FIELDS, SAN JUAN COUNTY, UTAH

by

David E. Eby, Eby Petrography & Consulting, Inc.
Stephen T. Nelson, Brigham Young University
and
Thomas C. Chidsey, Jr., and Craig D. Morgan (retired), Utah Geological Survey

CHAPTER 7:
ISOTOPE GEOCHEMISTRY, BUG, CHEROKEE, TIN CUP MESA, AND PATTERSON CANYON FIELDS, SAN JUAN COUNTY, UTAH

INTRODUCTION

Diagenesis played a major role in the development of reservoir heterogeneity in Bug and Cherokee fields and probably throughout the Paradox Formation fields (figures 3.1 and 4.12). Stable isotope geochemistry provides insights into the chemical differences between preserved remnants of depositional components from various diagenetic events in carbonate rocks as recognized from core examination and thin section petrography. A graph of carbon versus oxygen isotope compositions for a range of carbonate rock types from various published sources as compiled by Roylance (1990) is shown on figure 7.1. Broad fields of carbon and oxygen isotope compositions for various carbonate rock settings are indicated, including modern marine ("subsea") cements, various marine skeletons and sediments, deepwater ("pelagic") limestones, Pleistocene carbonates, and meteoric carbonates ("speleothems and veins").

Previous Work

The only previously published isotope composition analyses for lower Desert Creek rocks for the study area were completed at the Marathon Petroleum Technology Lab in Littleton, Colorado, for the M.S. thesis work of Roylance (1984). That data and the location of the wells sampled are in tables 7.1 and 7.2, and on figures 3.7 and 7.2. Brinton (1986) collected and interpreted a robust data set of carbon and oxygen isotopes (84 samples) from four cores in Ismay field, Utah and Colorado (figure 1.3), which is outside the study area. Comments about the general isotopic ranges of various diagenetic rock components within the Ismay zone in cores from Ismay and Greater Aneth fields (outside of the Blanding sub-basin project area) have been published by Dawson (1988).

Methodology

Isotopic composition analyses for carbon and oxygen were completed for a variety of whole rock and diagenetic phases for core samples from the lower Desert Creek zone from Bug field and the upper Ismay zone from Cherokee field (tables 7.1, 7.3, and 7.4). In addition, a series of samples from whole rock, dolomite, and various cement generations were selected from an upper Ismay buildup in the Bonito No. 41-6-85 well (NE1/4NE1/4 section 6, T. 38 S., R. 25 E., SLBL&M, Patterson Canyon field, San Juan County, Utah) containing well-cemented oolitic beds and phylloid-algal mound fabrics (table 7.5, figure 7.3). Individual samples were collected as powdered rock using a Dremel drill

equipped with precision bits. All analyses were completed at the Brigham Young University (BYU) Department of Geology Stable Isotope Laboratory, Provo, Utah. The internal standard used in the BYU lab is the UCLA Carrara marble (table 7.6). The accepted values for this internal standard were matched consistently during the analysis of the Paradox core samples selected for this study. All isotopic compositions are reported relative to Vienna PeeDee Belemnite (VPDB) (see Land, 1980, figure 6 for definition relative to Standard Mean Ocean Water or SMOW).

RESULTS AND INTERPRETATION

Carbon and Oxygen Isotopes from the Lower Desert Creek Zone

Values obtained in this study were compared to stable carbon and oxygen isotopic measurements reported by Roylance (1984, 1990), and included here on figure 7.2 and in table 7.2. Eight powdered samples were collected and analyzed from two Bug field wells (table 7.3). The samples include dolomitized phylloid-algal mound fabrics and breccias, cream-colored dolomitized internal sediments, and dolomitized void-filling cements (mostly botryoids and blunt-ended fibrous fans). Annotated close-up core photos (figure 7.4) show the approximate locations of the drilled and powdered samples from the May-Bug No. 2 and Bug No. 4 wells. A plot of carbon versus oxygen compositions for all Bug field samples obtained in this study is shown on figure 7.5 (see also table 7.3). Comparison of the new data with previously reported Bug field isotope compositions (Roylance, 1984, 1990) is shown on figure 7.6.

Carbon Isotopic Compositions, Bug Field

Carbon isotopic compositions for the eight Bug field dolomite samples (figure 7.4) all cluster very close around a mean $\delta^{13}C_{VPDB}$ value of +4.43‰ (range of +4.03‰ to +4.77‰). Interestingly, the range of $\delta^{13}C_{VPDB}$ values is slightly larger for the Bug No. 4 well (+4.52‰ to +4.77‰) than for the May-Bug No. 2 well (+4.03‰ to +4.49‰), although their means (+4.68‰ versus 4.28‰) are not significantly different. The carbon isotope values for Bug field dolomites are remarkably similar for all the rock components analyzed, including "whole rock" samples from the phylloid-algal mound fabrics and associated marine sediments, internal sediments within shelter pores, and early cements lining original pores.
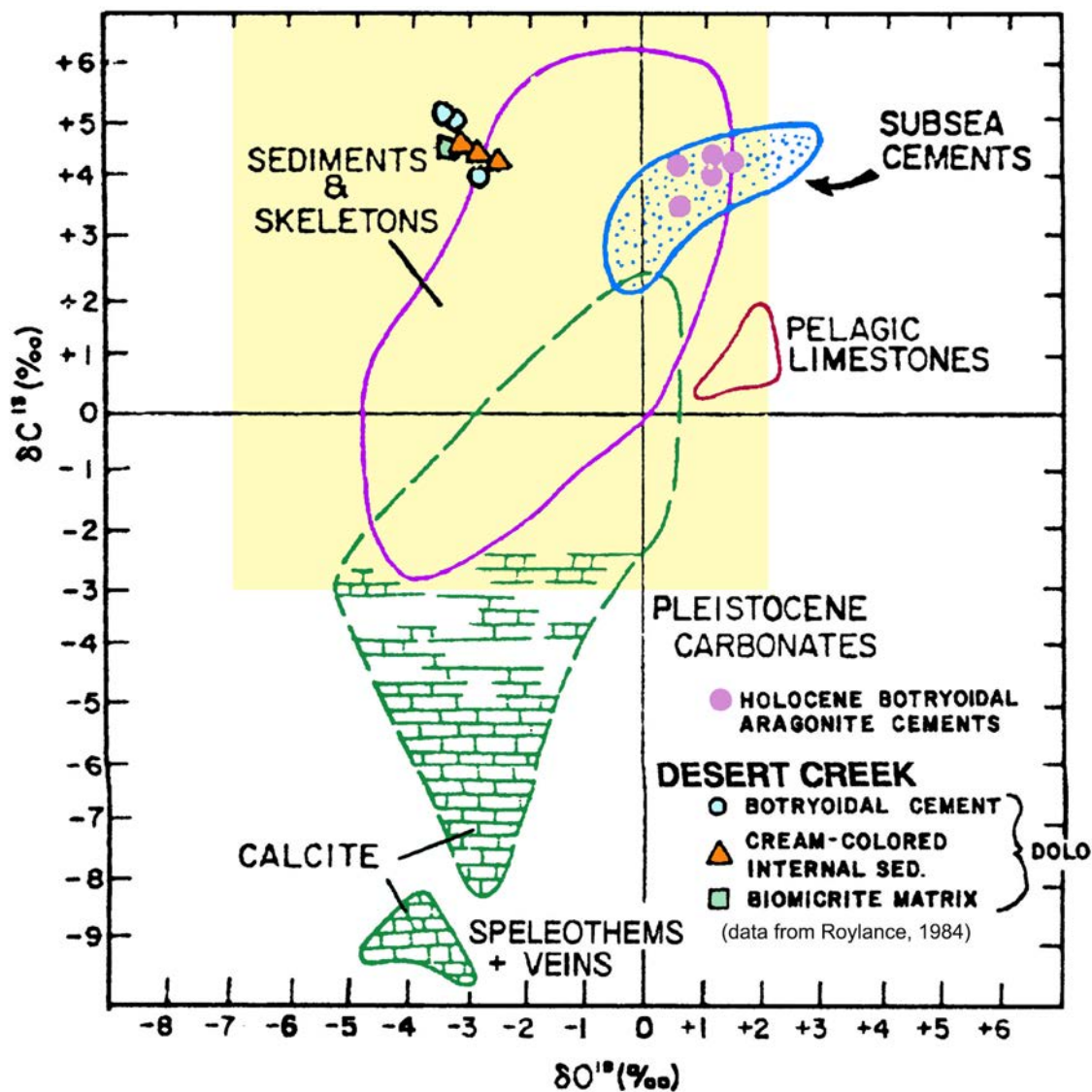
Figure 7.1. *Carbon versus oxygen isotope compositions. Other compositional lithofacies compiled from various published work (modified from James and Ginsburg, 1979, by Roylance, 1990). The yellow area in this crossplot is the same part of the graph shown on figures 7.2, 7.5, 7.6, 7.7, 7.9, and 7.11.*

Table 7.1. *Location of cores used in the isotope geochemistry study.*

Zones	Well Name	Location
Lower Desert Creek	*May-Bug 2 (this study)	NE1/4SW1/4 sec. 7, T36S, R26E UT
	* Bug 4 (this study)	NE1/4SW1/4 sec. 16, T36S, R26E UT
	* Bug 13 (Roylance, 1984)	NE1/4NW1/4 sec. 17, T36S, R26E UT
	* Bug 16 (Roylance, 1984)	NE1/4SW1/4 sec. 17, T36S, R26E UT
	Tin Cup Mesa 1-25	SW1/4NW1/4 sec. 25, T38S, R25E UT
Upper Ismay	ϒCherokee 22-14 (this study)	SE1/4NW1/4 sec. 14, T38S, R23E UT
	ϒCherokee 33-14 (this study)	NE1/4NW1/4 sec. 14, T38S, R23E UT
	Bonito 41-6-85 (this study)	NE1/4NE1/4 sec. 6, T38S, R25E UT

*Well locations are shown on figure 3.7
ϒWell locations are shown on figure 3.10

Table 7.2. *Previous stable carbon and oxygen isotope data from lower Desert Creek zone, Bug and Tin Cup Mesa fields (analyses from Roylance, 1984).*

Sample Groups:	$\delta^{13}C_{VPDB}$	$\delta^{18}O_{VPDB}$
Bug Field – Lower Desert Creek Cores		
Dolomitized Whole Rock Matrix (biomicrite in algal bafflestone)		
Bug 13: 5940.7'C	+4.7	-3.3
Dolomitized Internal Sediment (within phylloid-algal bafflestone)		
Bug 13: 5939.3'A	+4.4	-2.9
Bug 13: 5940.7'A	+4.3	-2.5
Bug 16: 6313.4'A	+4.8	-3.3
Dolomitized Botryoidal Cements		
Bug 13: 5939.3'B	+5.0	-3.3
Bug 13: 5940.7'B	+4.0	-2.9
Bug 16: 6313.4'B	+5.2	-3.4
Tin Cup Mesa Field – Lower Desert Creek Cores		
Limestone Whole Rock Matrix (calcite fraction [micrite and crinoid, bryozoan and brachiopod fragments] of dolomitized bioclastic wackestone)		
Tin Cup Mesa 1-25: 5667' calcite	+0.9	-3.3
Dolomite Fraction of Whole Rock Matrix (dolomitized micrite matrix of bioclastic wackestone)		
Tin Cup Mesa 1-25: 5667' dolomite	+0.9	-1.6
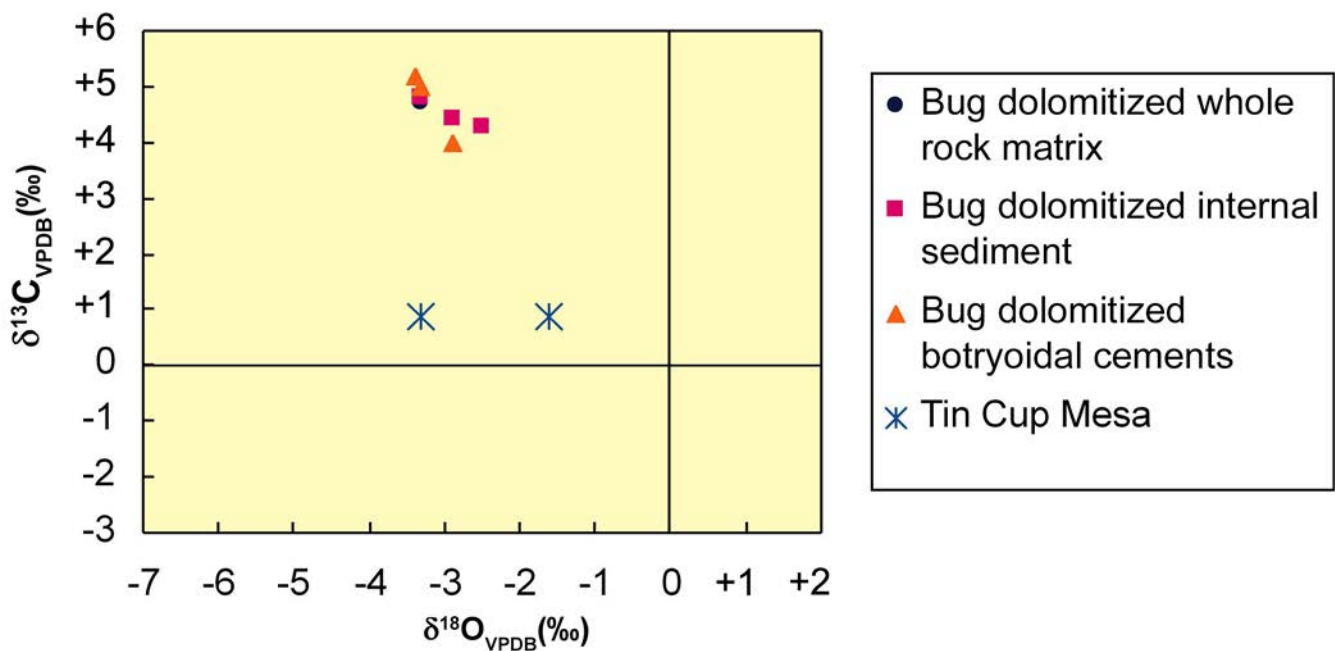
Figure 7.2. *Carbon versus oxygen isotopic compositions for Bug and Tin Cup Mesa fields determined by Roylance (1984).*

Table 7.3. Stable carbon and oxygen isotope data from lower Desert Creek zone, Bug field dolomites, completed for this study.

Sample Groups:	$\delta^{13}C_{VPDB}$	$\delta^{18}O_{VPDB}$
Bug Field – Lower Desert Creek Cores		
Whole Rock Dolomite		
May-Bug 2: 6304'A (phylloid-algal mound & marine sediment)	+4.49	-4.72
May-Bug 2: 6315'B (phylloid-algal mound fabric)	+4.03	-4.42
Dolomitized Internal Sediment (cream-colored)		
May-Bug 2: 6304'B	+4.30	-4.50
May-Bug 2: 6315'A	+4.16	-4.15
Bug 4: 6297.4'B	+4.52	-4.67
Dolomitized Micro-Boxwork Fabric (probably botryoidal cements)		
May-Bug 2: 6304'C	+4.40	-4.56
Bug 4: 6289.7'	+4.77	-4.58
Bug 4: 6297.4'A	+4.76	-4.46

Table 7.4. Stable carbon and oxygen isotope data from upper Ismay zone, Cherokee field, completed for this study.

Sample Groups:	$\delta^{13}C_{VPDB}$	$\delta^{18}O_{VPDB}$
Cherokee Field – Upper Ismay Cores		
Whole Rock		
Cherokee 22-14: 5827.7' (mostly dolomite, w/ moldic porosity)	+5.41	-2.90
Cherokee 22-14: 5836.8' (limestone; phylloid-algal mound fabric)	+5.02	-4.55
Cherokee 33-14: 5781.2'A (mostly dolomite)	+4.67	-6.08
Micro-Porous Dolomite Zones (often w/ pyrobitumen)		
Cherokee 22-14: 5768.7'	+3.57	-2.92
Cherokee 33-14: 5781.2'B	+4.85	-4.54

Table 7.5. Stable carbon and oxygen isotope data from upper Ismay buildup zone, Bonito No. 41-6-85 core, Patterson Canyon field, completed for this study.

Sample Groups:	$\delta^{13}C_{VPDB}$	$\delta^{18}O_{VPDB}$
Whole Rock (dolomitized oolite)		
Bonito 41-6-85: 5544'A	+4.53	-5.10
Dolomitized Cements (in oolite)		
Bonito 41-6-85: 5544'B	+4.51	-5.15
Calcite Cements (within phylloid-algal buildup)		
Bonito 41-6-85: 5592'A (black cement)	+6.30	-5.10
Bonito 41-6-85: 5592'B (gray cement)	+5.67	-5.68
Bonito 41-6-85: 5592'C (brown cement? w/sediment?)	+5.56	-5.87
Bonito 41-6-85: 5592'D (white cap cement; no sediment)	+5.73	-5.05
Bonito 41-6-85: 5592'E (coarse blocky cement)	+5.69	-6.41
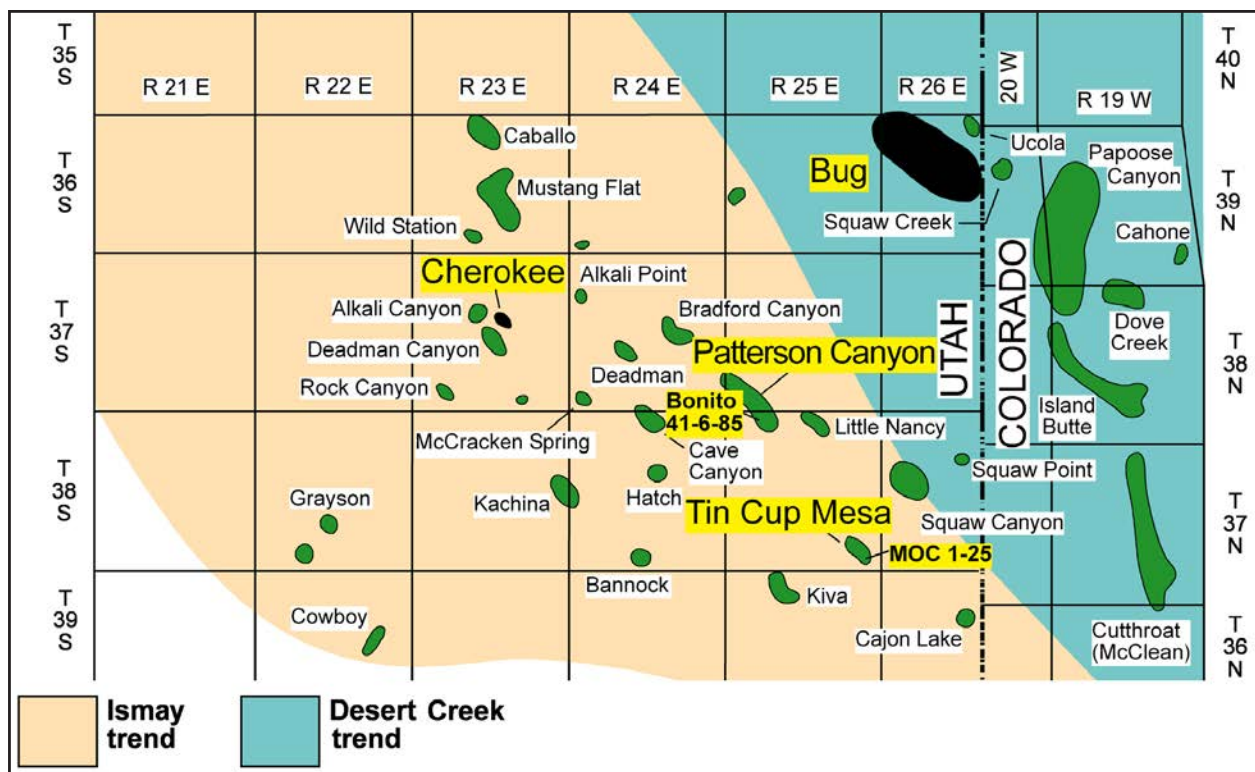
Figure 7.3. *Project study area and fields (case-study fields in black) within the Desert Creek and Ismay producing trends, Utah and Colorado. Fields sampled for isotope analyses are highlighted in yellow.*

Table 7.6. *Brigham Young University lab calibration to an internal standard.*

Sample No.	$\delta^{13}C_{VPDB}$ *	$\delta^{18}O_{VPDB}$ *
UCLA-1/17/2003	+2.59	-2.01
UCLA-4/9/2003	+2.44	-2.23
UCLA-4/10/2003	+2.35	-2.33
UCLA-2/18/2003	+2.58	-1.92
UCLA-2/10/2003	+2.49	-1.83
UCLA-2/6/2003	+2.45	-2.06
UCLA-6/30/2003	+2.56	-1.89
mean +2.49		-2.04
1 std. dev. 0.09		0.18

*UCLA Carrara Marble, with accepted values of $\delta^{13}C_{VPDB}$ = +2.495 and $\delta^{18}O_{VPDB}$ = -2.027

The mean value of $\delta^{13}C_{VPDB}$ for all Bug field samples in this study is also very close to the mean of +4.6‰ (range of +4.0‰ to +5.2‰) for seven samples from two other Bug field cores (Bug No. 13 and Bug No. 16) analyzed by Marathon's lab (see table 3, p. 125 in Roylance, 1984; figure 7.2). Despite dolomitization, all of the lower Desert Creek samples from Bug field analyzed in this study, as well as analyzed by Marathon, show carbon isotope compositions that are very close in value to modern marine carbonates ("sediments and skeletons" on figure 7.1) and Holocene botryoidal marine aragonite cements (James and Ginsburg, 1979; "subsea cements" on figure 7.1).

Furthermore, carbon isotopic compositions for former aragonite marine cements from the Late Permian Capitan Reef complex in southeastern New Mexico are calculated to be about +5.3‰ by Given and Lohmann (1985). Hence, it appears that the carbon isotope geochemistry of all of the lower Desert Creek dolomites at Bug field have retained a strong influence from Pennsylvanian marine water composition. Meteoric waters, which typically would tend to lower the carbon isotope values significantly (Hudson, 1975), do not appear to have had any effect on the composition of these lower Desert Creek dolomites.
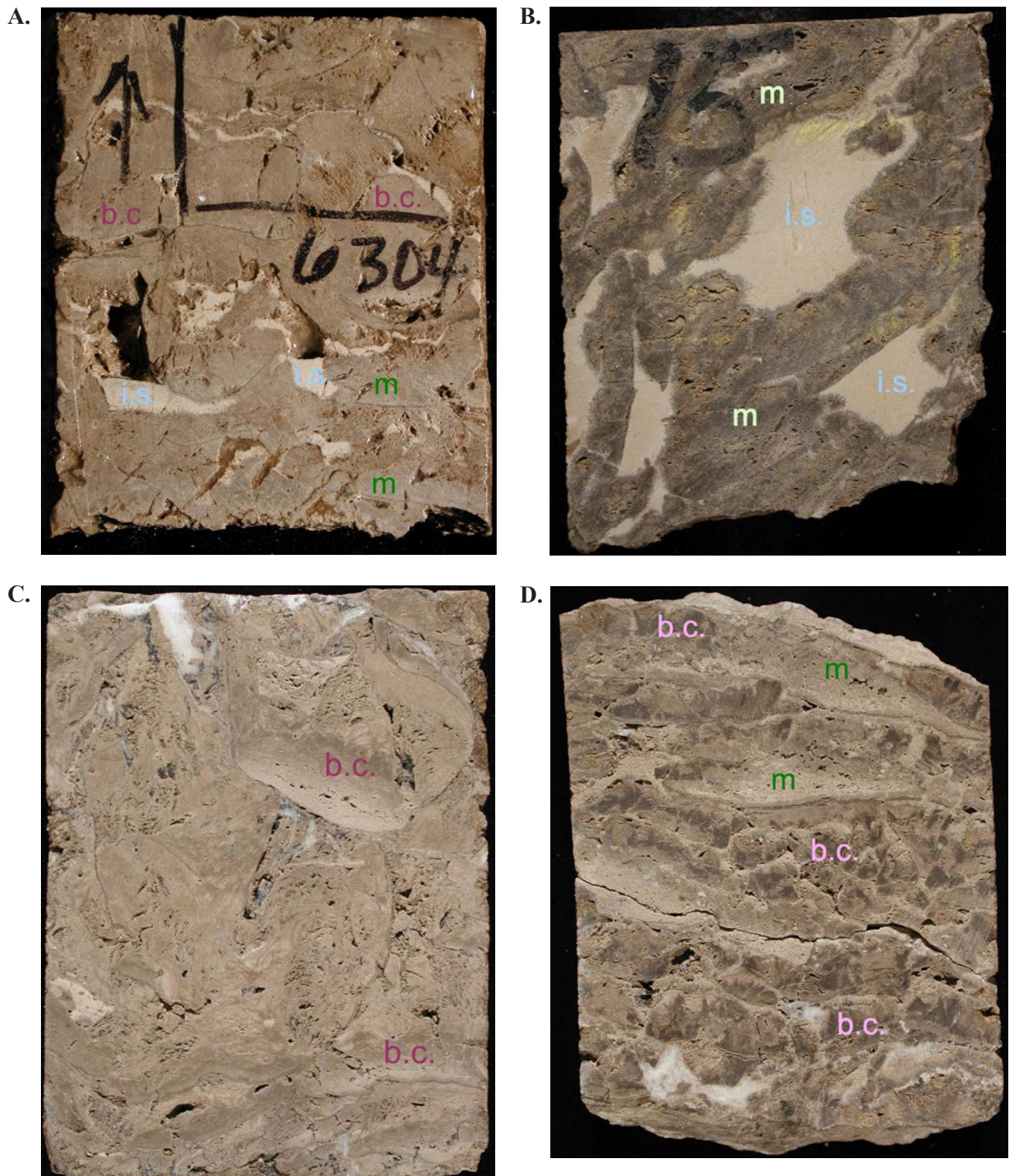
Figure 7.4. *Core photographs of typical Bug field components sampled for stable carbon and oxygen isotope analysis. **(A)** May-Bug No. 2 well: 6304 feet (1921 m) – the "whole rock" dolomitized phylloid-algal mound fabric (m; sample 6304'A) in medium gray, the dolomitized cream-colored internal sediment (i.s.; sample 6304'B), and dark gray dolomitized botryoidal cements (b.c.; sample 6304'C), as well as associated micro-boxwork fabrics. **(B)** May-Bug No. 2 well: 6315 feet (1925 m) – the "whole rock" dolomitized phylloid-algal mound fabric (m; sample 6315'B) in dark gray and the dolomitized cream-colored internal sediment (i.s.; sample 6315'A). **(C)** Bug No. 4 well: 6289.7 feet (1917.1 m) – dolomitized, dark gray botryoidal cements (b.c.; sample 6289.7') displaying micro-boxwork fabric. **(D)** Bug No. 4 well: 6297.5 feet (1919.5 m) – "whole rock" dolomitized phylloid-algal mound fabric (m; sample 6297.5'B) and dark gray dolomitized botryoidal cements (b.c.; sample 6297.5'A) as well as associated micro-boxwork fabrics.*
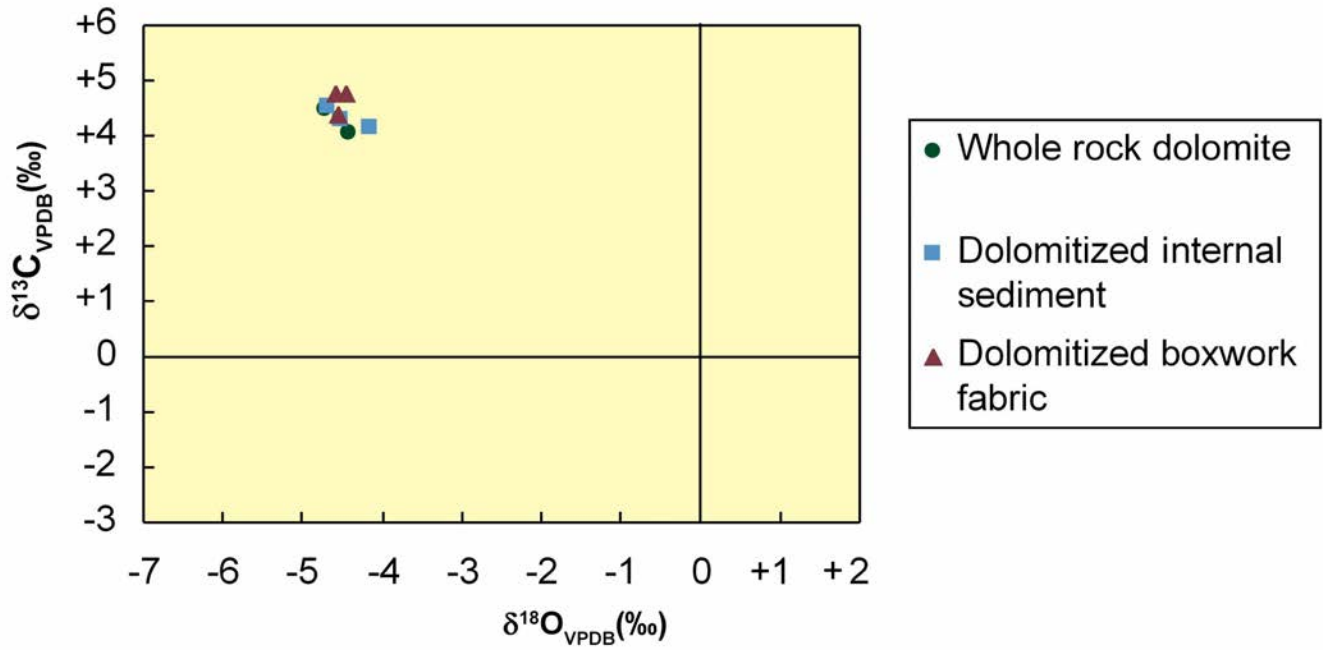
Figure 7.5. *Carbon versus oxygen isotopic compositions for Bug field dolomites completed for this study.*
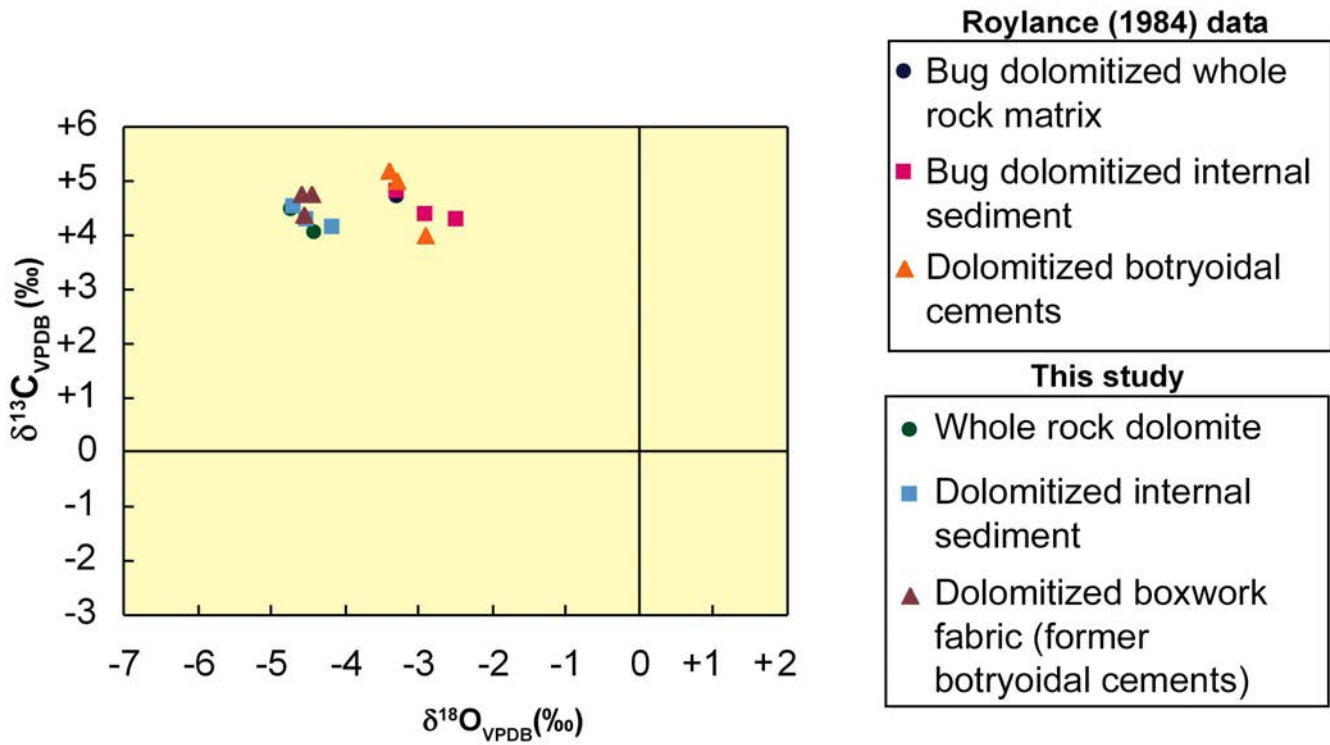
Figure 7.6. *Graph comparing carbon versus oxygen isotopic compositions for Bug field dolomites by Roylance (1984) versus those completed for this study.*

Oxygen Isotopic Compositions, Bug Field

Oxygen isotopic compositions for the eight Bug field dolomite samples (figure 7.5 and table 7.3) also cluster in a very narrow range around a mean $\delta^{18}O_{VPDB}$ value of -4.51‰ (range of -4.15‰ to -4.72‰). There is no significant difference in oxygen values between the two Bug wells studied. However, the oxygen compositions in the dolomites sampled here for May-Bug No. 2 and Bug No. 4 are significantly different from the values reported by Roylance (1984, 1990, for seven samples processed from the same stratigraphic interval in the Bug No. 13 and Bug No. 16 wells) (figures 7.5 and 7.6, table 7.2). The mean $\delta^{18}O_{VPDB}$ for the latter wells is -3.1‰ (range of -2.5‰ to -3.4‰). Thus, the oxygen values in the May-Bug No. 2 and Bug No. 4 cores are more negative by nearly 1.5‰. There are only three possible sources for the differnces: (1) a fluid of different composition, (2) dolomitization at a different temperature, or (3) both. The oxygen isotope composition data from the Bug No. 13 and Bug No. 16 cores, which are situated near the center of the Bug field buildup (figure 3.7), are rather close to the values for modern marine carbonates ("sediments and skeletons" on figure 7.1) and to values inferred for unaltered Pennsylvanian marine cements (Lohmann, 1983).

Oxygen isotopic compositions for former aragonite and magnesium calcite marine cements from the Late Permian Reef complex in southeastern New Mexico are calculated to be between -2.8‰ and -2.5‰ by Given and Lohmann (1985, 1986). The lighter oxygen values obtained from samples in the May-Bug No. 2 and Bug No. 4 cores, which are located along the margins or flanks of Bug field (figure 3.7), may be indicative of exposure to higher temperatures, to fluids depleted in ^{18}O relative to sea water, or to hypersaline waters (Land, 1980, 1982) during burial diagenesis.

Carbon and Oxygen Isotopic Compositions, Tin Cup Mesa Field

Two samples of regional, non-reservoir, open-marine lower Desert Creek zone from Tin Cup Mesa field were analyzed by Marathon's lab for carbon and oxygen isotope composition (MOC No. 1-25 well [NW1/4NW1/4 section 25, T. 38 S., R. 25 E., SLBL&M]; figure 7.3, table 7.2). The isotopic values for these samples (a limestone and a dolomite) are significantly different from the Bug field reservoir dolomites (figures 7.2 and 7.7). The biggest contrast is the much lighter (by greater than 3‰) $\delta^{13}C_{VPDB}$ values in the Tin Cup Mesa lower Desert Creek samples than at Bug field. For $\delta^{18}O_{VPDB}$ values, the dolomite sample is significantly heavier (at -1.6‰) than the limestone (calcite fraction) sample (at -3.3‰) at Tin Cup Mesa field. The most probable reasons for these differences is that the Tin Cup Mesa reservoir may have experienced more meteoric diagenesis, which usually reduced both carbon and oxygen isotope values.
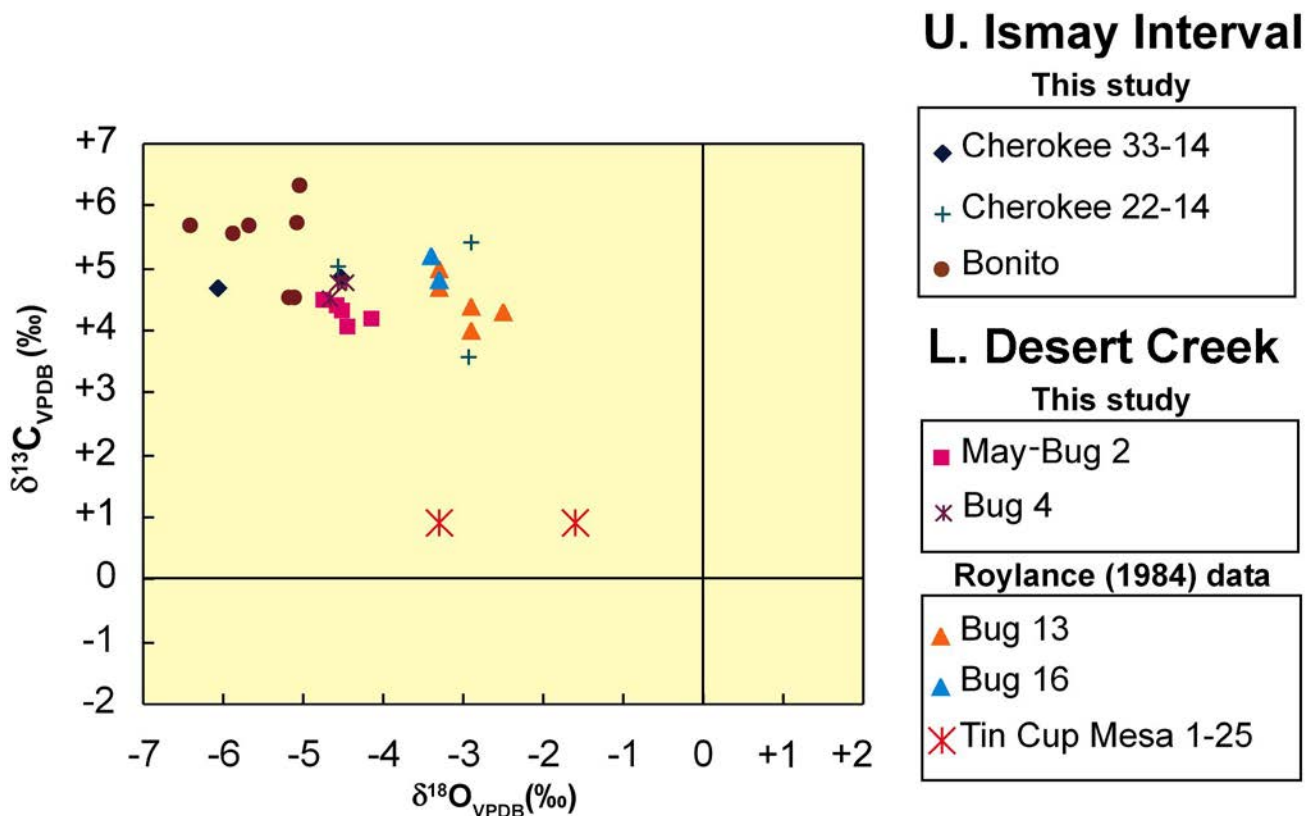
Figure 7.7. Summary of carbon versus oxygen isotopic compositions for all components sampled for this study and previously published data by Roylance (1984).

Carbon and Oxygen Isotopes from the Upper Ismay Zone

Isotopic composition analyses for carbon and oxygen were completed for a variety of whole rock and diagenetic phases for core samples from the upper Ismay zone in Cherokee field (figures 7.3 and 3.12; table 7.1). Five powdered samples were drilled and analyzed from two cored, upper Ismay wells at Cherokee field (table 7.3). The samples include typical dolomitized calcarenite (bioclastic grainstone), limestone phylloid-algal fabric, dolomitized cryptalgal (stromatolitic) laminites, and microcrystalline-microporous dolomite. Annotated close-up core photos (figure 7.8) show the approximate locations of the drilled and powered samples from the Cherokee Federal No. 22-14 and Cherokee Federal No. 33-14 wells. A plot of carbon versus oxygen compositions for all Cherokee field samples obtained in this study is shown on figure 7.9 (see also table 7.4).

Carbon Isotopic Compositions, Cherokee Field

Carbon isotopic compositions for the five upper Ismay dolomite samples from Cherokee field (figure 7.9) have a mean $\delta^{13}C_{VPDB}$ value of +4.70‰ (range of +3.57‰ to +5.11‰). Although the mean carbon isotopic composition appears to be higher in the upper Ismay carbonate samples from Cherokee field than in the lower Desert Creek dolomites at Bug field, the values are not distinguishable at the 95% confidence level (t-test). In addition, the limestone (calcite) sample from representative phylloid-algal mound fabrics displays a $\delta^{13}C_{VPDB}$ value within the same range as the dolomite samples (table 7.4). Brinton (l986, p. 217–218) reported a possible mean marine $\delta^{13}C_{VPDB}$ value of +3.9‰ during the time of Ismay deposition from analysis of unaltered brachiopods in cores from Ismay field on the Aneth Platform to the south (figure 1.3). Carbon isotopic compositions for former aragonite marine cements from the Late Permian Capitan Reef complex in southeastern New Mexico are about +5.3‰ (Given and Lohmann, 1985), suggesting that the fluids responsible for upper Ismay carbonates within Cherokee field have slightly heavier carbon isotope compositions than marine brachiopods at Ismay field, or slightly lighter than late Paleozoic seawater. However, as with the Bug field dolomite samples, Cherokee field carbonates fall within the same range of carbon isotope compositions as modern marine sediments, skeletons, and marine cements (see figure 7.1). A number of possible reasons for this include (1) meteoric diagenesis or time or both, and (2) fractionation occuring between aragonite (now inverted?) and bicarbonate is larger than that occurring between calcite and bicarbonate (Veizer and others, 1999).

The $\delta^{13}C_{VPDB}$ values of Cherokee field upper Ismay components overlap or are slightly heavier than the diagenetic components reported by Dawson (1988) in Ismay field for meteoric-phreatic cements ($\delta^{13}C_{VPDB}$ = +2.5‰ to +4.8‰) and are uniformly heavier than either deep burial ferroan calcite

cements ($\delta^{13}C_{VPDB}$ = +1.8‰ to +3.2‰) or saddle dolomites (mean $\delta^{13}C_{VPDB}$ = +3.4‰). The range of $\delta^{13}C_{VPDB}$ values at Cherokee field has a better overlap with values reported from marine botyroidal-fibrous cements and "neomorphosed matrix sediments" in Ismay field cores (Brinton, 1986) that range between +4.2‰ to +5.0‰. In addition, Brinton (1986, figure 62) shows that various forms of microcrystalline dolomite in Ismay field have isotopic values that cluster between +3.0‰ and +6.0‰ for $\delta^{13}C_{VPDB}$. As with the lower Desert Creek dolomites in Bug field, it does not appear that meteoric waters, which typically would precipitate carbonates with more depleted carbon isotope values, have had major effects on the composition of the Ismay carbonate components in Cherokee field. Rather, it is likely that most of the carbonates present within the Ismay zone (as well as throughout the lower Desert Creek zone) have retained a marine-influenced isotope composition throughout marine cementation as well as through post-burial recycling of marine carbonate components during dolomitization, stylolitization, dissolution, and late cementation. Such an explanation is in agreement with the model for the positive carbon isotope values of many ancient carbonates proposed by Hudson (1975).

Oxygen Isotopic Compositions, Cherokee Field

Oxygen isotopic compositions for the Cherokee field limestone and dolomite samples (figure 7.9 and table 7.4) form a wide range of values around a mean $\delta^{18}O_{VPDB}$ value of -4.20‰ (range of -2.90‰ to -6.08‰). As with the carbon isotope data, there is no significant difference between the oxygen isotope compositions from lower Desert Creek dolomite samples in Bug field and the upper Ismay limestones and dolomites from Cherokee field. There is no apparent pattern in the Cherokee field $\delta^{18}O_{VPDB}$ values other than the deeper samples contain the more depleted (more negative) values. However, the range of values is probably too wide to suggest a depth-related temperature increase for the lowered $\delta^{18}O_{VPDB}$ values. A similar range of $\delta^{18}O_{VPDB}$ values was reported by Dawson (1988) from a variety of cement generations from Ismay field cores. Only very late ferroan calcites and saddle dolomites in Dawson's (1988) data displayed more negative oxygen isotope compositions than the Cherokee field limestones and dolomites.

Brinton (l986, p. 217–218) reported a possible mean marine $\delta^{18}O_{VPDB}$ value of -4.7‰ (similar to values for the Carboniferous in Veizer and others, 1999, p. 72–75), during the time of Ismay deposition, from analysis of unaltered brachiopods from Ismay field core. This proposed Ismay marine value is very close to two of the Cherokee field values (see table 7.4), and to the mean value of all the samples. However, two of the samples (at -2.90‰ and -2.92‰) are significantly heavier than Brinton's (1986) marine $\delta^{18}O_{VPDB}$ value calculated from unaltered marine fossils. They are closer to Given and Lohmann's (1985, 1986) marine diagenesis as determined from former aragonite and magnesium calcite marine cements in the Capitan Reef in West Texas. These heavier $\delta^{18}O_{VPDB}$ sam-

A.

B.

C.

D.
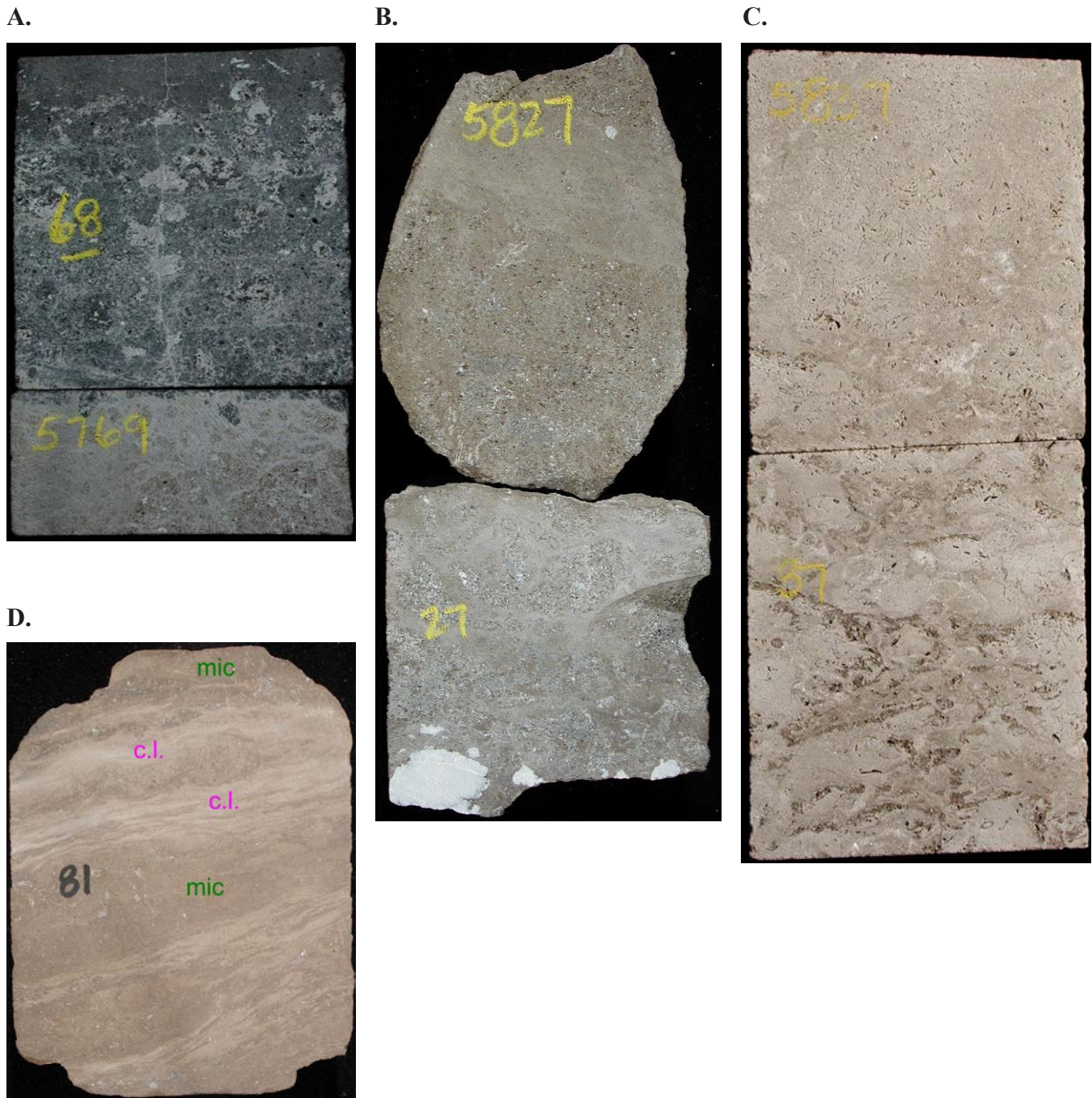
Figure 7.8. Core photographs of typical Cherokee field components sampled for stable carbon and oxygen isotope analysis. (A) Cherokee Federal No. 22-14 well: 5768.7 through 5769.2 feet (1758.3–1758.5 m) – microporous dolomite surrounded by black pyrobitumen was drilled at 5768.7 feet (1758.3 m). (B) Cherokee Federal No. 22-14 well: 5827 feet (1776 m) – a "whole rock" sample of dolomitized calcarenite (bioclastic grainstone) was drilled at 5827.7 feet (1776.3 m). Significant moldic porosity is present in this interval. (C) Cherokee Federal No. 22-14 well: 5837 feet (1779 m) – a "whole rock" limestone sample of phylloid-algal mound fabric was drilled at 5826.8 feet (1176.0 m). (D) Cherokee Federal No. 33-14 well: 5781 feet (1762 m) – both the "whole rock" dolomitized cryptalgal laminite (c.l.; sample 5781.2'A) and microporous dolomite (mic; sample 5781.2'B).
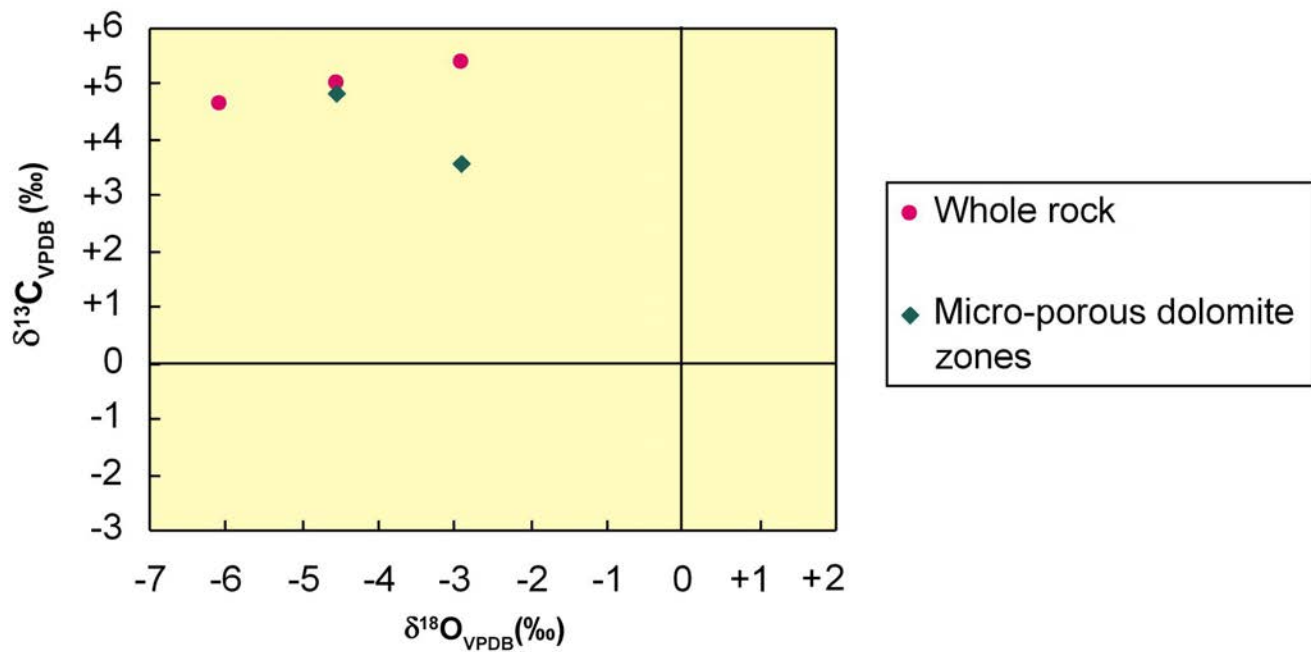
Figure 7.9. *Carbon versus oxygen isotopic compositions for Cherokee field components completed for this study.*

ples (both dolomites) contain oxygen values similar to two cement-filled crinoids and many of the microcrystalline dolomites analyzed by Brinton (1986). One of the dolomitized samples in Cherokee field, from cryptalgal laminites, has a much lighter oxygen composition (-6.08‰). Only certain saddle dolomite cements, late equant calcite spars, and neomorphosed calcites commonly had such light compositions in Brinton's (1986) research on Ismay field cores. The depleted $\delta^{18}O_{VPDB}$ value of this one dolomite sample (Cherokee Federal No. 33-14 sample 5781.2'A) suggests neomorphism, cementation, and/or dolomitization from warm or isotopically light subsurface waters.

Carbon and Oxygen Isotopic Compositions, Patterson Canyon Field

Carbon and oxygen isotopic analysis was completed on various whole rock and diagenetic cement generations from the upper Ismay oolite/phylloid-algal buildup along the southwest margin of Patterson Canyon field (figure 7.3, table 7.1). The Bonito No. 41-6-85 well cored approximately 25 feet (8 m) of very well cemented, phylloid-algal mound limestone (a "reef wall" at the margin of the Patterson Canyon phylloid-algal reservoir) and 31 feet (10 m) of overlying tight oolitic and pelloidal calcarenites. Two samples were drilled from core near the top of the oolitic grainstone section, and five samples were drilled from the cements near the base of the well-cemented mound section. Annotated close-up core photos (figure 7.10) show the approximate locations of the drilled and powdered samples from the oolite and "reef cementstone" interval selected in the Bonito No. 41-6-85 well. This particular core was analyzed, despite its location outside of either of the two case-study fields (Bug and Cherokee) because of the spec-

tacular development of cements that display visual characteristics suggesting different generations of development, most of which appear to have been early, or prior to significant burial. A plot of carbon versus oxygen compositions for all Bonito No. 41-6-85 limestone samples obtained in this study is shown on figure 7.11 (see also table 7.5).

Carbon isotopes: Carbon isotopic compositions for the seven upper Ismay limestone samples in the core from the cemented buildup in Patterson Canyon field have a mean $\delta^{13}C_{VPDB}$ value of +5.43‰ (range of +4.51‰ to +6.30‰). These values are distinguishable at the 95% confidence level (t-test) from the Cherokee field carbonate samples and at the 90% level from the Bug field dolomites, but like the Bug and Cherokee values of $\delta^{13}C_{VPDB}$, they are much heavier than the mean value of +0.56‰ (standard deviation of 1.55‰) for a large sampling (n = 272) of Phanerozoic marine limestones (Hudson, 1975). However, the samples can be divided into two populations with regard to carbon isotopic composition. The five calcite samples from the deeper cemented phylloid-algal buildup have a mean $\delta^{13}C_{VPDB}$ value of +5.79 ‰ (range of +5.56‰ to +6.30‰) whereas the oolite and cement samples from the capping grainstone have a mean $\delta^{13}C_{VPDB}$ value of +4.52‰ (range of +4.51‰ to +4.53‰). Since both of these carbon isotope populations are significantly heavier than Brinton's (1986) value for unaltered brachiopods from Ismay field, it is likely that an isotopically heavier fluid, possibly from concentrated (higher salinity) or closed-system sea water, is recorded in both populations.

Interestingly, Given and Lohmann's (l985) calculated $\delta^{13}C_{VPDB}$ value (+5.3‰) from Late Paleozoic marine cements from the Permian Basin reef front falls between the

A.

B.

Figure 7.10. *Core photographs of whole rock and cement components sampled for stable carbon and oxygen isotope analysis in the upper Ismay buildup in the Bonito No. 41-6-85 well, Patterson Canyon field.* ***(A)*** *Sample depth: 5544 feet (1690 m) – both the "whole rock" limestone (an oolitic grainstone; sample 5544'A) and calcite cement bands (cem; sample 5544'B) along bedding.* ***(B)*** *Sample depth: 5592 feet (1704 m) – five calcite cement generations were sampled for isotopic analysis. Sample 5592'A – black cements that appear to have originally been botryoidal cement fans. Sample 5592'B – gray marine cements. Sample 5592'C – brown cements containing sediments at the bottoms of pores, which often display geopetal relationships. Sample 5592'D – white cements that fill the tops of geopetal cores. Sample 5592'E – coarse, blocky calcite spar cements.*
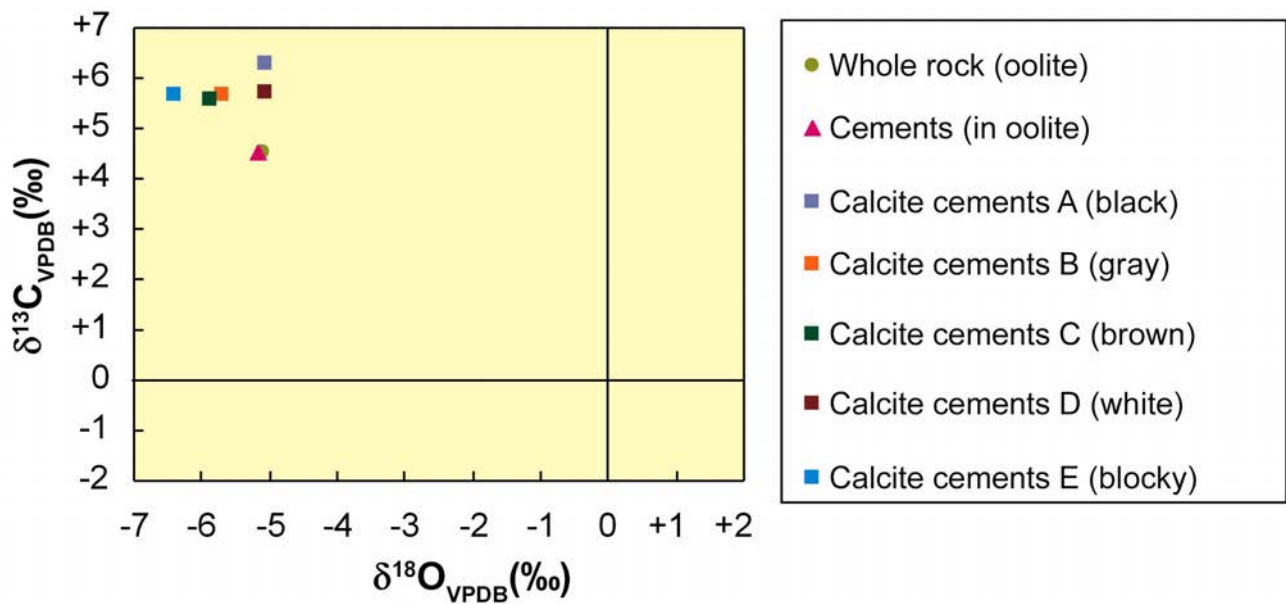
Figure 7.11. *Carbon versus oxygen isotopic compositions for whole rock and cement components in an upper Ismay buildup, Bonito No. 41-6-85 well, Patterson Canyon field, completed for this study.*

two Bonito No. 41-6-85 well populations. It does not appear that meteoric waters, which typically would precipitate calcites with more depleted carbon isotope values, were involved in the diagenesis of the tight Patterson Canyon carbonate buildup. Thus there must be another cause for the significant difference in $\delta^{13}C_{VPDB}$ values between the well-cemented oolite samples and the cements present in the underlying reef. Clearly the waters were somehow different in composition between the phylloid-algal mound cements and the lithified oolites. One possible scenario is that the waters responsible for the several generations ("A" through "E") of mound cement were confined to a "closed hydrologic system" that allowed a fluid with heavier carbon to evolve. The oolite and cement bands therein may have been in a more open system allowing water exchange such that waters with a composition slightly lighter than Brinton's (1986) proposed Ismay marine value (derived from unaltered brachiopods) were involved in the lithification and diagenesis of the capping oolite.

Oxygen isotopes: Oxygen isotopic compositions for the seven upper Ismay limestone samples of the cemented buildup in Patterson Canyon field form a moderate range of $\delta^{18}O_{VPDB}$ values around a mean of -5.48‰ (range of -5.05‰ to -6.41‰). As with the carbon isotope data, there is a significant difference (at the 95% confidence level) between the Bonito No. 41-6-85 well oxygen isotope compositions and those from both the lower Desert Creek dolomites and the upper Ismay at Cherokee field. There is no significant difference in the $\delta^{18}O_{VPDB}$ values between the deeper mound, early cement samples (mean value of -5.62‰) and the overlying lithified oolite (mean of -5.58‰). All seven of the Bonito No. 41-6-85 limestone samples, regardless of component or cement type, are lighter on average by about 1.0‰ than the

Bug and Cherokee field samples. These Patterson Canyon samples' $\delta^{18}O_{VPDB}$ values from diagenetic components are also lighter than either Brinton's (1986) marine $\delta^{18}O_{VPDB}$ value calculated from unaltered marine fossils or Given and Lohmann's (1985) values of -2.8‰ to -2.5‰ for former aragonite and magnesium calcite marine cements from the Late Permian Reef complex in southeastern New Mexico. The reasons for these significant differences are not immediately clear. The oxygen isotope signatures possibly indicate waters with depleted ^{18}O characteristics evolved in the mound cavities and ooid grainstone pores, without any influence by hypersaline waters. Alternatively, the limestones in this sample set may have all been modified via neomorphism by isotopically light subsurface waters.

CHAPTER 8:

CAPILLARY PRESSURE/MERCURY INJECTION ANALYSIS, BUG AND CHEROKEE CASE-STUDY FIELDS, SAN JUAN COUNTY, UTAH

---

by

David E. Eby, Eby Petrography & Consulting, Inc.
and
Thomas C. Chidsey, Jr., Utah Geological Survey

CHAPTER 8:
CAPILLARY PRESSURE/MERCURY INJECTION ANALYSIS, BUG AND CHEROKEE CASE-STUDY FIELDS, SAN JUAN COUNTY, UTAH

INTRODUCTION

The Bug and Cherokee case-study fields (figure 1.3) were chosen for capillary pressure/mercury injection analysis due to the quality and amount of core available from those fields. Capillary pressure/mercury injection analysis evaluates reservoir fluid saturation and relates pore aperture size and distribution to porosity and permeability (Pittman, 1992). These data were used to assess reservoir potential and quality by: (1) determining the most effective pore systems for oil storage versus drainage, (2) identifying reservoir heterogeneity, (3) predicting potential untested compartments, (4) inferring porosity and permeability trends, and (5) matching diagenetic processes, pore types, mineralogy, and other attributes to porosity and permeability distribution. High-pressure mercury-injection porosimetry (MIP) measurements were conducted on five core samples (table 8.1; appendix K). The core samples include (1) a dolomitic phylloid-algal bafflestone with both early marine cement and leaching from the May-Bug No. 2 well (6304 feet [1921 m]), (2) a dolomitic phylloid-algal bafflestone with internal sediment and leaching, also from the May-Bug No. 2 well (6315 feet [1925 m]), (3) a dolomitic phylloid-algal bafflestone with both early marine cement and leaching from the Bug No. 4 well (6289.1 feet [1916.8 m]), (4) a dolomitic peloidal packstone to grainstone with anhydrite replacement and bitumen plugging from the Cherokee Federal No. 22-14 well (5768.7 feet [1758.2 m]), and (5) a micritic dolomitic mudstone to wackestone with a large amount of bitumen from the Cherokee Federal No. 33-14 well (5781.2 feet [1762.0 m]).

METHODOLOGY

Capillary pressure/mercury injection analysis was conducted by TerraTek, Inc., Salt Lake City, Utah (now part of Schlumberger). Core plugs were obtained from the two Cherokee wells and three of the eight Bug wells that were cored. Core plugs were no more than 2 inches (5 cm) in length. Prior to MIP testing, the samples were dried in a low-temperature convection oven, and then ambient helium porosity and grain density measurements were conducted on each sample (table 8.1). These porosity values, along with the volume of mercury injected into each sample, were used to calculate cumulative saturation. The samples were also visually examined for open fractures that can contribute to anomalous results at low injection pressures. None of the samples tested contained open fractures or coring-induced cracks.

RESULTS AND INTERPRETATION

All samples tested exhibited 100% mercury saturation at pressures less than 10,000 pounds per square inch (psi) (68,950 kPa) injection pressure. The selected reservoir rock samples vary in porosity from 11% to 24% and have grain densities of 2.8 to 2.9 g/cm^3. Pore-throat-radius histograms and saturation profiles are presented on figures 8.1 through 8.7.

Bug Field

Pore-Throat Radii

Three capillary pressure/mercury injection tests were run on samples from Bug field: two from the May-Bug No. 2 well (6304 feet [1921 m] and 6315 feet [1925 m]), and one from the Bug No. 4 well. The sample from 6304 feet (1921 m) from the May-Bug No. 2 well reveals that the distribution of pore-throat radii is trimodal (figure 8.1). Mode 1 ranges from 20 to 10 microns (the modal class is 10.65 microns) and accounts for 2% to 4% of the pore space, having 20% of the pores saturated on the cumulative injection curve. Mode 2 ranges from 6.9 to 4.5 microns (the modal class is 5.0 microns) and accounts for 10% to 12% of the pore space, with 10% of the pores saturated on the cumulative injection curve. The minor

Table 8.1. *Well core-plug samples selected for capillary pressure/mercury injection analysis.*

Sample Depth (ft)	Well Name	Porosity (%)	Grain Density (g/cm³)
6304.0	May-Bug 2	11.06	2.865
6315.0	May-Bug 2	22.24	2.834
6289.1	Bug 4	12.45	2.857
5768.7	Cherokee 22-14	24.38	2.875
5781.2	Cherokee 33-14	20.89	2.934
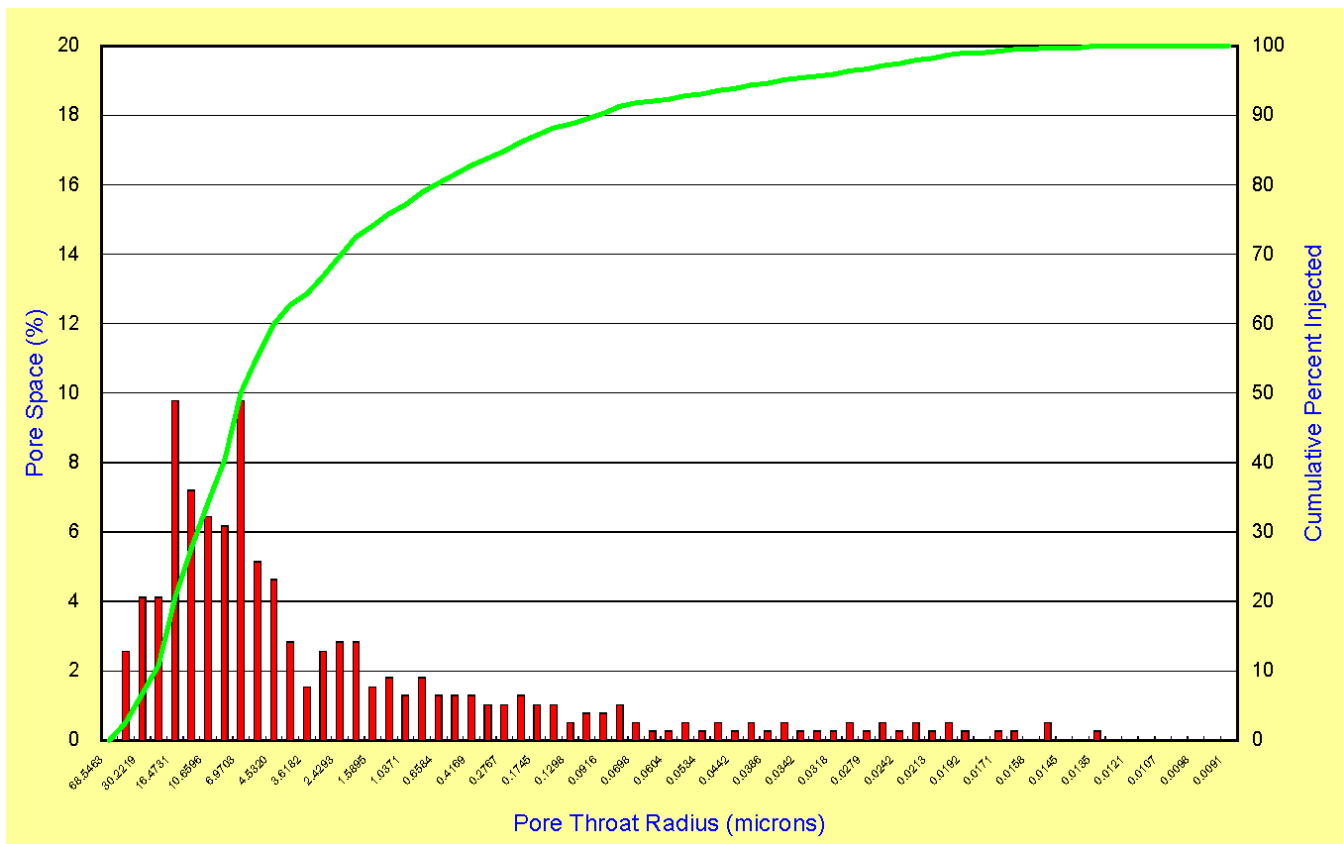
Figure 8.1. *Pore throat radius histogram – sample depth, 6304 feet (1921 m) – May-Bug No. 2 well.*
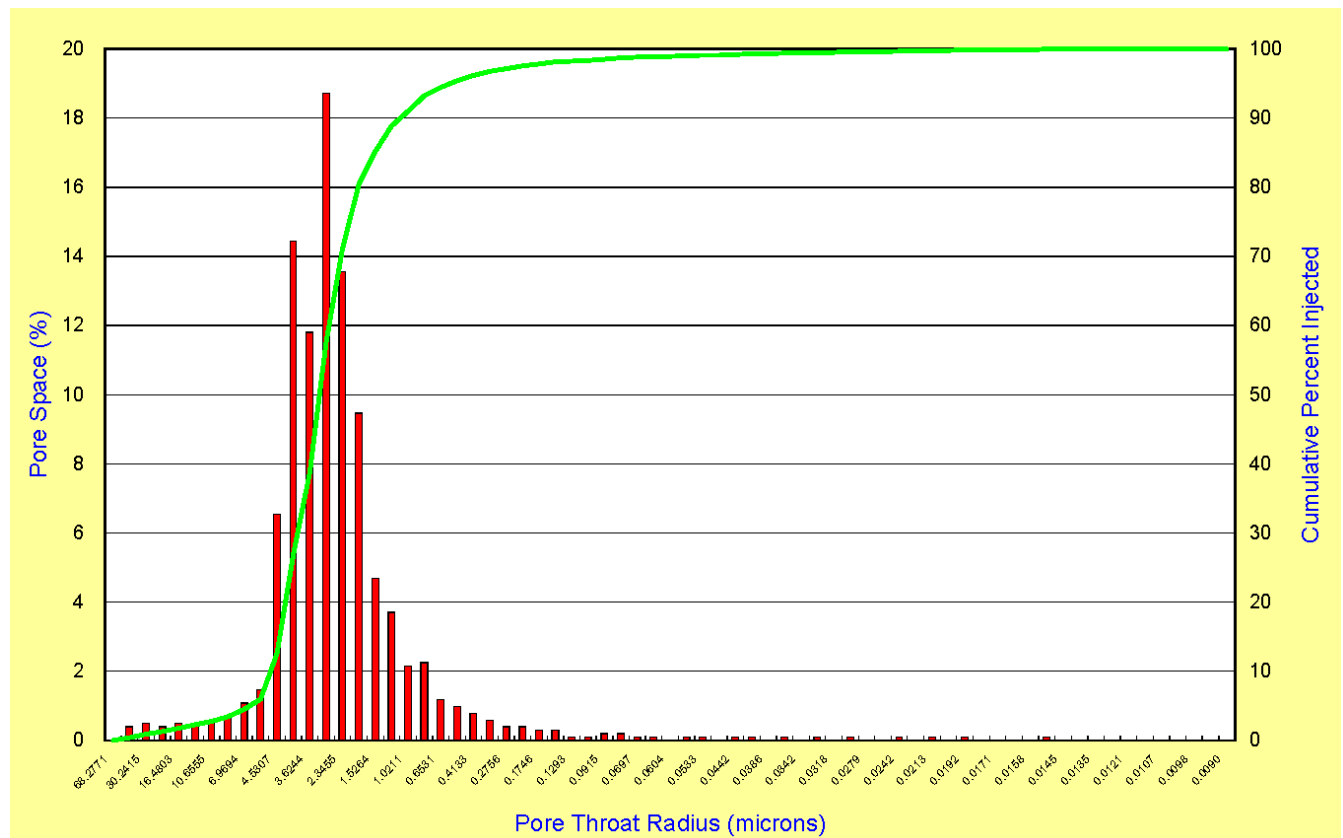
Figure 8.2. *Pore throat radius histogram – sample depth, 6315 feet (1925 m) – May-Bug No. 2 well.*
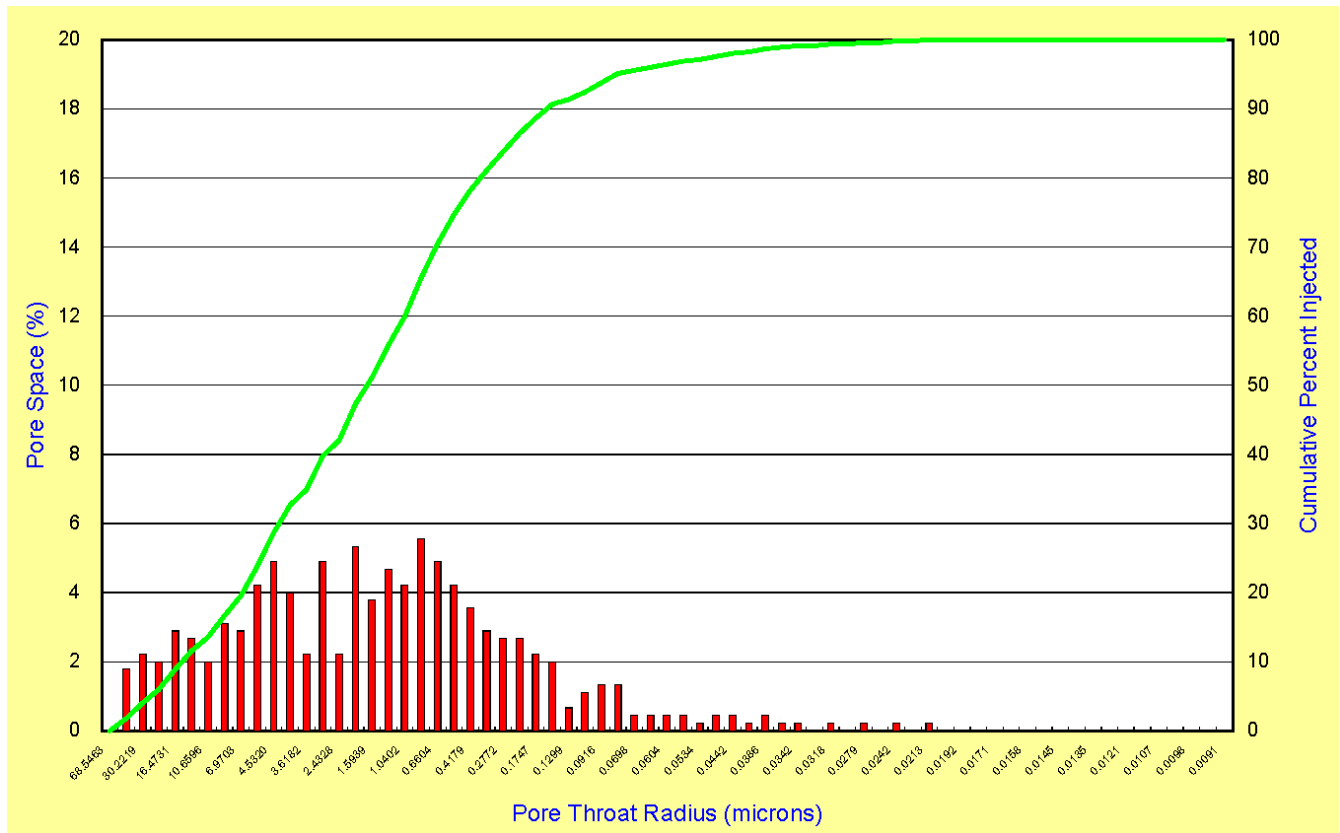
Figure 8.3. *Pore throat radius histogram – sample depth, 6289.1 feet (1916.9 m) – Bug No. 4 well.*
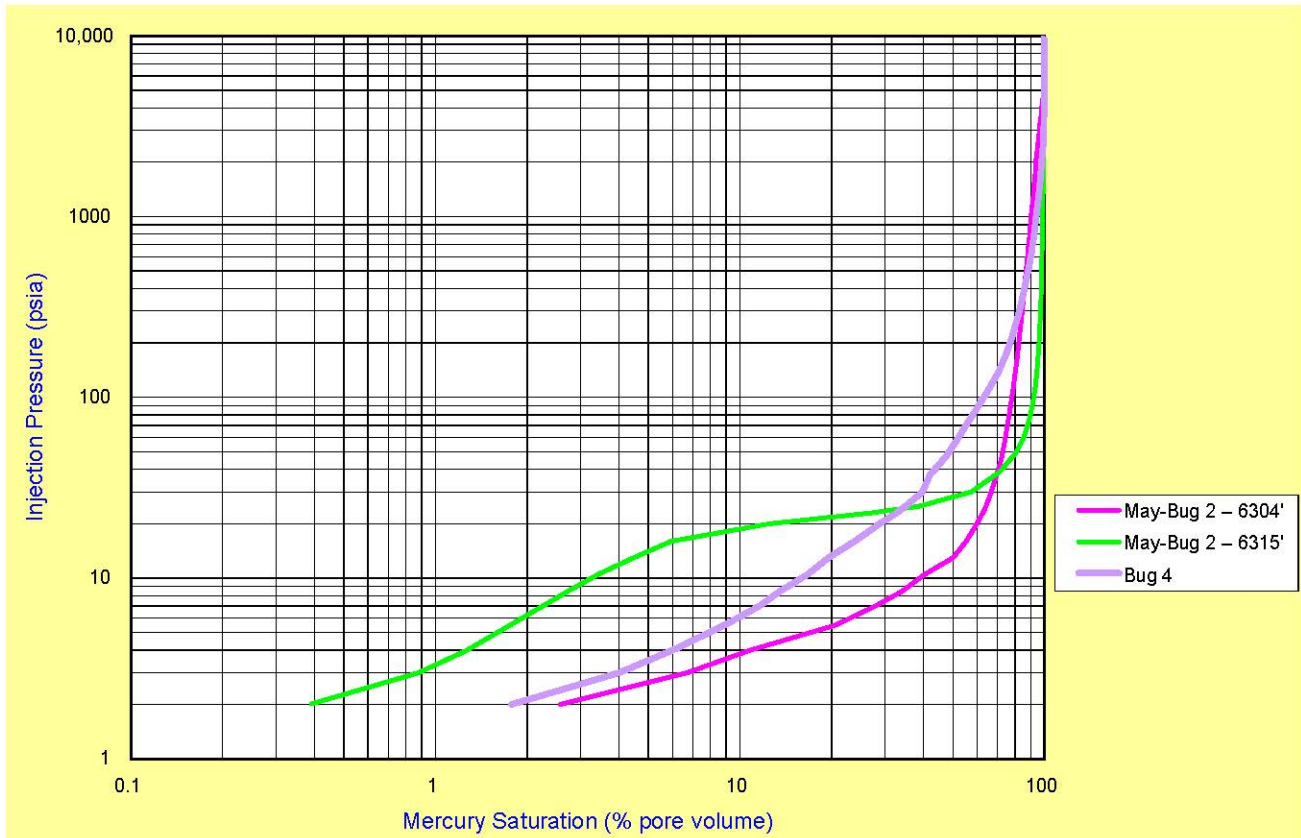
Figure 8.4. *Saturation profiles, May-Bug No. 2 and Bug No. 4 wells.*
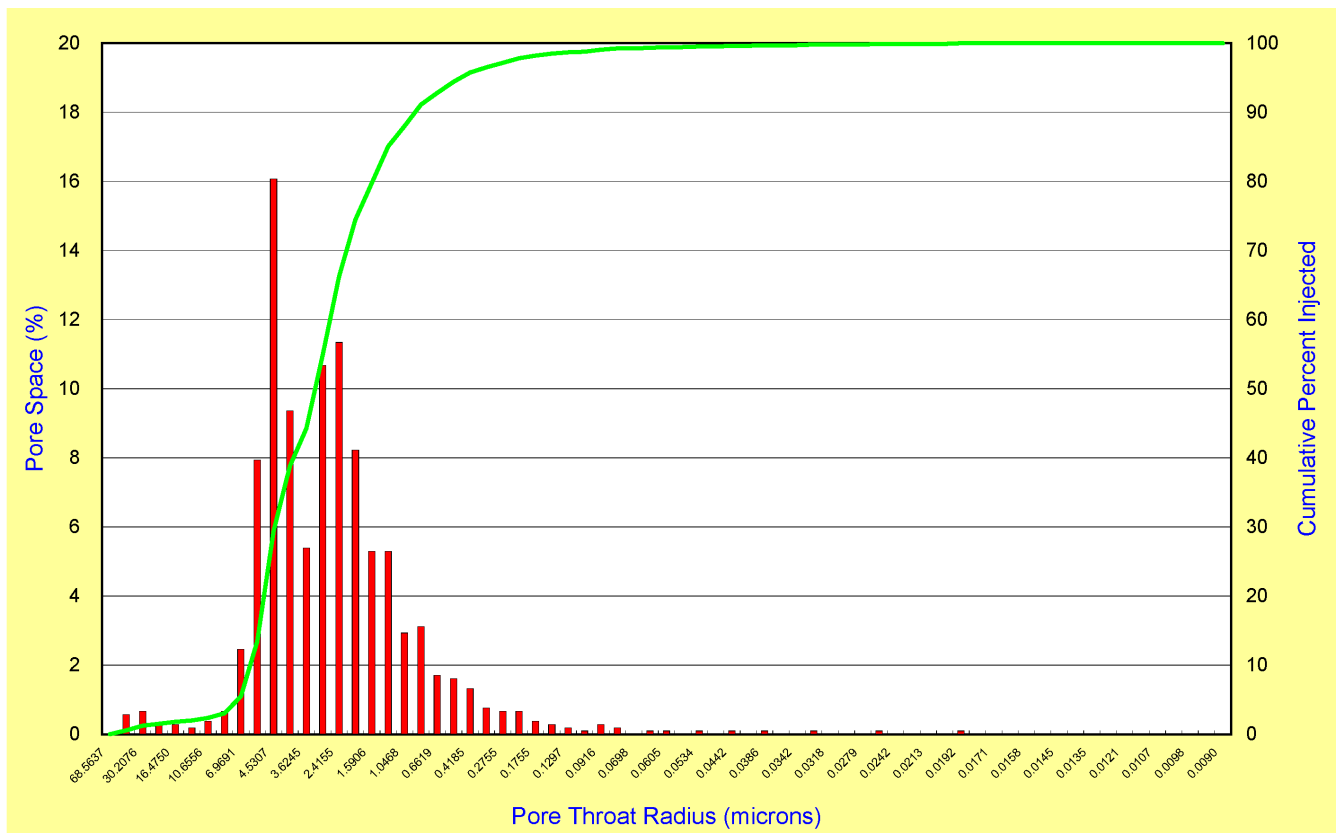
Figure 8.5. *Pore throat radius histogram – sample depth, 5768.7 feet (1758.3 m) – Cherokee Federal No. 22-14 well.*
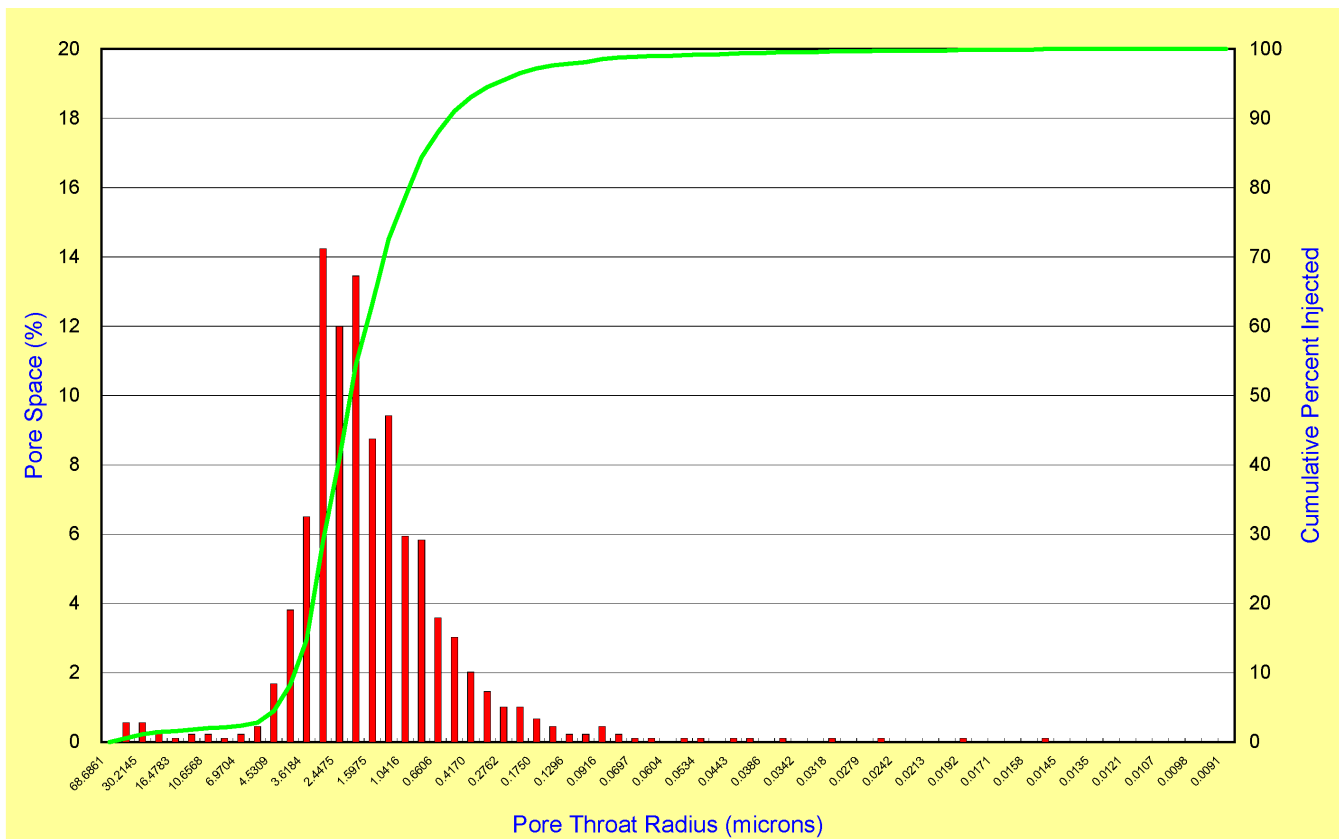
Figure 8.6. *Pore throat radius histogram – sample depth, 5781.2 feet (1762.1 m) – Cherokee Federal No. 33-14 well.*
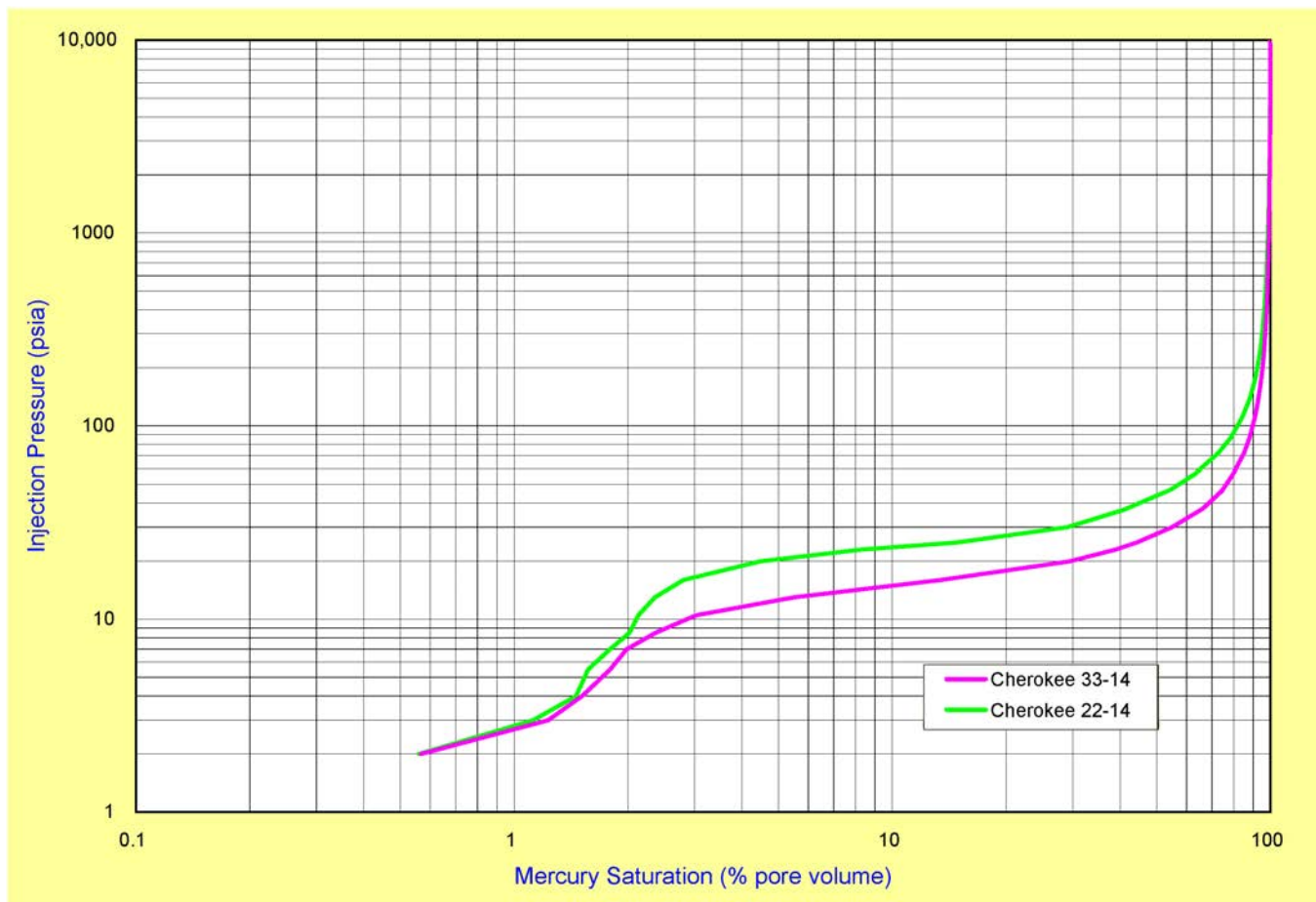
Figure 8.7. Saturation profiles, Cherokee Federal No. 22-14 and Cherokee Federal No. 33-14 wells.

mode 3 ranges from 3.0 to 1.5 microns (the modal class is 2.0 microns) and accounts for 13% to 15% of the pore space, also with 10% of the pores saturated on the cumulative injection curve. Modes 1 and 2 account for 30% of the injection and need 16% porosity to be effective for oil and 17.5% porosity for gas production. The measured porosity is 11.1%.

For the sample from 6315 feet (1925 m) from the May-Bug No. 2 well, the distribution of pore-throat radii appears to be unimodal (figure 8.2). The primary mode ranges from 4.5 to 1.5 microns (modal class is 2.3 microns) and accounts for 2% to 17% of the pore space, having 75% saturation of the cumulative curve. This primary mode needs 18% porosity to be effective for oil and 19.5% porosity for gas production. The measured porosity is 22.2%.

The distribution of pore-throat radii in the Bug No. 4 well is trimodal (figure 8.3). Mode 1 ranges from 5.5 to 3.6 microns (the modal class is about 4.0 microns) and accounts for 4.2% to 6.3% of the pore space, having 10% of the pores saturated on the cumulative injection curve. Mode 2 ranges from 2.4 to 1.0 microns (the modal class is 1.6 microns) and accounts for 8.3% to 10.3% of the pore space, also with 10% of the pores saturated on the cumulative injection curve. Mode 3 ranges from 1.0 to 0.4 microns (the modal class is 0.66 microns) and

accounts for 12.3% to 14.3% of the remaining pore space, again with 10% of the pores saturated on the cumulative injection curve. Modes 1 and 2 account for 20% of the injection and need 11% porosity to be effective for oil production. Mode 3 needs 18% porosity to be effective for gas production. The measured porosity is 12.3%.

Saturation Profiles

The saturation profile for the sample from 6304 feet (1921 m) from the May-Bug No. 2 well shows mode 1 covers 1% to 60% of the mercury saturation and requires injection pressure of 1 to 20 psi (7–138 kPa) (figure 8.4). Mode 2 covers 60% to 75% of the mercury saturation and requires injection pressure of 20 to 50 psi (138–345 kPa). The first 50% of the mercury saturation requires 15 psi (103 kPa); the second 45% requires 400 psi (2758 kPa).

The saturation profile for the sample from 6315 feet (1925 m) from the May-Bug No. 2 well shows the primary mode covers 6% to 60% of the mercury saturation and requires injection pressure of 15 to 30 psi (103–207 kPa) (figure 8.4). The first 50% of the mercury saturation requires 28 psi (193 kPa); the second 45% requires 400 psi (2758 kPa).

The saturation profile for the Bug No. 4 well sample shows mode 1 covers 4% to 28% of the mercury saturation and requires injection pressure of 3 to 20 psi (21–138 kPa) (figure 8.4). Mode 2 covers 45% to 70% of the mercury saturation and requires injection pressure of 40 to 150 psi (276–1034 kPa). Mode 3 covers 88% to 92% of the mercury saturation and requires injection pressure of 500 to 1500 psi (3448–10,343 kPa). The first 50% of the mercury saturation requires 55 psi (379 kPa); the second 45% requires 2000+ psi (13,782+ kPa).

Relatively high injection pressures are required to occupy more than the last 70% of the pores (figure 8.4). The steeper saturation profiles indicate a significant amount of micro-boxwork porosity, and thus, an excellent target for horizontal drilling.

Cherokee Field

Pore-Throat Radii

The pore-throat-radius histograms for both the Cherokee Federal No. 22-14 and Cherokee Federal No. 33-14 well samples (5768.7 feet [1758.2 m] and 5781.2 feet [1762.0 m], respectively) (figures 8.5 and 8.6) show that half of the pore size distribution falls under 2.0 microns, or in the microporosity realm. For the Cherokee Federal No. 22-14 well sample, the distribution of pore-throat radii appears to be trimodal. Mode 1 ranges from 7.0 to 3.6 microns (the modal class [the most abundant radii in the mode] is 4.0 microns) and accounts for 3.8% to 8% of the pore space, with 30% of the pores saturated on the cumulative injection curve. Mode 2 ranges from 2.4 to 1.04 microns (the modal class is 1.6 microns) and accounts for 10% to 15% of the pore space, also with 30% of the pores saturated on the cumulative injection curve. Mode 3 ranges from 0.7 to 0.13 microns (the modal class is 0.7 microns) and accounts for the remaining pore space, but with 20% of the pores saturated on the cumulative injection curve. Modes 1 and 2 account for 60% of the injection and need 16% porosity to be effective for oil and gas production. Mode 3 needs 19.5% porosity to be effective for oil (1.0 micron radii) and gas (0.5 micron radii) production. The measured porosity is 24.4%.

For the Cherokee Federal No. 33-14 well sample, the distribution of pore-throat radii appears to be unimodal. The primary mode ranges from 3.0 to 1.04 microns (modal class is 2.0 microns) and accounts for 6% to 15% of the pore space, but only 40% saturation of the cumulative curve at 2.0 microns. Thus, the Cherokee Federal No. 33-14 is a poorer producer than the Cherokee Federal No. 22-14. This primary mode needs 15.5% porosity to be effective for oil and 19.5% porosity for gas production. The measured porosity is 20.1%.

Saturation Profiles

The saturation profile for the Cherokee Federal No. 22-14 well sample shows mode 1 covers 2% to 30% of the mercury saturation (percent of the pore volume) and requires injection pressure of 2 to 20 psi (14–138 kPa) (figure 8.7). Mode 2 covers 30% to 70% of the mercury saturation and requires injection pressure of 20 to 40 psi (138–276 kPa) and is the most important in terms of contribution to production. The first 50% of the mercury saturation requires 28 psi (193 kPa) and is thus a good pore system; the second 45% requires 400 psi (2758 kPa). Most pores are filled under 1000 psi (6895 kPa).

The saturation profile for the Cherokee Federal No. 33-14 well sample shows the primary mode covers 2.5% to 70% of the mercury saturation and requires injection pressure of 15 to 70 psi (103–483 kPa) (figure 8.7). The first 50% of the mercury saturation requires 45 psi (310 kPa); the second 45% requires 600 psi (4137 kPa).

As in Bug field, both samples show that a relatively high injection pressure is required to occupy more than the last 70% of the pores (figure 8.7). The Cherokee Federal No. 33-14 well sample has a steeper saturation profile than the Cherokee Federal No. 22-14 well sample indicating a greater amount of microporosity, and corresponding to the lower IFP (336 BOPD and 349 MCFGPD for the Cherokee Federal No. 33-14 well compared to 688 BOPD and 78,728 MCFGPD for the Cherokee Federal No. 22-14 well). However, the data suggest that the well still has potential for untapped reserves.

CHAPTER 9:
WELL-TEST AND PRODUCTION ANALYSIS, BUG AND CHEROKEE CASE-STUDY FIELDS, SAN JUAN COUNTY, UTAH

by

Thomas C. Chidsey, Jr., Utah Geological Survey

CHAPTER 9:
WELL-TEST AND PRODUCTION ANALYSIS, BUG AND CHEROKEE CASE-STUDY FIELDS, SAN JUAN COUNTY, UTAH

INTRODUCTION

Well-test and production data were analyzed for the Bug and Cherokee case-study fields (figure 1.3). These data were compiled through two principal tasks: (1) review of existing well-completion data, and (2) determination of production history from production reports available through the Utah Division of Oil, Gas and Mining. This information was merged with the various geological characterization studies to identify production "sweet spots" and potential horizontal drilling candidates, both in wells and fields.

WELL-TEST DATA EVALUATION

Well-test data can provide key insight into the nature of reservoir heterogeneities, and also deliver "large-scale" quantitative data on actual reservoir properties and lithofacies from case-study reservoirs. Although a number of well tests have

been conducted in all of the target reservoirs, only the IFP well tests (the calculated average daily rates usually based on the first 30 days of production) were determined to provide quantitative reservoir property information. Initial potential flow well tests were graphed and plotted for each well (figures 9.1 through 9.4). The graphs include both oil (in BOPD) and gas (in MCFGPD) production.

In Bug field, the highest IFPs were recorded from the Bug No. 1, May-Bug No. 2, Bug No. 9, and Bug No. 4 wells (figures 9.1 and 9.2), located structurally downdip from the updip porosity pinch out that forms the trap and in the main part of the lower Desert Creek zone carbonate buildup (figures 3.7 and 3.12); Bug No. 9 was tested from the thickest section of the mound. These wells penetrated both the phylloid-algal mound and the shoreline carbonate island lithofacies of the carbonate buildup. The lowest recorded IFPs were from wells closest to the updip porosity pinch out, or just downdip from the oil/water contact (figures 9.1, 9.2, and 3.7). These wells penetrated only the phylloid-algal mound lithofacies (figure 3.12).
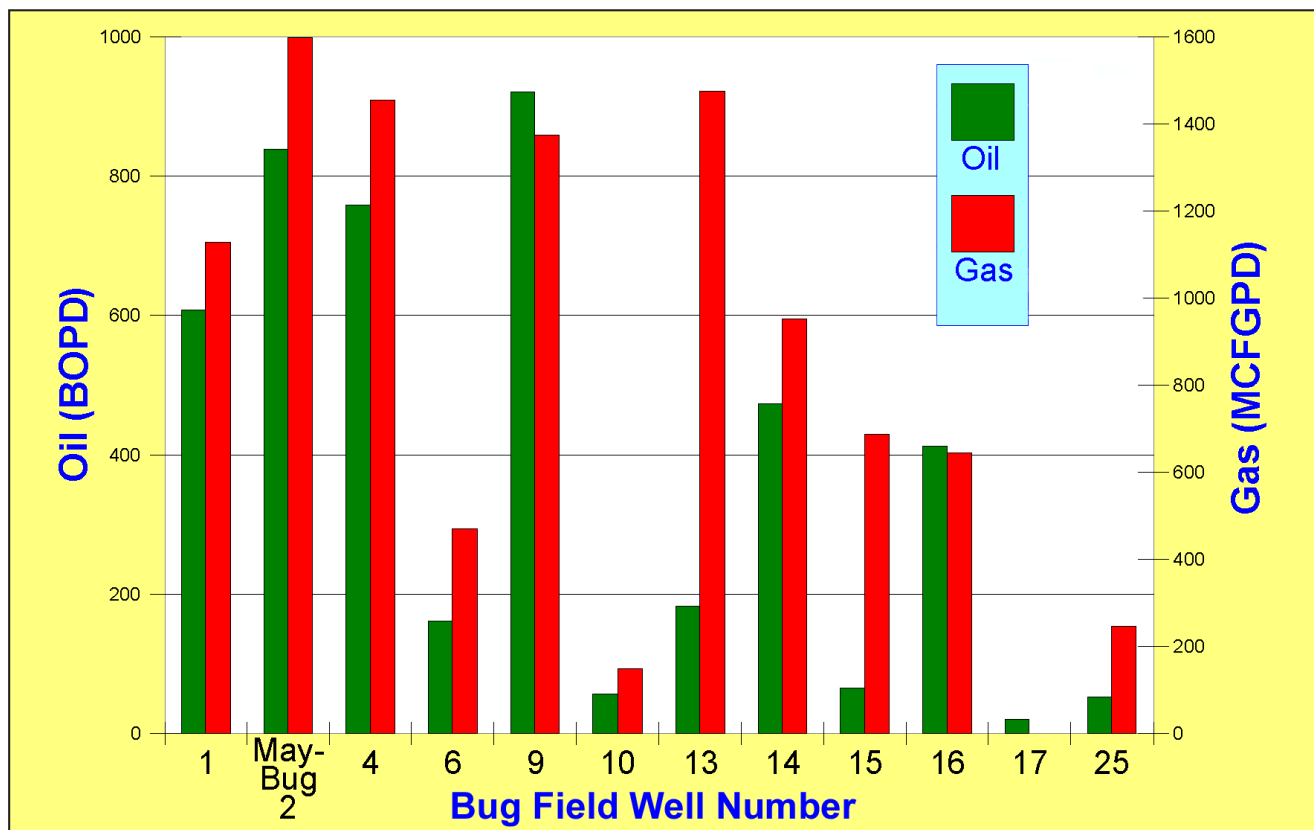
Figure 9.1. *Initial flowing potential (the calculated average daily rates usually based on the first 30 days of production) of oil (in BOPD) and gas (in MCFGPD) from lower Desert Creek producing wells in Bug field (data source: Utah Division of Oil, Gas and Mining).*

In Cherokee field, the highest IFP was recorded from the Cherokee Federal No. 22-14 well (figures 9.3 and 9.4), located on the crest of the structural nose where the thickest part of the upper Ismay zone mound lithofacies developed (figures 3.10 and 3.14). The lowest recorded IFP was from the Cherokee Federal No. 11-14 well (figures 9.3 and 9.4), located on the structural low and on the thin flank of the mound buildup (figures 3.10 and 3.14). Both wells had relatively high gas-to-oil ratios (GOR) in comparison to the other two producing field wells (figure 9.3) in the southeastern part of the field (figure 9.4).

CUMULATIVE PRODUCTION

In Bug field, oil and gas production peaked in 1982 and steadily declined ever since (figure 9.5). The largest volumes of oil have been produced from the May-Bug No. 2 and Bug No. 14 wells (figure 9.6). These wells, plus the Bug No. 4, Bug No. 9, and Bug No. 16 wells, have each produced over 200,000 barrels of oil. Although these wells penetrated the phylloid-algal mound and the shoreline carbonate island lithofacies (figure 3.12), there are other wells that penetrated this same lithofacies combination, such as Bug No.13 well, but
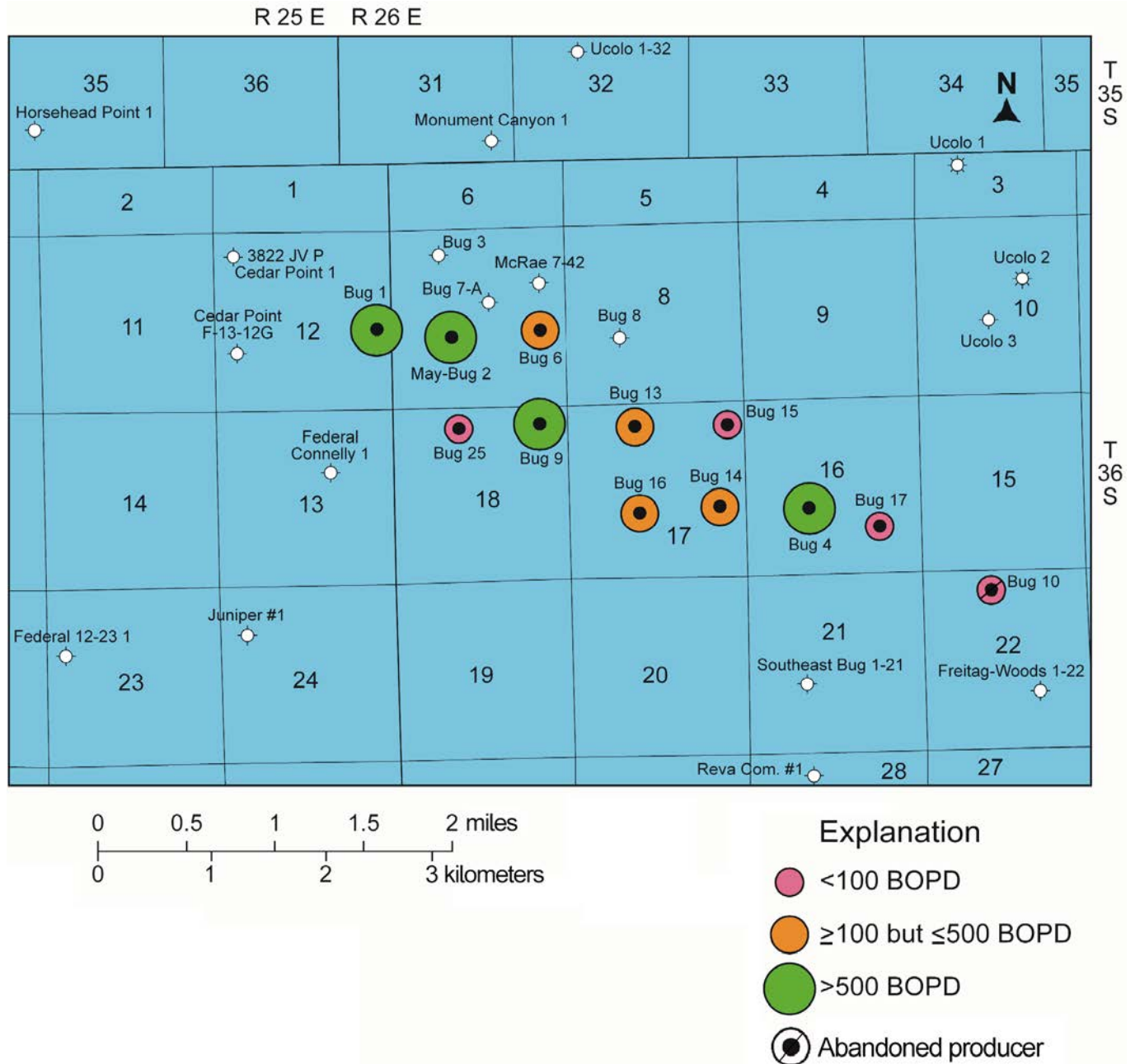
Figure 9.2. *Bubble map of initial flowing potential of oil (in BOPD) from lower Desert Creek producing wells in Bug field (data source: Utah Division of Oil, Gas and Mining).*
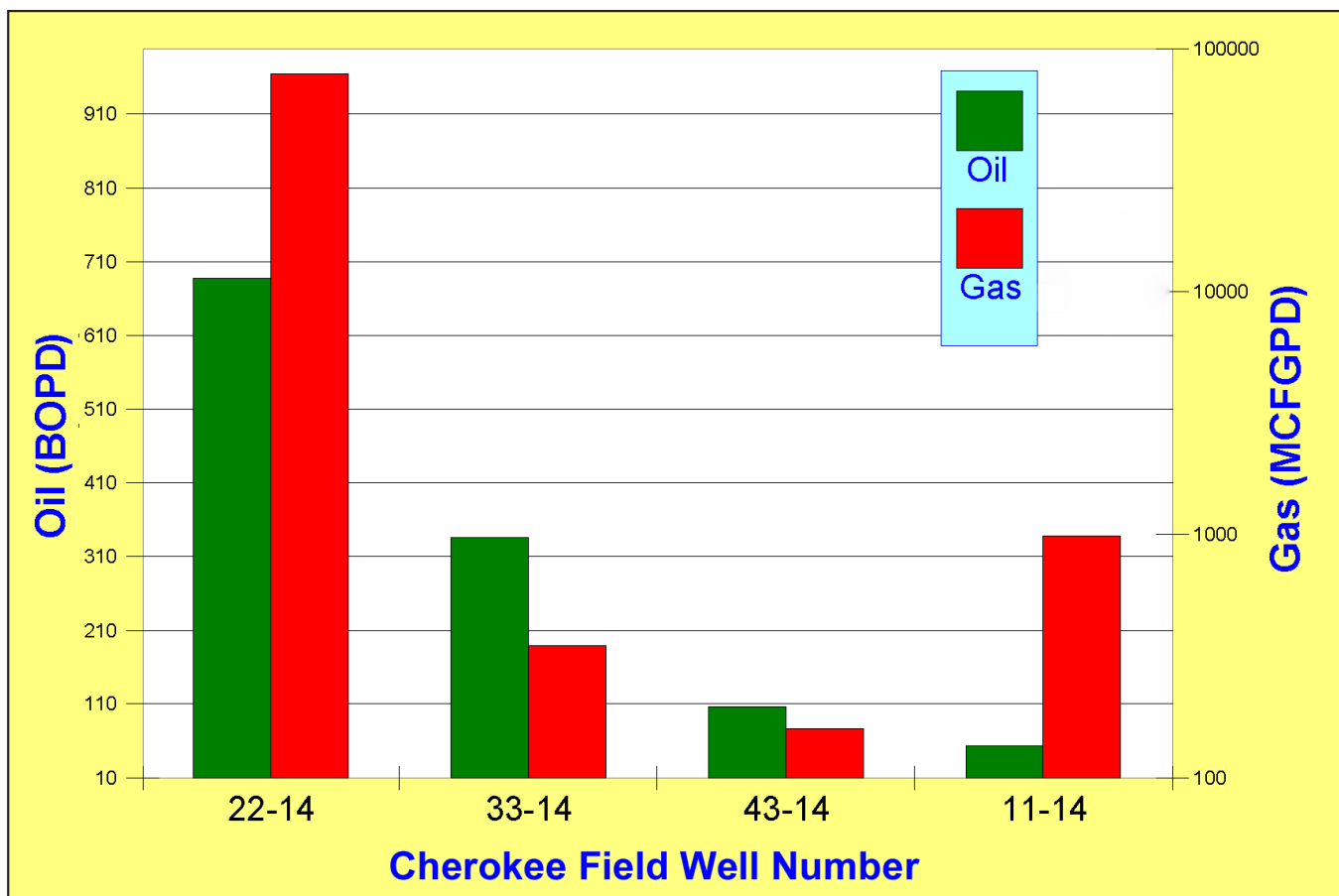
Figure 9.3. *Initial flowing potential of oil (in BOPD) and gas (in MCFGPD) from upper Ismay producing wells in Cherokee field (data source: Utah Division of Oil, Gas and Mining).*

have produced lower volumes of oil. Such lower-producing wells may have encountered fewer microfractures and less micro-boxwork porosity (figure 3.27), a prime diagenetic pore type in this dolomitized reservoir, which is thought to account for the greatest hydrocarbon storage and flow capacity in the field. The lowest volumes of hydrocarbon production are from wells closest to the updip porosity pinch out (Bug Nos. 6, 15, and 17; figure 9.6) or farther downdip near the oil/water contact (Bug No. 25) (figure 3.7). These wells penetrated only the phylloid-algal mound lithofacies (figure 3.12). The Bug No. 13 and Bug No. 15 wells are the structurally highest wells in the field and are located near a presumed gas cap, thus their production history shows high GORs (figure 9.7).

Oil and gas production from Cherokee field has also steadily declined since peaking in the late 1980s (figure 9.8). The largest volume of oil has been produced from the Cherokee Federal No. 33-14 well (figure 9.9); the highest volume of gas has been produced from the Cherokee Federal No. 22-14 well (figure 9.10). Both wells are located where the crest of the structural nose coincides with the thickest part of the mound lithofacies (figures 3.10 and 3.14). The Cherokee Federal No. 22-14 well is slightly higher structurally than the Cherokee Federal No. 33-14 well, possibly accounting for the significantly greater volume of gas production. These wells pene-

trate both the phylloid-algal mound and the crinoid/fusulinid-bearing carbonate sand lithofacies of the carbonate buildup (figure 3.14). The Cherokee Federal No. 33-14 well may have encountered a significantly thicker section of microporosity and microfractures than other wells resulting in greater oil production. Microporosity is present in cores from both the Cherokee Federal No. 33-14 and Cherokee Federal No. 22-14 wells (figure 3.30). This unique pore type represents the greatest hydrocarbon storage capacity and potential horizontal drilling target in the field. The lowest volumes of hydrocarbon production are from wells on the flanks of both the structure and the mound. These wells are likely close to the oil/water contact (its exact elevation is unknown) and have penetrated only the phylloid-algal mound buildup.
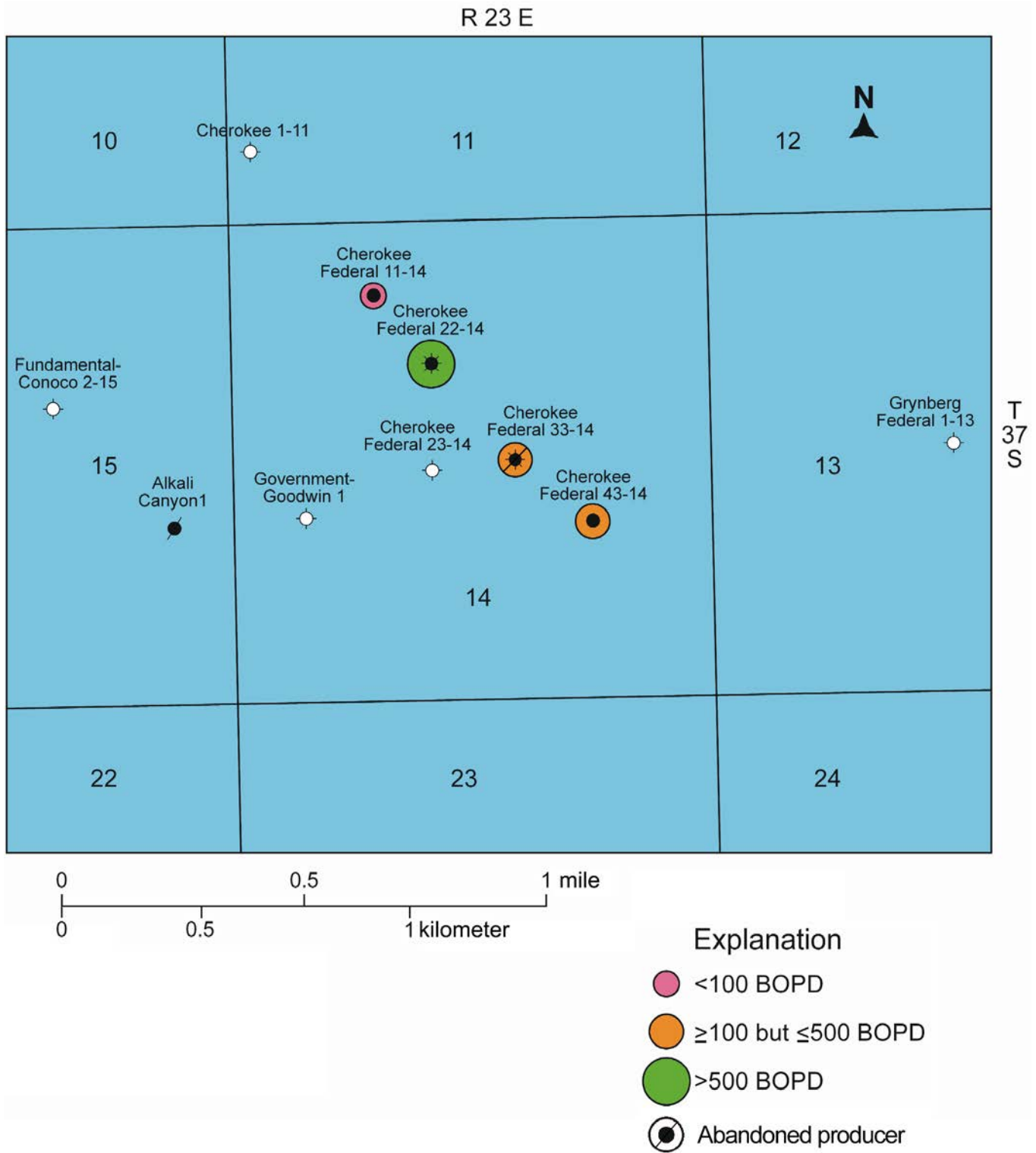
Figure 9.4. *Bubble map of initial flowing potential of oil (in BOPD) from upper Ismay producing wells in Cherokee field (data source: Utah Division of Oil, Gas and Mining).*
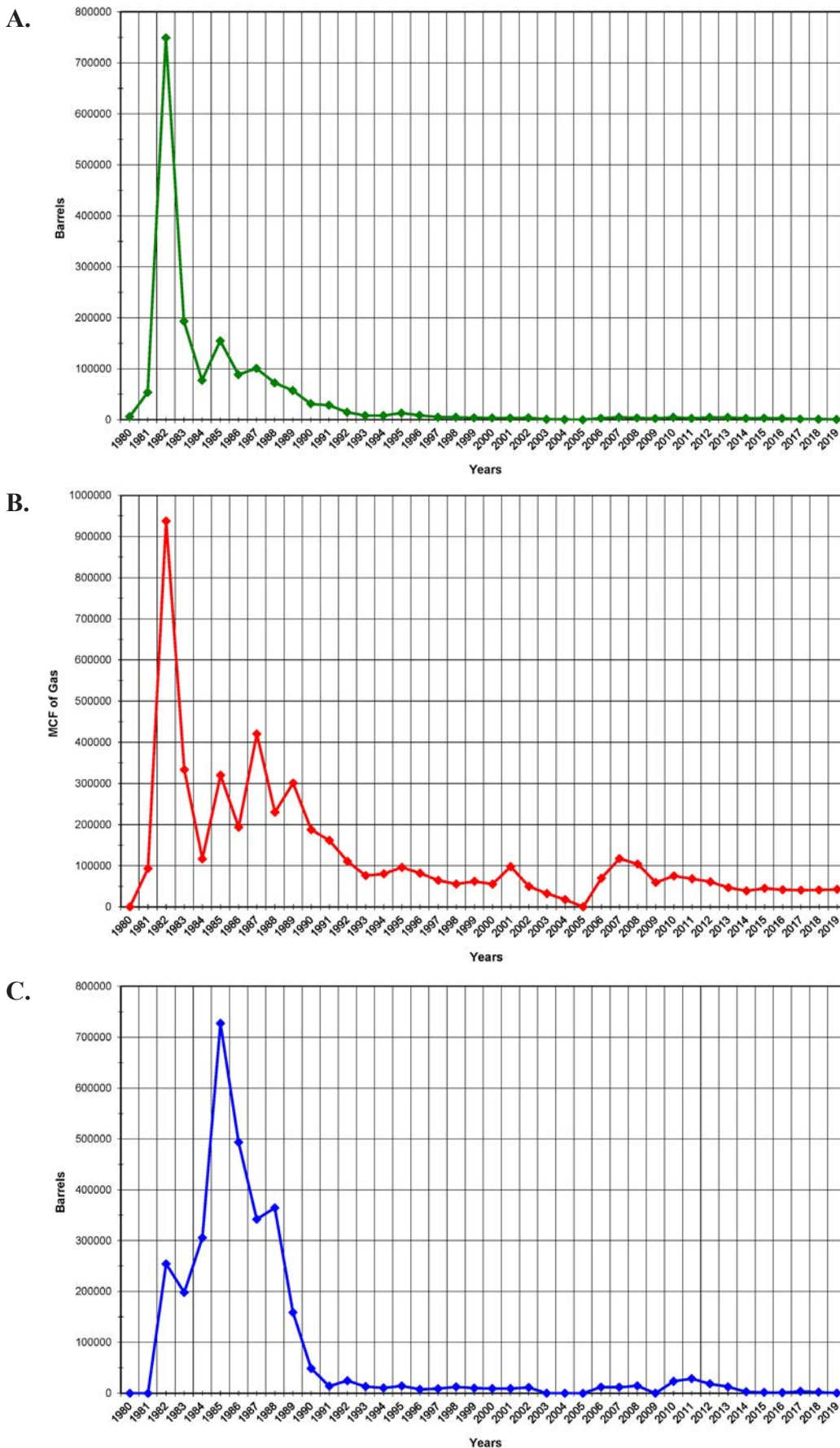
Figure 9.5. *Historical oil **(A)**, gas **(B)**, and water **(C)** production for Bug field through 2019 (Utah Division of Oil, Gas and Mining, 2020).*
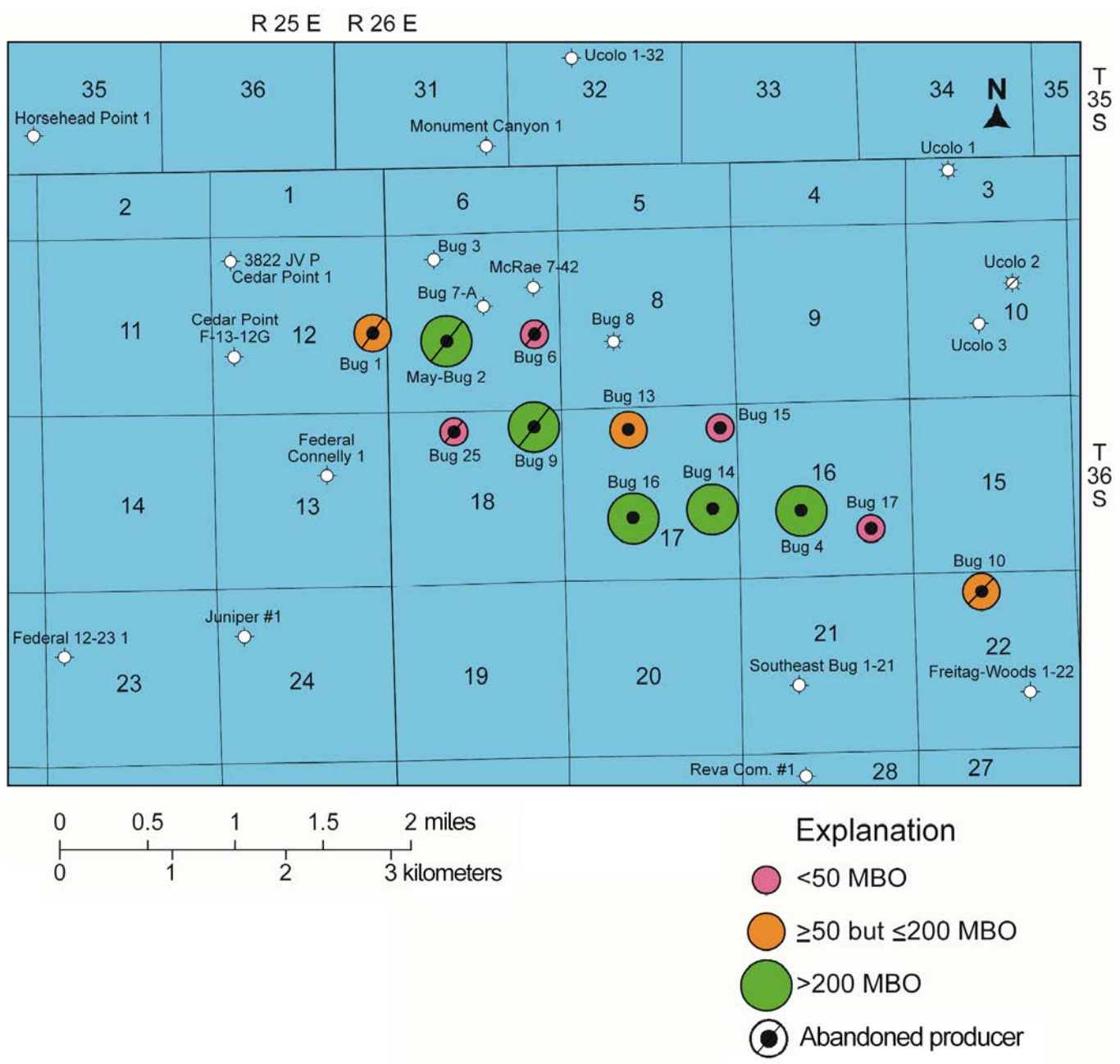
Figure 9.6. *Bubble map of cumulative production of oil (in thousands of barrels [MBO]) from lower Desert Creek producing wells in Bug field as of January 1, 2020 (Utah Division of Oil, Gas and Mining, 2020).*
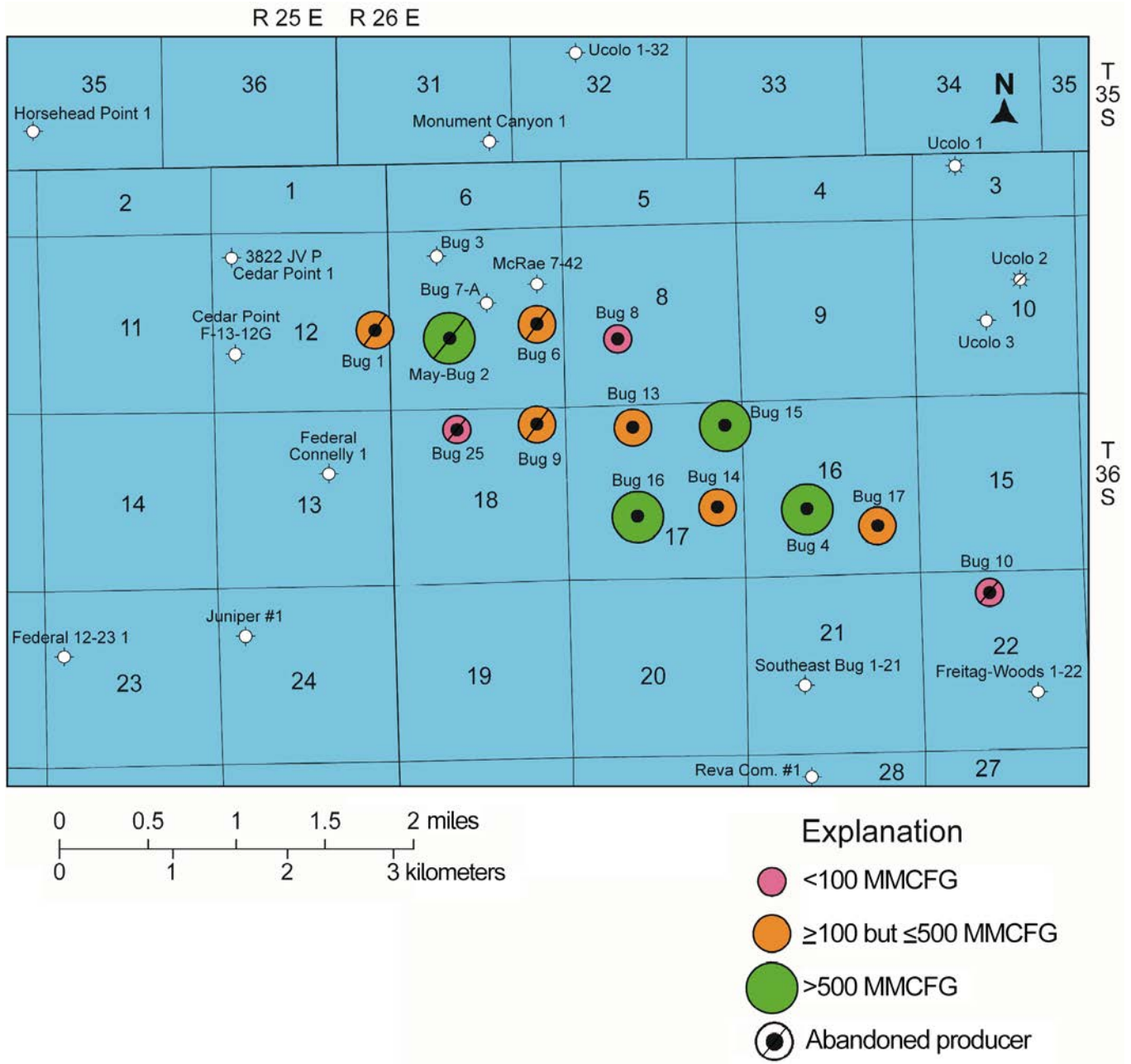
Figure 9.7. Bubble map of cumulative production of gas (in million cubic feet [MMCFG]) from lower Desert Creek producing wells in Bug field as of January 1, 2020 (Utah Division of Oil, Gas and Mining, 2020).
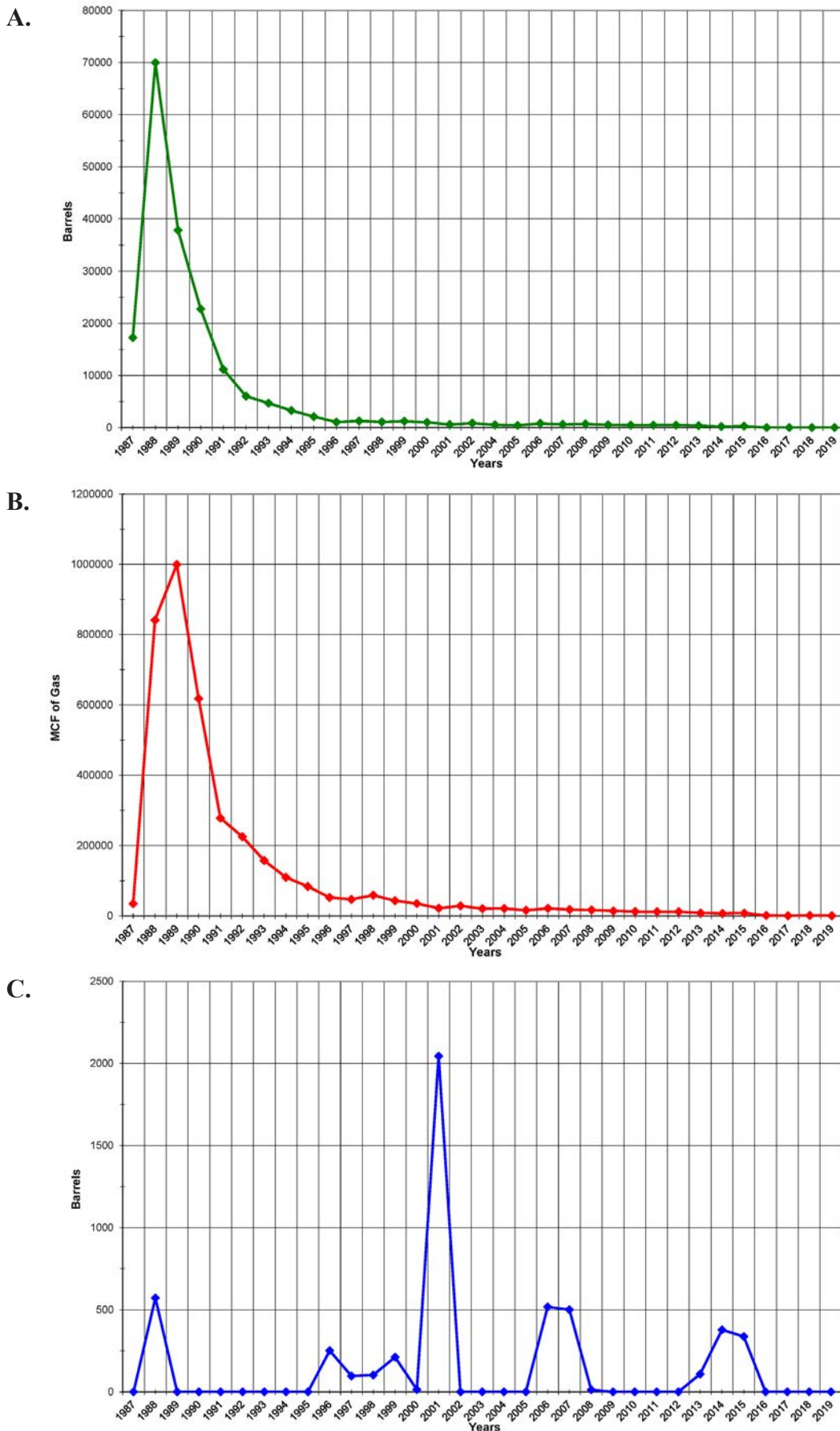
Figure 9.8. *Historical oil **(A)**, gas **(B)**, and water **(C)** production for Cherokee field through 2019 (Utah Division of Oil, Gas and Mining, 2020).*
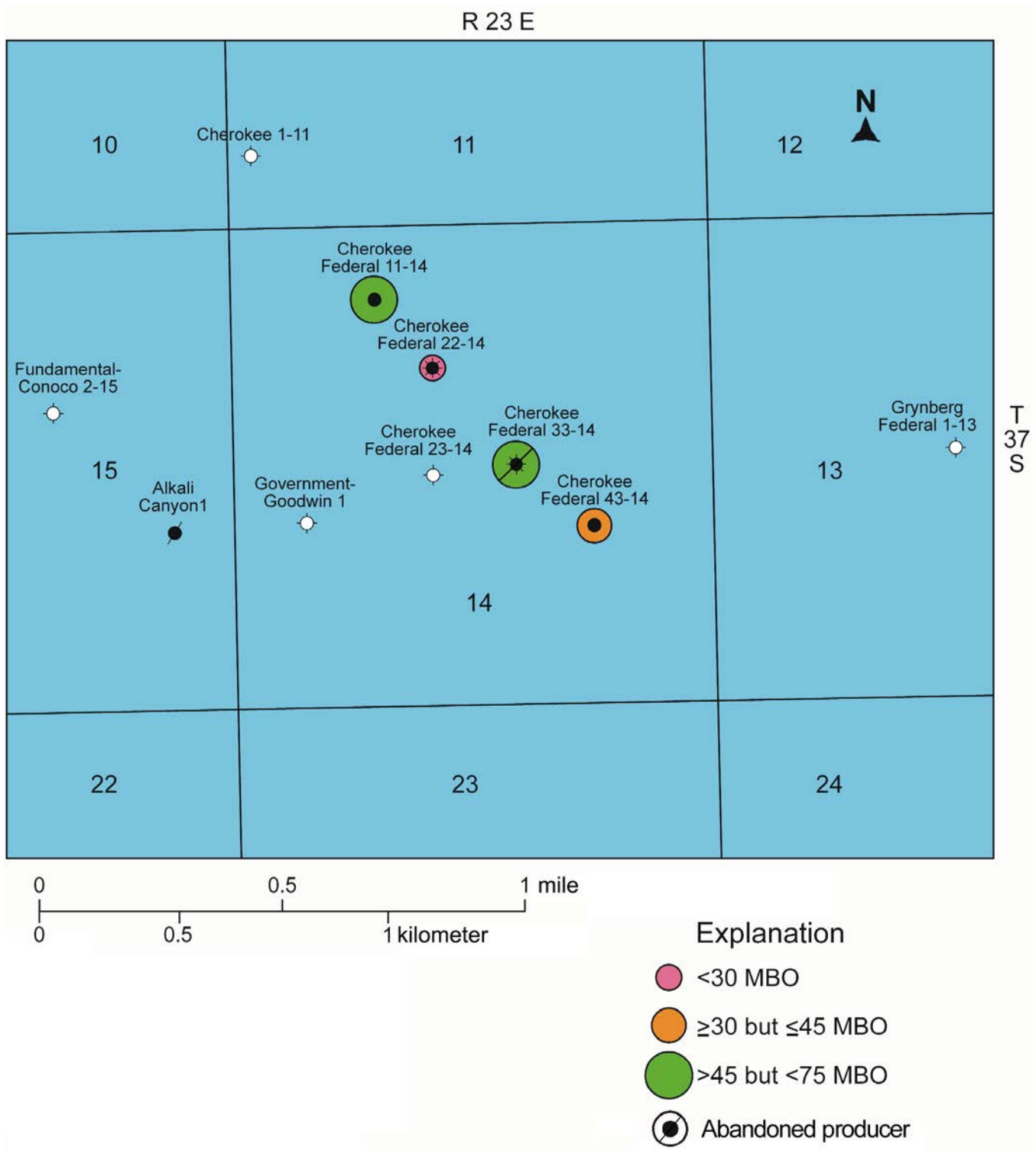
Figure 9.9. *Bubble map of cumulative production of oil (in thousands of barrels [MBO]) from upper Ismay producing wells in Cherokee field as of January 1, 2020 (Utah Division of Oil, Gas and Mining, 2020).*
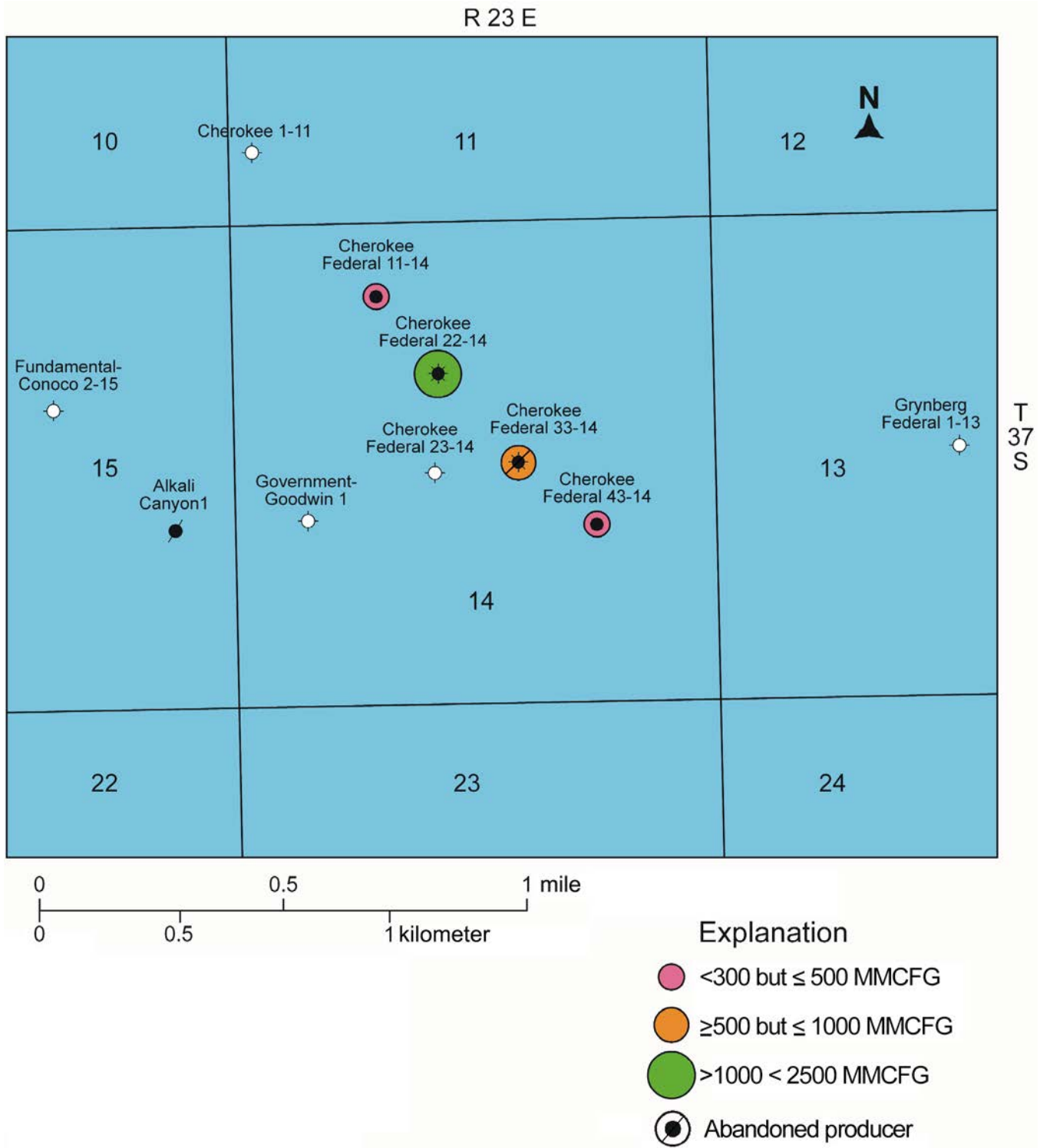
Figure 9.10. Bubble map of cumulative production of gas (in million cubic feet [MMCFG]) from upper Ismay producing wells in Cherokee field as of January 1, 2020 (Utah Division of Oil, Gas and Mining, 2020).

CHAPTER 10:
HORIZONTAL DRILLING OPPORTUNITIES

---

by

Thomas C. Chidsey, Jr., Utah Geological Survey
and
David E. Eby, Eby Petrography & Consulting, Inc.

CHAPTER 10:
HORIZONTAL DRILLING OPPORTUNITIES

INTRODUCTION

Multilateral wellbores can be drilled from an existing single wellbore (figure 1.4) (Chambers, 1998). These laterals may be horizontal or deviated to reach different bottom-hole locations. The laterals are drilled from the main wellbore. Branches are drilled from a horizontal lateral into the horizontal plane. Laterals may be opposed to each other or stacked. Multilaterals are drilled for cost saving reasons or reservoir production reasons associated with improved drainage or injection. They provide a means for increasing contact with the pay zones and, in the case of our study, would target untapped reservoir compartments.

Historical Aspects

Beginning in the 1990s, horizontal drilling was proven to be a viable alternative to conventional vertical drilling. With the exception of the giant Greater Aneth field (figure 1.3), the value of horizontal drilling has not been demonstrated in any of the over 100 smaller shallow-shelf carbonate reservoirs in the southern Paradox Basin. The reservoirs are heterogeneous due to lithofacies changes and extensive diagenesis within the Ismay and Desert Creek zones, leaving untapped compartments. To date, only two short-radius horizontal wells have been drilled (in the 1990s) in small Ismay (Knockando) and Desert Creek (Mule) fields (figure 1.3); neither wellbore was hydraulically fractured, only treated with acid. The results from these wells were disappointing in terms of encountering the objective reservoir lithofacies and production (Chidsey, 2002).

Reservoirs developed in carbonate reefs that have successfully been drilled with horizontal wells include pinnacle reefs in the Alberta Basin, the Madison Group in the Williston Basin, Permian Basin reefs, and Devonian and Silurian pinnacle reefs in the Michigan Basin. The purpose of horizontal drilling for these carbonate reservoirs was to (1) solve water-, solvent-, and/or gas-coning problems, (2) control water production, (3) improve light oil production, and (4) encounter off-reef lithofacies or karsted reef surfaces. These drilling programs were not designed to encounter untapped reservoir compartments. The results of these drilling projects are summarized by Jones (1992), LeFever (1992), and Wood and others (1996). The horizontal wells, some of which are hydraulically fractured, in these plays have generally higher success rates than vertical wells, and have higher initial flowing potentials (20% to 50%), lower drilling costs, and require fewer wells to drain a reservoir than vertical wells.

Greater Aneth Field Horizontal Drilling Program

Greater Aneth oil field, Utah's largest oil producer, was discovered in 1956. Located on the Aneth platform part of the Paradox Basin in extreme southeastern Utah (figures 1.1 and 1.3), Greater Aneth represents a "typical" mature western U.S. oil field. More than 100 short horizontal laterals have been drilled in the field. Combined with waterflooding and carbon dioxide (CO_2) flooding programs, horizontal drilling has successfully increased production after years of decline and increased the estimated ultimate recovery well beyond earlier predictions at Greater Aneth field. The lessons learned from horizontal drilling at Greater Aneth can also be applied when targeting untested reservoir potential, described in previous chapters, for the case-study fields and the many similar, small fields throughout the Blanding sub-basin north of the Aneth platform (figure 1.3).

Field Overview

Greater Aneth is a stratigraphic trap with fractures and small faults. The field produces oil and gas primarily from the Desert Creek zone sealed by the organic-rich, overlying Gothic shale, both within the Paradox Formation (figure 1.2).

The Desert Creek at Greater Aneth field is a complex reservoir representing a variety of environments: open-marine shelf, shallow-marine oolitic shoals, phylloid-algal mounds, and low-energy restricted shelf. Carbonate fabrics consist of limestone (algal boundstone/bafflestone and oolitic, peloidal, and skeletal grainstone and packstone) and finely crystalline dolomite.

The net reservoir thickness of the Desert Creek zone at Greater Aneth is 50 feet (15 m) over a 48,260-acre (19,530 ha) area. Porosity averages 10% in interparticle, moldic, and intercrystalline networks enhanced by fractures; permeability averages 10 mD, ranging from 3 to 30 mD.

Cumulative production as of September 1, 2020, was 496,514,536 BO, 469 BCFG, and 2,037,102,414 BW (Utah Division of Oil, Gas and Mining, 2020). In-place total oil reserves for Greater Aneth field are estimated at 1.1 billion barrels (Peterson and Ohlen, 1963; Babcock, 1978a, 1978b, 1978c, 1978d; Peterson, 1992; Moore and Hawks, 1993).

Waterfloods

The largest waterflood program in the Paradox Basin and one of the largest in Utah is in Greater Aneth field. Waterflooding in the field began in 1961 (Babcock, 1978b). Until horizontal drilling technology was developed in the 1990s, the waterflood

programs at Greater Aneth used a radial five-spot flow pattern where streamlines of water displace oil from a point source of injection to point sources of production, leaving some parts of the reservoir poorly swept (figure 10.1A) (Amateis and Hall, 1997). The extensive horizontal drilling program in Greater Aneth changed the five-spot flow pattern to line-drive injection patterns (figure 10.1B) and improved both lateral and vertical sweep efficiencies over that of the previous vertical wells (Amateis and Hall, 1997).

Production and injection laterals were drilled into the Desert Creek porosity intervals to more efficiently sweep oil that vertical wells could not reach. Horizontal laterals were drilled as injector-producer pairs in opposing, northwest and southeast directions, offset about 1800 feet (550 m) diagonally to parallel horizontal producing wells (figure 10.1B). This allowed the line-drive flow to maintain reservoir pressure and more uniformly sweep oil from injection to producing wells (Amateis and Hall, 1997). In addition, every other row of wells was left as vertical wells, resulting in significant cost savings and provided a method to produce or inject into intervals not horizontally drilled. Amateis and Hall (1997) estimated a 5% to 10% increase in recovery of the OOIP using the line-drive flow pattern based on reservoir simulation.

Carbon Dioxide Floods

Carbon dioxide flooding is an enhanced oil recovery technique used in mature West Texas fields (over 20% of that area's production) and elsewhere. However, only one field in Utah (and in the Paradox Basin) is under CO_2 flood—Greater Aneth. Carbon dioxide flooding is relatively low risk, significantly increases oil recovery, and extends the life of a field by 20 to 30 years. Ultimate oil recovery may increase by over 40% with CO_2 flooding (8% to 16% due to CO_2 flooding alone) (Lambert and others, 1995). Chidsey (2002) proposed using CO_2 flooding to increase production and reserves in small fields of the southern Paradox Basin.

The application of horizontal drilling techniques to the CO_2 flooding programs at Greater Aneth field has been a major sucess. Evaluating potential areas of Greater Aneth field for CO_2 flooding involved several screening criteria, which can be applied to fields in the Blanding sub-basin. The most important criterion was that CO_2 miscibility needed to be attainable over a major part of the reservoir, requiring widespread good injectivity and reservoir connectivity. Therefore, understanding reservoir lithofacies, heterogeneity, and petrophysical properties was critical in planning CO_2 flooding programs at Greater Aneth field. The reservoir should be deeper than 2500 feet (760 m) and the API gravity of the oil greater than 25° (Hsu and others, 1995). The average depth to the Desert Creek zone at Greater Aneth is over 5500 feet (1680 m) and the API gravity of the oil ranges from 40° to 42°, comparable to fields in the Blanding sub-basin. The maximum viscosity must be 10 to 12 centipoise (cP) (Lambert and others, 1995); the viscosity of Greater Aneth oil is 0.54 cP.

Prospective CO_2 flooding candidates had performed well during waterflood programs where they established favorable sweep efficiency, acceptable throughput rates, and good voidage balance (Hsu and others, 1995). Limiting factors to CO_2 flood programs include complex reservoir heterogeneity, which can create non-uniform displacement fronts.

The Devonian Ouray Formation and Mississippian Leadville Limestone, at McElmo Dome field on the eastern edge of the Paradox Basin in southwest Colorado (figure 1.1), supply CO_2 to Greater Aneth field (and Permian Basin fields) via an 8-inch pipeline. McElmo Dome field produces nearly pure CO_2 with reserves estimated at 2.5 TCFG (Tremain, 1993).

Carbon dioxide flooding began at Greater Aneth in 1985. The production response was evident after between one and two years through a water-alternating-gas (WAG) program, shown schematically on figure 10.2. Oil production increased from
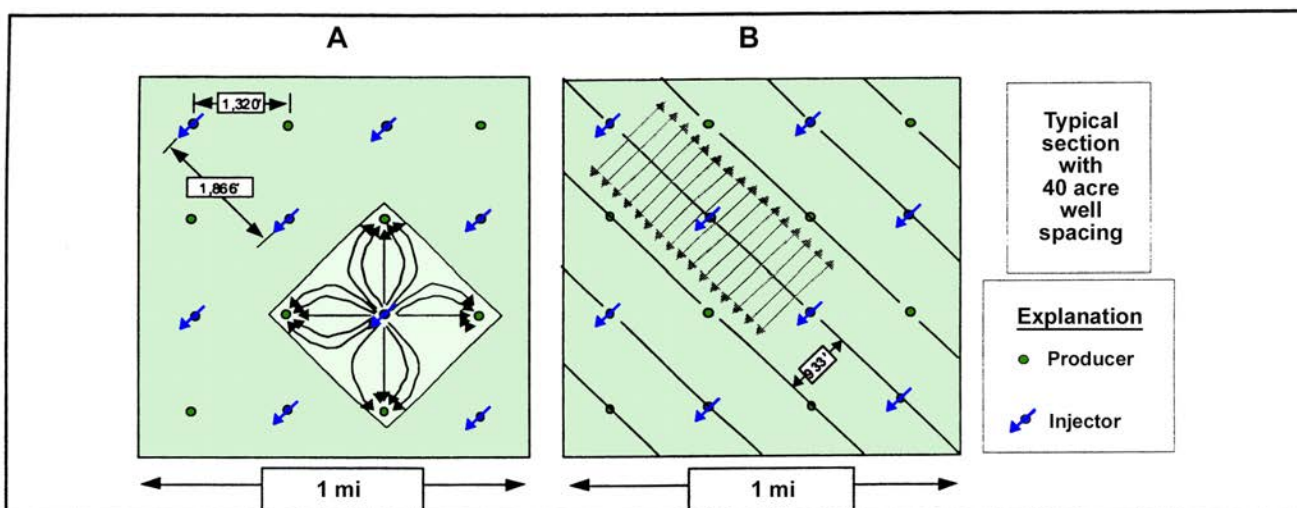
Figure 10.1. *Waterflood flow patterns at Greater Aneth field.* **(A)** *Vertical wells in a five-spot radial flow pattern.* **(B)** *Line-drive flow pattern using horizontal wells. After Amateis and Hall (1997).*

5500 to 6500 BOPD, peaking after a ten-year period (Lambert and others, 1995). Incremental recovery from CO_2 flooding is estimated at 33 million BO or an incremental recovery efficiency of 9.3% (Jim Rutledge, Los Alamos National Laboratory, verbal communication, July 26, 2007).

A pilot CO_2 flood using horizontal wells (lateral) was conducted in the northwestern part of the field in 1998. The horizontal laterals were drilled in vuggy, phylloid-algal dolomitic bafflestone. Although the project was brief, rapid CO_2 breakthrough occurred after which it was abandoned. The operator determined that the best intervals for CO_2 flooding were not phylloid-algal bafflestone but oolitic grainstone and packstone.

Horizontal Drilling

Extensive and successful horizontal drilling programs in Greater Aneth field were carried out primarily in the northwestern and southeastern parts of the field. Short-reach or horizontal lateral drilling programs at Greater Aneth field included wells with two opposed sets of three stacked parallel laterals with lengths of 860 to 960 feet (260–290 m), similar to that shown schematically on figure 1.4. The purpose of this program was to encounter subzones that were basically untouched by waterflooding, discussed in the previous section, and to slant through vertical barriers to overcome permeability problems and increase production (Amateis, 1995).

Parasequence boundaries, non-algal zones, OOIP, net pay, and sweep efficiency (described in the section above) were the main criteria used to choose the location of horizontal laterals. In addition, horizontal laterals were drilled in northwest and southeast directions perpendicular to small-scale, southwest-northeast-trending normal faults (5 to 40 feet [2–12 m] of vertical offset) and fracture zones that likely divide the reservoir into segments. Production tests averaged 700 BOPD with rates as high as 1127 BOPD and 461 BW per day.

HORIZONTAL DRILLING TARGETS IN THE BLANDING SUB-BASIN

Regional Lithofacies Perspective

The Utah portion of the Blanding sub-basin shows the development of "clean carbonate" packages that contain a variety of the productive reservoir lithofacies (see Chapter 2 and appendix C). These clean carbonates abruptly change laterally into thick anhydrite packages. Isochore maps of the upper Ismay clean carbonates and the locally thick anhydrites are consistent with a broad carbonate shelf containing several small intra-shelf basins. The intra-shelf basin centers filled with anhydrite following carbonate sedimentation on the remainder of the carbonate shelf.
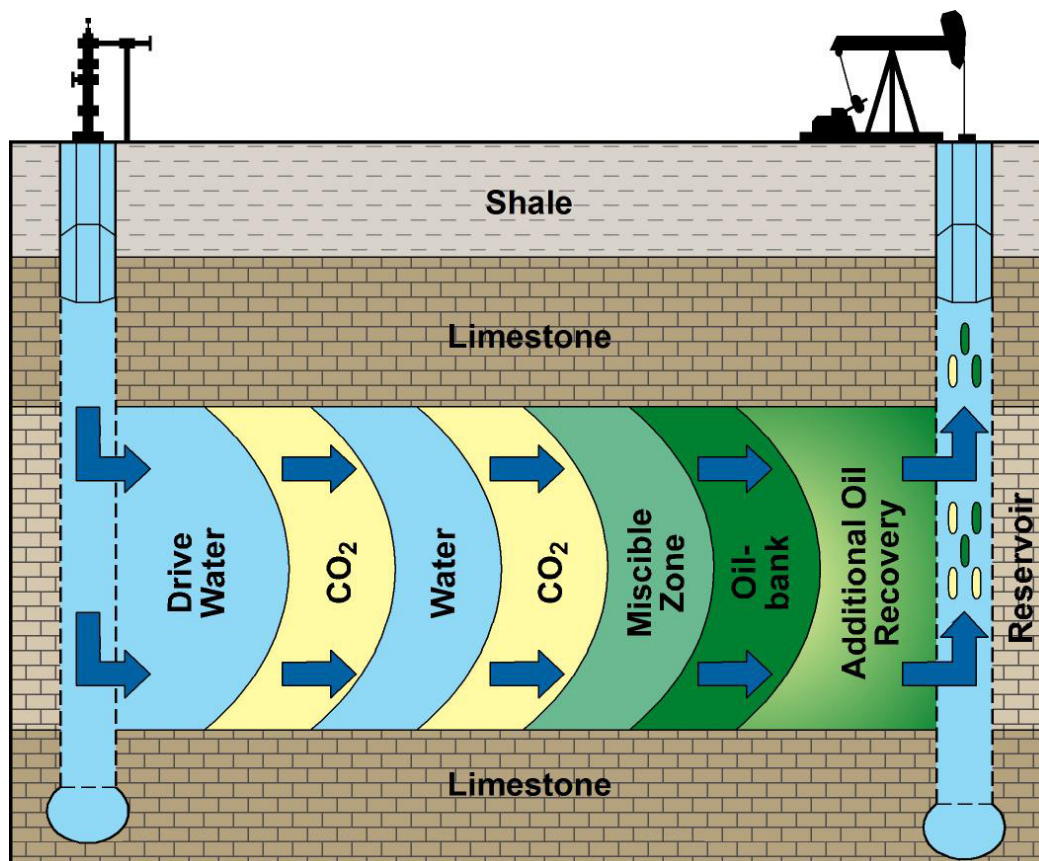
Figure 10.2. Schematic diagram showing water-alternating-gas (WAG) CO_2 injection.

Lithofacies and reservoir controls imposed by the anhydritic intra-shelf basins should be considered when selecting the optimal location and orientation of any horizontal drilling for undrained reserves, as well as identifying new exploration trends. Projections of the inner shelf/tidal flat and mound trends around the intra-shelf basins identify potential exploration targets (figures 2.18 and 2.19), which could be developed using horizontal drilling techniques. Drilling horizontally from known phylloid-algal reservoirs along the inner shelf/tidal flat trend could encounter previously undrilled porous buildups.

Intra-shelf basins are not present in the lower Desert Creek zone of the Blanding sub-basin. However, drilling horizontally from productive mound lithofacies along linear shoreline trends could also encounter previously undrilled porous Desert Creek intervals and buildups.

Reservoir Zones

Carbonate buildups and extent of field potential shown on isochore maps of the upper Ismay and lower Desert Creek and structure contour maps on the top of the upper Ismay zone and the Chimney Rock shale, for Bug and Cherokee fields, respectively, also reveal possible horizontal drilling targets.

In Bug field, the thickness of the lower Desert Creek clean carbonate (see appendix E) displays an elongate, northwest-southeast-trending carbonate buildup depicting the typical, nearshore, shoreline-linear lithofacies tracts of the Desert Creek zone in the northern Blanding sub-basin. Small saddles at Bug and other elongate fields in the Blanding sub-basin may represent intermound troughs between subsidiary buildups. Intermound troughs may be filled with low-permeability wackestone and mudstone, thus acting as barriers or baffles to fluid flow. The relatively small size and abundance of intermound troughs over short distances, as observed in outcrop along the San Juan River for example, suggests caution should be used when correlating these lithofacies between development wells (Chidsey and others, 1996a). Lithofacies that appear correlative and connected from one well to another may actually be separated by low-permeability lithofacies and carbonate rock fabrics which inhibit flow and decrease production potential. Horizontal wells, or laterals, increase the chance of successful drainage where these troughs are present.

In Cherokee field, the six porosity units (figures 3.15 through 3.20) in the Ismay zone could be tested with horizontal laterals from existing wellbores. In addition, horizontal laterals could test the potential of each individual limestone and dolomite unit identified in core. These two lithologies have distinct diagenetic characteristics and pore types, which are often separated from each other by various baffles and barriers. Mutiple porosity units as well as limestone and dolomite units are likely present in other small Ismay fields in the Blanding sub-basin.

The reservoir quality of Bug and Cherokee fields, and most likely all Desert Creek and Ismay fields in the Blanding sub-basin, has been affected by multiple generations of dissolution, anhydrite plugging, and various types of cementation that act as barriers or baffles to fluid flow. Extensive, early-stage micro-boxwork porosity due to dissolution related to subaerial exposure of the carbonate buildup is the most significant diagenetic characteristic of the Desert Creek zone at Bug field (figure 3.27). Intense, late-stage microporosity development along hydrothermal solution fronts is the most significant diagenetic characteristic of the Ismay zone at Cherokee field (figure 3.30). Based on crossplots of permeability and porosity data, the reservoir quality of the rocks in Bug and Cherokee fields is most dependent on pore types and diagenesis. The micro-boxwork porosity in Bug field and the microporosity in Cherokee field represent important targets for undrained reserves by using horizontal drilling techniques.

Horizontal Drilling Strategies

Three strategies for horizontal drilling are recommended for Bug, Cherokee, and similar fields in the Paradox Basin (figure 10.3). All strategies involve drilling stacked, parallel horizontal laterals or high-angle drill holes. Depositional lithofacies are targeted in both the Desert Creek and Ismay zones where, for example, multiple buildups (algal mounds and calcarenites) can be penetrated with two opposed sets of stacked, parallel horizontal laterals (figure 10.3A).

Much of the elongate, brecciated, beach-mound, depositional lithofacies and micro-boxwork porosity in the Desert Creek zone of Bug field and other similar fields could be penetrated by opposed sets of stacked, parallel horizontal laterals (figure 10.B). Finally, the hydrothermally induced microporosity in the Ismay zone of Cherokee and other fields does not appear to be lithofacies dependent and therefore could be drained with radially stacked, horizontal laterals and splays (figure 10.3C).
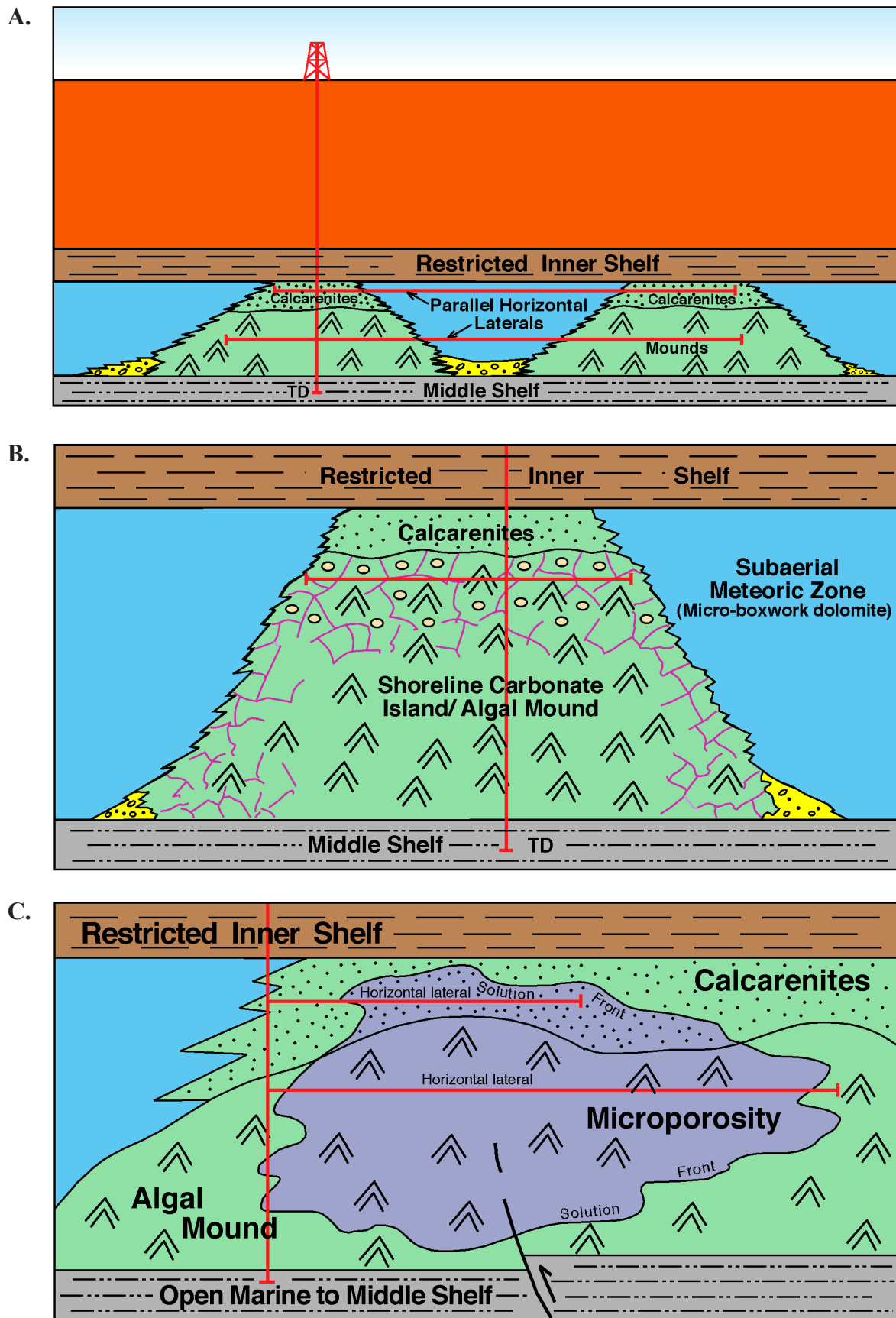
Figure 10.3. *Schematic diagram of strategies for horizontal drilling in Bug and Cherokee fields, Utah: **(A)** depositional lithofacies in the Desert Creek and Ismay zones of Bug and Cherokee fields, **(B)** depositional lithofacies and diagenetic fabrics (micro-boxwork porosity) in the Desert Creek zone of Bug field, and **(C)** microporosity in the Ismay zone of Cherokee field.*

CHAPTER 11:
SUMMARY AND CONCLUSIONS

by

Thomas C. Chidsey, Jr., Utah Geological Survey

CHAPTER 11:
SUMMARY AND CONCLUSIONS

The Paradox Basin of Utah, Colorado, Arizona, and New Mexico contains nearly 100 small oil fields producing from carbonate buildups within the Pennsylvanian (Desmoinesian) Paradox Formation. These fields typically have 1 to 10 vertical wells with primary production ranging from 700,000 to 2,000,000 barrels of oil per field and a 15% to 20% recovery rate of OOIP. Millions of barrels of oil will not be recovered from these small fields because of inefficient recovery practices and undrained heterogeneous reservoirs.

The two main producing zones of the upper Paradox Formation are informally named the Desert Creek and the Ismay. The Desert Creek zone is dominantly dolomite, comprising regional, nearshore, shoreline trends with highly aligned, linear lithofacies tracts. The Desert Creek produces oil and gas in fields in the central Blanding sub-basin. The Ismay zone is dominantly limestone, comprising small, equant buildups of phylloid-algal material; locally variable, inner-shelf, skeletal calcarenites; rare, open-marine, bryozoan mounds; and anhydrite caps. The Ismay produces oil and gas from fields in the southern Blanding sub-basin. Both the Desert Creek and Ismay buildups generally trend northwest-southeast. Various lithofacies changes and extensive diagenesis have created complex reservoir heterogeneity within these two diverse zones.

Two case-study fields were selected for local-scale reservoir characterization and evaluation: Bug field in the Desert Creek trend and Cherokee field in the Ismay trend, San Juan County, Utah. Geological characterization on a local scale focused on reservoir heterogeneity, quality, and lateral continuity, as well as possible reservoir compartmentalization. This study utilized representative cores, geophysical logs, and thin sections to characterize and grade each field in the Blanding sub-basin for drilling horizontal laterals from existing development wells.

The primary objective of this study was to increase hydrocarbon recovery and reserves from small fields in the Paradox Basin before they are abandoned. Our evaluation of regional lithofacies and case studies, summarized below, provides the information for future successful horizontal drilling programs to occur in similar Paradox Basin fields and other shallow-shelf carbonate deposits in the Permian Basin, Silurian pinnacle and patch reefs of the Michigan and Illinois Basins, and shoaling carbonate island trends of the Williston Basin, and elsewhere.

REGIONAL LITHOFACIES EVALUATION

1. The depositional environments of the Desert Creek and Ismay zones, based on core descriptions, show that the controlling factors were water depth, salinity, prevailing wave energy, and, in the case of phylloid-algal growth, paleostructural position. Lithofacies from the middle shelf, principally the phylloid-algal mounds, form the dominant producing reservoirs in the Desert Creek and Ismay zones.

2. Examination of lower Desert Creek cores identified open marine, middle shelf, proto-mound, and phylloid-algal mound lithofacies. Upper Ismay cores include seven depositional lithofacies: open marine, middle shelf, inner shelf/tidal flat, bryozoan mounds, phylloid-algal mounds, quartz sand dunes, and anhydritic salinas.

3. Regional log-based cross sections within the Utah part of the Blanding sub-basin show the development of "clean carbonate" packages, which contain all of the productive reservoir lithofacies. These clean carbonates abruptly change laterally into thick anhydrite packages. Isochore maps of the upper Ismay clean carbonates and the locally thick anhydrites are consistent with a broad carbonate shelf containing several small intra-shelf basins. The intra-shelf basin centers filled with anhydrite following carbonate sedimentation on the carbonate shelf.

4. Separating the upper Ismay zone lithofacies into two intervals (upper and lower parts) and mapping each interval individually delineated very prospective reservoir trends that contain porous, productive buildups. The mapped lithofacies trends clearly define anhydrite-filled intra-shelf basins. Intra-shelf basins are not present in the lower Desert Creek zone of the Blanding sub-basin.

CASE-STUDY FIELDS

1. The log-based correlation scheme developed for the study ties the typical, vertical, core-derived sequence or cycle of depositional lithofacies from Bug and Cherokee case-study fields to their corresponding gamma-ray and neutron-density geophysical logs. The correlation scheme identifies major zone contacts, seals or barriers, baffles, producing or potential reservoirs, and depositional lithofacies. Seals or barriers include anhydrite layers and shales. Baffles are those rock units that restrict fluid flow in some parts of the field but may develop enough porosity and permeability in other parts through diagenetic processes or lithofacies changes to provide a conduit for fluid flow or even oil storage. In Bug field, the porosity unit is the entire Desert Creek mound. However, geophysical logs often exhibit a "false porosity" for some units, which led to wasteful completion attempts. The cores reveal these zones to actually

represent barriers or baffles to fluid flow. Log-defined units with real porosity represent potential targets for horizontal drilling. In Cherokee field for example, six porosity units were identified in the upper Ismay zone; however, the low-ermost exhibited a false porosity on geophysical logs and is incapable of fluid flow.

2. The typical vertical sequence of lithofacies from the case-study fields, as determined from conventional core and tied to its corresponding log response, helped identify reservoir and non-reservoir rock (such as false porosity zones on geophysical well logs) and determine potential units suitable for horizontal drilling projects.

3. Structure contour maps on the top of the Desert Creek and Ismay zones as well as seals such as the Chimney Rock shale, and isochore maps of various units of the lower Desert Creek and Ismay for case-study fields show carbonate buildup trends, lithofacies distribution, defined limits of field potential, and also indicate possible horizontal drilling targets.

4. The diagenetic fabrics and porosity types found in the various hydrocarbon-bearing rocks of the case-study fields are indicators of reservoir flow capacity, storage capacity, and potential for horizontal drilling. The reservoir quality of these fields has been affected by multiple generations of dissolution, anhydrite plugging, and various types of cementation, which act as barriers or baffles to fluid flow. The thin sections from Bug field show extensive, early-stage micro-boxwork porosity due to dissolution related to sub-aerial exposure of the carbonate buildup. The most significant and unique diagenetic characteristic observed in thin sections from Cherokee field was intense, late-stage micro-porosity development along hydrothermal solution fronts.

5. Based on crossplots of permeability and porosity data, the reservoir quality of the rocks in the case-study fields is most dependent on pore types and diagenesis.

Scanning Electron Microscopy (SEM) and Pore Casting

1. Scanning electron microscope and/or pore casting analyses helped disclose the diagenetic fabrics and porosity types found in the various hydrocarbon-bearing units of Bug and Cherokee fields.

2. All samples exhibit microporosity in the form of micro-boxwork porosity (primarily in Bug field) or intercrystalline (primarily in Cherokee field). Dissolution has contributed to porosity in most samples. It has created moldic, vuggy, and channel porosity. All samples contain dolomite. Anhydrite, calcite, smectite clays, and pyrobitumen are present in some samples. The dominant cement occluding porosity and permeability in the Cherokee wells is anhydrite.

3. The general diagenetic sequence for these samples, based on SEM and pore casting analyses, is: (1) deposition of calcite cement, (2) dissolution, (3) dolomitization, (4) dissolution, (5) fracturing, (6) calcite cementation, (7) quartz cementation, (8) clay deposition, (9) anhydrite cementation, and (10) pyrobitumen emplacement.

Epifluorescence (EF) Analysis

1. Epifluorescence petrography makes it possible to clearly identify grain types and shapes, within both limestone and dolomite reservoir intervals in upper Ismay zone thin sections from cores examined in this study. In particular, identification of peloids, skeletal grain types, and coated grains is enhanced in rocks where these grains have been poorly preserved, partially leached, or completely dolomitized.

2. Depositional textures that are frequently occult or poorly preserved can often be clearly distinguished using blue-light EF microscopy. In many of the microporous limestones and finely crystalline dolomites of the upper Ismay reservoir at Cherokee field, the differences between muddy and calcarenitic fabrics can only be clearly appreciated with fluorescence lighting.

3. Epifluorescence petrography clearly and rapidly images pore spaces that cannot otherwise be seen in standard viewing under transmitted polarized lighting. In addition, the cross-sectional size and shape of pores are enhanced.

4. Much of the upper Ismay zone porosity is very heterogeneous and poorly connected as viewed under EF. In particular, microporosity within some of the upper Ismay reservoir section in Cherokee field can be resolved much more clearly than with transmitted polarized lighting. The EF examination helps in seeing the dissolution origin of most types of the microporosity. Transmitted polarized lighting does not image microporosity in carbonate samples very well, even though blue-dyed epoxy can be impregnated into even very small pores. This porosity does not show up very well because the pores are much smaller than the thickness of the thin section, hence carbonate crystallites on either side of micropores are seen rather than the pores. In addition, opaque bitumen linings prevent light from passing through some of the pores to the observer. Without the aid of the EF view, the amount of visible open pore space would be underestimated in the plane-light image.

5. Where dolomitization has occurred, EF petrography often shows the crystal size, shape, and zonation far better than transmitted plane or polarized lighting. This information is often very useful when considering the origin and timing of dolomitization as well as evaluating the quality of the pore system within the dolomite.

6. Permeability differences within these dolomite and limestone samples are also enhanced by EF because of the dif-

ferential oil saturations between the lower-permeability areas and the more permeable lithologies. Low-permeability carbonates from this study area show bright yellow fluorescence due to trapped live oil that is retained within tighter parts of the reservoir system. More permeable rocks show red fluorescence due to the epoxy fluorescence where oil has almost completely drained from the better-quality parts of the reservoir.

7. Fluorescence of dense, "muddy" limestone and dolomite containing abundant, closely spaced, wispy stylolite seams often reveals some very interesting textural and porosity information. Under plane transmitted light, these types of samples appear to be a dense lime mudstone whereas EF examination clearly shows distinct grain-supported peloids. More importantly, EF frequently reveals small compartments of good porosity separated from much tighter rocks by subhorizontal stylolitic seams. Hence, some of the stylolites and wispy seams with concentrations of insoluble residues act as barriers to vertical fluid flow between the porous compartments. Epifluorescence also suggests that the origin of the porosity may be related to dissolution of the peloidal limestone matrix after the formation of the stylolites.

Cathodoluminescence (CL) Analysis

1. Examination of lower Desert Creek dolomites and upper Ismay limestones under CL makes it possible to more clearly identify grain types and shapes, early cements (such as botryoidal, fibrous marine, bladed calcite cements), and brecciated phylloid-algal mound fabrics. In addition, identification of pelleted fabrics in muds, as well as various types of skeletal grains, is improved by CL examination in rocks where these grains have been poorly preserved, partially leached, or completely dolomitized. In many ways, CL imaging of samples complements the types of information derived from EF of carbonate thin sections.

2. Cathodoluminescence imaging clearly and rapidly images pore spaces that cannot be easily seen in standard viewing under transmitted, plane-polarized light. In addition, the detail of cross-sectional size, shape, and boundaries of pores is enhanced. This information is often useful when considering the origin and timing of dolomitization as well as evaluating the quality of the pore system within the dolomite.

3. Imaging of microfractures as well as dissolution along microstylolites, is greatly facilitated under CL. Many open microfractures cannot be easily seen in a normal 3-μm-thick petrographic thin section, especially within dense, lower Desert Creek dolomites. Routine CL examination of the same thin section often reveals the presence of individual microfractures or microfracture swarms.

4. Examination of saddle dolomites, when present within the clean carbonate intervals of the lower Desert Creek or up-

per Ismay intervals, can provide more information about these late, elevated temperate (often hydrothermal) mineral phases. For instance, saddle dolomites from the Cherokee Federal No. 22-14 well showed nice growth banding. They also exhibited the difference between replacement and cement types of saddle dolomites under CL.

Isotope Geochemistry

1. Diagenesis is the main control on the quality of Desert Creek and Ismay reservoirs. Much of the porosity development occurred in a mesogenetic (burial) setting, mostly post-dating stylolitization. Maximum porosity is developed as dissolution adjacent to stylolites, especially in phylloid-algal mounds. It is likely that most of the carbonates present within the lower Desert Creek (as well as throughout the Ismay zone) have retained a marine-influenced isotope geochemistry through marine cementation as well as post-burial recycling of marine carbonate components during dolomitization, stylolitization, dissolution, and late cementation. Such an explanation agrees with the model for the positive carbon isotope values of many ancient carbonates.

2. Carbon isotopic compositions for Bug field dolomite samples have a mean $\delta^{13}C_{VPDB}$ value of +4.43‰. Despite dolomitization, all of the lower Desert Creek samples from Bug field show carbon isotope compositions that are very close in value to modern marine carbonates and Holocene botryoidal marine aragonite cements.

3. The carbon isotope geochemistry of the lower Desert Creek dolomites at Bug field has retained a strong influence from Pennsylvanian marine water composition. Meteoric waters do not appear to have had any affect on the composition of these lower Desert Creek dolomites.

4. Oxygen isotopic compositions for the Bug field dolomite samples have a mean $\delta^{18}O_{VPDB}$ value of -4.51‰. The lighter oxygen values obtained from wells located along the margins or flanks of Bug field may be indicative of exposure to higher temperatures, to fluids depleted in ^{18}O relative to sea water, or to hypersaline waters during burial diagenesis.

5. The wells in Bug field having the lightest oxygen isotope compositions in the lower Desert Creek dolomites have produced significantly greater amounts of hydrocarbons.

6. Carbon isotopic compositions for the upper Ismay dolomite samples at Cherokee field have a mean $\delta^{13}C_{VPDB}$ value of +4.70‰. As with the Bug field dolomite samples, the Cherokee field carbonates fall within the same range of carbon isotope compositions as modern marine sediments, skeletons, and marine cements. Meteoric waters, which typically would precipitate carbonates with more depleted carbon isotope values, have not had major effects on the composition of the Ismay carbonate components.

7. Oxygen isotopic compositions for the Cherokee field limestone and dolomite samples form a wide range of values around a mean $\delta^{18}O_{VPDB}$ value of -4.20‰. There is no significant difference between the oxygen isotope compositions from lower Desert Creek dolomite samples in Bug field and the upper Ismay limestones and dolomites from Cherokee field.

8. One of the dolomitized samples in Cherokee field, from cryptalgal laminites, has a much lighter oxygen composition. The depleted $\delta^{18}O_{VPDB}$ value of this one dolomite sample suggests neomorphism, cementation, and/or dolomitization from warm or isotopically light subsurface waters.

9. Carbon isotopic compositions for upper Ismay limestone samples in the cemented buildup of Patterson Canyon field have a mean $\delta^{13}C_{VPDB}$ value of +5.43‰. However, the samples can be divided into two populations with regard to carbon isotopic composition: isotopically heavier mound cemented and isotopically lighter oolite and cement bands. Mound cements in Patterson Canyon field were confined to a "closed hydrologic system" that allowed a fluid with heavier carbon to evolve. The oolite and cement bands therein may have been in a more open system allowing water exchange such that waters with a composition slightly lighter were involved in the lithification and diagenesis of the capping oolite. Oxygen isotopic compositions for upper Ismay limestone samples of the cemented buildup in Patterson Canyon field have a mean $\delta^{18}O_{VPDB}$ value of -5.48‰, lighter than Bug and Cherokee samples. The oxygen isotope signatures indicate waters with depleted ^{18}O characteristics evolved in the mound cavities and ooid grainstone pores, without any influence by hypersaline waters. Alternatively, the limestones in this sample set may have all been modified via neomorphism by isotopically light subsurface waters.

Capillary Pressure /Mercury Injection Analysis

1. Capillary pressure/mercury injection analyses were used to assess reservoir potential and quality in Bug and Cherokee fields by (1) determining the most effective pore systems for oil storage versus drainage, (2) identifying reservoir heterogeneity, (3) predicting potential untested compartments, (4) inferring porosity and permeability trends, and (5) matching diagenetic processes, pore types, mineralogy, and other attributes to porosity and permeability distribution.

2. The pore-throat-radius histograms for Bug field show that some zones likely have significant microporosity (micro-boxwork porosity), whereas other zones are dominated by moldic porosity. Steeper saturation profiles for Bug field indicate a significant amount of micro-boxwork porosity and excellent targets for horizontal drilling.

3. The pore-throat-radius histogram for both the Cherokee Federal No. 22-14 and Cherokee Federal No. 33-14 wells shows that half of the pore size distribution falls under 2.0 microns or in the microporosity realm. The saturation profiles for both wells show that a relatively high injection pressure is required to occupy more than the last 70% of the pores. The Cherokee Federal No. 33-14 well has a steeper saturation profile than the Cherokee Federal No. 22-14 well indicating a greater amount of microporosity and thus, a high potential for untapped reserves.

Production Analysis

1. Production "sweet spots" and potential horizontal drilling candidates were identified for Bug and Cherokee fields. In Bug field, the highest IFPs and largest volumes of oil were recorded from wells located structurally downdip from the updip porosity pinch out that forms the trap, and in the main part of the lower Desert Creek zone carbonate buildup. These wells penetrated both the phylloid-algal mound and the shoreline carbonate island facies where significant micro-boxwork porosity has likely developed—the diagenetic pore type with the greatest hydrocarbon storage and flow capacity in this dolomitized reservoir.

2. In Cherokee field, the highest IFPs as well as the largest volumes of oil and gas produced are from wells located on the crest of the structural nose where the upper Ismay zone buildup developed and in the thickest part of the mound facies. These wells penetrated both the phylloid-algal mound and the crinoid/fusulinid-bearing, carbonate sand facies of the carbonate buildup where there may be a thick section of microporosity. This unique pore type represents the greatest hydrocarbon storage capacity and potential horizontal drilling target in the field.

HORIZONTAL DRILLING OPPORTUNITIES

1. With the exception of the giant Greater Aneth field, the value of horizontal drilling has not been demonstrated in any of the small shallow-shelf carbonate reservoirs in the Paradox Basin. These reservoirs are heterogeneous due to lithofacies changes and extensive diagenesis within the Desert Creek and Ismay zones leaving untapped compartments. Production and injection laterals could be drilled into the porosity zones to sweep oil that vertical wells could not reach.

2. Whereas initial production rates may be encouraging from laterals, high early declines will likely indicate the need for injection support. Half of horizontal laterals may be converted to injection to maintain reservoir pressure and maximize sweep efficiency.

3. Lithofacies and reservoir controls imposed by the anhydritic intra-shelf basins should be considered when selecting the optimal location and orientation of any horizontal

drilling for undrained reserves, as well as identifying new exploration trends. In the Desert Creek zone, drilling horizontally from productive mound lithofacies along linear shoreline trends could also encounter previously undrilled porous intervals and buildups. In the Ismay zone, projections of the inner shelf/tidal flat and mound trends around the intra-shelf basins identify potential exploration targets, which could be developed using horizontal drilling techniques. Drilling horizontally from known phylloid-algal reservoirs along the inner shelf/tidal flat trend could encounter previously undrilled porous buildups.

4. Strategies for horizontal drilling were developed for case-study and similar fields in the Paradox Basin. All strategies involve drilling stacked, parallel horizontal laterals. Depositional lithofacies are targeted in both the Desert Creek and Ismay zones where, for example, multiple buildups can be penetrated with two opposed sets of stacked, parallel horizontal laterals. Much of the elongate, brecciated beach-mound depositional lithofacies in the Desert Creek zone of Bug field and similar fields could be penetrated by opposed sets of stacked, parallel horizontal laterals. Similarly, a second strategy involves penetrating multiple zones of diagenetically enhanced reservoir intervals in these mound buildups. The microboxwork porosity in Bug field and microporosity in Cherokee field as well as other fields in the Desert Creek and Ismay trends, represent important sites for untapped hydrocarbons and possible targets for horizontal drilling. The hydrothermally induced microporosity in the Ismay zone of Cherokee field does not appear to be lithofacies dependent and therefore it and other fields in the trend could be drained with radially stacked, horizontal laterals and splays.

5. Horizontal wells could be stimulated with hydraulic fracturing as well as acid treatments. We recommend engineering studies to determine the specific methods that would be most appropriate for relatively thin carbonate reservoir zones in the Desert Creek and Ismay zones—i.e. fluid types (including flow enhancers, scale preventers, bactericids) and amounts, proppants, injection rates, pressure, etc.

6. Finally, we recommend three-dimensional seismic surveys to help identify not only untested carbonate buildups but adjacent debris fans/aprons that represent additional horizontal drilling targets.

ACKNOWLEDGMENTS

REFERENCES

Allan, J.R., and Wiggins, W.D., 1993, Dolomite reservoirs—geochemical techniques for evaluating origin and distribution: American Association of Petroleum Geologists, Continuing Education Course Note Series 36, 129 p.

Amateis, L.J., 1995, Application of sequence stratigraphic modeling to integrated reservoir management at Aneth Unit, Greater Aneth field, Utah: Society of Petroleum Engineers, SPE 030534, p. 35–49.

Amateis, L.J., and Hall, S., 1997, Drilling multilaterals in a complex carbonate reservoir, Aneth field, Utah, *in* Coalson, E.B., Osmond, J.C., and Williams, E.T., editors, Innovative petroleum technology in the Rocky Mountain area: Rocky Mountain Association of Geologists Guidebook, p. 125–135.

Baars, D.L., 1966, Pre-Pennsylvanian paleotectonics—key to basin evaluation and petroleum occurrences in Paradox Basin, Utah and Colorado: American Association of Petroleum Geologists Bulletin, v. 50, no. 10, p. 2082–2111.

Baars, D.L., 1983, The Colorado Plateau—a geologic history: Albuquerque, University of New Mexico press, 179 p.

Baars, D.L., and Stevenson, G.M., 1981, Tectonic evolution of the Paradox Basin, Utah and Colorado, *in* Wiegand, D.L., editor, Geology of the Paradox Basin: Rocky Mountain Association of Geologists Guidebook, p. 23–31.

Baars, D.L., and Stevenson, G.M., 1982, Subtle stratigraphic traps in Paleozoic rocks of Paradox Basin, *in* Halbouty, M.T., editor, The deliberate search for the subtle trap: American Association of Petroleum Geologists Memoir 32, p. 131–158.

Babcock, P.A., 1978a, Aneth (Aneth Unit), San Juan County, Utah, *in* Fassett, J.E., editor, Oil and gas fields in the Four Corners area: Four Corners Geological Society Guidebook, v. II, p. 577–579.

Babcock, P.A., 1978b, Aneth (McElmo Creek Unit), San Juan County, Utah, *in* Fassett, J.E., editor, Oil and gas fields in the Four Corners area: Four Corners Geological Society Guidebook, v. II, p. 580–583.

Babcock, P.A., 1978c, Aneth (Ratherford Unit), San Juan County, Utah, *in* Fassett, J.E., editor, Oil and gas fields in the Four Corners area: Four Corners Geological Society Guidebook, v. II, p. 584–586.

Babcock, P.A., 1978d, Aneth (White Mesa Unit), San Juan County, Utah, *in* Fassett, J.E., editor, Oil and gas fields in the Four Corners area: Four Corners Geological Society Guidebook, v. II, p. 587–590.

Barker, C.E., and Kopp, O.C., editors, 1991, Luminescence microscopy—quantitative and qualitative aspects: Society for Sedimentary Geology (SEPM) Short Course 25 Notes, p. 1–7.

Bebout, D.G., and Loucks, R.G., 1984, Handbook for logging carbonate rocks: Bureau of Economic Geology, University of Texas at Austin, Handbook 5, 43 p.

Blakey, R., and Ranney, W., 2008, Ancient landscapes of the Colorado Plateau: Grand Canyon, Grand Canyon Association, p. 29–38.

Brinton, L., 1986, Deposition and diagenesis of Middle Pennsylvanian (Desmoinesian) phylloid algal banks, Paradox Formation, Ismay zone, Ismay field and San Juan Canyon, Paradox Basin, Utah and Colorado: Golden, Colorado School of Mines, M.S. thesis, 315 p.

Budd, D.A., Hammes, U., and Ward, W.B., 2000, Cathodoluminescence in calcite cements—new insights on Pb and Zn sensitizing, Mn activation, and Fe quenching at low trace-element concentrations: Journal of Sedimentary Petrology, v. 70, p. 217–226.

Burruss, R.C., 1981, Hydrocarbon fluid inclusions in studies of sedimentary diagenesis, *in* Hollister, L.S., and Crawford, M.L., editors, Fluid inclusions—applications in petrology: Mineralogical Association of Canada Short Course Notes, v. 6, p. 138–156.

Burruss, R.C., 1991, Practical aspects of fluorescent microscopy of petroleum fluid inclusions, *in* Barker, C.E., and Kopp, O.C., editors, Luminescence microscopy—quantitative and qualitative aspects: Society for Sedimentary Geology (SEPM) Short Course 25 Notes, p. 1–7.

Burruss, R.C., Cercone, K.R., and Harris, P.M., 1986, Timing of hydrocarbon migration—evidenced from fluid inclusions in calcite cements, tectonics and burial history, *in* Schneidermann, N., and Harris, P.M., editors, Carbonate cements: Society for Sedimentary Geology (SEPM) Special Publication 36, p. 277–289.

Cander, H.S., Kauffman, J., Daniels, L.D., and Meyers, W.J., 1988, Regional dolomitization in the Burlington-Keokuk Formation (Mississippian), Illinois and Missouri—constraints from cathodoluminescent zonal stratigraphy, *in* Shukla, V., and Baker, P.A., editors, Sedimentology and geochemistry of dolostones: Society for Sedimentary Geology (SEPM) Special Publication No. 43, p. 129–144.

Cannizzaro, C.R., 1985, Depositional analysis of the upper Ismay and lower Desert Creek intervals (Pennsylvanian) of the southern Paradox Basin: Troy, New York, Rensselaer Polytechnic Institute, M.S. thesis, 85 p.

Cather, M.E., Morrow, N.R., Brower, K.R., and Buckley, J.S., 1989a, Uses of epi-fluorescent microscopy in evaluation of Mesaverde tight gas sands [abs.]: American Association of Petroleum Geologists Bulletin, v. 73, p. 1150–1151.

Cather, M.E., Morrow, N.R., and Klich, I., 1989b, Applications of fluorescent dye staining techniques to reservoir studies of tight gas sands, Measverde Group, southwestern Colorado [abs.]: American Association of Petroleum Geologists Bulletin, v. 73, p. 342.

Cercone, K.R., and Pedone, V.A., 1987, Fluorescence (photoluminescence) of carbonate rocks—instrumental and analytical sources of observational error: Journal of Sedimentary Petrology, v. 57, p. 780–782.

Chambers, M.R. 1998, Multilateral technology gains broader acceptance: O&G Journal, v. 96, no. 47, p. 47–52.

Chidsey, T.C., Jr., compiler and editor, 2002, Increased oil production and reserves utilizing secondary/tertiary recovery techniques on small reservoirs in the Paradox Basin, Utah—final report: U.S. Department of Energy (NETL/NPTO) Oil Recovery, Field Demonstrations, Program Class II, compact disc, 174 p.

Chidsey, T.C., Jr., compiler and editor, 2007, Heterogeneous shallow-shelf carbonate buildups in in the Paradox Basin, Utah and Colorado—targets for increased oil production and reserves using horizontal drilling techniques—final report: U.S. Department of Energy, National Petroleum Technology Laboratory Class II Oil Revisit Program, Contract No. DE-FC26-00BC15128, compact disc, 155 p.

Chidsey, T.C., Jr., and Eby, D.E., 2000, Facies of the Paradox Formation, southeastern Utah, and modern analogs—tools for exploration and development [abs.]: American Association of Petroleum Geologists, Annual Convention Program with Abstracts, v. 9, p. A26.

Chidsey, T.C., Jr., and Eby, D.E., 2009, Regional lithofacies trends in the upper Ismay and lower Desert Creek zones in the Blanding sub-basin of the Paradox Basin, Utah, *in* Houston, W.S., Wray, L.L., and Moreland, P.G., editors, The Paradox Basin revisited—new developments in petroleum systems and basin analysis: Rocky Mountain Association of Geologists Special Publication, p. 436–470.

Chidsey, T.C., Jr., and Eby, D.E., 2017, Potential oil-prone areas in the Cane Creek shale play, Paradox Basin, Utah, identified by epifluorescence microscope techniques: Utah Geological Survey Special Study 160, 170 p., https://doi.org/10.34191/SS-160.

Chidsey, T.C., Jr., Brinton, L., Eby, D.E., and Hartmann, Kris, 1996a, Carbonate mound reservoirs in the Paradox Formation—an outcrop analogue along the San Juan River, southeastern Utah, *in* Huffman, A.C., Jr., Lund, W.R., and Godwin, L.H., editors, Geology and resources of the Paradox Basin: Utah Geological Association Publication 25, p. 139–156.

Chidsey, T.C., Jr., Eby, D.E., and Lorenz, D.M., 1996b, Geological and reservoir characterization of small shallow-shelf fields, southern Paradox Basin, Utah, *in* Huffman, A.C., Jr., Lund, W.R., and Godwin, L.H., editors, Geology and resources of the Paradox Basin: Utah Geological Association Publication 25, p. 39–56.

Choquette, P.W., and Pray, L.C., 1970, Geologic nomenclature and classification of porosity in sedimentary carbonates: American Association of Petroleum Geologists Bulletin, v. 54, no. 2, p. 207–250.

Colorado Oil & Gas Conservation Commission, 2020, Colorado oil and gas information system (COGIS)—production data inquiry: Online, <oil-gas.state.co.us/cogis/ProductionSearch2.asp>, accessed December 2020.

Coniglio, M., Zheng, Q., and Carter, T.R., 2003, Dolomitization and recrystallization of Middle Silurian reefs and platformal carbonates of the Guelph Formation, Michigan Basin, southwestern Ontario: Bulletin of Canadian Petroleum Geology, v. 51, p. 177–199.

Crawley-Stewart, C.L., and Riley, K.F., 1993, Cherokee, *in* Hill, B.G., and Bereskin, S.R., editors, Oil and gas fields of Utah: Utah Geological Association Publication 22, non-paginated.

Dansereau, P., and Bourque, P.A., 2001, The Neigette breccia—remnant of the West Point reef tract in the Matapedia Valley area, and witness to Late Silurian synsedimentary faulting, Gaspe Belt, Northern Appalachians, Quebec: Bulletin of Canadian Petroleum Geology, v. 49, p. 327–345.

Dawson, W.C., 1988, Ismay reservoirs, Paradox Basin—diagenesis and porosity development, *in* Goolsby, S.M., and Longman, M.W., editors, Occurrence and petrophysical properties of carbonate reservoirs in the Rocky Mountain region: Rocky Mountain Association of Geologists, p. 163–174, 442–443.

Denton, G.H., and Hughes, T.J., 1983, Milankovitch theory of ice ages—hypothesis of ice-sheet linkage between regional insolation and global climate: Quaternary Research, v. 20, p. 125–144.

Doelling, H.H., 2010, Geology of Arches National Park, *in* Sprinkel, D.A., Chidsey, T.C., Jr., and Anderson P.B., editors, Geology of Utah's parks and monuments (third edition): Utah Geological Association Publication 28, p. 11–36.

Dorobek, S.L., Read, J.F., Niemann, J.M., Pong, T.C., and Haralick, R.M., 1987, Image analysis of cathodoluminescence-zoned calcite cements: Journal of Sedimentary Petrology, v. 57, p. 766–770.

Dravis, J.J., 1988, Deep-burial microporosity in Upper Jurassic Haynesville oolitic grainstones, East Texas: Sedimentary Geology, v. 63, p. 325–341.

Dravis, J.J., 1991, Carbonate petrography—update on new techniques and applications: Journal of Sedimentary Petrology, v. 61, p. 626–628.

Dravis, J.J., 1992, Burial dissolution in limestones and dolomites—criteria for recognition and discussion of controls—a case study approach (Part 1—Upper Jurassic Haynesville limestones, East Texas; Part 2—Devonian Upper Elk Point dolomites, western Canada): American Association of Petroleum Geologists Bulletin/Canadian Society of Petroleum Geologists Short Course on Subsurface Dissolution Porosity in Carbonates, Calgary, Canada, 171 p.

Dravis, J.J., and Yurewicz, D.A., 1985, Enhanced carbonate petrography using fluorescence microscopy: Journal of Sedimentary Petrology, v. 55, p. 795–804.

Dunham, R.J., 1962, Classification of carbonate rocks according to depositional texture, *in* Ham, W.E., editor, Classification of carbonate rocks: American Association of Petroleum Geologists Memoir 1, p. 108–121.

Eby, D.E., Chidsey, T.C., Jr., and Morgan, C.D., 2008, The use of epifluorescence techniques to determine potential oil-prone areas in the Mississippian Leadville Limestone, northern Paradox Basin, Utah [abs.]: Rocky Mountain Natural Gas Geology and Resource Conference, Rocky Mountain Section of the American Association of Petroleum Geologists and Colorado Oil & Gas Association Official Program with Abstracts, p. 88–89.

Eby, D.E., and Hager, R.C., 1986, Fluorescence petrology of San Andres dolomites—H.O. Mahoney lease, Wasson field, Yoakum County, Texas: Permian Basin Section, Society for Sedimentary Geology (SEPM) Publication 86-26, p. 37–38.

Embry, A.R., and Klovan, J.E., 1971, A Late Devonian reef tract on northeastern Banks Island, Northwest Territories: Canadian Petroleum Geologists Bulletin, v. 19, p. 730–781.

Fairchild, I.J., 1983, Chemical studies of cathodoluminescence of natural dolomites and calcites: Sedimentology, v. 30, p. 572–583.

Fetzner, R.W., 1960, Pennsylvanian paleotectonics of the Colorado Plateau: American Association of Petroleum Geologists Bulletin, v. 44, no. 8, p. 1371–1413.

Filippelli, G.M., and DeLaney, M.L., 1992, Quantifying cathodoluminescent intensity with an on-line camera and exposure meter: Journal of Sedimentary Petrology, v. 62, p. 724–725.

Frahme, C.W., and Vaughn, E.B., 1983, Paleozoic geology and seismic stratigraphy of the northern Uncompahgre front, Grand County, Utah, *in* Lowell, J.D., editor, Rocky Mountain foreland basins and uplifts: Rocky Mountain Association of Geologists Guidebook, p. 201–211.

Frank, J.R., Carpenter, A.B., and Oglesby, T.W., 1982, Cathodoluminescence and composition of calcite cement in Taum Sauk Limestone (Upper Cambrian), southeast Missouri: Journal of Sedimentary Petrology, v. 52, p. 631–638.

Frank, T.D., Lohmann, K.C., and Meyers, W.J., 1996, Chemostratigraphic significance of cathodoluminescence zoning in syntaxial cement—Mississippian Lake Valley Formation, New Mexico: Sedimentary Geology, v. 105, p. 29–50.

Gardner, K.L., 1980, Impregnation technique using colored epoxy to define porosity in petrographic thin sections: Canadian Journal of Earth Sciences, v. 17, p. 1104–1107.

Gies, R.M., 1987, An improved method for viewing micropore systems in rocks with the polarizing microscope: Society of Petroleum Engineers Formation Evaluation, v. 2, p. 209–214.

Given, R.K., and Lohmann, K.C., 1985, Derivation of the original isotopic composition of Permian marine cements: Journal of Sedimentary Petrology, v. 55, p. 430–439.

Given, R.K., and Lohmann, K.C., 1986, Isotopic evidence for the early meteoric diagenesis of the reef facies, Permian reef complex of West Texas and New Mexico: Journal of Sedimentary Petrology, v. 56, p. 183–193.

Goldhammer, R.K., Oswald, E.J., and Dunn, P.A., 1994, High frequency, glacio-eustatic cyclicity in Middle Pennsylvanian of the Paradox Basin—an evaluation of Milankovitch forcing, *in* DeBoer, P.L., and Smith, D.G., editors, Orbital forcing and cyclic sequences: Special Publication of the International Association of Sedimentologists 19, p. 243–283.

Goldstein, R.H., 1988, Cement stratigraphy of Pennsylvanian Holder Formation, Sacramento Mountains, New Mexico: American Association of Petroleum Geologists Bulletin, v. 72, p. 425–438.

Goldstein, R.H., 1991, Practical aspects of cement stratigraphy with illustrations from Pennsylvanian limestone and sandstone, New Mexico and Kansas, *in* Barker, C.E., and Kopp, O.C., editors, Luminescence microscopy—quantitative and qualitative aspects: Society for Sedimentary Geology (SEPM) Short Course 25 Notes, p. 123–131.

Gregg, J.M., and Karakus, M., 1991, A technique for successive cathodoluminescence and reflected light microscopy: Journal of Sedimentary Petrology, v. 61, p. 613–635.

Guihaumou, N., Szydlowskii, N., and Padier, B., 1990, Characterization of hydrocarbon fluid inclusions by infrared and fluorescence microspectrometry: Mineralogical Magazine, v. 54, p. 311–324.

Harr, C.L., 1996, Paradox oil and gas potential of the Ute Mountain Ute Indian Reservation, *in* Huffman, A.C., Jr., Lund, W.R., and Godwin, L.H., editors, Geology of the Paradox Basin: Utah Geological Association Publication 25, p. 13–28.

Harry, D.L., and Mickus, K.L., 1998, Gravity constraints on lithospheric flexure and the structure of the late Paleozoic Ouachita orogen in Arkansas and Oklahoma, south-central North America: Tectonics, v. 17, no. 2, p. 187–202.

Heckel, P.H., 1977, Origin of phosphatic black shale facies in Pennsylvanian cyclothems of mid-continent North America: American Association of Petroleum Geologists Bulletin, v. 61, no. 7, p. 1045–1068.

Heckel, P.H., 1983, Diagenetic model for carbonate rocks in midcontinent Pennsylvanian eustatic cyclothems: Journal of Sedimentary Petrology, v. 53, p. 733–759.

Heckel, P.H., 1986, Sea-level curve for Pennsylvanian eustatic marine transgressive-regressive depositional cycles along midcontinent outcrop belt, North America: Geology, v. 14, p. 330–334.

Hemming, N.G., Meyers, W.J., and Grams, J.C., 1989, Cathodoluminescence in diagenetic calcites—the roles of Fe and Mn as deduced from electron probe and spectrophotometric measurements: Journal of Sedimentary Petrology, v. 59, p. 404–411.

Hintze, L.F., and Kowallis, B.J., 2009, Geologic history of Utah: Provo, Utah, Brigham Young University Geology Studies Special Publication 9, 225 p.

Hite, R.J., 1960, Stratigraphy of the saline facies of the Paradox Member of the Hermosa Formation of southeastern Utah and southwestern Colorado, *in* Smith, K.G., editor, Geology of the Paradox Basin fold and fault belt: Four Corners Geological Society, Third Field Conference Guidebook, p. 86–89.

Hite, R.J., 1970, Shelf carbonate sedimentation controlled by salinity in the Paradox Basin, southeast Utah, *in* Ran, J.L., and Dellwig, L.F., editors, Third symposium on salt: Northern Ohio Geological Society, v. 1, p. 48–66.

Hite, R.J., Anders, D.E., and Ging, T.G., 1984, Organic-rich source rocks of Pennsylvanian age in the Paradox Basin of Utah and Colorado, *in* Woodward, Jane, Meissner, F.F.,

and Clayton, J.L., editors, Hydrocarbon source rocks of the greater Rocky Mountain region: Rocky Mountain Association of Geologists Guidebook, p. 255–274.

Hite, R.J., and Buckner, D.H., 1981, Stratigraphic correlation, facies concepts and cyclicity in Pennsylvanian rocks of the Paradox Basin, *in* Wiegand, D.L., editor, Geology of the Paradox Basin: Rocky Mountain Association of Geologists 1981 Field Conference, p. 147–159.

Hudson, J.D., 1975, Carbon isotopes and limestone cements: Geology, v. 3, p. 19–22.

Hsu, C., Koinis, R.L., and Fox, C.E., 1995, Technology, experience speed CO_2 flood design: Oil & Gas Journal, v. 93, no. 43, p. 51–59.

Imbrie, J., and Imbrie, J.Z., 1980, Modeling the climatic response to orbital variations: Science, v. 207, p. 943–953.

James, N.P., and Ginsburg, R.N., 1979, The seaward margin of Belize barrier and atoll reefs: International Association of Sedimentologists Special Publication 3, 191 p.

Jones, G.S., 1992, A geologist's perspective on horizontal drilling in a pinnacle reef, Rainbow Basin, Alberta, *in* Schmoker, J.W., Coalson, E.B., and Brown, C.A., editors, Geological studies relevant to horizontal drilling— examples from western North America: Rocky Mountain Association of Geologists Guidebook, p. 171–175.

Kirby, K.C., and Tinker, S.W., 1992, The Keg River/Winnipegosis petroleum system in northeast Alberta [abs.]: American Association of Petroleum Geologists Annual Convention, Official Program with Abstracts, v. 1, p. A66.

Kitcho, C.H., 1981, Characteristics of surface faults in the Paradox Basin, *in* Wiegnand, D.L., editor, Geology of the Paradox Basin: Rocky Mountain Association of Geologists Guidebook, p. 1–21.

Kluth, C.F., 1986, Plate tectonics of the Ancestral Rocky Mountains: American Association of Petroleum Geologists Memoir 41, p. 353–369.

Kluth, C.F., and Coney, P.J., 1981, Plate tectonics of the Ancestral Rocky Mountains: Geology, v. 9, p. 10–15.

LaFlamme, A.K., 1992, Replacement dolomitization in the Upper Devonian Leduc and Swan Hills Formations, Caroline area, Alberta, Canada [abs.]: American Association of Petroleum Geologists Annual Convention, Official Program with Abstracts, v. 1, p. A70.

Lambert, M.R., Anthony, T.L., Calvin, M.W., Gutierrez, S., Markley, D.K., and Smith, D.P., 1995, Implementing CO_2 floods—no more delays!: Society of Petroleum Engineers, SPE Paper 35187, 15 p.

Land, L.S., 1980, The isotopic and trace elements geochemistry of dolomite—the state of the art, *in* Zenger, D.H., Dunham, J.B., and Ethington, R.L., editors, Concepts and models of dolomitization: Society for Sedimentary Geology (SEPM) Special Publication 28, p. 87–110.

Land, L.S., 1982, Dolomitization: American Association of Petroleum Geologists Short Course Note Series No. 24, 20 p.

LaVoie, D., Chi G., and Fowler, M.G., 2001, The Lower Devonian Upper Gaspe Limestones in eastern Gaspe—carbonate diagenesis and reservoir potential: Bulletin of Canadian Petroleum Geology, v. 49, p. 346–365.

LaVoie, D., and Morin, C., 2004, Hydrothermal dolomitization in the Lower Silurian Sayabee Formation in northern Gaspe—Matapedia (Quebec)—constraint on timing of porosity and regional significance for hydrothermal reservoirs: Bulletin of Canadian Petroleum Geology, v. 52, p. 256–269.

LeFever, J.A., 1992, Horizontal drilling in the Williston Basin, United States and Canada, *in* Schmoker, J.W., Coalson, E.B., and Brown, C.A., editors, Geological studies relevant to horizontal drilling—examples from western North America: Rocky Mountain Association of Geologists Guidebook, p. 177–197.

Lohmann, K.C., 1983, Diagenetic history of carbonate reservoirs—integration of petrographic and geochemical techniques, *in* Wilson, J.L., Wilkinson, B.H., Lohmann, K.C., and Hurley, N.F., editors, New ideas and methods of exploration for carbonate reservoirs: Dallas Geological Society, unpaginated.

Machel, H.G., 2000, Application of cathodoluminescence to carbonate diagenesis, *in* Pagel, M., Barbin, V., Blanc P., and Ohnenstetter, D., editors, Cathodoluminescence in geosciences: New York, Springer, p. 271–301.

Machel, H.G., and Burton, E.A., 1991, Factors governing cathodoluminescence in calcite and dolomites and their implications for studies of carbonate diagenesis, *in* Barker, C.E., and Kopp, O.C., editors, Luminescence microscopy—quantitative and qualitative aspects: Society for Sedimentary Geology (SEPM) Short Course 25 Notes, p. 37–57.

Marshall, D.J., 1988, Cathodoluminescence of geological materials: Winchester, Massachusetts, Allen & Unwin, 128 p.

Marshall, D.J., 1991, Combined cathodoluminescence and energy dispersive spectroscopy, *in* Barker, C.E., and Kopp, O.C., editors, Luminescence microscopy—quantitative and qualitative aspects: Society for Sedimentary Geology (SEPM) Short Course 25 Notes, p. 27–36.

Martin, G.W., 1983, Bug, *in* Fassett, J.E., editor, Oil and gas fields of the Four Corners area, volume III: Four Corners Geological Society, p. 1073–1077.

Matheny, J.P., and Longman, M.W., 1996, Lower Desert Creek reservoirs in the Paradox Basin—examples of phylloid algae filling depositional lows related to salt dissolution, *in* Longman, M.W., and Sonnenfeld, M.D., editors, Paleozoic systems of the Rocky Mountain region: Society for Sedimentary Geology (SEPM) Rocky Mountain Section Guidebook, p. 267–282.

Meyers, W.J., 1974, Carbonate cement stratigraphy of the Lake Valley Formation (Mississippian), Sacramento Mountains, New Mexico: Journal of Sedimentary Petrology, v. 44, p. 837–861.

Meyers, W.J., 1978, Carbonate cements—their regional distribution and interpretation in Mississippian limestones of southwestern New Mexico: Sedimentology, v. 25, p. 371–400.

Meyers, W.J., 1991, Cement stratigraphy—an overview, *in* Barker, C.E., and Kopp, O.C., editors, Luminescence microscopy—quantitative and qualitative aspects: Society for Sedimentary Geology (SEPM) Short Course 25 Notes, p. 133–148.

Miller, J., 1988, Cathodoluminescence microscopy, *in* Tucker, M., editor, Techniques in sedimentology: Oxford, Blackwell Publications, p. 174–190.

Moore, T.R., and Hawks, R.L., 1993, Greater Aneth, *in* Hill, B.G., and Bereskin, S.R., editors, Oil and gas fields of Utah: Utah Geological Association Publication 22 (Addendum), non-pagenated.

Nuccio, V.F., and Condon, S.M., 1996, Burial and thermal history of the Paradox Basin, Utah and Colorado, and petroleum potential of the Middle Pennsylvanian Paradox Formation, *in* Huffman, A.C., Jr., Lund, W.R., and Godwin, L.H., editors, Geology of the Paradox Basin: Utah Geological Association Publication 25, p. 57–76.

Ohlen, H.R., and McIntyre, L.B., 1965, Stratigraphy and tectonic features of Paradox Basin, Four Corners area: American Association of Petroleum Geologists Bulletin, v. 49, no. 11, p. 2020–2040.

Oline, W.F., 1996, Bug, *in* Hill, B.G., and Bereskin, S.R., editors, Oil and gas fields of Utah: Utah Geological Association Publication 22 Addendum, non-paginated.

Parrish, J.T., 1982, Upwelling and petroleum source beds, with reference to the Paleozoic: American Association of Petroleum Geologists Bulletin, v. 66, no. 6, p. 750–774.

Peterson, J.A., 1966, Stratigraphic vs. structural controls on carbonate-mound accumulation, Aneth area, Paradox Basin: American Association of Petroleum Geologists Bulletin, v. 50, no. 10, p. 2068–2081.

Peterson, J.A., 1992, Aneth field—U.S.A., Paradox Basin, Utah, *in* Foster, N.H., and Beaumont, E.A., editors, Stratigraphic traps III: American Association of Petroleum Geologists Treatise of Petroleum Geology—Atlas of Oil and Gas Fields, p. 41–82.

Peterson, J.A., and Hite, R.J., 1969, Pennsylvanian evaporite-carbonate cycles and their relation to petroleum occurrence, southern Rocky Mountains: American Association of Petroleum Geologists Bulletin, v. 53, p. 884–908.

Peterson, J.A., and Ohlen, H.R., 1963, Pennsylvanian shelf carbonates, Paradox Basin, *in* Bass, R.O., editor, Shelf carbonates of the Paradox Basin: Four Corners, Geological Society Symposium, 4th Field Conference, p. 65–79.

Pittman, E.D., 1992, Relationship of porosity and permeability to various parameters derived from mercury injection-capillary pressure curves for sandstone: American Association of Petroleum Geologists Bulletin, v. 76, no. 2, p. 191–198.

Pray, L.C., and Wray, J.L., 1963, Porous algal facies (Pennsylvanian) Honaker Trail, San Juan Canyon, Utah, *in* Bass, R.O., editor, Shelf carbonates of the Paradox Basin: Four Corners Geological Society Guidebook, p. 204–234.

Radke, B.M., and Mathis, R.L., 1980, On the formation and occurrence of saddle dolomite: Journal of Sedimentary Petrology, v. 50, p. 1149–1168.

Ritter, S.M., and Gianniny, G.L., 2012, Geological guide to Honaker Trail, San Juan River gorge (near Goosenecks State Park), Southeastern Utah, *in* Anderson, P.B., and Sprinkel, D.A., editors, Geologic road, trail, and Lake guides to Utah's parks and monuments (3rd edition): Utah Geological Association Publication 29, 32 p.

Rost, F.W.D., 1992, Fluorescence microscopy, v. 1: New York, Cambridge University Press, 253 p.

Roylance, M.H., 1984, Depositional and diagenetic control of petroleum entrapment in the Desert Creek interval, Paradox Formation, southeastern Utah and southwestern Colorado: Lawrence, University of Kansas, M.S. thesis, 191 p.

Roylance, M.H., 1990, Depositional and diagenetic history of a Pennsylvanian algal-mound complex—Bug and Papoose Canyon fields, Utah and Colorado: American Association of Petroleum Geologists Bulletin, v. 74, p. 1087–1099.

Scholle, P.A., and Ulmer-Scholle, D.S., 2003, A color guide to the petrography of carbonate rocks: American Association of Petroleum Geologists Bulletin Memoir 77, p. 427–440.

Sipple, R.F., and Glover, E.D., 1965, Structures in carbonate rocks made visible by luminescence petrography: Science, v. 150, p. 1283–1287.

Skinner, M.R., 1996, Carbonate microfacies and conodont biostratigraphy of the subsurface upper Ismay interval (Desmoinesian, Paradox Formation), Mustang Flat oil field, Utah: Provo, Utah, Brigham Young University, M.S. thesis, 110 p.

Soeder, D.J., 1990, Applications of fluorescent microscopy to study of pores in tight rocks: American Association of Petroleum Geologists Bulletin, v. 74, p. 30–40.

Stevenson, G.M., and Baars, D.L., 1986, The Paradox—a pull-apart basin of Pennsylvanian age, *in* Peterson, J.A., editor, Paleotectonics and sedimentation in the Rocky Mountain region: American Association of Petroleum Geologists Memoir 41, p. 513–539.

Stevenson, G.M., and Baars, D.L., 1987, The Paradox—a pull-apart basin of Pennsylvanian age, *in* Campbell, J.A., editor, Geology of Cataract Canyon and vicinity: Four Corners Geological Society, 10th Field Conference, p. 31–55.

Teichmuller, M., and Wolf, M., 1977, Application of fluorescence microscopy in coal petrology and oil exploration: Journal of Microscopy, v. 109, p. 49–73.

Tremain, C.M., 1993, Low-BTU gas in Colorado, *in* Hjellming, C.A., editor, Atlas of major Rocky Mountain gas reservoirs: New Mexico Bureau of Mines and Mineral Resources, p. 172.

Utah Division of Oil, Gas and Mining, 2020, Oil and gas summary production report by field, August 2020: Online, https://oilgas.ogm.utah.gov/oilgasweb/publications/monthly-rpts-by-fld.xhtml, accessed December 2020.

van Gijzel, P., 1967, Palynology and fluorescence microscopy: Reviews of Paleobotany and Palynology, v. 1, p. 49–79.

Veizer, J., Ala, D., Azmy, K., Bruckschen, P., Buhl, D., Bruhn, F., Carden, G.A., Diener, A., Ebneth, S., Godderis, Y., and Jasper, T., 1999, $^{87}Sr/^{86}Sr$, $\delta^{13}C$ and $\delta^{18}O$ evolution of Phanerozoic seawater: Chemical Geology, v. 161, no. 1-3, p. 59–88.

Walker, G., and Burley, S., 1991, Luminescence petrography and spectroscopic studies of diagenetic minerals, *in* Barker, C.E., and Kopp, O.C., editors, Luminescence microscopy—quantitative and qualitative aspects: Society for Sedimentary Geology (SEPM) Short Course 25 Notes, p. 83–96.

Wood, J.R., Allan, J.R., Huntoon, J.E., Pennington, W.D., Harrison, W.B., Taylor, E., and Tester, C.J., 1996, Horizontal well taps bypassed Dundee oil in Crystal field, Michigan: Oil & Gas Journal, October, p. 60–63.

Wood, R.E., and Chidsey, T.C., Jr., 2015, Oil and gas fields map of Utah: Utah Geological Survey Circular 119, scale 1:700,000, https://doi.org/10.34191/C-119.

Wray, L.L., Apeland, A.D., Hemborg, T., and Brchan, C., 2002, Oil and gas fields map of Colorado: Colorado Geological Survey Map Series 33, scale 1:500,000.

Yanguas, J.E., and Dravis, J.J., 1985, Blue fluorescent dye technique for recognition of microporosity in sedimentary rocks: Journal of Sedimentary Petrology, v. 55, p. 600–602.

APPENDIX A:

REGIONAL PARADOX FORMATION CROSS SECTIONS, BLANDING SUB-BASIN, UTAH

Link to supplemental data download:
https://ugspub.nr.utah.gov/publications/bulletins/b-140/b-140-a.pdf

APPENDIX B:

REGIONAL PARADOX FORMATION STRUCTURE AND ISOCHORE MAPS, BLANDING SUB-BASIN, UTAH

Link to supplemental data download:
https://ugspub.nr.utah.gov/publications/bulletins/b-140/b-140-b.pdf

APPENDIX C:

REGIONAL PARADOX FORMATION FACIES MAPS, BLANDING SUB-BASIN, SAN JUAN COUNTY, UTAH

Link to supplemental data download:
https://ugspub.nr.utah.gov/publications/bulletins/b-140/b-140-c.pdf

APPENDIX D:

**GEOPHYSICAL WELL LOG/CORE DESCRIPTIONS AND CORE PHOTOGRAPHS,
BUG AND CHEROKEE FIELDS, SAN JUAN COUNTY, UTAH**

Link to supplemental data download:
https://ugspub.nr.utah.gov/publications/bulletins/b-140/b-140-d.zip

APPENDIX E:

CROSS SECTIONS AND FIELD MAPS, BUG AND CHEROKEE FIELDS, SAN JUAN COUNTY, UTAH

Link to supplemental data download:
https://ugspub.nr.utah.gov/publications/bulletins/b-140/b-140-e.pdf

APPENDIX F:

THIN SECTION DESCRIPTIONS, BUG AND CHEROKEE FIELDS, SAN JUAN COUNTY, UTAH

Link to supplemental data download:
https://ugspub.nr.utah.gov/publications/bulletins/b-140/b-140-f.pdf

APPENDIX G:

**POROSITY/PERMEABILITY CROSSPLOTS, BUG AND CHEROKEE FIELDS,
SAN JUAN COUNTY, UTAH**

Link to supplemental data download:
https://ugspub.nr.utah.gov/publications/bulletins/b-140/b-140-g.pdf

APPENDIX H:

THIN SECTION SCANNING ELECTRON MICROSCOPY AND PORE CASTING, BUG AND CHEROKEE FIELDS, SAN JUAN COUNTY, UTAH

Link to supplemental data download:
https://ugspub.nr.utah.gov/publications/bulletins/b-140/b-140-h.pdf

APPENDIX I:

THIN SECTION EPIFLUORESCENCE, BUG AND CHEROKEE FIELDS, SAN JUAN COUNTY, UTAH

Link to supplemental data download:
https://ugspub.nr.utah.gov/publications/bulletins/b-140/b-140-i.pdf

APPENDIX J:

THIN SECTION CATHODOLUMINESCENCE, BUG AND CHEROKEE FIELDS, SAN JUAN COUNTY, UTAH

Link to supplemental data download:
https://ugspub.nr.utah.gov/publications/bulletins/b-140/b-140-j.pdf

APPENDIX K:

CAPILLARY PRESSURE/MERCURY INJECTION ANALYSIS, BUG AND CHEROKEE FIELDS, SAN JUAN COUNTY, UTAH

Link to supplemental data download:
https://ugspub.nr.utah.gov/publications/bulletins/b-140/b-140-k.zip